République Algérienne Démocratique et Populaire
Ministère de L'Enseignement Supérieur et de la Recherche Scientifique
Université Sétif 1 - Ferhat Abbas

FACULTE DE TECHNOLOGIE

Thèse

Présentée au Département d'électrotechnique pour l'obtention du

diplôme de **Doctorat 3ème cycle**

En : Electrotechnique

Spécialité : Energies Renouvelables

Par : Badreddine Bendriss

Sujet

Contribution à l'Optimisation du Fonctionnement des Réseaux de Distribution en Présence de Génération Distribuée

Soutenue publiquement, le 16/10/2025, devant le jury composé de :

M.	GHERBI Ahmed	Professeur	Université de Setif 1	Président
M.	SAYAH Samir	Professeur	Université de Setif 1	Directeur de thèse
M.	HAMOUDA Abdellatif	Professeur	Université de Setif 1	Co-directeur de thèse
M.	HALIS Abderrahmane	M.C.A	Université de Setif 1	Examinateur
M.	BEDOUI Samir	M.C.A	Université d'OEB	Examinateur
M.	BELILA Hassen	M.C.A	Université d'OEB	Examinateur

People's Democratic Republic of Algeria
Ministry of Higher Education and Scientific Research
University Setif 1 - Ferhat Abbas

FACULTY OF TECHNOLOGY

Thesis

Presented to Department of Electrotechnics in fulfillment of the requirement for the degree of **Doctorate 3rd cycle**

In : Electrotechnic

Speciality : Renewable Energies

By : Badreddine Bendriss

Subject

Contribution to the Optimization of Distribution Grid Operation in the Presence of Distributed Generation

Publicly defended, on 16/10/2025, before a jury composed of :

M.	GHERBI Ahmed	Professor	University of Setif 1	Chairman
M.	SAYAH Samir	Professor	University of Setif 1	Thesis supervisor
M.	HAMOUDA Abdellatif	Professor	University of Setif 1	Thesis co-supervisor
M.	HALIS Abderrahmane	Assoc. Prof. A	University of Setif 1	Examiner
M.	BEDOUI Samir	Assoc. Prof. A	University of OEB	Examiner
M.	BELILA Hassen	Assoc. Prof. A	University of OEB	Examiner

DEDICATION

I would like to dedicate this thesis to ...

My cherished parents, with deep gratitude, I express my heartfelt appreciation for their unwavering support, affection, and love, as well as the countless prayers that have sustained me throughout my academic journey. I pray Allah blesses them with good health, happiness, and a long fulfilling life.

to my beloved family, whose endless support, kindness, and faith have been the cornerstone of my academic path. I am eternally grateful for the bond we share, and I dedicate this work to all of you with love and appreciation.

To my fiancée, whose boundless love, continuous encouragement, and belief in me have been my greatest source of strength. Thank you for standing by my side and inspiring me to keep going, even in the hardest moments.

To my nephew Racime, your presence has brought joy and light into the family.

To myself, for the countless hours of effort, the sacrifices, and the perseverance in the face of every challenge. I ask Allah to reward me with all good things, to help me keep striving, learning, and to grant me the strength to continue.

To Gaza, a land of resilience and enduring hope; to her children who dream beneath shattered skies, and to her people who face unimaginable hardship with unwavering dignity and strength; May this humble work stand as a quiet tribute to your courage, a whisper of solidarity carried across borders. You are not forgotten.

Badreeddine Bendriss

Acknowledgements

First and foremost, I express my deepest thanks to Allah, the Almighty, whose limitless mercy, have guided me through every challenge with patience, courage and strength.

All my sincere gratitude goes to my thesis supervisor, Professor Samir SAYAH, at the Department of Electrical Engineering, Ferhat Abbas University of Setif, for granting me the opportunity to pursue a doctoral thesis under his supervision. I am profoundly thankful for his guidance, encouragement, and generous assistance throughout my research journey. His expertise, thoughtful advice, and insightful suggestions have significantly enriched this work. I am especially grateful for the trust and academic freedom he offered me, which allowed me to develop both intellectually and personally.

I extend my heartfelt gratitude to my co-supervisor, Professor Abdellatif HAMOUDA, at the Institute of Optics and Fine Mechanics, Ferhat Abbas University of Setif, for his valuable advice, insightful guidance, and wise suggestions. His constructive feedback and the depth of our discussions provided me with a clearer and more profound understanding of the various aspects of the subject, which greatly contributed to the successful completion of this work.

I would also like to express my deepest and sincere gratitude to Prof. Ahmed GHERBI, who honored me by accepting to be the president of this jury. My heartfelt thanks also go to all members of jury, Dr. Samir BEDOUI, Associate Prof. at the University of Oum Elbouaghi, Dr. Hassen BELILA Associate Prof. at the University of Oum Elbouaghi and Dr. Abderrahmene HALIS, Associate Prof. at the University of Setif 1 who honored me by agreeing to serve as examiners on this jury.

My heartfelt appreciation goes to my dear friend, Dr. Selman DJEFFAL, at National School of Polytechnic of Constantine, for his support in overcoming the hardest challenges, and for providing me with tools, knowledge, and guidance that have been crucial in navigating this journey.

To my friend, Dr. Amine BEN ALAYA, at the National Engineering School of Tunis, whose invaluable companionship and enriching exchange of knowledge and academic ideas contributed to my journey.

To my colleagues, the Phd students, whose support and camaraderie enriched my academic journey. I extend my warmest thanks.

Publications

Journal Articles (Ranked A)

1. B. Bendriss, S. Sayah, and A. Hamouda, "Efficient multi-objective optimization approach for solving optimal DG placement and sizing problem in distribution systems," Journal of Engineering Research, 2024. doi: 10.1016/j.jer.2024.10.017.

2. B. Bendriss, S. Sayah, and A. Hamouda, "A novel improved Frilled Lizard algorithm for solving the optimal planning problem of renewable energy sources within distribution grids under uncertainties," Energy Conversion and Management, 2025. doi: 10.1016/j.enconman.2024.119465.

Conference Proceedings

International conferences

1. B. Bendriss, S. Sayah, and A. Hamouda, "Optimization of distributed generations within radial distribution systems to enhance system performance," in IEEE International Conference on Electrical Engineering and Advanced Technologies (ICEEAT), Batna, Algeria, 2023, pp. 1–6. doi: 10.1109/ICEEAT60471.2023.10426213.

2. B. Bendriss, S. Sayah, and A. Hamouda, "Jellyfish search optimizer for optimal planning of DG units considering load levels," in IEEE International Conference on Advances in Electrical and Communication Technologies (ICAECOT), Setif, Algeria, 2024, pp. 1–6. doi: 10.1109/ICAECOT62402.2024.10829294.

3. B. Bendriss, S. Sayah, and A. Hamouda, "Optimization of distributed generations placement and sizing in radial distribution system through ABC algorithm," in International Conference on Engineering, Natural Sciences, and Technological Developments (ICENSTED), Konya, Turkey, 19-21 July 2024.

4. B. Bendriss, S. Sayah, and A. Hamouda, "Optimizing Renewable Energy Integration in Radial Distribution Systems Considering Uncertainties in Power Generation," in International Conference on Multidisciplinary Sciences and Technological Developments (ICMUSTED), Konya, Turkey, 13-15 December 2024.

National conferences

1. B. Bendriss, S. Sayah, and A. Hamouda, "Grey Wolf Optimization Algorithm for Optimal Allocation of Distributed Generations in Radial Distribution Systems", in National Conference of Applied Sciences and Engineering (NCASE), ENSTA, Alger, Algeria, 2024.

2. B. Bendriss, S. Sayah, and A. Hamouda, "Enhanced Optimization of Distributed Generation Allocation in Radial Distribution Networks for Loss Minimization", in the Third Algerian Symposium on Renewable Energy & Materials (ASREM'25), Medea, Algeria, April 2025.

3. B. Bendriss, S. Sayah, and A. Hamouda, "Smart incorporation of renewable distributed generations for power loss reduction and voltage profile enhancement in radial distribution grids", in the First National Conference on Renewable Energies and Advanced Electrical Engineering (NC-REAEE'25), M'sila, Algeria, May 2025.

4. B. Bendriss, S. Sayah, and A. Hamouda, "A Novel Approach for Optimal Placement and Sizing of Distributed Generation in Radial Distribution Networks", in the 3^{rd} National Conference on Materials Sciences and Engineering (MSE'25), held at Hassiba Benbouali University of Chlef, Algeria, June 2025.

5. B. Bendriss, S. Sayah, and A. Hamouda, "Solving the Optimal Capacitor Bank Installation Problem in Radial Distribution Networks", in the National Conference on Advanced Materials for Sustainable Energy Transition (NC – AMSET2025), Medea, Algeria, June 2025.

بِسْمِ ٱللَّهِ ٱلرَّحْمَٰنِ ٱلرَّحِيمِ

"وَمَآ أُوتِيتُم مِّنَ ٱلْعِلْمِ إِلَّا قَلِيلًا"

(سورة الإسراء، الآية 85)

Abstract

Nowadays, the integration of renewable energy source-based distributed generation (RES-based DG) into radial distribution grids has increased significantly, caused by technological advancements, technical requirements, financial incentives, and ecological concerns. RES deployment remains one of the most effective and viable strategies for meeting the growing demand for electricity and reinforcing the distribution systems' performance. This integration hinges on identifying optimal locations and determining the appropriate power outputs of RES units when injected into radial distribution grids. However, this task is complicated due to the inherent stochastic nature of RES power generation, particularly from wind turbines (WTs) and solar photovoltaic (SPV) arrays, along with the fluctuations in load demand, necessitating the adoption of robust and advanced planning strategies. To this end, this thesis proposes to develop an appropriate time-varying probability load-generation model based on Weibull and Beta probability density functions (PDFs) to estimate the stochastic power output from WTs and SPV arrays, respectively. This model is based on hourly seasonal data, including wind speed, solar irradiance, and ambient temperature, collected over a specified time frame and location. An improved Frilled Lizard Optimization (IFLO) algorithm is developed and proposed for strategic RES planning, aiming to minimize total power losses, improve voltage profiles, and enhance voltage stability while adhering to operational constraints. The IFLO algorithm incorporates three advanced strategies: fitness distance balance, quasi-opposite-based learning, and Cauchy mutation, to strengthen its search capabilities and prevent convergence to local optima traps. The proposed method effectively determines the optimal locations, rated capacities of SPV strings and WTs, and the power factor of WTs. Its performance is validated through simulations on the IEEE 69-bus medium-scale and 85-bus large-scale distribution grids. Simulation results decisively demonstrate that optimal RES allocation significantly improves system performance. Furthermore, the suggested technique outperforms other recent and effective optimization algorithms, including the grey wolf optimizer (GWO), jellyfish search optimizer (JSO), black-winged kite algorithm (BKA), and the original frilled lizard optimization (FLO), in solving the optimal planning problem of RES integration under both deterministic and probabilistic scenarios.

Keywords: Renewable energy sources planning, Radial distribution grid, Probability density function, Wind turbine, Solar photovoltaic, Optimization algorithms.

Resumé

De nos jours, l'intégration des énergies renouvelables basée sur la génération distribuée (RES-based DG) dans les réseaux de distribution a considérablement augmenté, en raison des avancées technologiques, des exigences techniques, des incitations financières et des préoccupations écologiques. Le déploiement des RES constitue l'une des stratégies de planification les plus efficaces et viables pour répondre à la demande croissante d'électricité et renforcer la performance du réseau de distribution. Cette intégration repose sur la détermination des emplacements appropriés pour les RES et de leur production optimale lorsqu'ils sont injectés dans un réseau de distribution radial. Cependant, ce processus est compliqué en raison de la nature stochastique de la production d'énergie renouvelable, notamment des éoliennes et des panneaux solaires photovoltaïques, ainsi que par les fluctuations de la demande de charge, ce qui nécessite des stratégies de planification robustes et avancées. À cet effet, cette thèse propose de développer un modèle probabiliste de charge-production basé sur les fonctions de densité de probabilité de Weibull et de Beta pour estimer la production stochastique des éoliennes et des panneaux photovoltaïques, respectivement. Ce modèle repose sur des données horaires saisonnières, comprenant la vitesse du vent, l'irradiance solaire et la température ambiante, collectées sur une période et un site spécifiés. Une version améliorée de l'algorithme d'optimisation du lézard à collerette (IFLO) est développée et proposée pour la planification stratégique de l'intégration des ressources renouvelables. L'objectif est de minimiser les pertes totales d'énergie, d'améliorer les profils de tension et de renforcer la stabilité de tension tout en respectant les contraintes opérationnelles. L'algorithme IFLO intègre trois stratégies avancées : FDB, QOBL et CM pour renforcer ses capacités de recherche et empêcher la convergence vers des optima locaux. La technique proposée permet d'identifier efficacement les emplacements optimaux, les puissances nominales des chaînes de panneaux photovoltaïques et des éoliennes, ainsi que le facteur de puissance des éoliennes. La validation de l'approche est réalisée à travers des simulations sur les réseaux de distribution à moyenne et grande échelle IEEE à 69 et 85 bus respectivement. Les résultats de simulation démontrent de manière concluante que l'allocation optimale des ressources renouvelables améliore les performances du système. De plus, la technique proposée surpasse d'autres algorithmes d'optimisation récents et efficaces, tels que l'optimiseur du loup gris (GWO), l'optimiseur de recherche des méduses (JSO), l'algorithme du milan à ailes noires (BKA) et l'algorithme original du lézard à collerette (FLO), dans la résolution du problème de planification optimale de l'intégration des RES dans des scénarios déterministes et probabilistes.

Mots clés : Planification des sources renouvelable, Réseau de distribution radial, Densité de probabilité, Éolienne, Solaire photovoltaïque, Algorithmes d'optimisation.

الملخص

في الوقت الحاضر، شهد دمج التوليد الموزع المعتمد على مصادر الطاقة المتجددة في شبكات التوزيع ازديادًا ملحوظًا، نتيجةً للتطورات التكنولوجية، والمتطلبات الفنية، والحوافز المالية، والاعتبارات البيئية. ويُعد نشر مصادر الطاقة المتجددة أحد أكثر الخيارات التخطيطية فاعلية وقابلية للتطبيق لتلبية الطلب المتزايد على الكهرباء وتعزيز أداء نظام التوزيع. تعتمد هذه العملية التكاملية على تحديد المواقع المناسبة لمصادر الطاقة المتجددة وقيم الطاقة المثلى التي يتم حقنها في شبكة التوزيع الشعاعية. ومع ذلك، فإن هذه المهمة معقدة بسبب الطبيعة العشوائية المتأصلة في توليد الطاقة المتجددة، ولا سيما من توربينات الرياح ومصفوفات الخلايا الشمسية الكهروضوئية، إلى جانب التقلبات في الطلب على الأحمال، مما يستلزم تطوير استراتيجيات تخطيطية متقدمة وقوية. وفي هذا الإطار، تهدف هذه الأطروحة إلى تطوير نموذج حمل-توليد احتمالي المتغير مع الزمن يعتمد على دالتي الكثافة الاحتمالية Weibull و Beta لتقدير التوليد العشوائي للطاقة من توربينات الرياح ومصفوفات الخلايا الكهروضوئية على التوالي. ويستند هذا النموذج إلى بيانات موسمية زمنية بالساعة، تشمل سرعة الرياح، وشدة الإشعاع الشمسي، ودرجة الحرارة، تم جمعها خلال فترة زمنية وموقع محددين. كما تم تطوير خوارزمية محسّنة تُدعى "خوارزمية السحلية المزركشة المحسنة" (IFLO) وتُقترح لتخطيط دمج مصادر الطاقة المتجددة بشكل استراتيجي، بهدف تقليل فقدان الطاقة، وتحسين ملفات الجهد، وتعزيز استقرار جهد النظام، مع الالتزام بالقيود التشغيلية. وتتضمن خوارزمية IFLO ثلاث استراتيجيات متقدمة لتعزيز قدراتها البحثية ومنع انحصارها في الحلول المحلية المثلى، وهي: توازن المسافة مع الملائمة (Fitness Distance Balance)، والتعلم القائم على القيم شبه المعاكسة (Quasi-Opposite-Based Learning)، والطفرات المستندة إلى توزيع كوشي (Cauchy Mutation). تحدد التقنية المقترحة بفعالية المواقع والسعات المثلى لسلاسل الخلايا الكهروضوئية وتوربينات الرياح، وعامل القدرة الخاص بتوربينات الرياح. تم التحقق من دقة المنهجية من خلال إجراء محاكاة على شبكتي توزيع بقدرتين متوسطتين وكبيرتين، هما شبكة IEEE ذات 69 نقطة وشبكة ذات 85 نقطة. وأظهرت نتائج المحاكاة بشكل قاطع أن التخطيط الأمثل لمواقع مصادر الطاقة المتجددة يؤدي إلى تحسين أداء النظام. علاوة على ذلك، تفوقت التقنية المقترحة على عدد من خوارزميات الحديثة والفعالة الأخرى، بما في ذلك خوارزمية الذئب الرمادي (GWO)، وخوارزمية البحث لقناديل البحر (JSO)، وخوارزمية طائرالحدأة سوداء الجناحين (BKA)، بالإضافة إلى خوارزمية السحلية المزركشة الأصلية (FLO)، وذلك في حل مشكلة التخطيط الأمثل لدمج مصادر الطاقة المتجددة عبر كل من السيناريوهات الحتمية والاحتمالية.

الكلمات المفتاحية: تخطيط مصادر الطاقة المتجددة، شبكة التوزيع الشعاعية، دالة كثافة الاحتمال، التوربينات الرياح، الخلايا الكهروضوئية الشمسية، خوارزميات التحسين.

Table of contents

List of figures xv

List of tables xviii

List of abbreviations xviii

General introduction 1

1. Research objectives and contributions . . . 2
2. Thesis structure . . . 3

1 Overview of Power System and Distributed Generations 5

1.1 Introduction . . . 5
1.2 Electrical Power system topology . . . 6
1.2.1 Production . . . 7
1.2.2 Transmission . . . 7
1.2.3 Distribution grids . . . 8
1.2.4 Consumption . . . 9
1.3 Distributed Generations (DGs) . . . 9
1.4 Various forms of renewable energy-based DGs . . . 11
1.4.1 Wind energy . . . 11
1.4.1.1 Wind turbines components . . . 12
1.4.1.2 Working principle of a wind turbine . . . 13
1.4.1.3 Wind Turbine Development . . . 14
1.4.1.4 Benefits of Wind Energy . . . 15
1.4.1.5 Drawbacks of Wind Energy . . . 16
1.4.2 Photovoltaic solar energy . . . 16
1.4.2.1 Solar panels construction . . . 17
1.4.2.2 Photovoltaic effect . . . 18
1.4.2.3 Different types of photovoltaic cells . . . 19
1.4.2.4 Benefits of Solar Energy . . . 20

1.4.2.5 Drawbacks of Solar Energy . . . 21
1.4.3 Geothermal energy . . . 21
1.4.3.1 Benefits of geothermal energy . . . 21
1.4.3.2 Drawbacks of geothermal energy . . . 22
1.4.4 Hydropower . . . 22
1.4.5 Biomass energy . . . 23
1.5 Renewable energy sources integration into the distribution grids . . . 24
1.5.1 Technical benefits . . . 24
1.5.1.1 Power losses reduction . . . 24
1.5.1.2 Voltage profile and stability improvement . . . 25
1.5.2 Economical benefits . . . 26
1.5.3 Environmental benefits . . . 26
1.6 Literature review on DG integration into the distribution grid and research gaps exploration . . . 26
1.7 Conclusion . . . 31

2 Load Flow Analysis in Distribution Grids 32
2.1 Introduction . . . 32
2.2 Importance of radial distribution grids analysis . . . 33
2.3 Structure of a radial distribution grid . . . 34
2.4 Per unit system . . . 34
2.5 Power and current flowing in the branches . . . 35
2.6 Load flow solution of a radial distribution grid . . . 36
2.7 The backward/forward sweep method . . . 36
2.7.1 Initialisation . . . 37
2.7.2 Branch currents . . . 37
2.7.2.1 Load current . . . 37
2.7.2.2 Branch currents of a minor line . . . 37
2.7.2.3 Branch currents of a sub-lateral line . . . 38
2.7.2.4 Branch currents of a lateral line . . . 38
2.7.2.5 Branch currents of the main line . . . 39
2.7.3 Voltage magnitude at each bus . . . 39
2.7.4 Convergence criterion . . . 39
2.7.5 Active and reactive power losses . . . 40
2.7.6 Voltage deviation . . . 40
2.7.7 Voltage stability analysis in distribution grids . . . 41
2.8 Flowchart of the backward/forward sweep method . . . 42
2.9 Numerical applications on a radial distribution grid . . . 42

2.9.1 Test system 1: the IEEE 69-bus system . . . 44
2.9.2 Test system 2: the IEEE 85-bus system . . . 46
2.9.3 Test system 3: the actual Portuguese 94-bus system . . . 49
2.10 Conclusion . . . 52

3 Methods for Modeling Uncertainty in Power Systems 53
3.1 Introduction . . . 53
3.2 Uncertainty modeling methods . . . 54
3.3 Probability density functions . . . 56
3.3.1 Discrete probability distributions . . . 56
3.3.2 Continuous probability distributions . . . 57
3.3.3 Common types of continuous PDFs . . . 57
3.3.3.1 Gaussian (Normal) distribution . . . 59
3.3.3.2 Weibull distribution . . . 60
3.3.3.3 Beta distribution . . . 62
3.4 Modern power systems uncertainties modeling . . . 63
3.4.1 Load modeling . . . 63
3.4.2 Renewable energy resources (RESs) modeling . . . 64
3.4.2.1 Wind speed modeling . . . 64
3.4.2.2 Solar irradiance modeling . . . 65
3.4.2.3 Power generation model . . . 65
3.5 Conclusion . . . 68

4 Optimization and Metaheuristic Algorithms 69
4.1 Introduction . . . 69
4.2 Optimization process . . . 70
4.3 Formulation of the optimization problem . . . 71
4.3.1 Objective function . . . 71
4.3.2 Control parameters . . . 72
4.3.3 Constraints . . . 72
4.4 Optimization methods . . . 73
4.4.1 Conventional methods . . . 73
4.4.1.1 Analytical techniques . . . 73
4.4.1.2 Deterministic techniques . . . 73
4.4.2 Metaheuristic methods . . . 74
4.5 Various optimization algorithms . . . 74
4.5.1 Grey wolf optimization (GWO) algorithm . . . 75
4.5.1.1 Hunting strategy: Exploration phase . . . 76

4.5.1.2 Attacking strategy: exploitation phase 77
4.5.2 Jellyfish search optimizer (JSO) algorithm 78
4.5.2.1 Ocean current 79
4.5.2.2 Jellyfish swarm motions 79
4.5.3 Black-winged kite algorithm (BKA) 80
4.5.3.1 Initialization phase 81
4.5.3.2 Attacking behavior 82
4.5.3.3 Migration behavior 82
4.5.4 Frilled lizard optimization (FLO) algorithm 84
4.5.4.1 Initialization 84
4.5.4.2 Hunting Strategy: Exploration phase 85
4.5.4.3 Moving up the Tree: Exploitation phase 86
4.6 Improved Frilled Lizard Optimization (IFLO) algorithm 88
4.6.1 Fitness Distance Balance (FDB) 88
4.6.2 Quasi-Opposite-Based Learning (QOBL) 89
4.6.3 Cauchy Mutation (CM) 90
4.7 Simulation results 90
4.7.1 IFLO evaluation on standard benchmark functions 91
4.7.1.1 Analysis of the statistical results 91
4.7.1.2 Analysis of convergence curves 95
4.7.1.3 Analysing data using Boxplots 96
4.8 Conclusion 98

5 Solving the Optimal Planning Problem of Renewable Energy Sources in Distribution Grids 100
5.1 Introduction 100
5.2 RES-based DG planning without uncertainties 101
5.2.1 Problem Description 101
5.2.2 System limitations 102
5.2.2.1 Equality constraints 102
5.2.2.2 Inequality constraints 103
5.2.3 Simulation Results and Discussions 103
5.2.3.1 Scenario 1: DGs integration operating at unity-PF . . 104
5.2.3.2 Scenario 2: DGs integration operating at optimal-PF . 108
5.3 RES planning considering uncertainties 112
5.3.1 Problem description with uncertainty 112
5.3.1.1 Objective functions 112
5.3.1.2 System constraints 114

5.3.2 Data analysis 116
5.3.3 Simulation Results and Discussions 118
5.4 Conclusion 125

Conclusion and Future Work **127**

References **129**

Appendix A Load and line data **147**

Appendix B Benchmark test functions **161**

List of figures

1.1 Architecture of modern power system 6
1.2 Meshed structure of an electrical transmission network 7
1.3 Radial scheme of a distribution system 9
1.4 Hourly electricity consumption in France (Source: RTE [20]) 10
1.5 Grid-connected wind turbine 12
1.6 Inside components of a Nacelle (Source: Vestas [35]) 14
1.7 Evolution in size and height of wind turbines over time (height in feet, where 1 ft = 0.3048 m) (Source: EERE [39]) 15
1.8 Main components of grid-connected PV systems 17
1.9 Principal elements of a solar panel 18
1.10 Description of the photovoltaic effect 18
1.11 Back and front of a monocrystalline silicon cell [46] 19
1.12 Polycrystalline silicon cell [50] 20
1.13 Thin Film solar cell [50] 20
1.14 Geothermal energy principle [52] 22
1.15 Hydropower energy production principle [55] 23
1.16 Biomass power generation 23
1.17 Comprehensive DG Benefits 25

2.1 Structure of a radial distribution grid 34
2.2 Representation of a two-bus in the radial distribution grid 35
2.3 Flowchart of the load flow solution 43
2.4 Single line diagram of 69-bus distribution grid 44
2.5 Active and reactive power losses across the branches of the 69-bus distribution grid 45
2.6 Voltage profile of the 69-bus distribution grid 45
2.7 Voltage stability index values of the 69-bus distribution grid 46
2.8 Single line diagram of 85-bus distribution grid 47

2.9 Active and reactive power losses across the branches of the 85-bus distribution grid . . . 48
2.10 Voltage profile of the 85-bus distribution grid . . . 48
2.11 Voltage stability index values of the 85-bus distribution grid . . . 49
2.12 Single line diagram of the actual Portuguese 94-bus distribution grid . . . 50
2.13 Active and reactive power losses across the branches of 94-bus distribution grid . . . 50
2.14 Voltage profile of 94-bus distribution grid . . . 51
2.15 Voltage stability index values of 94-bus distribution grid . . . 51

3.1 Summary of uncertainty modeling approaches used in the literature . . . 55
3.2 Probability over an interval $[a, b]$ . . . 57
3.3 Curves of typical continuous PDFs [153] . . . 58
3.4 Gaussian PDFs with chosen values of μ and σ^2 . . . 60
3.5 Weibull PDF with chosen values of k and c . . . 61
3.6 Beta PDFs with chosen values of α and β . . . 63
3.7 Non-linear power curve of a wind turbine . . . 67

4.1 Steps for solving an optimization problem . . . 71
4.2 Local optima and global optima . . . 75
4.3 Hierarchical levels of the grey wolves [186] . . . 76
4.4 (a) Surrounding the prey, (b) Attacking the prey [186] . . . 77
4.5 Pseudo code of the GWO algorithm . . . 78
4.6 Jellyfish movements in ocean [188] . . . 79
4.7 Pseudo code of the JFO algorithm . . . 81
4.8 (a) Black-winged kites hovering in the air, waiting for attack, and (b) hovering in the air, searching for prey [189] . . . 83
4.9 Pseudo code of the BKA algorithm . . . 84
4.10 Frilled lizard taken from Pinterest . . . 85
4.11 Pseudo code of the FLO algorithm . . . 87
4.12 Pseudo code of the proposed IFLO algorithm . . . 91
4.13 Comparative convergence analysis of algorithms on benchmark functions 95
4.13 Comparative convergence analysis of algorithms on benchmark functions (continued) . . . 96
4.14 Statistical comparison of various optimizers using boxplots on test function 97
4.14 Statistical comparison of various optimizers using boxplots on test function (Continued) . . . 98

5.1 Equivalent two-bus model of the grid . . . 102

5.2 Convergence curves for single DG optimisation at Unity-PF 106
5.3 Convergence curves for two DG optimisation at Unity-PF 106
5.4 Convergence curves for three DG optimisation at Unity-PF 107
5.5 Voltage profile of RDG before and after DG integration at unity-PF . . 107
5.6 Convergence curves for one DG optimization at Optimal-PF 110
5.7 Convergence curves for two DG optimization at Optimal-PFs 110
5.8 Convergence curves for three DG optimization at Optimal-PFs 111
5.9 Voltage profile of RDG before and after DG integration at optimal-PFs 111
5.10 Seasonal hourly load profile 117
5.11 Geographical location of the studied area shown on Google Maps . . . 117
5.12 Weibull PDF of wind speed for the 22^{nd} hour of summer (for $k = 3.4217$ and $c = 9.8850$). 118
5.13 Beta PDF of solar irradiance for the 14^{th} hour of spring (for μ=0.4042 and σ= 0.1012) 118
5.14 Seasonal hourly average temperature 119
5.15 Optimization flow process for addressing the optimal planning problem of RESs into the RDG 119
5.16 Predicted hourly seasonal power generated by wind farms 122
5.17 Predicted hourly seasonal power generated by SPV farms 122
5.18 Seasonal voltage profiles for the 85-bus RDG without RESs integration 123
5.19 Seasonal voltage profiles for the 85-bus RDG in the presence of RESs . 123
5.20 Seasonal power losses for the 85-bus RDG without and with the integration of RESs 124
5.21 Minimum VSI recorded at prior and after the integration of RESs for each season and hour 124
5.22 Convergence behavior of various algorithms addressing the optimal planning problem of RESs in the 85-bus RDG 125

List of tables

1.1 Voltage classifications table 8
1.2 Classification of DG by power range and technology [24, 25] 11

3.1 Voltage-dependent load types and their corresponding exponents [165] . 64

4.1 Setting parameters of each algorithm 92
4.2 Statistical results of optimization algorithms on the benchmark functions 93
4.2 Statistical results of optimization algorithms on the benchmark functions (Continued) 94

5.1 Results of integrating 1, 2, and 3 DGs with unity power factor into the RDG 105
5.2 Results of integrating 1, 2, and 3 DGs with optimal power factor into the RDG 109
5.3 Technical Parameters of SPV and WT unit 120
5.4 Parameters values limitations 120
5.5 Optimal planning results for RESs integration into the 85-bus RDG . . 121
5.6 Fitness value comparison of algorithms 125

A.1 Bus data for 69-bus test system 147
A.1 Bus data for 69-bus test system (Continued) 148
A.2 Line data for 69-bus test system 149
A.2 Line data for 69-bus test system (Continued) 150
A.3 Bus Data for 85-Bus Test System 151
A.3 Bus Data for 85-Bus Test System (Continued) 152
A.4 Line data for 85-bus test system 153
A.4 Line data for 85-bus test system (Continued) 154
A.5 Bus Data for the actual Portuguese 94-Bus System 155
A.5 Bus Data for the actual Portuguese 94-Bus System (Continued) 156
A.5 Bus Data for the actual Portuguese 94-Bus System (Continued) 157

A.6 Line data for the actual Portuguese 94-bus system 158
A.6 Line data for the actual Portuguese 94-bus system (Continued) 159
A.6 Line data for the actual Portuguese 94-bus system (Continued) 160

B.1 Unimodal functions. 161
B.2 Multimodal functions. 161
B.3 Fixed-dimension multimodal benchmark functions. 162

List of abbreviations

RES	Renewable Energy Sources
SPV	Solar Photovoltaic
DG	Distributed Generation
BFS	Backward/Forward Sweep
WT	Wind Turbine
GWO	Grey Wolf Optimization
JSO	Jellyfish Search Optimization
FLO	Frilled Lizard Optimization
BKA	Black Winged Kite Algorithm
LV	Low Voltage
HV	High Voltage
ELV	Extra Low Voltage
HVDC	High Voltage Direct Current
IFLO	Improved Frilled Lizard Optimization
PDF	Probability Density Function
KCL	Kirchhoff's Current Law
KVL	Kirchhoff's Voltage Law
UV	Ultra Violet
FDB	Fitness Distance Balance
CM	Cauchy Mutation
QOBL	Quasi-Opposite-Based Learning
DC	Direct Current
AC	Alternating Current
toe	Tons of Oil Equivalent
IEEE	Institute of Electrical and Electronics Engineers
p.u.	per unit
VD	Voltage Deviation
VSI	Voltage Stability Index
SD	Standard Deviation

CDF	Cumulative Distribution Function
V	Variance
EERE	Energy Efficiency and Renewable Energy
WOA	Whale Optimization Algorithm
HHO	Harris Hawks optimization
DOA	Dingo Optimization Algorithm
CDO	Chernobyl Disaster Optimizer
CPU	Central Processing Unit
MATLAB	Matrix Laboratory
RAM	Random Access Memory
RDG	Radial Distribution Grid
PF	Power Factor
RST	Reliability Test System
VMPP	Voltage at Maximum Power Point
IMPP	Current at Maximum Power Point
PV	Photovoltaic
Voc	Open-Circuit Voltage
FF	Filling Factor
Isc	Short-Circuit Current
MPP	Maximum Power Point
CO_2	Carbon Dioxide
SO_2	Sulfur Dioxide
NO_x	Nitrogen Oxides
MCS	Monte Carlo Simulation
NSGA	Non Dominated Sorting Genetic Algorithm
PSO	Particle Swarm Optimization
kW	Kilowatt
kVar	Kilovolt-Amperes Reactive
PME	Point Estimate Method
EV	Electric Vehicle

General introduction

The global surge in electricity consumption has become increasingly evident due to economic development, modernization, increased household usage, improved quality of life, and the construction of new facilities to support growing populations. This trend places increasing pressure on existing power distribution systems [1]. The distribution stage is particularly significant as it bridges the transmission network and electricity consumers. These systems are primarily structured in a radial configuration with a unidirectional flow of electricity from centralized power plants to end users, making them prone to several operational challenges, including voltage drops, high power losses, difficulties in maintaining power quality, and deterioration in system stability. Such issues negatively affect the overall performance and reliability of the distribution grid [2, 3].

Traditionally, meeting the escalating electricity demand has predominantly focused on augmenting the power plant capacities through further combustion. However, this approach is neither economically efficient nor environmentally sustainable, as it relies heavily on fossil fuels [4].

The integration of renewable energy sources (RESs)-based distributed generation (DG) into radial distribution systems has become a central focus in modern power system planning and operation. RES technologies, such as wind turbines (WT) and solar photovoltaic (SPV) systems, present a sustainable alternative for meeting the increasing electricity demand and reducing fossil fuel dependency. Unlike traditional centralized power plants, RESs are cost-effective and environmentally friendly, referring to small-scale power sources placed closer to consumption points [5, 6], offering a range of benefits to the distribution grid, including the reduction of system losses, improvement of the voltage profile, enhancement of system stability, and alleviation of heavy loads. It is therefore important to improve the reliability and efficiency of the distribution grid. Besides, by curbing carbon dioxide emissions, RES-based DG units play a crucial role in addressing environmental concerns, placing them as essential components of sustainable power systems.

However, these benefits can only be achieved through a judicious and strategic integration of DG units, which entails determining appropriate locations, sizes, and power factor settings within the distribution grid [7]. Improperly located or sized DGs can negatively impact system performance, resulting in increased power losses, poor voltage profiles, system instability, reverse power flow, malfunctioning of protection devices, voltage violations at injection buses, and thermal limits in distribution lines [8, 9]. Consequently, the effective integration of RES-based DGs remains a crucial challenge for researchers and engineers, necessitating advanced optimization techniques and accurate planning.

Nonetheless, the inherent intermittent nature and unpredictability of RESs pose further challenges and complications in optimal distribution grid planning with RESs. Unlike conventional power generation, which can be reliably scheduled and dispatched, wind and solar power generation are particularly dependent on weather conditions. WTs rely on wind speed, while SPV systems are influenced by solar irradiance and ambient temperature at a specific time and geographic location. This uncertainty introduces variability and intermittency into the grid, making it difficult to ensure a stable and reliable power supply. These dependencies, coupled with fluctuations in load demand, make the proper integration of RESs into the distribution network even more complex. Effectively addressing these uncertainties requires advanced forecasting techniques, adaptive grid management strategies, and investments in grid modernization to accommodate the unique characteristics of renewable energy generation. Such measures are essential for maximizing the effectiveness of RES integration and ensuring a stable, reliable, and sustainable power system [10].

1. Research objectives and contributions

The primary objective of this thesis is to develop a methodology for the optimal planning problem of RES integration into the distribution grid, accounting for hourly fluctuations in WT and SPV power output influenced by environmental factors, including wind speed, solar irradiance, and ambient temperature, as well as time-varying load demand based on real historical collected data from the study area over a seasonal planning horizon. This modeling provides insights into the combined impact of RES generation and demand variability on grid dynamics throughout the designated time frame. A key aspect of this research is the development of a novel optimization technique to solve the optimal planning problem of RESs, specifically WTs and SPV array systems, within radial distribution grids. The proposed algorithm, termed the Improved Frilled Lizard Optimization (IFLO), integrates fitness distance balance, quasi-opposite-based learning and Cauchy mutation strategies to enhance its searching capabilities between

exploration and exploitation phases and avoid falling into local optimal traps. The suggested technique is thoroughly assessed through extensive statistical comparison against other recent and efficient meta-heuristic optimization techniques. The study aims to minimize power losses, improve the voltage profile, and enhance voltage stability through both single- and multi-objective optimization problem formulation. Accordingly, it determines the optimal location and rating capacities of SPV strings and WTs, as well as the power factor of WTs, while ensuring compliance with operational constraints across distribution grids of varying scales and complexities. To address the inherent uncertainty of the problem, we have implemented advanced forecasting techniques using Weibull and Beta probability distribution functions. Through this exhaustive approach, the research aims to enhance operational efficiency and reinforce the resilience of distribution grids with the increasing RES integration.

2. Thesis structure

The research work presented in this thesis is divided into five chapters.

Chapter 1 provides a comprehensive overview of power systems and distribution generation, emphasizing DG technologies, particularly those based on RES such as photovoltaics and wind turbines, reflecting a shift towards sustainable energy solutions driven by environmental concerns and economic incentives. Additionally, the chapter includes a thorough literature review of existing techniques and their applications in solving optimization problems for efficient DG integration, highlighting their significant implications for modern energy systems.

Chapter 2 is dedicated to studying the load flow problem in radial distribution grids, emphasizing the critical importance of determining the steady-state operating condition of the electrical power systems. The chapter introduces the backward/forward sweep method as a solution technique, recognized for its computational efficiency and robustness in addressing the distinctive topological characteristics of radial grid structures. Its performance is evaluated on the IEEE 69-bus, 85-bus, and the actual Portuguese 94-bus distribution grids, demonstrating its effectiveness in solving load flow problems for various radial configurations.

Chapter 3 presents the theoretical foundations and mathematical concepts essential for modeling uncertainty parameters in modern power systems. It focuses on the inherent uncertainty of RES with a time-varying load model. The chapter explores a range of methodologies for uncertainty modeling, including probabilistic, possibilistic, and hybrid approaches, as well as robust optimization and interval analysis. By introducing tools such as probability distribution functions based on hourly patterns,

we emphasized their role in representing uncertainty and determining optimal operating conditions.

Chapter 4 provides an overview of optimization principles and definitions, followed by an exploration of widely used nature-inspired metaheuristic algorithms for solving optimization problems, such as Grey Wolf Optimization (GWO) and Jellyfish Search Optimization (JSO), alongside two recently developed algorithms, namely, the Black-Winged Kite Algorithm (BKA) and the Frilled Lizard Optimization (FLO), all of which are proposed and implemented in this study. Furthermore, the chapter introduces the Improved Frilled Lizard Optimization (IFLO) algorithm, which integrates advanced strategies to enhance exploration and exploitation capabilities, achieving more effective solutions. The performance of IFLO is then evaluated across 23 benchmark test functions and compared against several state-of-the-art optimization algorithms to assess its competitiveness and robustness.

Chapter 5 is dedicated to presenting the results and discussion derived from the application of our proposed IFLO algorithm. The chapter examines the advantages of employing IFLO over the original FLO and several recently developed metaheuristic algorithms, including GWO, JSO, and the BKA, in addressing the optimal planning problem for RES integration. This chapter is divided into two main parts. The first part addresses a single-objective optimization problem without considering uncertainties in load or generation, focusing exclusively on minimizing active power losses within the IEEE 69-bus medium-scale distribution system. The second part involves a more complex and realistic case study applied to the IEEE 85 bus large-scale distribution system. Here, a multi-objective optimization framework is adopted, considering seasonal uncertainties in both load and generation.

Finally, a general conclusion of this research work and exploration of future perspectives are presented.

Chapter 1

Overview of Power System and Distributed Generations

1.1 Introduction

Electrical energy has become an indispensable resource worldwide, integral for daily life and the economic stability of nations. Consequently, the demand for reliable, sustainable, and cost-efficient power networks that operate efficiently, provide uninterrupted service, and maintain high energy quality is critical for fostering the growth and development of modern societies. Besides, production methods and generation technologies are expected to undergo significant changes in the coming decades.

Distribution systems are the primary interface for delivering electricity to end users, bridging the gap between high-voltage transmission networks and consumers at medium and low voltage levels. To meet the demands of a dynamic and sustainable energy future, distribution networks must evolve into flexible and intelligent infrastructures capable of seamlessly integrating local and renewable energy sources.

Over time, economic development and growing environmental concerns related to global climate change have catalyzed significant transformations in distribution networks. Originally designed to transport power unidirectionally from centralized generation to consumers. However, the increasing penetration of decentralized energy production, particularly from renewable sources within the distribution grids, has fundamentally altered this pattern. Today, distribution systems must accommodate bidirectional power flows, manage intermittent generation, and address challenges including grid stability, voltage regulation, and efficient power flow management. These evolving challenges necessitate innovative solutions to ensure that future networks can handle the dynamic needs of modern power systems while advancing sustainability goals.

This chapter opens with a comprehensive overview of the general structure of power systems, with a particular emphasis on distribution grids. It then explores various forms of decentralized generation, specifically focusing on wind turbines and solar photovoltaic systems, which will be considered in this thesis. These generation units are categorized according to their energy sources and their ability to deliver active and reactive powers, offering benefits and drawbacks of each one. The chapter concludes with an in-depth literature review of optimization techniques and the associated challenges for the optimal integration of distributed generation into distribution grids.

1.2 Electrical Power system topology

The power system is a critical infrastructure organized across various voltage levels to ensure the efficient and reliable transmission of electrical energy from generation plants to end users. A typical power system comprises interconnected components, including generation, transmission, distribution, and consumption [11]. Figure 1.1 illustrates the general architecture of a modern power system.

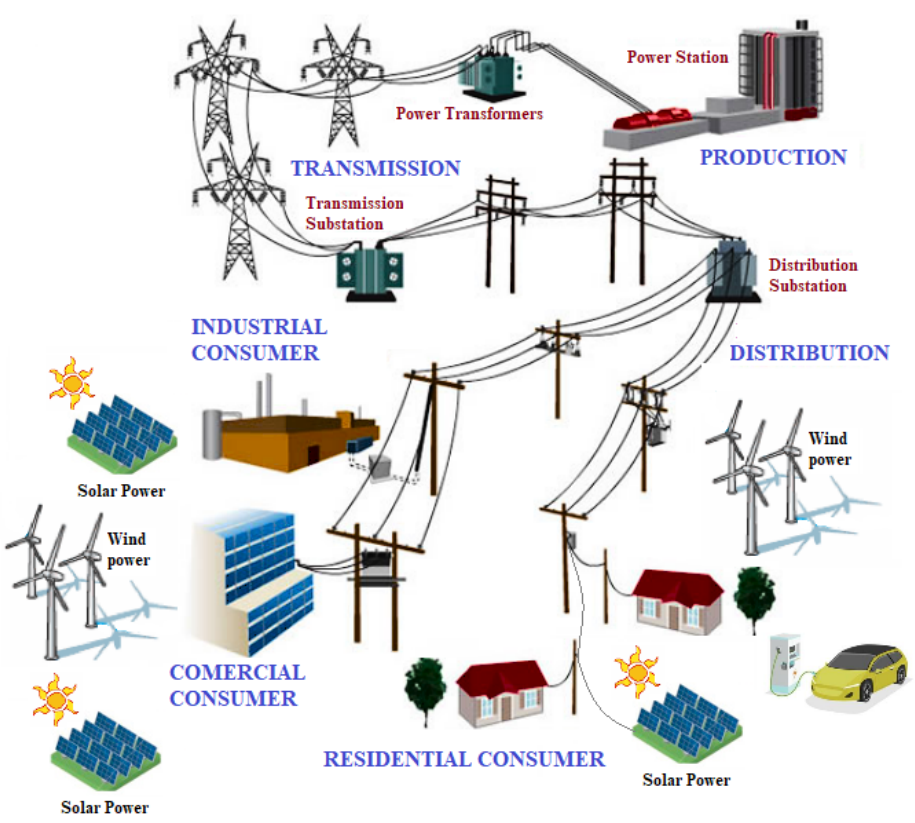

Figure 1.1: Architecture of modern power system

1.2.1 Production

Energy production relies on controllable primary sources, such as thermal power plants using fossil fuels, nuclear power plants, hydroelectric plants, and others. These power plants generally use large synchronous alternators, which convert mechanical energy into electricity through mechanically coupled turbines, driven by steam, gas, or hydraulic energy. These systems are connected to the transmission grid via a group transformer. The active power output of these units generally ranges from 100 MW for low-capacity thermal power plants to 1650 MW for the largest units of nuclear power plants [12].

1.2.2 Transmission

Transmission networks are designed to transport electrical energy over long distances, from generation centers to substations that serve distribution systems. Typically ranging from 63 kV to 400 kV in Algeria [13], the transmission networks operate at high voltage levels to minimize transmission line real losses. From a topographical perspective, transmission networks are often meshed or interconnected, as shown in Figure 1.2, to ensure safe operation. This configuration enables the aggregation of electricity produced by large power plants and efficiently transporting it to consumption areas. Additionally, interconnected systems enhance the economical and safe operation of power generation facilities by compensating for different uncertainties, ensuring reliability and flexibility across the entire grid [14].

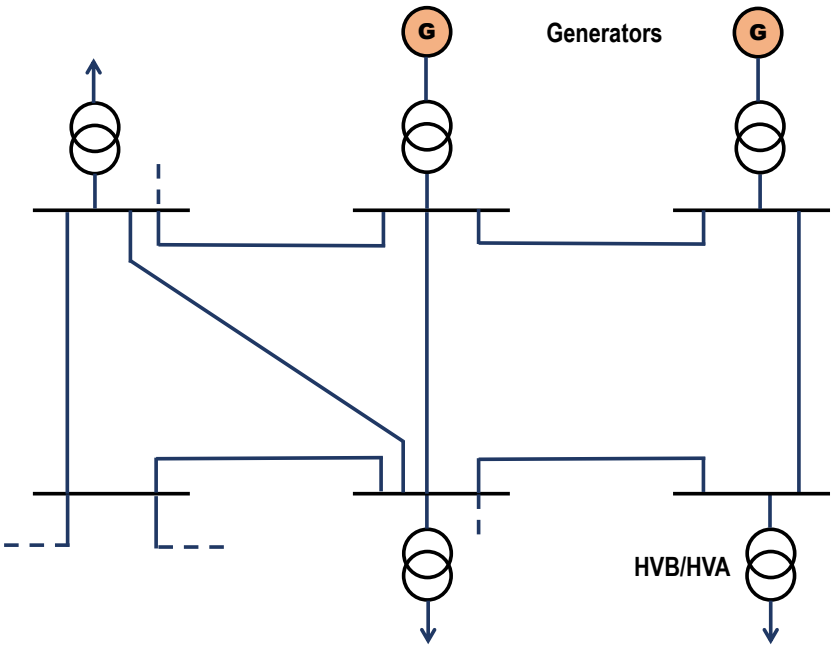

Figure 1.2: Meshed structure of an electrical transmission network

The current standards in effect in Algeria, as defined by SONELGAZ[1], classify voltage levels as follows:

Table 1.1: Voltage classifications table

Voltage Classification		**Nominal Voltage (Un in Volts)**	
		AC Voltage	**DC Voltage**
Extra Low Voltage (ELV)		$U_n \leq 50V$	$U_n \leq 120$
Low Voltage (LV)	LVA	$50 < U_n \leq 500$	$120 < U_n \leq 750$
	LVB	$500 < U_n \leq 1000$	$750 < U_n \leq 1500$
High Voltage (HV)	HVA	$1000 < U_n \leq 50\,000$	$1500 < U_n \leq 75\,000$
	HVB	$U_n > 50\,000$	$U_n > 75\,000$

1.2.3 Distribution grids

Distribution grids represent the most important substructure of an electrical system, serving as the final interface that connects the transmission network to end users. These grids operate at voltage levels below 50 kV, corresponding to the medium voltage or HVA and low voltage (LV) ranges. In Algeria, the nominal voltage level for HVA distribution grids is 10 kV and 30 kV [15]. These voltage levels provide an effective balance to limit voltage drops, minimize the number of required substation sources (HTB/HTA connection nodes), and alleviate challenges associated with high voltages, including investment costs and the protection of both properties and individuals [16].

In most cases, distribution grids operate in a radial configuration. This structure simplifies the protection system, as power flows unidirectionally from the HVB/HVA source substations to the HVA/LV substations and ultimately to end consumers, as demonstrated in Figure 1.3. This unidirectional flow facilitates rapid fault detection and isolation. Additionally, the radial structure easily ensures network maintenance and energy counting at source substations [17].

The feeders comprise single-phase, three-phase, and bi-phase busbar assemblies, enabling the interconnection of outgoing lines and transformers that step down the voltage to suitable levels for end use and secondary distribution [18]. Additionally, backup operating schemes are strategically placed between source substations to minimize the number of impacted customers during failures [19].

[1]Société Nationale de l'Électricité et du Gaz (National Company of Electricity and Gas)

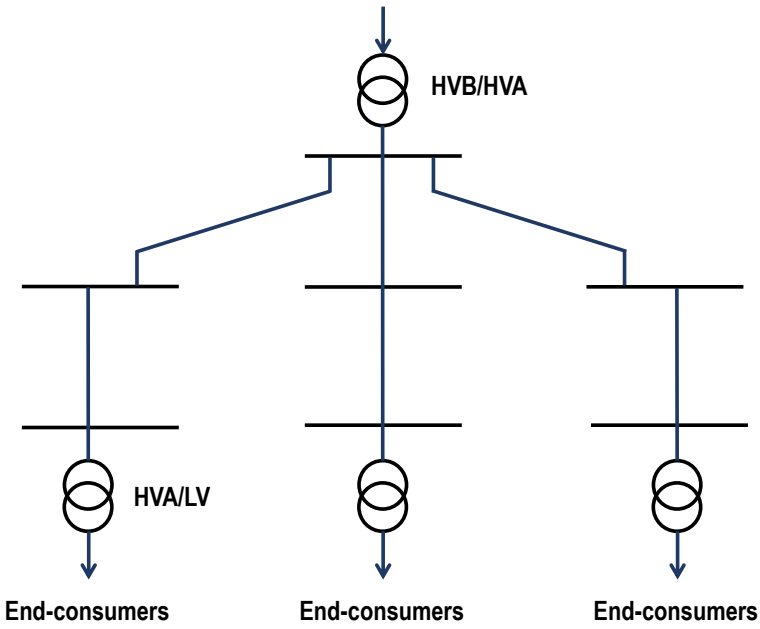

Figure 1.3: Radial scheme of a distribution system

1.2.4 Consumption

The electricity produced is primarily consumed by the three main sectors: industrial, commercial, and residential. Electricity demand, referred to as loads, is characterized by active and reactive power consumption and varies based on time, weather conditions, and economic activities, reflecting the dynamic nature of energy consumption.

Power values measured over a specific time interval are used to calculate key metrics, such as maximum (peak) power and average power. By monitoring currents at transformer stations between transmission and distribution grids, consumption curves, known as load curves, are plotted to visualize the evolution of loads over time (See Figure 1.4) [20]. These curves enable network operators to predict future consumption patterns. Such data is essential in developing production planning strategies and optimizing network management.

1.3 Distributed Generations (DGs)

Distributed power generation (DG) technology is an emerging complementary infrastructure to traditional power systems, regarded as a small-scale, decentralized production of electricity located near consumption sites. DG units are typically integrated into medium or LV grids within distribution systems [21]. These units are categorized into non-renewable and renewable DG technologies based on the type of

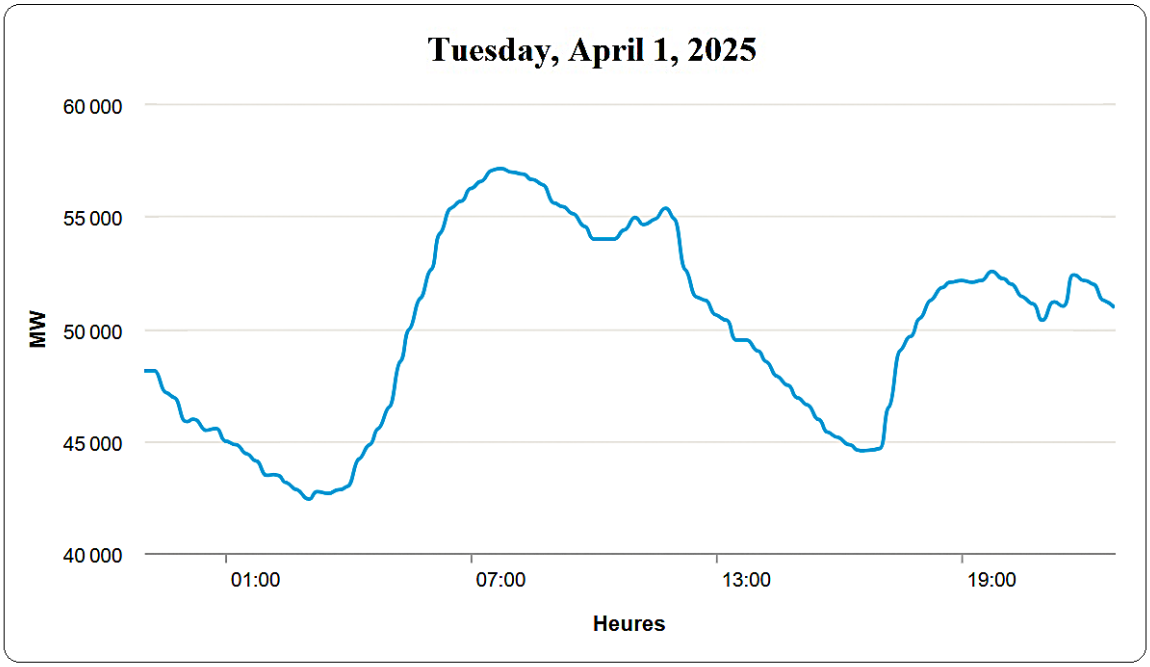

Figure 1.4: Hourly electricity consumption in France (Source: RTE [20])

energy source utilized. The former includes conventional DG technologies, such as fossil fuel-based generators, which have been widely deployed in distribution systems as backup generation or cogeneration without significant interaction with distribution networks. The latter encompasses wind, solar photovoltaic, biomass, geothermal, and hydropower generators, which are increasingly adopted in distribution grids due to environmental concerns and associated incentives such as reducing dependence on fossil fuels, making these renewable sources attractive options for distribution grids reinforcement [22].

Unlike fossil fuel-based DG technologies, which allow for power output control, the power generation from renewable DG technologies is non-controllable. Decentralized generation units differ from centralized generation units in that they are small-scale generating units, often connected to the distribution grids [11]. They can be classified based on their rated power output, which is influenced by the availability of primary energy sources, such as wind and solar irradiance. This factor plays a key role in determining suitable sites for these generators during the planning stage [23]. The power output of distributed generators ranges from a few watts to several megawatts. Table 1.2 presents DG classification according to their power output range [24, 25].

The following section provides a brief overview of renewable energy-based DGs, focusing on wind and solar photovoltaic technologies to be considered in this research.

Table 1.2: Classification of DG by power range and technology [24, 25]

Categories	Power Range	DG Technology
Micro DG	$\sim 1\,\mathrm{W} < 5\,\mathrm{kW}$	Solar PV system
Small DG	$5\,\mathrm{kW} < 5\,\mathrm{MW}$	Wind turbine, Fuel cell, Biomass...
Medium DG	$5\,\mathrm{MW} < 50\,\mathrm{MW}$	Geothermal
Large DG	$50\,\mathrm{MW} <\sim 300\,\mathrm{MW}$	Hydrogen Energy System

1.4 Various forms of renewable energy-based DGs

Renewable energy-based DGs utilize sustainable sources such as solar, wind, and hydropower to generate electricity. These sources are naturally renewable, making them an environmentally friendly alternative to conventional energy systems. However, their intermittent nature can limit consistent power output, as generation depends on resource availability and weather conditions. Despite this, renewable DGs offer significant advantages, including minimal environmental impact and a positive contribution to the overall efficiency of the power system. These systems help reduce reliance on fossil fuels, lower greenhouse gas emissions, and support more sustainable energy production [26, 27]. The following subsections offer a concise overview of wind, solar, geothermal, hydropower, and biomass energy technologies.

1.4.1 Wind energy

Wind turbine (WT) generators capture the kinetic energy of the wind and convert it into mechanical energy through the rotation of the blades. The rotational speed of the shaft, driven by the blade motion, is increased by a gearbox. This mechanical energy is then converted into electrical energy via an alternator. This energy source is increasingly popular due to its technological development and strong environmental appeal. Although investment costs are relatively high, the primary energy is free, and the environmental impact is relatively low [28].

A wind farm comprises multiple wind turbines placed several hundred meters apart, interconnected via an underground network, and integrated into the distribution grid through an interconnection substation.

Algeria, a vast territory with diverse geography and contrasting climates, holds substantial potential for renewable energy development, particularly in solar and wind power.

National political authorities recognize this potential and have been addressing the issue for several years. However, they still rely heavily on fossil fuels, especially oil, which is integral to the country's economy.

Algeria has a single wind farm located in Adrar, spanning 30 hectares, with an installed capacity of 10 megawatts (MW). This clean and renewable energy source is integrated into the electrical grid, enhancing the energy supply of Adrar Wilaya. The country plans to expand this capacity to 400 MW by 2030-2035, as part of the renewable energy program outlined by the Ministry of Energy and Mines [29].

1.4.1.1 Wind turbines components

Figure 1.5 illustrates a typical grid-connected wind turbine installation. The main components of the wind turbine are a tower, three rotor blades, and a nacelle. The essential electrical and electronic components necessary for the efficient and safe conversion of wind energy into electricity are housed within the nacelle and the tower base. These include power control systems (pitch and yaw), the generator, and power electronics [30].

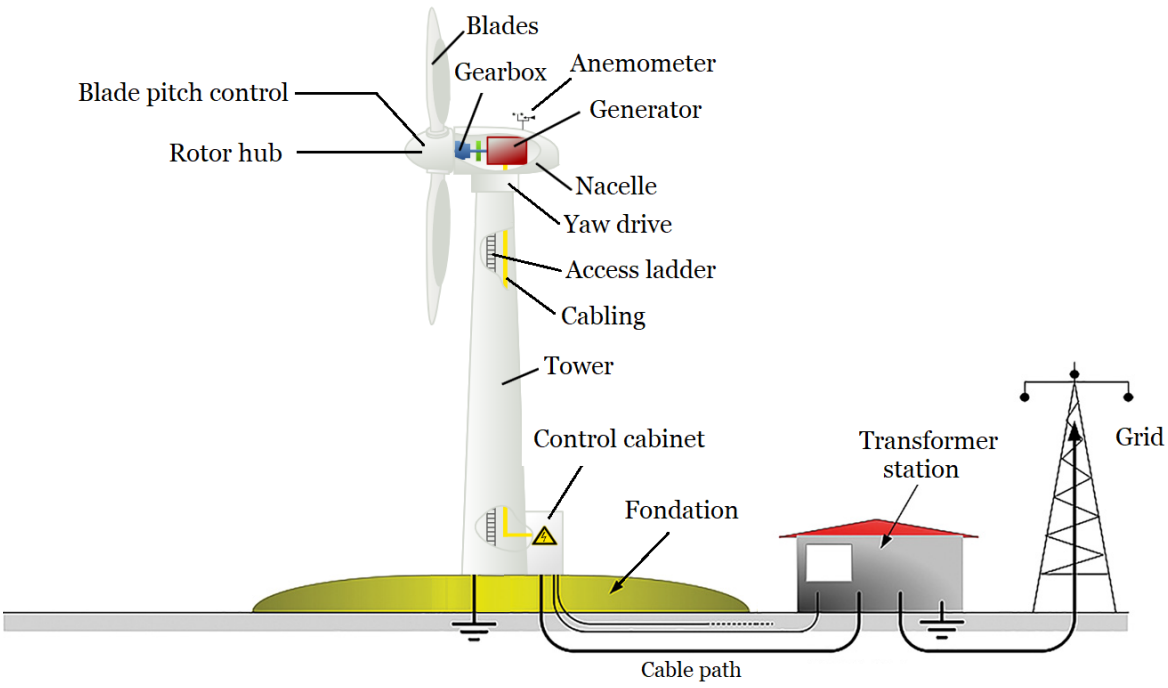

Figure 1.5: Grid-connected wind turbine

- **Tower:** Its primary role is to carry the rotor-nacelle assembly, preventing the blades from touching the ground. Additionally, it positions the rotor at an optimal height to minimize the effects of the wind gradient near the ground, thereby

enhancing energy capture. Some manufacturers offer towers of varying heights for the same rotor-nacelle assembly to better adapt to different installation sites [31, 32].

- **Rotor:** The rotor is an essential component responsible for capturing wind energy and converting it into mechanical energy. It consists of the blades and the main shaft, with the hub linking these elements. To maximize energy capture, the rotor is designed to operate at optimal speeds and angles, adjusting according to wind conditions. In modern wind turbines, the rotor is often coupled with a pitch control system that adjusts the blade angles, ensuring maximum efficiency and preventing damage from high wind speeds [33].

- **Nacelle:** The nacelle houses the key components of a wind turbine, including the gearbox, generator, and control systems. Its primary function is to support and protect these critical elements while ensuring efficient energy conversion. Additionally, the nacelle is designed to rotate in accordance to the wind direction, optimizing the rotor's alignment for maximum energy capture [34]. Figure 1.6 illustrates a cross-sectional view of a Vestas-type nacelle [35], showcasing its main components.

1.4.1.2 Working principle of a wind turbine

The process begins when the wind flows over the three rotor blades, causing them to rotate due to their aerodynamic design, with speeds between 10 and 30 rpm [36]. This blades rotation turns the main shaft, which is connected to the rotor through the hub. The mechanical energy generated by the rotor's motion is transmitted through the low-speed shaft to a gearbox, which amplifies the rotational speed, transferring it to the high-speed shaft to match the generator's operating speed at 1500 rpm [37]. The generator then converts this mechanical energy into electrical energy through electromagnetic induction, delivering alternating current. The current intensity varies with wind speed; as wind speed increases, the lift on the rotor increases, resulting in increasing power generation by the generator [36]. When the wind reaches the rated speed, determined by the manufacturer and depending on the wind turbine's type and size, the turbine operates at its rated power.

Modern wind turbines often include a pitch control system, which adjusts the angle of the blades using the hydraulic unit to optimize their efficiency based on wind speed. Additionally, a yaw control system enables the nacelle to rotate horizontally and continuously align with the wind direction, guided by the wind measurement system placed at the rear of the nacelle. In high wind speed conditions, the rotor spins freely,

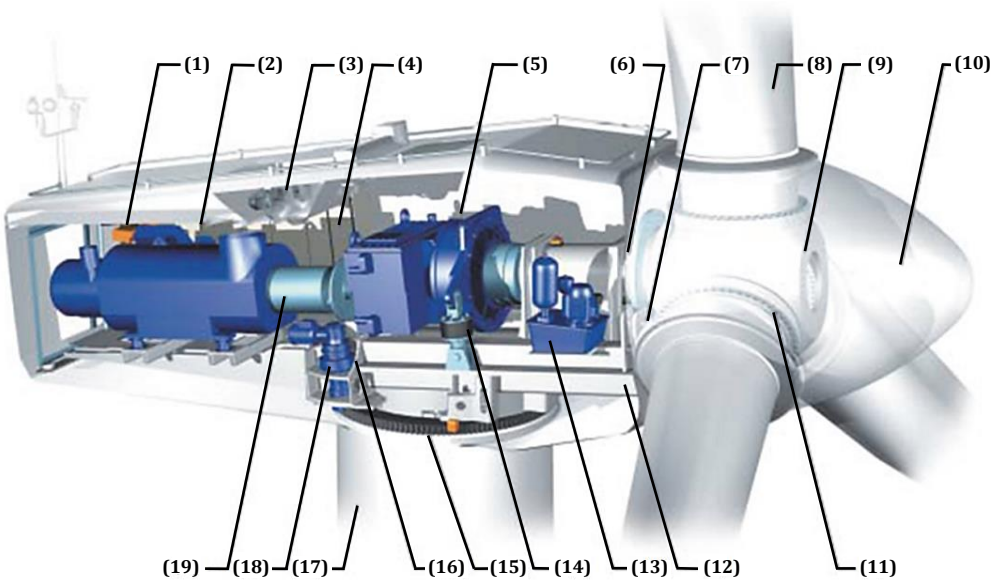

(1): Service crane	(8): Blade	(14): Shock absorbers
(2): Generator	(9): Hub	(15): Yaw ring
(3): Cooling system	(10): Hub cover	(16): Brake
(4): Top control unit	(11): Blade bearing	(17): Tower
(5): Gearbox	(12): Bed frame	(18): Yaw gears
(6): Main shaft with two bearing	(13): Hydraulic unit	(19): Transmission high speed shaft
(7): Rotor lock system		

Figure 1.6: Inside components of a Nacelle (Source: Vestas [35])

causing the wind turbine to stop producing electricity to ensure equipment safety and minimize wear. Once the wind speed decreases, the wind turbine automatically resumes operation. All these processes are fully automated and managed by a computer. In case of an emergency shutdown, a brake system on the high-speed shaft is operated to ensure the turbine's safety [36–38].

From an electrical engineering point of view, wind turbines are nothing more than electricity-generating power plants, similar to hydroelectric or diesel-powered systems. They must meet standard conditions for grid-connected systems, ensuring safety, supervision, and power quality.

1.4.1.3 Wind Turbine Development

Wind power generators have experienced substantial advancements over the years. Manufacturers have continuously scaled up wind turbines for both onshore and offshore applications, as larger turbine sizes have led to enhanced performance and reduced

costs. By capturing more energy from the wind, these advancements aim to make wind-generated electricity quite economical in more regions.

By 2035, the capacity of a single offshore wind turbine is projected to reach a maximum of 20 MW, further reinforcing the trend of increasing turbine power and dimensions. This trend is illustrated in Figure 1.7 [39], which shows the correlation between the increase in turbine size and power generation.

Future wind turbine development will not only focus on increasing power capacity but also on critical design improvements. These include advancements in rotor blade aerodynamics, wind farm operational management, and maintenance and fault diagnosis systems. Such refinements are intended to optimize wind farm efficiency, reliability, and availability [40, 41].

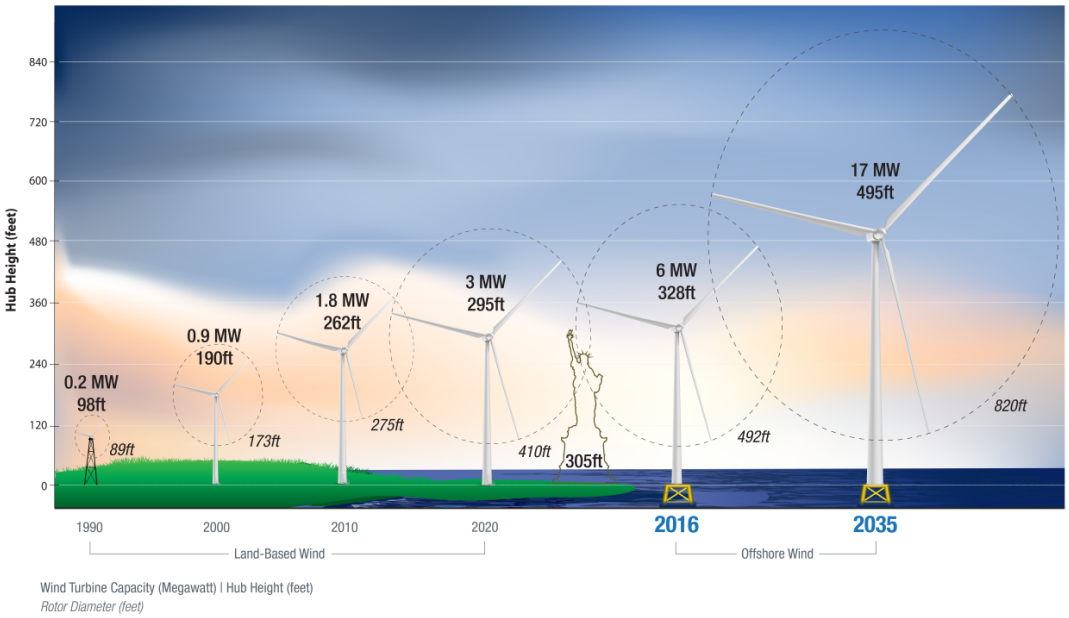

Figure 1.7: Evolution in size and height of wind turbines over time (height in feet, where 1 ft = 0.3048 m) (Source: EERE [39])

1.4.1.4 Benefits of Wind Energy

Wind energy offers numerous benefits:

- ✓ Wind energy is a limitless resource that reduces reliance on fossil fuels, providing a sustainable energy solution.
- ✓ It is environmentally friendly, producing no emissions, which significantly helps reduce pollution.

- ✓ Wind energy systems have low operational and maintenance costs.
- ✓ Wind turbines can potentially export reactive power for network support.
- ✓ Wind energy projects contribute to stimulating the local economy by creating job opportunities and driving infrastructure development.

1.4.1.5 Drawbacks of Wind Energy

The main drawbacks of wind energy are:

- ✓ Intermittent power generation
- ✓ The noise from turbines can be disruptive.
- ✓ Although operational costs are low, installation can be expensive.
- ✓ Large wind farms require substantial land
- ✓ Wind turbines are most effective in regions with sufficient wind

1.4.2 Photovoltaic solar energy

Solar energy is the most widely used renewable resource, recognized for its abundance and extensive deployment. Photovoltaic (PV) panels directly capture solar radiation and convert it into electricity through the properties of semiconductor materials. It consists of cells arranged in an array, which may be fixed or equipped with a tracking system to optimize solar capture and maximize power generation. These systems produce direct current (DC), which is converted into alternating current (AC) using inverters, and can operate with or without energy storage depending on the desired application [42]. Figure 1.8 illustrates the main components of a grid-connected PV system.

The global evolution towards sustainable energy has led numerous countries to increase the prioritization of solar power. Large-scale solar power plants are currently under development across the world. In Algeria, the national electricity company, SONELGAZ, offers financial incentives to encourage property owners to invest in solar energy.

Various studies on Algeria's solar energy potential reveal its vast capacity for exploitation and development. Indeed, Algeria, with an area of over two million square kilometers, receives approximately 300 billion tons of oil equivalent (toe) per year in solar energy. In terms of solar irradiation, the energy received daily on a horizontal surface of 1 m^2 is around 5 kWh across almost the entire national territory [43, 44].

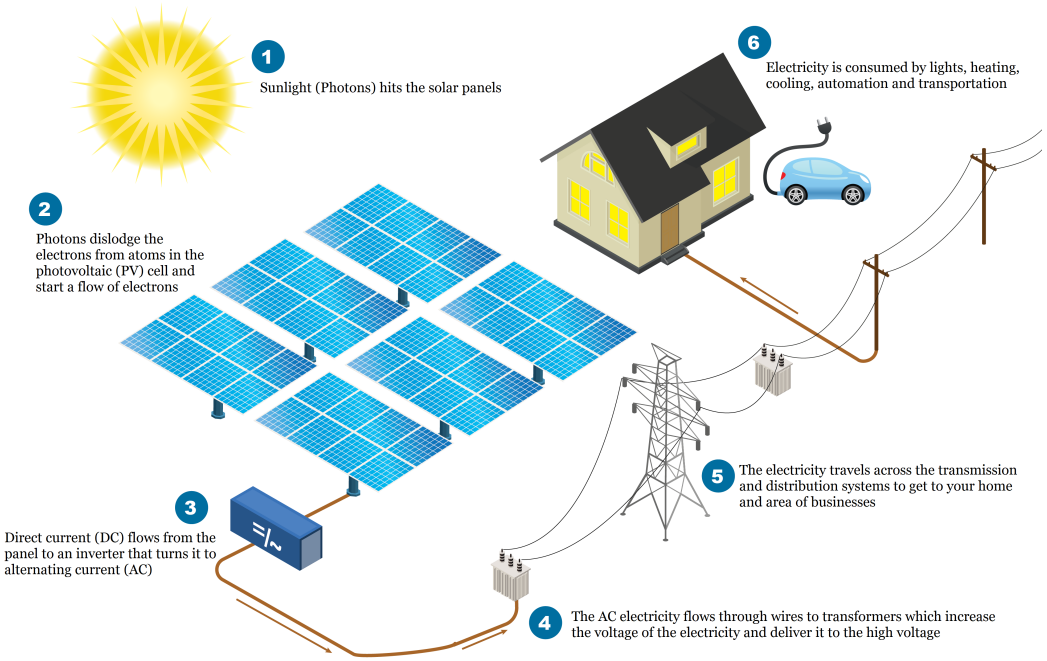

Figure 1.8: Main components of grid-connected PV systems

Algeria has made significant strides in solar energy development since the inauguration of its first solar power plant in 2011. As of 2023, the country operates around 24 large-scale solar power plants connected to the main grid, with a total installed capacity of 437 MW. Furthermore, plans are in place to expand this capacity to 4 GW by 2025 through major projects launched in 2023.

1.4.2.1 Solar panels construction

The construction of solar panels is concentrated on optimizing efficiency, durability, and adaptability to various environmental conditions. While advancements in photovoltaic technology have improved performance, the fundamental design of solar panels has remained largely unchanged. Most solar panels consist of a structured assembly of photovoltaic cells, typically made from crystalline silicon, encapsulated between protective layers. These layers include a transparent glass cover at the front and a polymer back sheet at the rear, all enclosed within an aluminum frame (see Figure 1.9) [45].

Once installed, solar panels must endure diverse and often extreme environmental conditions throughout their operational lifespan, which typically exceeds 25 years. They are continuously exposed to fluctuating temperatures, humidity, wind loads, and Ultraviolet (UV) radiation, all of which can degrade panel materials over time. Despite being engineered for durability, solar panels may still experience structural

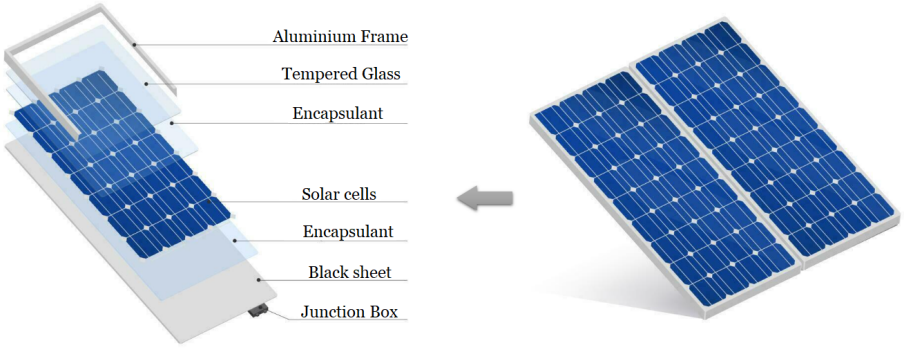

Figure 1.9: Principal elements of a solar panel

and electrical failures, such as cell micro-cracks, water ingress, and delamination of protective layers. To ensure long-term performance, manufacturers emphasize the use of high-quality materials and advanced encapsulation techniques that enhance resistance to environmental stressors.

1.4.2.2 Photovoltaic effect

The photovoltaic effect is the fundamental physical process that directly converts sunlight into electricity by generating and transporting positive and negative electric charges within a semiconductor material, as depicted in Figure 1.10.

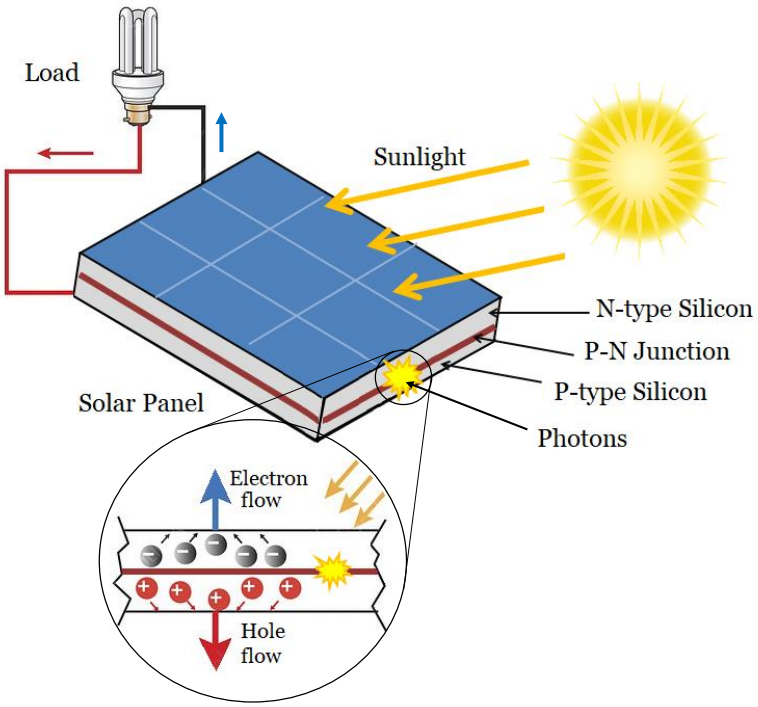

Figure 1.10: Description of the photovoltaic effect

A solar cell is typically made from silicon, which is composed of two layers: an N-type silicon layer, which has an excess of free electrons, and a P-type silicon layer, which has an abundance of holes (electron deficiencies), that are joined together to create a P-N junction. When photons from solar radiation strike the semiconductor, their energy excites electrons, driving the excess electrons from the N-type silicon to diffuse into the P-type silicon. Consequently, the initially N-doped region acquires a positive charge, while the initially P-doped region becomes negatively charged. This charge separation creates a potential difference, allowing electrons to flow through an external circuit, producing direct current (DC) electricity [46, 47].

1.4.2.3 Different types of photovoltaic cells

There are various types of solar cells, also known as photovoltaic cells, each distinguished by its efficiency and cost. However, regardless of the type, their energy conversion efficiency remains relatively low, typically between 8% and 23%. Currently, three main technologies of photovoltaic cells exist [46]:

- **Monocrystalline silicon cell:** Monocrystalline cells are the first commercially available solar cells, fabricated from a block of silicon crystallized into a single crystal (see Figure 1.11). To fabricate these, a seed crystal is drawn from a mass of molten silicon, forming a cylindrical ingot with a single, continuous crystal lattice structure. This ingot is then mechanically sliced into thin wafers (silicon slices). After applying an anti-reflective coating and adding the front and rear metal contacts, the cell is wired and packaged with many others into a complete solar panel [48, 49]. Monocrystalline silicon cells are highly efficient, but their manufacturing process is slow and energy-intensive, making them more expensive than their polycrystalline or thin-film counterparts [50].

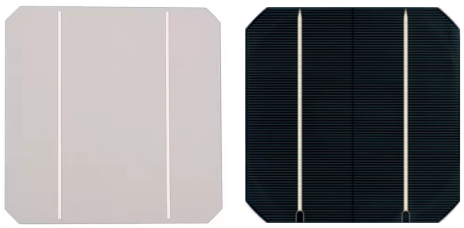

Figure 1.11: Back and front of a monocrystalline silicon cell [46]

- **Polycrystalline silicon cell:** Polycrystalline (or multi-crystalline) cells consist of multiple small crystal grains, rather than a single uniform crystal structure (see Figure 1.12). They are typically made by casting a cube-shaped ingot from molten silicon, which is then sawed and packaged similarly to monocrystalline

cells. A key advantage of polycrystalline cells over monocrystalline silicon is that they are less expensive to produce and require 2 to 3 times less energy during manufacturing [49, 50].

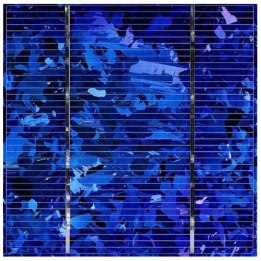

Figure 1.12: Polycrystalline silicon cell [50]

- **Thin film cells:** Thin-film solar cells are made by depositing thin layers of semiconductor materials onto substrates such as glass or plastic. Amorphous silicon (a-Si) is a common material used, requiring less than 1% of the silicon needed for crystalline cells. While cheaper to produce and less energy intensive, these cells have lower efficiency due to less ordered atomic structures and experience a 20% drop in efficiency early on. Thin-film cells are lightweight, flexible, and cost-effective, with ongoing improvements enhancing their performance and broadening their applications (see Figure 1.13) [50].

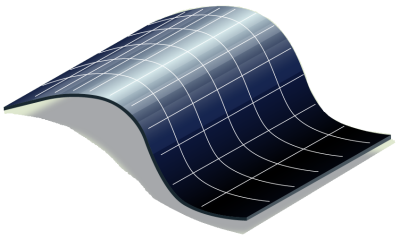

Figure 1.13: Thin Film solar cell [50]

1.4.2.4 Benefits of Solar Energy

The use of solar energy offers several benefits. It belongs to the large family of renewable energies. The electricity it generates has no environmental impact and does not require raw materials. Other benefits include:

- ✓ Panels can be installed on various surfaces, such as walls or roofs.
- ✓ Reliable and abundant, as the sun is an unlimited energy source.
- ✓ Operates silently, making it ideal for residential and urban use.

- ✓ Practical and cost-free, as it generates electricity even in remote areas.
- ✓ No fuel costs, as power is directly derived from sunlight.
- ✓ Designed to withstand harsh weather conditions, requiring minimal maintenance.
- ✓ Surplus electricity can be sold to offset the initial investment in the long term.

1.4.2.5 Drawbacks of Solar Energy

Although solar energy provides many benefits, there are some drawbacks to consider:

- ✓ The upfront investment in solar panels and related equipment can be expensive due to high initial installation costs.
- ✓ Solar energy is weather-dependent, intermittent, and unavailable at night.
- ✓ Large installations may require significant space, which could be a limitation in urban areas.
- ✓ Limitation of suitable locations depending on sunlight availability.
- ✓ Low efficiency
- ✓ Storing solar energy for use at night or during cloudy days requires additional equipment like batteries, which can be costly

1.4.3 Geothermal energy

Geothermal power plants harness the heat from underground water reservoirs, which can reach temperatures of up to 350°C in optimal locations, to generate electricity or provide direct heating. Hot water is pumped to the surface and passed through heat exchangers. The resulting steam drives a turbine connected to a generator, producing electrical energy, as illustrated in Figure 1.14. Dry rock extraction technology is also used, where cold water is injected into deep rock layers, heated by the Earth's heat, and then brought back to the surface as hot water [51, 52].

1.4.3.1 Benefits of geothermal energy

Geothermal energy offers several benefits, including being a renewable and sustainable energy source with no greenhouse gas emissions, making it environmentally friendly. It provides a reliable and consistent power supply, as geothermal systems are independent of weather conditions such as rain, sun, or wind, unlike some other renewable sources such as solar or wind energy. Additionally, it requires a small land area and can be used for both electricity generation and direct heating applications.

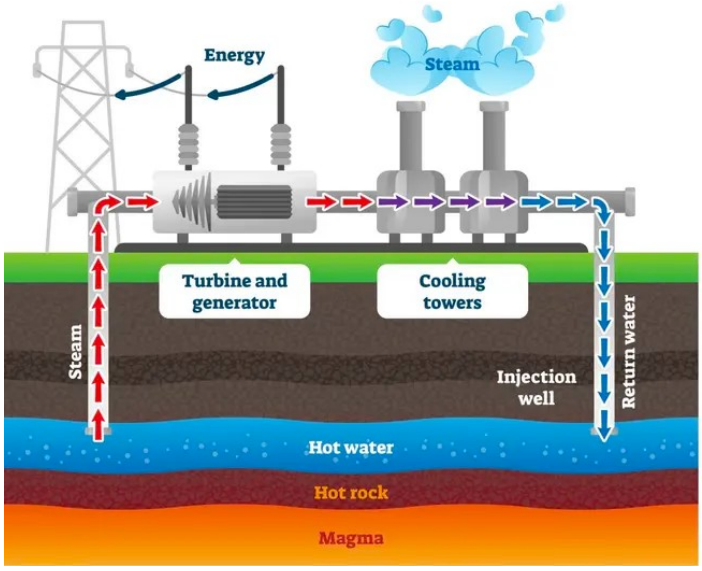

Figure 1.14: Geothermal energy principle [52]

1.4.3.2 Drawbacks of geothermal energy

The drawbacks include high initial costs for installation and drilling, specific location feasibility, and the potential for localized environmental impacts, such as land subsidence or the release of toxic gases from deep reservoirs. Furthermore, geothermal energy may not be feasible in areas where geothermal resources are not abundant or accessible.

1.4.4 Hydropower

Hydropower, or hydroelectric power, is one of the oldest and most widely used renewable energy sources. It is based on the potential and kinetic energy of water from rivers, lakes, or streams to drive a turbine, which then rotates a generator, converting mechanical energy into electrical energy (see Figure 1.15). The power generation of hydroelectric plants depends on the turbine flow rate and the available head height [53, 54].

Hydropower is one of the most cost-effective methods of electricity production, consuming no water or fuel. The water passing through the turbine remains unaffected and available for other uses, with no emissions produced. The lifespan of a hydroelectric plant is long, with some operating for over 100 years. Additionally, they contribute to water management by supporting irrigation and flood control. However, hydropower has some drawbacks, such as high initial construction costs, environmental impacts on aquatic ecosystems, and the displacement of communities due to dam construction. Furthermore, its efficiency depends on water availability, which can be affected by climate change and seasonal variations [53, 55].

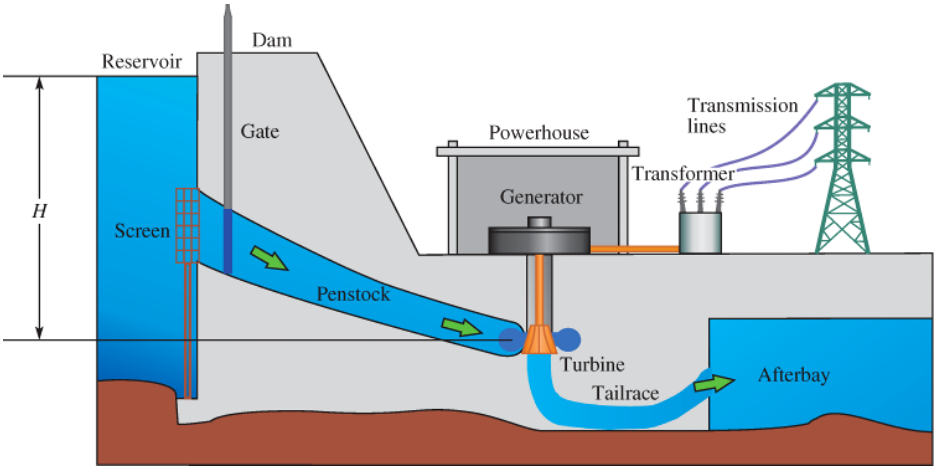

Figure 1.15: Hydropower energy production principle [55]

1.4.5 Biomass energy

Biomass energy is a form of renewable energy derived from organic materials, including wood, agricultural residues, animal waste, and industrial and domestic organic waste. These resources are converted into electrical energy through combustion, anaerobic fermentation, or chemical synthesis (Figure 1.16) [55]. It plays a significant role in the global transition to cleaner, more sustainable energy systems. This technology is increasingly used in rural areas.

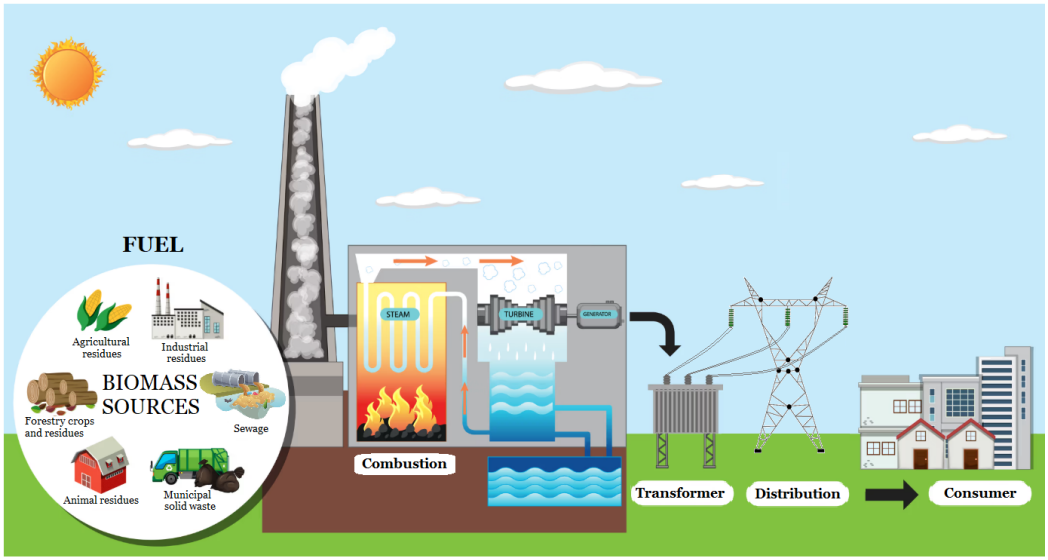

Figure 1.16: Biomass power generation

Biomass energy offers numerous benefits. On a global scale, it contributes to solid waste management while reducing a country's dependence on fossil fuels by converting organic materials into various energy forms [56]. For individuals, biomass energy

is a profitable and economically advantageous energy source due to its widespread availability and renewable nature when managed sustainably [57]. Additionally, this energy source generates low greenhouse gas emissions, making it an attractive option for waste management and energy production simultaneously.

Biomass is part of a shorter carbon cycle, meaning the carbon dioxide emitted during bio-energy combustion is reabsorbed by growing plants through photosynthesis, maintaining a balanced atmospheric carbon exchange [58].

The main drawback of biomass energy is its low energy efficiency. Additionally, excessive reliance on biomass can result in adverse environmental effects, including deforestation, soil erosion, and pollution [57].

1.5 Renewable energy sources integration into the distribution grids

In recent years, the integration of renewable energy sources (RESs) based-DG into distribution grids has been seen as an effective strategy in distribution system planning to meet the increasing electricity demand while enhancing the operational grid performance. RESs are cost-effective and environmentally friendly, referring to small-scale electricity generation placed near the end consumers [5, 6]. Integrating RESs at strategic locations and optimal sizes within the RDG offers numerous benefits, including reduced power losses, improved voltage profile, enhanced system stability, lower carbon emissions, load alleviation, and overall improvements in system reliability and efficiency. However, improper placement and sizing of DGs can negatively impact system performance, such as increased power losses, poor voltage profiles, system instability, reverse power flow, and improper functioning of protection devices [7, 8, 59]. Therefore, effectively integrating RESs into RDGs presents a crucial challenge for many researchers and engineers.

Generally, these benefits can be categorized into three main domains: technical, economic, and environmental [60], as summarized in Figure 1.17.

1.5.1 Technical benefits

1.5.1.1 Power losses reduction

Unlike transmission networks, distribution systems are characterized by a high resistance to reactance (R/X) ratio and significant voltage drops that could cause considerable power losses along the feeders. Studies have reported that approximately 13% of the total power generated is dissipated as line losses at the distribution level [61].

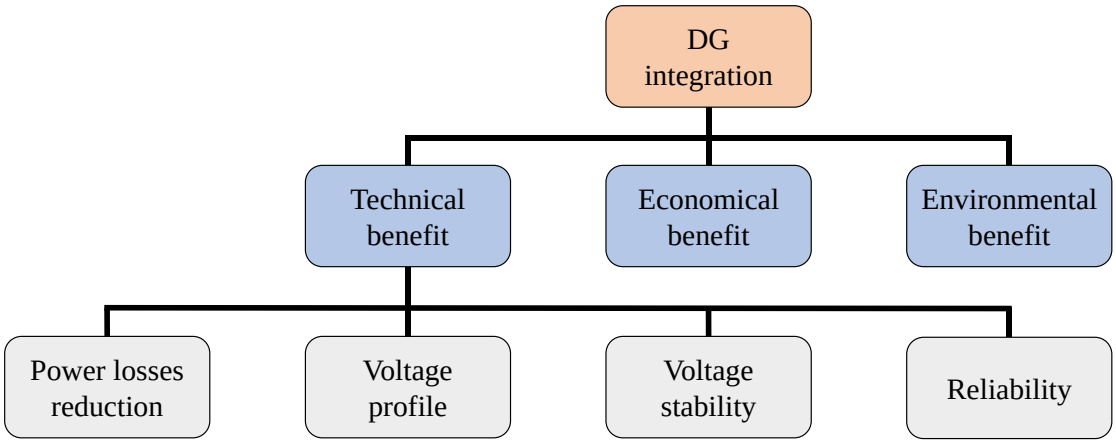

Figure 1.17: Comprehensive DG Benefits

Consequently, minimizing these losses remains a significant challenge for power distribution utilities worldwide. The impact of DG integration on system power losses is considered one of the important aspects of the planning stage. According to the literature, the optimal location and size of DG units are crucial factors in mitigating electrical losses. Properly integrated DG can significantly reduce these losses, whereas sub-optimal planning may lead to excessive power losses. Various researchers have proposed different methodologies to address the optimal planning problem of DG within radial distribution grids to minimize power losses, formulating it as the main objective function. In this regard, it has been assumed that the sum of total losses at all branches could represent network losses. While most studies have focused on minimizing total active power losses in distribution grids [62, 63], some have extended their scope to consider daily, monthly, and annual energy losses as objective functions [64, 65].

1.5.1.2 Voltage profile and stability improvement

The voltage profile in distribution grids, closely associated with power quality, is usually a secondary concern compared to energy losses from the utility viewpoint. However, the increasing penetration of intermittent renewable-based DG has attracted greater interest in maintaining a stable and reliable voltage profile at the distribution stage [66]. On the other hand, voltage stability, once mostly studied considerably at the transmission level [67], has become a recognized challenge in distribution systems, especially under heavily loaded system conditions with insufficient reactive power support. To mitigate such risks, recent studies emphasize the optimal placement and sizing of DG units can significantly enhance the voltage profile and system stability.

Some researchers focused solely on improving the voltage profile [5, 68, 69] or voltage stability [5, 69, 70] as a primary objective. However, most have aimed to minimize losses while improving the voltage profile and stability [3, 71, 72].

1.5.2 Economical benefits

The integration of DGs into distribution grids offers significant economic benefits, primarily through the reduction of power losses, which decreases energy costs. By generating electricity closer to consumption points, DG minimizes transmission and distribution costs while enhancing system efficiency. Additionally, DG integration can defer or eliminate the need for costly infrastructure upgrades, such as new substations or line reinforcements to accommodate increasing loads [72]. Moreover, the use of renewable energy-based DG units reduces fuel costs associated with conventional power generation. Industries may install their own DG units to partially meet their energy demands, reducing purchases from the grid [73, 74].

1.5.3 Environmental benefits

Utilizing renewable energy sources such as solar, wind, and biomass significantly reduces greenhouse gas emissions. According to published literature, approximately 80% of global pollution is attributed to the combustion of fossil fuels [24]. Numerous studies have confirmed that RES-based DG can reduce carbon emissions by approximately 40% [73]. The integration of DG reduces dependence on fossil-fuel-based power plants, thereby decreasing emissions of carbon dioxide (CO_2), sulfur dioxide (SO_2), and nitrogen oxides (NO_x) that result from the burning of fossil fuels in centralized power plants [75]. Ultimately, DG systems are environmentally friendly as they involve renewable energy resources in production. The widespread adoption of DG supports the transition to cleaner and more sustainable energy systems [72].

1.6 Literature review on DG integration into the distribution grid and research gaps exploration

Over the years, extensive research efforts have been conducted to address the optimal planning problem of distributed generations in radial distribution grids. These studies have explored diverse techniques, including analytical, heuristic, and meta-heuristic approaches. Early studies employed analytical methods [76–79], which, although their simplicity and computational efficiency, face significant challenges when applied to

complex problems involving numerous control variables or large search spaces. In recent decades, meta-heuristic methods have gained substantial research interest due to their effectiveness in solving complex real-world engineering problems that are often intractable using traditional approaches.

This review explores various optimization methodologies proposed in the academic literature to address the optimal planning problem of DGs in radial distribution grids, each considering specific objectives, either as a single or multi-objective problem formulation. These techniques include the equilibrium optimizer algorithm [80], the genetic algorithm [81], the jellyfish search optimizer [82], the whale optimization algorithm [83], the manta ray foraging optimization [63], the adaptive particle swarm optimization [62], and the improved wild horse optimization algorithm [84], to determine the optimal size and placement of DGs for minimizing power losses. In addition, the coyote optimization algorithm [85] has been applied to find the best site and size of DG units to reduce power loss, lower operating costs, and improve voltage stability. The arithmetic optimization algorithm [86], the artificial bee colony algorithm [3], the modified gravitational search algorithm [87], and the chimp sine cosine algorithm [88] were also implemented to identify the best site and location of DG units for reducing power losses and elevating the voltage profile. Further, methods like the improved golden jackal optimization [89], the quasi-oppositional chaotic symbiotic organisms search algorithm [5], the water flow optimization [90], the grey wolf optimization [91], the spider monkey optimization [92], and the electric eel foraging optimization [93] were applied to identify the optimal size and site of DG units to balance power loss reduction and voltage stability enhancement.

Regarding multi-objective approaches, an efficient multi-objective optimization technique was proposed in [72] to integrate wind turbines and solar photovoltaic arrays optimally into the IEEE 69-bus and real Portuguese 94-bus radial distribution grids. A multi-objective slime mold algorithm [94] was also introduced for solar resource allocation, aiming to achieve optimal voltage profile, minimize losses, and maximize renewable energy penetration levels. Moreover, the spider wasp optimization algorithm, presented in [95], was designed to solve the optimal power flow problem by balancing exploration and exploitation. Its multi-objective version leverages the Pareto concept and fuzzy membership functions to optimize fuel costs, emissions, and power losses, showing superior performance on IEEE 30 57- and 118-bus systems. The authors of [96] employed the competitive swarm optimizer to optimize DG and shunt capacitor placement on the IEEE-34 bus radial distribution grid, minimizing power loss, voltage deviation, and operating costs. In [97], the Osprey optimization algorithm was proposed to optimally site and size multiple DGs in radial distribution networks, minimizing

power losses and improving voltage stability. Additionally, the authors of [98] proposed a Lévy flight genetic algorithm for optimizing the placement and sizing of solar PV (SPV)-based DG in radial distribution grids. The approach improves voltage profiles, reduces active power loss, and minimizes energy loss costs, validated on the IEEE 33-bus system and a residential feeder in Nigeria. In [99], the authors developed a multi-objective energy management system for a multi-microgrid system using the multi-objective multi-version optimizer, achieving superior cost savings, reduced power losses, and optimal DG utilization. The authors of [100] developed a master-slave optimization framework for optimally integrating SPV systems into distribution grids using Multi-Objective Particle Swarm Optimization (MOPSO), Non-Dominated Sorting Genetic Algorithm 2 (NSGA-II), and a multi-objective ant lion optimizer. The three algorithms were implemented on 33- and 27-bus feeders. NSGA-II achieved the best performance in reducing energy losses and cutting operating costs. Also, a memory-based artificial gorilla troops optimizer [101] and zebra optimization algorithm [102] are presented to minimize grid power loss and enhance voltage profiles.

All the above mentioned studies have focused on addressing the DG sizing and location problem by considering peak load conditions. Additionally, the uncertainties associated with renewable sources have been overlooked. In contrast, other studies have addressed the integration of renewable energy sources, accounting for their intermittent nature and the variability of load demands within the distribution grid from multiple perspectives. For example, Kayal and Chanda [103] focused on optimizing the locations and capacities of mixed solar and wind energy sources in an Indian rural 28-bus distribution grid using the weighted aggregation particle swarm optimization algorithm to reduce power losses, enhance voltage stability, and improve network security while considering solar irradiance and wind speed uncertainties. Hemeida et al. [63] presented a methodology for optimizing DG placement in power systems considering load uncertainties. The approach utilizes Monte Carlo simulation to generate various load scenarios, employing four bio-inspired optimization techniques: grey wolf optimization, manta ray foraging optimization, satin bowerbird optimization, and whale optimization algorithm. The objective was to minimize active power loss, voltage deviation, and maximize the voltage stability index. In [104], the authors suggested a strategy for allocating SPV and battery energy storage systems using a modified Henry gas solubility optimization algorithm to minimize total system power loss, considering SPV generation uncertainties and time-varying loads. In [105], the authors introduced a genetic algorithm-based approach for optimizing capacitor banks and distributed SPV generation in unbalanced distribution grids, incorporating sensitivity analysis to identify optimal zones for SPV and capacitor placement while addressing load and

SPV generation uncertainties over a 24-hour planning horizon. Khasanov et al. [106] proposed an artificial ecosystem-based optimization with opposition-based learning to optimize the placement of SPV and WT-based DGs in IEEE 33-bus and 85-bus RDGs. The improved algorithm integrates five strategies to enhance search capability, balancing exploration and exploitation phases, effectively minimizing system power losses while addressing the stochastic nature of RESs. In [107], the rider optimization algorithm has been proposed to identify the optimal size and site of RES, specifically WTs, SPVs, and biomass-based DG units in standard 33 and 69-bus distribution grids. The study aimed to minimize total energy losses while considering wind speed and solar irradiation fluctuations. Ramadan et al. [108] employed the artificial hummingbird algorithm for optimal RES sizing and placement in IEEE 33-bus and real 94-bus RDGs, effectively minimizing costs, emissions, and voltage deviations while improving voltage stability under uncertainty. A pseudo-inspired gravitational search algorithm is introduced in [109] as a novel approach to optimize RESs allocation and sizing in IEEE 15-bus, 33-bus, and 69-bus distribution grids, considering SPV and wind output uncertainties, electricity prices, and load variations using probability distribution functions. Also, a two-stage optimization approach combined mixed-integer linear programming with the Mountain Gazelle Optimizer was proposed in [110] for optimal battery energy storage placement and sizing in radial distribution grids. A hybrid model is presented in [111] for integrating RESs into the IEEE 33-bus distribution grid, using a bi-directional long short-term memory network to manage SPV and wind generation uncertainties. This model, optimized with binary particle swarm optimization, aimed to minimize energy losses and voltage deviations while considering long-term and seasonal impacts. In [112], a two-stage stochastic mixed-integer non-linear programming model was proposed to optimize renewable energy integration in distribution systems over a ten-year horizon. Using NSGA-II for long-term planning and MOPSO for hourly operation, the approach minimized costs, power loss, and voltage deviation while incorporating uncertainties through Monte Carlo simulation. The authors of [113] optimized DG power output at fixed locations in Tanzanian distribution grids, using four metaheuristic algorithms to minimize revenue losses based on hourly load profiles and tariff categories (D1, T1, and T2). Duan et al. [114] optimized WT allocation in radial distribution grids using a multi-objective improved horse herd optimizer and an unscented transformation method to model uncertainties. Their approach minimized power loss, enhanced reliability, and reduced costs, outperforming conventional optimization algorithms. Hachemi et al. [115] developed an integration strategy for RES and compressed air energy storage in RDGs using the red-tailed Hawk optimization technique to enhance reliability indices and line loading. The method was validated on

IEEE 69-bus and 33-bus systems, considering the output power fluctuations of SPV and WT generation sources as well as load demand variations. Two modified versions of the Tasmanian Devil optimization algorithm were proposed in [116] to deal with the efficient power flow in conventional and renewable power systems. In [117], an improved moth flame optimization algorithm was proposed for optimal scheduling of dispatchable and non-dispatchable DGs, addressing energy loss in power grids under dynamic load conditions using 69-bus and 118-bus systems. The enhanced cheetah optimizer algorithm was developed in [118] for dynamic economic dispatch, integrating demand-side management and RES to improve grid security and reduce costs. Khasanov et al. [119] introduced a modified bald eagle search optimization algorithm for RES-based DG and battery energy storage placement and sizing in 33-bus and 118-bus radial distribution systems. In [120], an enhanced jellyfish search optimizer was proposed for the efficient energy management in multi-microgrids, integrating photovoltaic, wind, and biomass systems. The approach minimizes costs, improves voltage stability, and enhances system performance, validated on an 85-bus distribution system. Guven et al. [121] presented the quadratic interpolation-enhanced artificial gorilla troop optimizer for optimizing grid-connected hybrid RES. The technique improved the renewable energy fraction, reduced annual costs, and lowered energy costs.

Furthermore, the coronavirus herd immunity optimizer was introduced in [122] to improve power plant economic, environmental, and technical performance. Tested on IEEE 30-bus and 57-bus systems. The artificial hummingbird algorithm was employed in [123] for the optimal planning of multiple RES integration in distribution systems with uncertainties. A bi-level optimization strategy was proposed in [124] for regional integrated energy systems, reducing carbon emissions and operational costs. The study addresses uncertainties in renewable generation and demand response. In [125], a solution, the success history-based adaptive differential evolution algorithm, was developed for optimal DG allocation under uncertain conditions. Additionally, a weight-aggregated particle swarm optimization method was proposed in [126] for DG and capacitor bank placement in distribution networks, considering SPV and WT generation uncertainties and fluctuating demand patterns to enhance power efficiency and stability. Also, in [127], an efficient metaheuristic algorithm for optimizing photovoltaic renewable energy sources and capacitor bank placement in distribution networks was proposed to minimize energy losses and enhance voltage stability. Duan et al. [128] presented a fuzzy multi-objective framework that optimizes photovoltaic and wind energy integration in radial distribution networks under uncertainty, utilizing an improved gradient-based optimizer. The proposed method enhances system robustness and outperforms existing techniques in minimizing losses and costs.

Ultimately, most of these studies have addressed the optimal planning problem of RESs, taking into account uncertainties in load, solar irradiation, and wind speed. However, they have largely overlooked temperature-related uncertainties, which limit their scope. Further limitations in the existing literature include the assumption of fixed locations or sizes for RESs, as well as the neglect of some grid constraints, such as line thermal limits and the minimum allowable voltage limit. Furthermore, the majority of these approaches assumed that WTs operate at unity power factors, focusing solely on their location and size while neglecting the optimization of their power factor. This creates a gap in exploiting the full potential of WTs operating at optimal power factor, where both active and reactive power are injected to enhance the system performance.

The core objective of this research work is to rigorously address and bridge the aforementioned research gaps.

1.7 Conclusion

This chapter has presented a comprehensive overview of the fundamental concepts of power systems and the various types of renewable energy-based DG. We have explored their integration into modern radial distribution grids, emphasizing the associated technical, economic, and environmental benefits. Additionally, it provided an in-depth literature review on renewable DG integration in distribution grids, critically highlighting the research gaps in previous studies. When optimally sized and placed, DG units can effectively reduce power losses, enhance voltage profiles, and improve the stability and reliability of distribution systems. However, improper planning may result in adverse effects, underscoring the importance of optimization techniques in determining the optimal locations and capacities for DG allocation.

The subsequent chapter will delve into power flow analysis based on identifying the network topology using the backward/forward sweep method to assess the performance of radial distribution grids.

Chapter 2

Load Flow Analysis in Distribution Grids

2.1 Introduction

Load flow analysis, also known as power flow analysis, is essential for the effective operation and strategic planning of distribution systems. This process uses a structured mathematical approach to calculate bus voltages, phase angles, currents, and power flows through system branches, generators, and loads in steady-state conditions [129]. Consequently, it provides vital insights into grid performance, including power losses, voltage deviations, and overall system stability, enabling engineers to enhance the efficiency of the distribution grid.

Several methods have been proposed in the literature to solve the load flow problem in power systems. Among the most notable approaches are Newtonian methods, such as the Newton-Raphson method [130, 131], the decoupled Newton-Raphson method [132], and the fast decoupled Newton-Raphson method [133, 134]. These methods are widely used in transmission grids to solve the load flow problem effectively. However, their application to distribution grids, particularly large-scale systems, often leads to divergence due to the distinct characteristics of distribution grids as compared to transmission grids, including higher resistance-to-reactance (R/X) ratio, radial configuration, and a greater number of nodes and branches [135].

The backward/forward sweep (BFS) methods [136–138] have gained significant attention as an efficient and accurate alternative for load flow solutions in radial distribution grids. This iterative method is based mainly on two sweeps: the backward sweep, where branch currents are computed using Kirchhoff's current law (KCL), and the forward sweep, which calculates bus voltages using Kirchhoff's voltage law (KVL).

This dual sweep makes the approach particularly effective in addressing load flow problems in complex and large distribution systems [87, 138].

This chapter focuses on calculating load flow in radial distribution grids using the BFS method. This technique relies on understanding the grid's topology by analyzing the data from its buses and branches. The process begins by classifying each bus as a terminal, common, or intermediate bus, and each line as a main, lateral, sub-lateral, or minor line. This classification will subsequently be exploited to perform load flow calculations. The performance of the proposed BFS method is evaluated on the IEEE 69-bus, 85-bus, and the actual Portuguese 94-bus distribution grids, emphasizing its effectiveness in solving load flow problems for various radial configurations.

2.2 Importance of radial distribution grids analysis

The analysis of radial distribution grids is crucial, given their distinct characteristics and the specific operational challenges they pose. As the final stage in electricity delivery, distribution grids are predominantly deployed in urban and suburban areas, making them critical to system performance and customer satisfaction. These grids are distinguished by a single, unidirectional power flow path from the substation to load points. This straightforward topology offers several advantages, including reliability, efficient fault management, expedited service restoration, and cost-effective maintenance. However, these systems are prone to significant voltage drops and elevated power losses, primarily due to extended distances and higher line resistances.

Moreover, this analysis is vital to ensure voltage stability, maintaining power supply within acceptable voltage limits, a requirement for customer satisfaction, and the overall integrity of the electrical supply. Additionally, such analysis helps reduce energy losses, thereby improving the overall operational efficiency of the distribution grid. It also facilitates the optimal sizing and strategic placement of network components, such as transformers and capacitors, which are indispensable for effective load management in response to fluctuating residential and commercial demand patterns.

With the increasing integration of renewable energy sources, the complexity of electrical distribution systems has grown considerably. This development has amplified the importance of accurate analysis for effective load flow management. Such analysis is essential for understanding the grid behavior under varying load and operational conditions, particularly in light of the variability and intermittency associated with renewable energy sources. It supports decision-making in system planning, operational management, and infrastructure modernization. Hence, robust analysis is indispensable for system planning and expansion, to accommodate future demand growth and

enable the integration of emerging technologies, as power grids transition toward more decentralized and dynamic architectures.

2.3 Structure of a radial distribution grid

Radial distribution grids are typically structured for unidirectional power flow, originating from a single source at the reference bus (slack bus) to multiple loads. The buses within the grid are classified as terminal, common, or intermediate types, while the lines connecting these buses are categorized into main, lateral, sub-lateral, and minor lines. Figure 2.1 illustrates the general structure of a radial distribution grid.

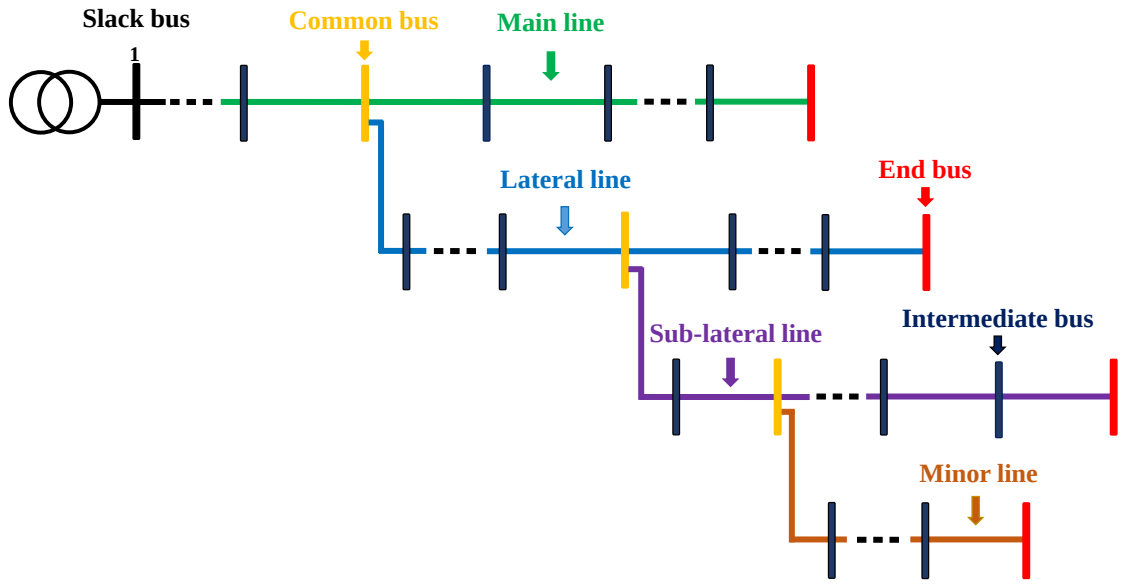

Figure 2.1: Structure of a radial distribution grid

2.4 Per unit system

The per unit (p.u.) system is a method for normalizing electrical quantities such as voltage, current, power, and impedance. Each quantity is expressed as a ratio of its actual value X to a predefined base value X_{base}, delivering a dimensionless value expressed in p.u. (or as a percentage of its base value) [11, 139]. This approach facilitates the comparison of parameter magnitudes and simplifies load flow calculations.

For a base voltage (V_{base}) in kV, a base power (S_{base}) in MVA, and an impedance Z in ohm (Ω), the resistance in per unit $Z_{p.u}$ is given by:

$$\bar{Z_{p.u}} = \bar{Z} \times \left(\frac{S_{base}}{V_{base}^2} \right) \tag{2.1}$$

The normalized active power $P_{p.u}$ as a function of the active power P in MW is given by:

$$P_{p.u} = \frac{P}{S_{base}} \tag{2.2}$$

The normalized reactive power $Q_{p.u}$ as a function of the reactive power Q in MVAr is given by:

$$Q_{p.u} = \frac{Q}{S_{base}} \tag{2.3}$$

2.5 Power and current flowing in the branches

A radial distribution grid consists of multiple branches, each modeled by a resistance in series with a pure inductance. Figure 2.2 illustrates the flow of active and reactive powers between two buses.

The active power transmitted from bus i to bus $i+1$ is expressed as follows [140]:

$$P_i = P'_{i+1} + R_i \left(\frac{P'^2_{i+1} + Q'^2_{i+1}}{V^2_{i+1}} \right) \tag{2.4}$$

where:

$$P'_{i+1} = P_{i+1} + P_{di+1} \tag{2.5}$$

P_{di} and P_{di+1} represent the active power demands at the bus i and $i+1$, respectively; P_i is the active power transmitted through the branch i.

The reactive power transmitted from bus i to bus $i+1$ is given by [140]:

$$Q_i = Q'_{i+1} + X_i \left(\frac{P'^2_{i+1} + Q'^2_{i+1}}{V^2_{i+1}} \right) \tag{2.6}$$

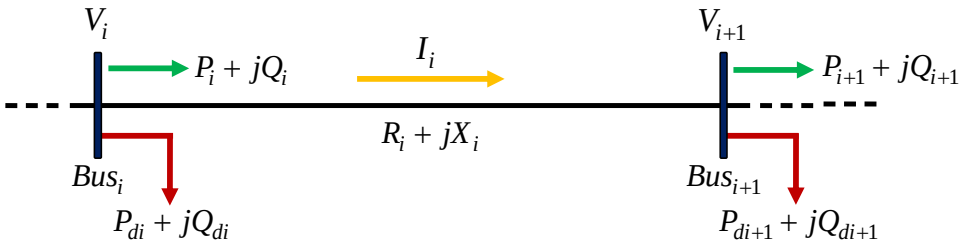

Figure 2.2: Representation of a two-bus in the radial distribution grid

where:

$$Q'_{i+1} = Q_{i+1} + Q_{di+1} \tag{2.7}$$

Q_{di} and Q_{di+1} represent the reactive power demands at the bus i and $i+1$, respectively; Q_i is the reactive power transmitted through the branch i.

The current flowing through a branch i is computed as follows [141]:

$$I_i = \frac{(V_i \angle\theta_i - V_{i+1} \angle\theta_{i+1})}{R_i + jX_i} \tag{2.8}$$

and

$$P_{di+1} - jQ_{di+1} = V^*_{i+1} I_i \tag{2.9}$$

2.6 Load flow solution of a radial distribution grid

Load flow calculation require two key inputs defining the distribution grid's characteristics: line and load data. These inputs are compiled into two tables. The line data table specifies the characteristics of the network conductors, while the load data table details the active and reactive power consumption at each bus. This data is essential for identifying the grid topology, allowing the calculation of branch currents, power transmitted through each branch, total active and reactive power losses and voltage levels at each bus. In this thesis, the load flow solution is carried out using the Backward/Forward Sweep (BFS) method. The following section details the BFS technique.

2.7 The backward/forward sweep method

The BFS method is an iterative technique used to solve power flow problems in radial distribution grids by applying Kirchhoff's current law (KCL) and Kirchhoff's voltage law (KVL). The backward sweep calculations begin from the last node (farthest bus or load point) and progress towards the first node (substation). KCL is applied to compute currents based on the power demands at each node. In the forward sweep, KVL is operated to update real and imaginary parts of the calculated node voltages by accounting for voltage drops across line impedances, starting from the first node towards the last node. These sweeps are repeated iteratively until the convergence criteria are met.

2.7.1 Initialisation

- Input network data: read linedata and busdata tables.
- Initialize the injected current ($I_i = 0$)
- Initialize voltage of all buses ($V_i = 1$ p.u.)
- Define the desired tolerance value (ϵ).

2.7.2 Branch currents

Currents in the system branches are determined during the backward sweep phase. This process begins by calculating the currents flowing through all loads connected at the buses. Subsequently, the currents flowing through the branches are computed in order, starting with the minor lines, then moving on to the sub-lateral lines, lateral lines, and finally the main line [136–138].

2.7.2.1 Load current

The injected current to each bus at iteration $k+1$ is calculated based on the power consumed by the connected load and the voltage magnitude at that bus at iteration k. For a given bus i, the injected current can be expressed as follows:

$$I_{d,i}^{k+1} = \frac{S_{d,i}^{*}}{V_i^{*,k}} \tag{2.10}$$

where $i = 1, 2, \ldots, N$, N is the total number of buses.

2.7.2.2 Branch currents of a minor line

The current flowing through a minor line branch can be calculated using [136]:

$$I_b = I_{b+1} + I_{d(b+1)} \tag{2.11}$$

where:

$$\begin{cases} b = (SB_m - 1), \ldots, (EB_m - 1) \quad \forall m, \quad m = 1, 2, \ldots, N_m, \\ I_{b+1} = 0, \quad \text{if} \quad (b+1) = EB_m \\ I_{bm,m} = I_b, \quad \text{if} \quad b = b_{slm} \end{cases} \tag{2.12}$$

N_m denotes the total number of minor lines, I_b and I_{b+1} are the currents of the branches b and $b+1$, respectively. SB_m is the starting bus of the m^{th} minor line, while

EB_m represents its ending bus. $I_{bm,m}$ is the branch current in the m^{th} minor line, and b_{slm} is the branch number connecting the sub-lateral line with the m^{th} minor line.

2.7.2.3 Branch currents of a sub-lateral line

The current flowing through a branch belonging to a sub-lateral line is written as follows [136]:

$$I_b = I_{b+1} + I_{d(b+1)} + \sum_{m=1}^{N_m} I_{bm,m} \tag{2.13}$$

where:

$$\begin{cases} b = (SB_{sl} - 1), \ldots, (EB_{sl} - 1) \quad \forall sl, \quad sl = 1, 2, \ldots, N_{sl} \\ I_{b+1} = 0 \quad \text{if} \quad (b+1) = EB_{sl} \\ I_{bm,m} = 0 \quad \text{if} \quad (b+1) \neq n_{slm} \quad \forall m, \quad m = 1, 2, \ldots, N_m \\ I_{bsl,sl} = I_b \quad \text{if} \quad b = b_{lsl} \end{cases} \tag{2.14}$$

N_{sl} denotes the total number of sub-lateral lines, SB_{sl} indicates the starting bus of the sl^{th} sub-lateral line, while EB_{sl} represents its ending bus. n_{slm} is the bus number in the sub-lateral line where the m^{th} minor line begins.

2.7.2.4 Branch currents of a lateral line

The current flowing through a branch belonging to a lateral line is written according to the following equation [136]:

$$I_b = I_{b+1} + I_{d(b+1)} + \sum_{sl=1}^{N_{sl}} I_{bsl,sl} \tag{2.15}$$

where:

$$\begin{cases} b = (SB_l - 1) \text{ up to } (EB_l - 1) \quad \forall l, \quad l = 1, 2, \ldots, N_l \\ I_{bsl,sl} = 0 \quad \text{if} \quad (b+1) \neq n_{lsl} \quad \forall sl, \quad sl = 1, 2, \ldots, N_{sl} \\ I_{b+1} = 0 \quad \text{if} \quad (b+1) = EB_l \\ I_{bl,l} = I_b \quad \text{if} \quad b = b_{Ml} \end{cases} \tag{2.16}$$

N_l denotes the total number of lateral lines. SB_l is the starting bus of the l^{th} lateral line, while EB_l represents its ending bus. $I_{bl,l}$ is the branch current in the l^{th} lateral line, b_{Ml} is the branch number connecting the main line with the l^{th} sub-lateral

line, n_{lsl} represents the common bus number in the lateral line from which the sl^{th} sub-lateral line begins.

2.7.2.5 Branch currents of the main line

The current flowing through a branch belonging to a main line is written according to the following equation [136]:

$$I_b = I_{b+1} + I_{d(b+1)} + \sum_{l=1}^{N_l} I_{bl,l} \tag{2.17}$$

where:

$$\begin{cases} b = 1, 2, \ldots, (EB_M - 1) \\ I_{bl,l} = 0, \quad \text{if} \quad (b+1) \neq n_{Ml}, \quad \forall l, \quad l = 1, 2, \ldots, N_l \\ I_{b+1} = 0, \quad \text{if} \quad (b+1) = EB_M \end{cases} \tag{2.18}$$

EB_M represents the ending bus of the main line, n_{Ml} is the number of the common bus in the main line where the l^{th} lateral line begins.

2.7.3 Voltage magnitude at each bus

The voltage magnitude at each bus is determined during the forward sweep, which is performed in ascending order, beginning at the source bus and progressing toward the system's terminal bus. This process calculates the voltage drop across each branch connecting buses i and $i+1$ (refer to Figure 2.2) at iteration $k+1$, as described by the following equation.

$$V_{i+1}^{k+1} = V_i^{k+1} - I_i^{k+1} \times Z_i, \quad i = 1, 2, \ldots, N_b \tag{2.19}$$

where, Z_i is the series impedance of branch i, N_b is the total number of branches in the system.

2.7.4 Convergence criterion

The backward and forward sweeps are repeated iteratively until the specified convergence criterion is met. The maximum difference in voltage magnitudes for two successive iterations is taken as the convergence criterion, as defined by:

$$max\left(\left|V_i^{k+1} - V_i^k\right|\right) < \epsilon, \quad i = 1, 2, \ldots, N \tag{2.20}$$

where V_i^{k+1} and V_i^k are the bus voltages at the $(k+1)^{\text{th}}$ and k^{th} iterations, respectively, ϵ is the desired tolerance, and N represents the total number of buses in the grid.

2.7.5 Active and reactive power losses

According to Figure 2.2, the active power loss in a branch i is calculated as:

$$P_{\text{Loss},i} = R_i \left(\frac{P_i^2 + Q_i^2}{|V_i|^2} \right) \tag{2.21}$$

The total active power losses in the system are determined by summing the losses of all branches, as defined in Equation (2.22):

$$P_{\text{T,Loss}} = \sum_{i=1}^{\text{Nb}} P_{\text{Loss},i} \tag{2.22}$$

The reactive power losses at the i^{th} branch are written as follows:

$$Q_{\text{Loss},i} = X_i \left(\frac{P_i^2 + Q_i^2}{|V_i|^2} \right) \tag{2.23}$$

The total reactive power losses in the system can be determined by summing the losses of all branches, as given in Equation (2.24):

$$Q_{\text{T,Loss}} = \sum_{i=1}^{\text{Nb}} Q_{\text{Loss},i} \tag{2.24}$$

2.7.6 Voltage deviation

The voltage deviation can be defined as the difference in voltage magnitude at bus i from the reference bus voltage (V_{ref}) equal to 1 p.u. The smaller the voltage deviation, the better the network voltage quality. The voltage deviation (VD) is expressed as follows [142]:

$$VD = \sum_{i=1}^{N} \left(V_i - V_{ref} \right)^2 \tag{2.25}$$

where, V_i is the voltage magnitude at bus i, and N is the total number of buses.

2.7.7 Voltage stability analysis in distribution grids

Voltage stability refers to the ability of an electrical system to maintain acceptable voltage levels at each bus after a disturbance. Various phenomena, such as line failures or load fluctuations, can lead to voltage drops across all buses, resulting in widespread network voltage collapse [143]. Numerous techniques for voltage stability analysis have been developed in the literature to evaluate the stability of distribution grids under diverse operating conditions and to provide effective control strategies [144]. Among these approaches, voltage stability indices are especially useful in assessing the stability of distribution grids.

In this study, we employ the voltage stability index (VSI) introduced by Chakravorty and Das [145], which can be derived from the simplified radial distribution grid diagram in Figure 2.2 and is represented by the following equations:

From Equations (2.8) and (2.9), we get:

$$|V_{i+1}|^4 - \left(|V_i|^2 - 2P_{di+1}\cdot R_i - 2Q_{di+1}\cdot X_i\right)|V_{i+1}|^2 + \left(P_{di+1}^2 + Q_{di+1}^2\right)\left(R_i^2 + X_i^2\right) = 0 \tag{2.26}$$

By replacing the terms $|V_i|^2 - 2P_{Li+1}\cdot R_i - 2Q_{Li+1}\cdot X_i$ and $\left(P_{Li+1}^2 + Q_{Li+1}^2\right)\left(R_i^2 + X_i^2\right)$ with b_i and c_i, respectively, the equation can be rewritten as:

$$|V_{i+1}|^4 - b_i|V_{i+1}|^2 + c_i = 0 \tag{2.27}$$

We can see that Equation (2.27) has four solutions, which are:

$$\frac{1}{\sqrt{2}}\left[b_i - \sqrt{b_i^2 - 4c_i}\right]^{\frac{1}{2}}$$

$$-\frac{1}{\sqrt{2}}\left[b_i - \sqrt{b_i^2 - 4c_i}\right]^{\frac{1}{2}}$$

$$-\frac{1}{\sqrt{2}}\left[b_i + \sqrt{b_i^2 - 4c_i}\right]^{\frac{1}{2}}$$

$$\frac{1}{\sqrt{2}}\left[b_i + \sqrt{b_i^2 - 4c_i}\right]^{\frac{1}{2}}$$

For realistic values where P, Q, R, X, and V are expressed in per unit, b_i is always positive. This is because the term $2\left(P_{Li+1}\cdot R_i + Q_{Li+1}\cdot X_i\right)$ is very small compared to $|V_i|^2$, and the term $4c_i$ is very small compared to b_i^2. As a result, $\left(b_i^2 - 4c_i\right)^{1/2}$ is almost equal to b_i, rendering the first two solutions of $|V_{i+1}|$ nearly zero and therefore

infeasible. The third solution is negative and hence not feasible. The fourth solution of $|V_{i+1}|$, being positive, is the feasible option.

Consequently, the solution to Equation (2.27) is:

$$|V_{i+1}| = \frac{1}{\sqrt{2}}\left[b_i + \sqrt{b_i^2 - 4c_i}\right]^{\frac{1}{2}} \tag{2.28}$$

From Equation (2.28), it can be noted that a valid solution for the load flow in the radial distribution grid exists if:

$$\left(b_i^2 - 4c_i\right) \geq 0 \tag{2.29}$$

By substituting the equations for b_i and c_i into Equation (2.29), we get:

$$VSI_{i+1} = |V_{i+1}|^4 - 4\left(P_{Li+1} \cdot X_i - Q_{Li+1} \cdot R_i\right)^2 - 4\left(P_{Li+1} \cdot R_i + Q_{Li+1} \cdot X_i\right)|V_i|^2 \geq 0 \tag{2.30}$$

where VSI_{i+1} is the voltage stability index of the $(i+1)^{th}$ bus.

For the stable operation of the radial distribution grid, VSI_{i+1} must be greater than or equal to 0. The authors of [145] state that the closer the value of VSI is to 1, the more stable the system becomes.

2.8 Flowchart of the backward/forward sweep method

Figure 2.3 presents the flowchart for solving the power flow problem using the backward/forward sweep method.

2.9 Numerical applications on a radial distribution grid

To demonstrate the effectiveness of the BFS method, it was implemented in MATLAB and applied to the IEEE 69-bus, IEEE 85-bus, and an actual Portuguese 94-bus radial distribution grids at a peak load condition [146–148]. This section demonstrates the practical application of the technique, showcasing its accuracy and efficiency in solving load flow problems. Key performance metrics, including active and reactive power losses, voltage profile, and stability, are analyzed to evaluate the grid's performance.

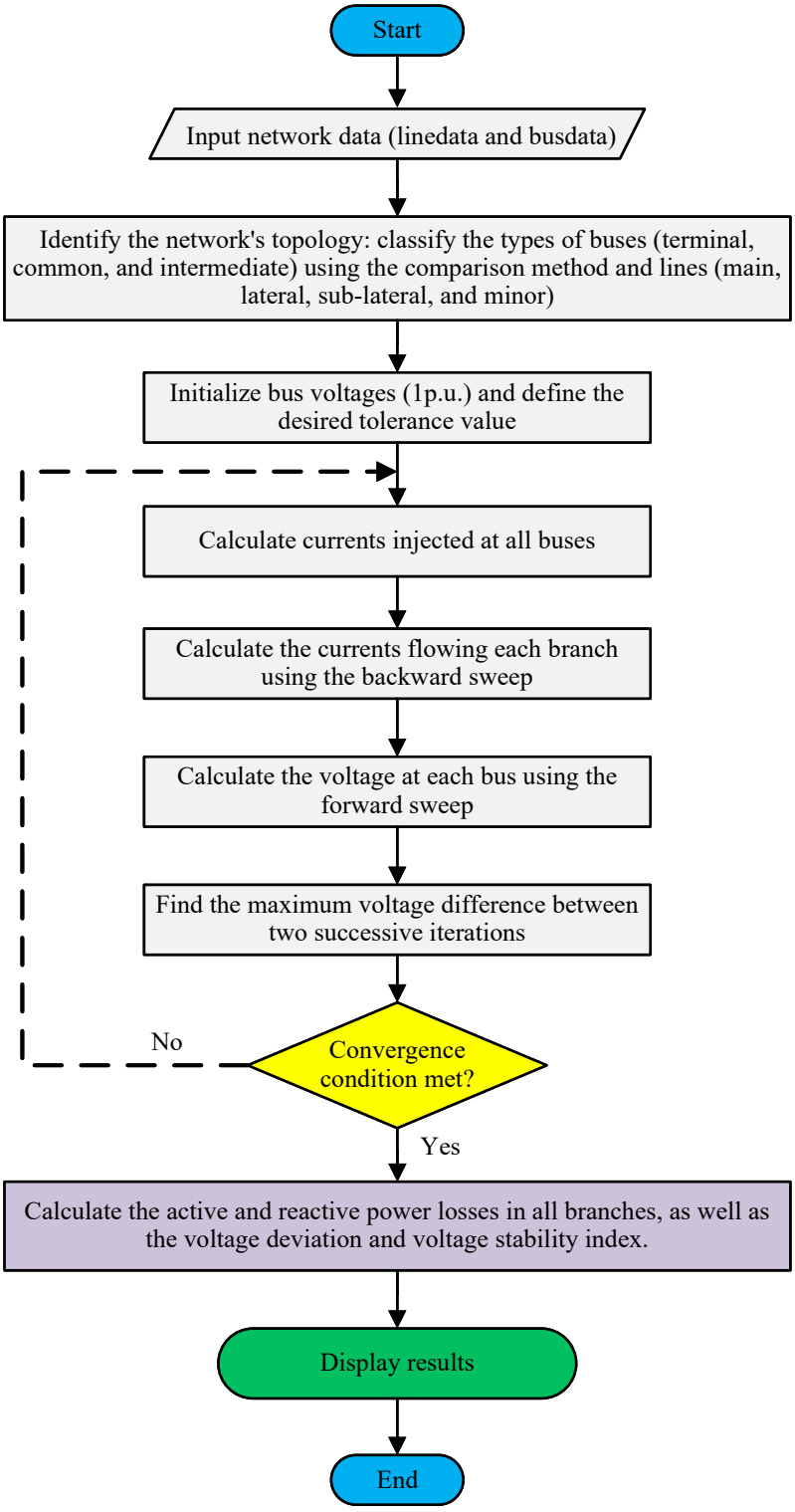

Figure 2.3: Flowchart of the load flow solution

2.9.1 Test system 1: the IEEE 69-bus system

The characteristics of the IEEE 69-bus distribution grid depicted in Figure 2.4 are as follows:

- Number of buses: 69;
- Number of branches: 68;
- Slack bus N° = 1;
- Base power: 100 MVA;
- Base voltage: 12.66 kV.

The detailed data for the IEEE 69-bus test system are provided in Appendices (A.1) and (A.2) [146].

Figure 2.5 illustrates the active and reactive power losses in each branch of the IEEE 69-bus distribution grid, derived after load flow calculation using the BFS method. The highest active power loss, $P_{\text{Loss}} = 49.6849\,\text{kW}$, and reactive power loss, $Q_{\text{Loss}} = 16.6773\,\text{kVAr}$, are observed at branch 6 (between buses 6 and 7). These losses are justified by the current flowing through the branch and its electrical characteristics, specifically resistance and reactance. The network's total active and reactive power

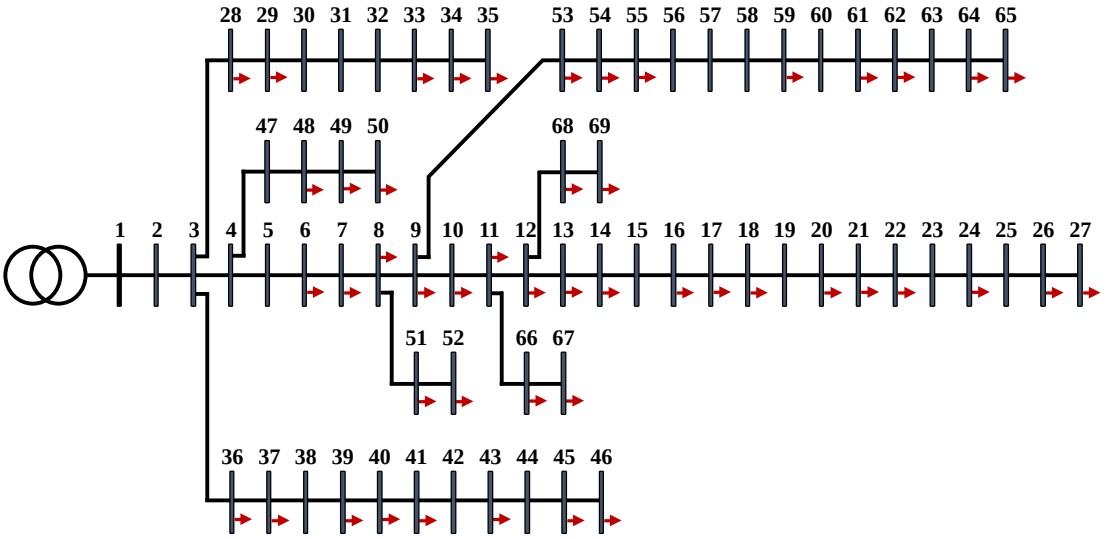

Figure 2.4: Single line diagram of 69-bus distribution grid

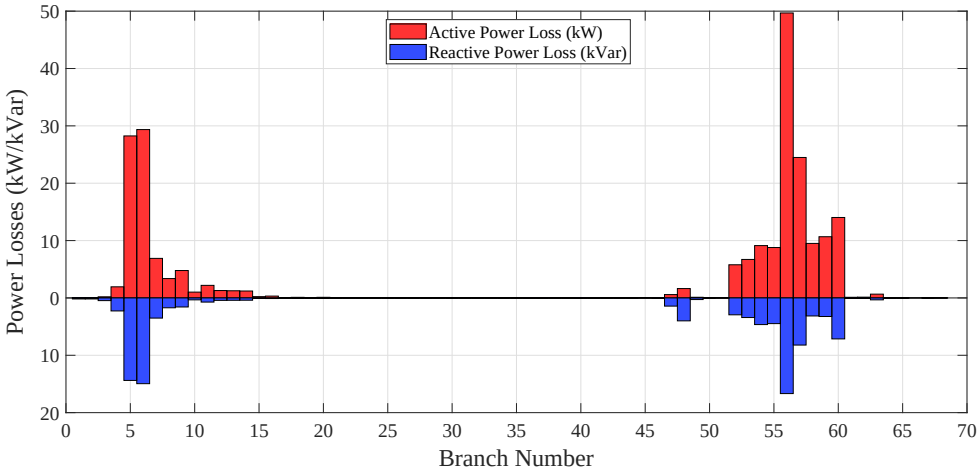

Figure 2.5: Active and reactive power losses across the branches of the 69-bus distribution grid

losses are 225.003 kW and 102.165 kVAr, respectively, representing 5.92% and 3.79% of the total load demand.

Figure 2.6 displays the voltage magnitudes at each bus within the IEEE 69-bus distribution grid, offering a clear overview of the voltage profile across the system. The figure highlights buses where the voltage levels may drop below acceptable limits, potentially leading to system instability or inefficiencies. Notably, the lowest voltage

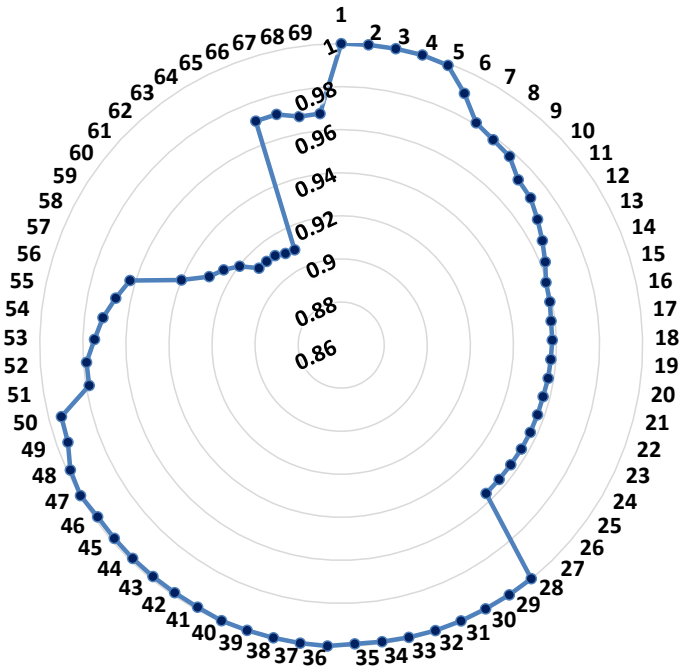

Figure 2.6: Voltage profile of the 69-bus distribution grid

magnitude, 0.9092 p.u., is observed at bus 65. The total voltage deviation across the network is 0.0993 p.u., which reflects the extent of voltage variations throughout the system.

Figure 2.7 illustrates the Voltage Stability Index (VSI) for each bus in the IEEE 69-bus distribution grid, providing valuable insights into the system's stability profile. At bus 65, the VSI is 0.6833, indicating a lower level of stability compared to other buses. A lower VSI value signifies that the bus is closer to voltage instability.

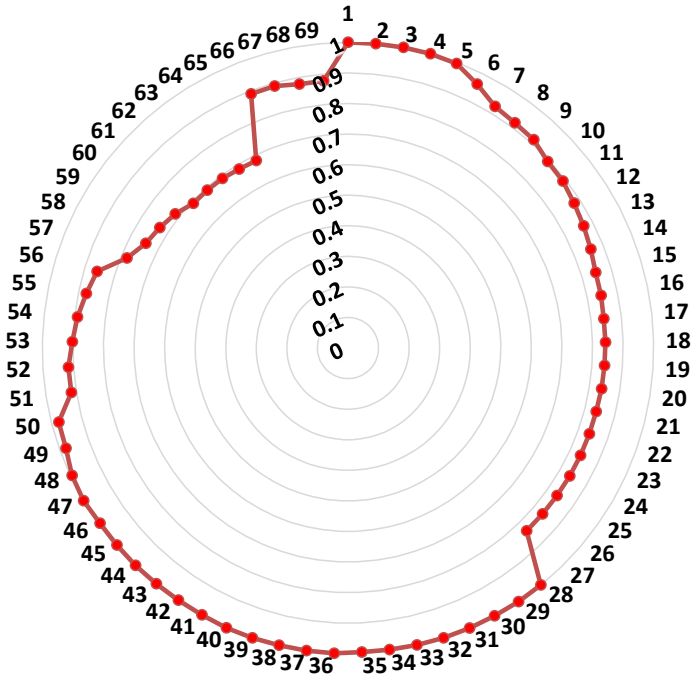

Figure 2.7: Voltage stability index values of the 69-bus distribution grid

2.9.2 Test system 2: the IEEE 85-bus system

The characteristics of the IEEE 85-bus distribution grid shown in Figure 2.8 are as follows:

- Number of buses: 85;
- Number of branches: 84;
- Slack bus N° = 1;
- Base power: 100 MVA;
- Base voltage: 11 kV.

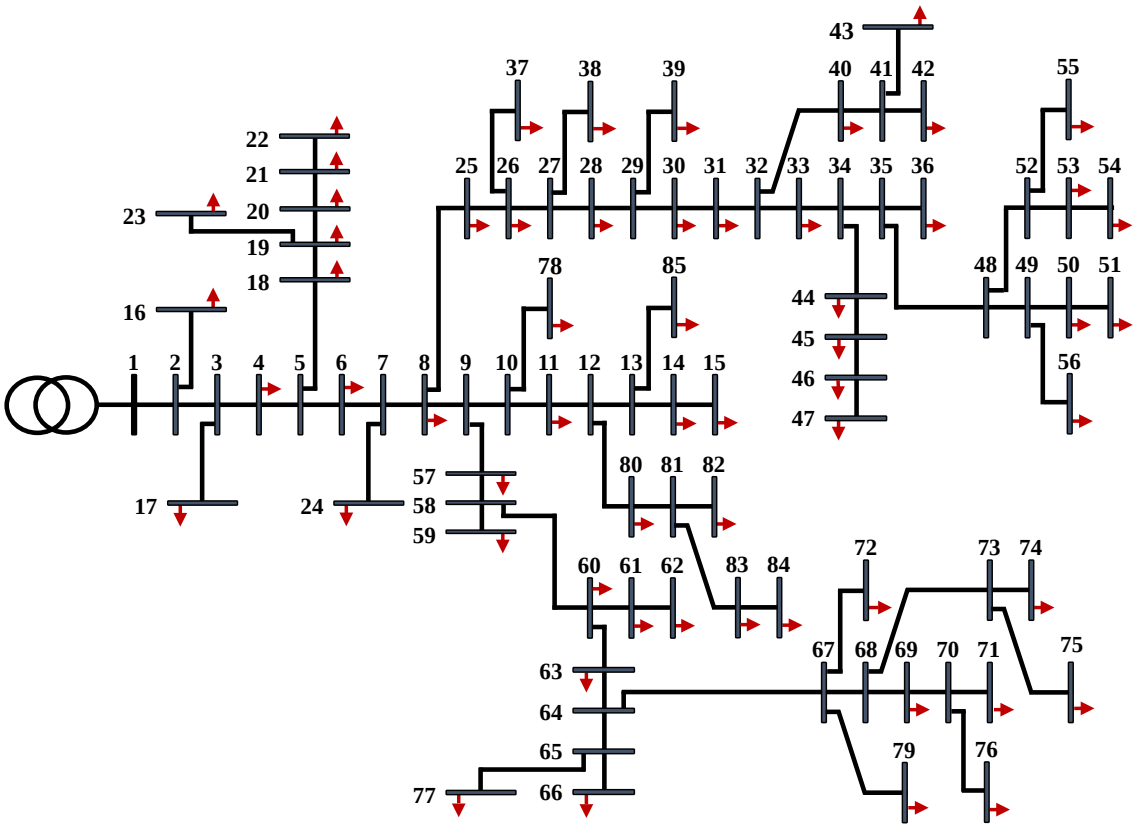

Figure 2.8: Single line diagram of 85-bus distribution grid

The detailed data for the test IEEE 85-bus system are provided in Appendices (A.3) and (A.4) [147].

Figure 2.9 illustrates the active and reactive power losses in each branch of the IEEE 85-bus distribution grid, obtained through load flow calculations using the BFS method. The highest active power loss, $P_{\text{Loss}} = 103.4935\,\text{kW}$, and reactive power loss, $Q_{\text{Loss}} = 70.8978\,\text{kVAr}$, appear at the 7^{th} branch. These losses are explained by the current flow and the electrical characteristics (resistance and reactance) of the branch. The total active and reactive power losses in the network are 316.1175 kW and 198.6021 kVAr, respectively, accounting for 12.30% and 7.57% of the total load demand.

Figure 2.10 shows the voltage magnitudes at each bus within the IEEE 85-bus radial distribution grid, providing an overview of the voltage profile across the system. The figure identifies buses where voltage levels fall below acceptable limits, which could result in potential system issues. The lowest voltage magnitude, 0.8713 p.u., is observed at bus 54, and the total voltage deviation of the network is 0.8214 p.u.

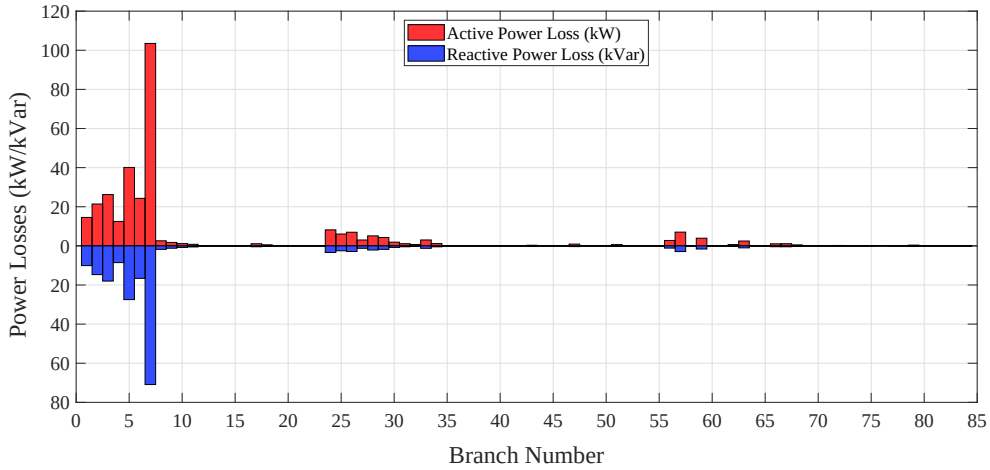

Figure 2.9: Active and reactive power losses across the branches of the 85-bus distribution grid

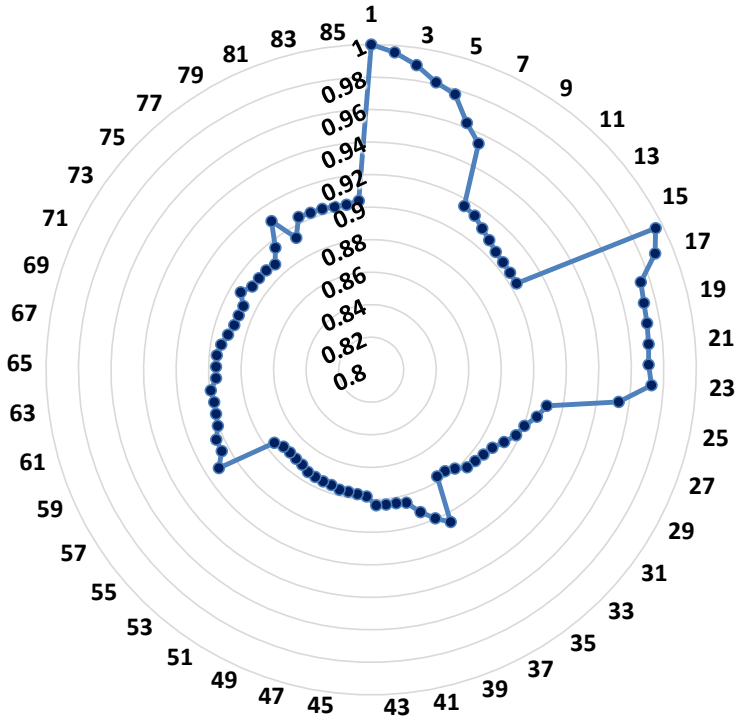

Figure 2.10: Voltage profile of the 85-bus distribution grid

Figure 2.11 presents the VSI at each bus in the IEEE 85-bus distribution grid, offering valuable insights into the system's stability profile. The lower level of stability is 0.5764, observed at bus 54, which suggests that the bus is closer to voltage instability.

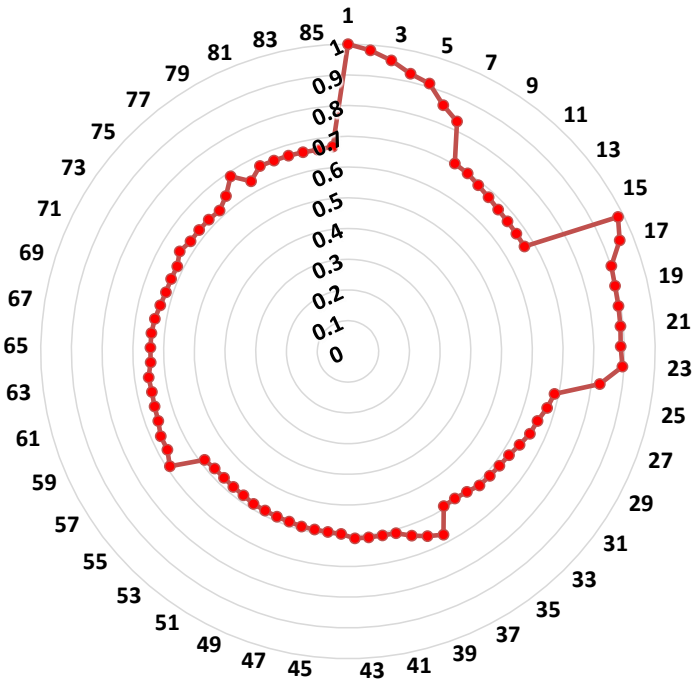

Figure 2.11: Voltage stability index values of the 85-bus distribution grid

2.9.3 Test system 3: the actual Portuguese 94-bus system

The characteristics of the actual Portuguese 94-bus system shown in Figure 2.12 are as follows:

- Number of buses: 94;
- Number of branches: 93;
- Slack bus N° = 1;
- Base power: 100 MVA;
- Base voltage: 11 kV.

The detailed data for the actual Portuguese 94-bus system are provided in the Appendices (A.5) and (A.6) [148].

Figure 2.13 illustrates the active and reactive power losses in each branch of the actual Portuguese 94-bus distribution grid, obtained through load flow analysis using the BFS method. The highest active power loss, $P_{\text{Loss}} = 48.5128\,\text{kW}$, and reactive power loss, $Q_{\text{Loss}} = 81.0831\,\text{kVAr}$, appear at the 9^{th} branch. These losses are explained by the current flowing through the branch and its electrical properties, specifically resistance and reactance. The total active and reactive power losses in the grid are

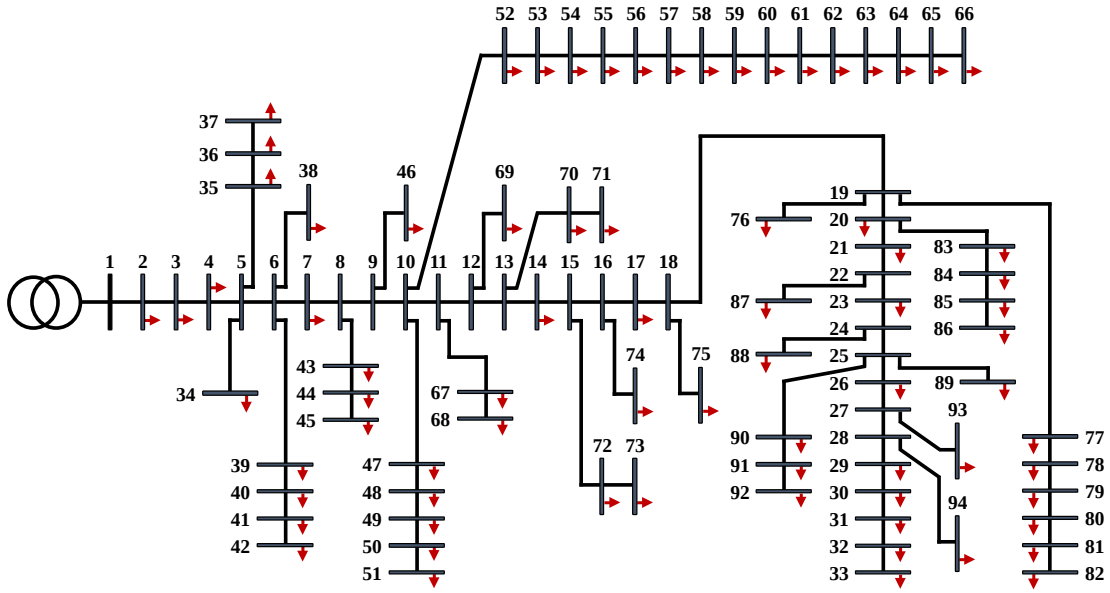

Figure 2.12: Single line diagram of the actual Portuguese 94-bus distribution grid

362.858 kW and 504.042 kVAr, respectively, accounting for 7.56% and 21.69% of the total load demand.

Figure 2.14 shows the voltage magnitudes at each bus within the 94-bus distribution grid, providing a clear overview of the voltage profile across the system. The figure identifies buses where voltage levels drop below acceptable limits, which could result in potential system operational issues. The lowest voltage magnitude, 0.8485 p.u., occurs at bus 92, and the total voltage deviation of the network is 1.0442 p.u.

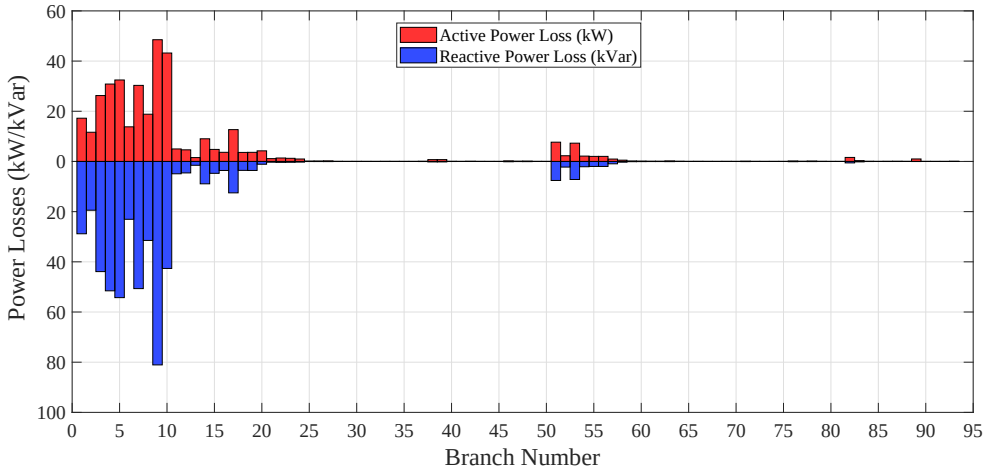

Figure 2.13: Active and reactive power losses across the branches of 94-bus distribution grid

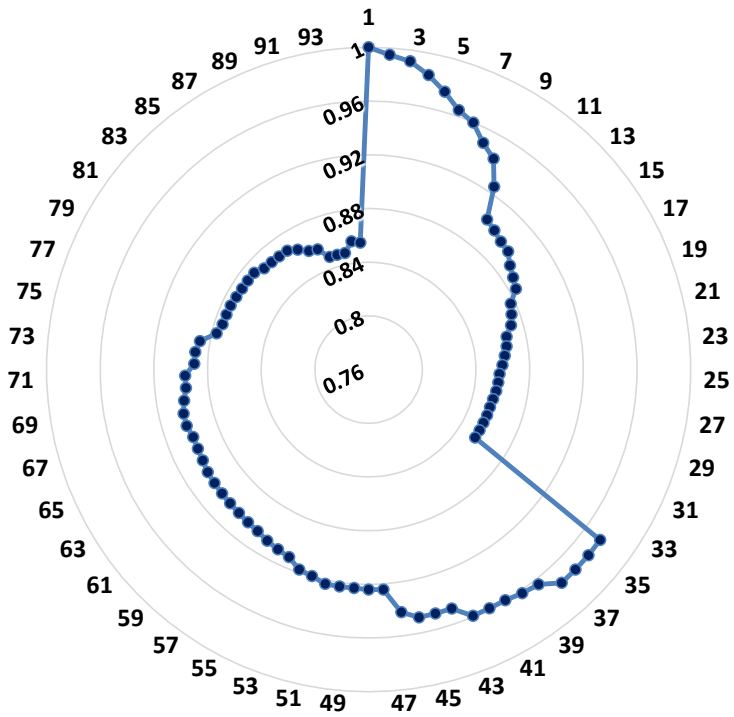

Figure 2.14: Voltage profile of 94-bus distribution grid

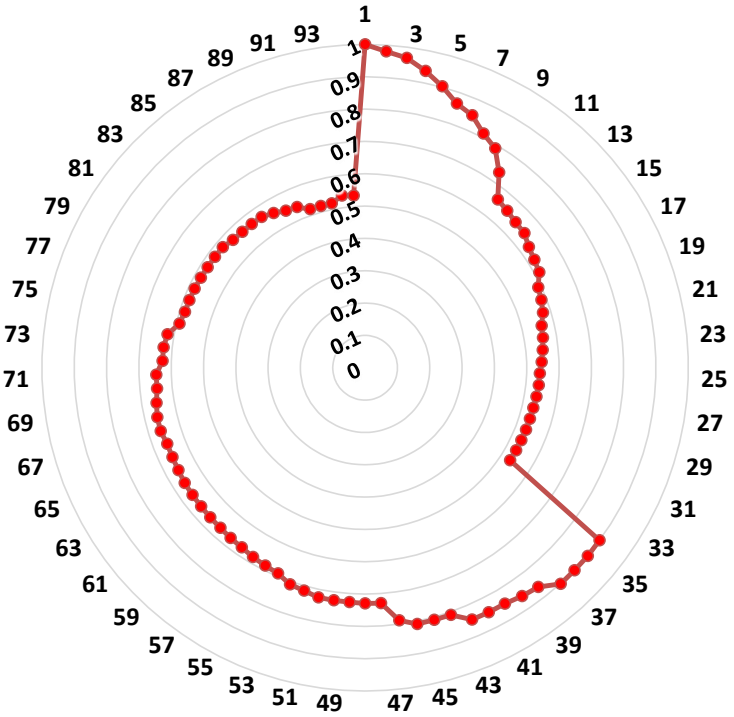

Figure 2.15: Voltage stability index values of 94-bus distribution grid

Figure 2.15 presents the VSI at each bus in the 94-bus distribution grid, offering valuable insights into the system's stability profile. The lower level of stability is 0.5183, observed at bus 92, which signifies that the bus is closer to voltage instability.

2.10 Conclusion

In this chapter, we have thoroughly explored the load flow analysis of a radial distribution grid. The study employed the backward/forward sweep method, known for its simplicity, speed, and robustness, to solve load flow problems efficiently. This technique is based on an understanding of the network's topology. Initially, we identified the types of buses (terminal, common, and intermediate buses) using the comparison method and lines (main, lateral, sub-lateral, and minor lines), ensuring an accurate representation of the system's structure. This topology was then used in the load flow calculation using the suggested method. The technique was tested on various distribution grids, including IEEE 69-bus, IEEE 85-bus, and the actual Portuguese 94-bus systems. The results demonstrated its effectiveness in providing reliable load flow solutions, highlighting its suitability for distribution system analysis.

Chapter 3

Methods for Modeling Uncertainty in Power Systems

3.1 Introduction

In recent years, the rapid evolution of power systems and advancements in energy generation technologies such as smart grids, microgrids, and renewable energy sources integrated with energy storage devices have created many new opportunities for enhancing power system operation and control. However, these innovations also pose significant challenges by increasing the complexity of planning and operating modern power system grids [149]. A critical challenge in this context is the inherent uncertainty in energy system parameters, particularly in modern renewable energy systems, where accurately describing the deterministic states of power grid parameters becomes increasingly difficult due to the high penetration level of renewable energy sources. This heightened uncertainty can expose power systems to operational and stability risks, necessitating the development of robust uncertainty modeling approaches to ensure reliable and secure system performance.

Typically, uncertainty is modeled using mathematical frameworks. Probability theory represents uncertain variables as a probability density function (PDF). The Monte Carlo simulation method, an iterative probabilistic technique, involves random sampling based on the probability distribution and evaluates the conventional equations of the employed algorithm. Although general and widely applicable, this method is computationally intensive, requiring significant processing time to achieve detailed results. The fuzzy set theory is another approach for assessing uncertainties within distribution grids [150, 151].

In this chapter, various uncertainty parameters modeling approaches for modern power systems are explored and systematically classified. The focus is placed on

probabilistic methods, with particular emphasis on the PDF to represent the random variability of renewable energy sources. This approach enables a more accurate representation of uncertain variables in modern distribution grid management, facilitating decision-making under uncertainty in the planning and operation stages.

3.2 Uncertainty modeling methods

Uncertainty modeling methods are commonly generic and not specifically designed for electric power systems. Modeling the uncertainties in electric power systems is just one scenario using these uncertainty modeling methods. Thus, the uncertainties in electric power systems are not the origins of uncertainty modeling methods but rather constitute a field for their application. The literature presents a range of uncertainty modeling techniques for modern power systems, classified into six principal categories [150–153]:

1. **Probabilistic methods** [154]**:** These methods are widely used to address power system uncertainties, where input parameters of a problem are random with a probability density function (PDF) shaped for them. The commonly known probabilistic approaches, or uncertainty modeling methods, are classified into numerical and analytical ones. The former includes various forms of Monte Carlo simulation (MCS), such as sequential MCS, Markov Chain MCS, pseudo-sequential MCS, and nonsequential MCS methods. The latter encompass scenario-based analysis, linearization, and PDF approximation methods.

2. **Possibilistic methods** [155]**:** It relies on fuzzy logic to model uncertainty, particularly useful when historical data is limited or incomplete. The fuzzy set theory describes uncertain input variables using membership functions. The most common techniques within this approach include the α-cut method, used to create crisp intervals from fuzzy sets, and defuzzification methods, which convert fuzzy outputs into precise values for decision-making.

3. **Hybrid possibilistic-probabilistic methods** [156]**:** Combining probabilistic and possibilistic approaches to handle the uncertain input parameters. The most commonly used techniques in this category are the fuzzy-scenario and fuzzy-MCS approaches.

4. **Information gap decision theory** [157]**:** This approach measures the deviation of errors between actual parameters and their estimations. It quantifies the extent to which an unknown parameter can vary while ensuring that the decision-maker achieves a guaranteed minimum income.

5. **Robust optimization** [158]**:** This approach employs uncertainty sets to describe the uncertainty of input parameters. It ensures that the obtained decisions remain feasible and optimal under the worst-case realization of uncertain parameters within the defined set.

6. **Interval analysis** [159]**:** This method assumes that uncertain parameters lie within predefined intervals. It focuses on determining the bounds of output variables by propagating the interval uncertainties through the model. Although similar to probabilistic modeling with a uniform PDF, interval analysis does not require probabilistic assumptions, making it suitable for handling bounding but non-stochastic uncertainties.

Figure 3.1 summarizes the various methodologies employed in the literature for modeling uncertainty in modern power systems. This visual representation offers a clear and concise overview of the diverse approaches used to address uncertainties in electric power systems, laying the foundation for a comprehensive understanding of the modeling techniques discussed.

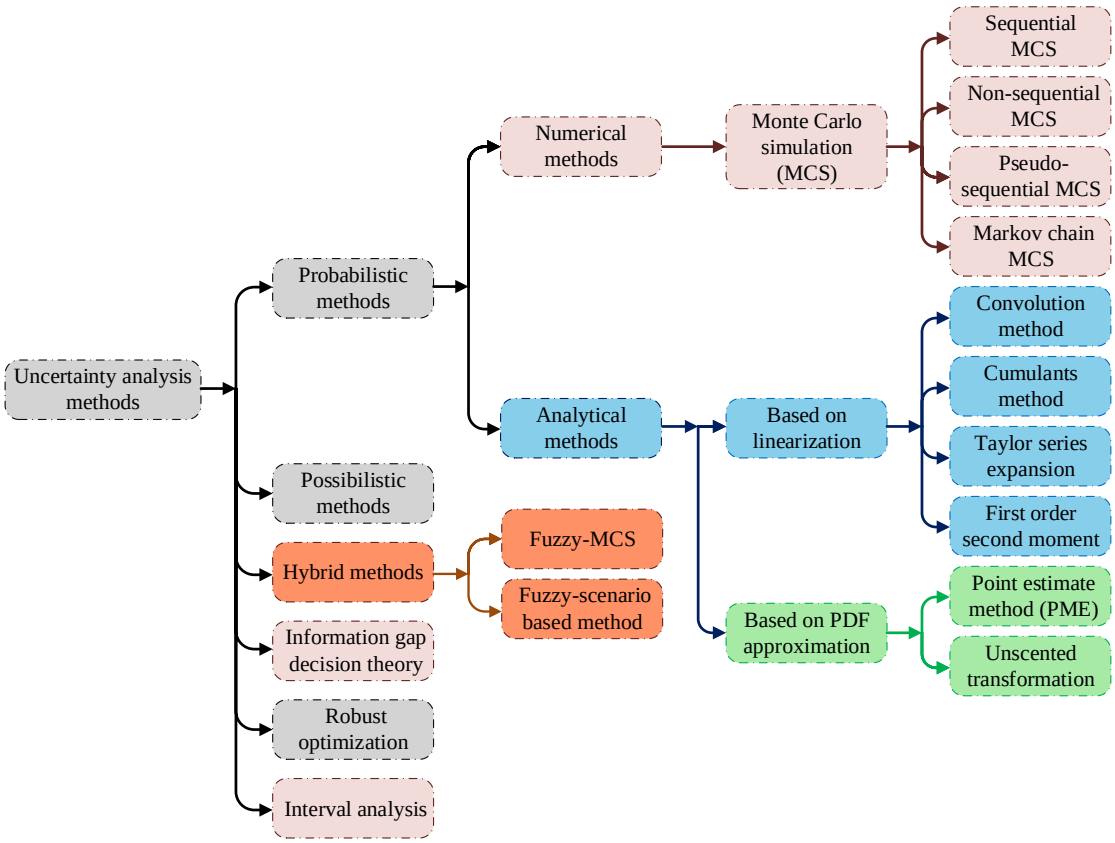

Figure 3.1: Summary of uncertainty modeling approaches used in the literature

3.3 Probability density functions

The PDF mathematically defines the possible range of values that a random variable may assume, along with the probability that the variable's value falls within any measurable subset of this range. The PDF can be continuous or discrete, depending on the nature of the phenomena under analysis. For continuous random variables, the PDF is continuous. Conversely, for discrete random variables, the probability distribution must be represented by a discrete function.

The Cumulative Distribution Function (CDF) describes the probability that a random variable is less than or equal to a specific number. It is inherently related to the PDF and is obtained by integrating the PDF, which accumulates the probabilities of all possible values. Consequently, the CDF is always an increasing function that takes values ranging from a minimum of 0 to a maximum of 1.

Mathematically, the CDF, denoted as $F(x)$, is defined by the following equation:

$$F(x) = \int_{-\infty}^{+\infty} f(x)\,dx \tag{3.1}$$

where, $f(x)$ is the PDF. Conversely, the PDF is obtained by differentiating the CDF as follows:

$$f(x) = \frac{d}{dx}F(x) \tag{3.2}$$

3.3.1 Discrete probability distributions

For discrete random variables X with possible values $x_1, x_2, \ldots, x_n$, the probability distribution is represented by a function that assigns a probability to each discrete value of X. The PDF function for discrete variable can be represented as follows [160]:

$$f(x_i) \geq 0, \quad \forall i \tag{3.3}$$

$$\sum_{i=1}^{n} f(x_i) = 1 \tag{3.4}$$

$$f(x_i) = P(X = x_i) \tag{3.5}$$

The PDF function is non-negative for all x values (Equation (3.3)). The sum of all probabilities associated with the PDF equals 1 (Equation (3.4)). The likelihood of the discrete variable x_i is given by Equation (3.5).

3.3.2 Continuous probability distributions

For a continuous random variable X, the PDF function can be represented as follows [160]:

$$f(x_i) \geq 0, \quad \forall i \tag{3.6}$$

$$\int_{-\infty}^{+\infty} f(x)\,dx = 1 \tag{3.7}$$

$$P(a \leq X \leq b) = \int_a^b f(x)dx \tag{3.8}$$

$$P(X = x_i) = 0 \tag{3.9}$$

The PDF function ($f(x)$) is non-negative for all values of x (Equation (3.6)). The integral of the PDF function over its entire domain is equal to 1 (Equation (3.7)), and the probability of the variable X falling within a range $[a,b]$ is given by Equation (3.8).

Continuous PDFs are defined over an infinite set of points within a continuous interval, where the probability of a single exact point is zero (Equation (3.9)). Hence, probabilities are determined over intervals, with the area under the curve between two distinct points representing the probability for that range, as illustrated in Figure 3.2.

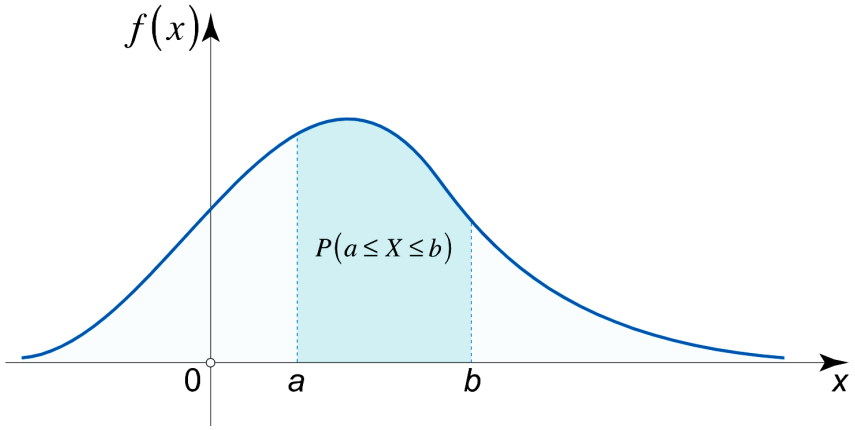

Figure 3.2: Probability over an interval $[a,b]$

3.3.3 Common types of continuous PDFs

Several probability distributions are widely employed in probability and statistics to model different types of continuous random variables. The most commonly used probability distributions are [161]:

- Gaussian distribution or Normal distribution
- Exponential distribution
- Gamma distribution
- Lognormal distribution
- Weibull distribution
- Beta distribution
- Uniform distribution

Figure 3.3 displays the typical curves of each probability distribution [153].

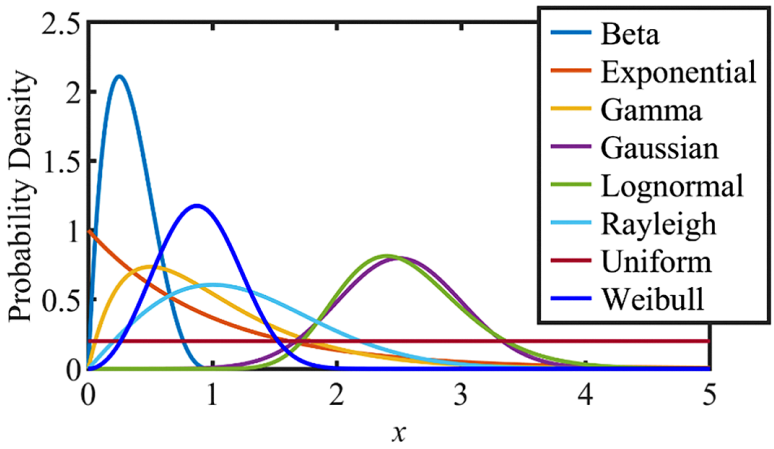

Figure 3.3: Curves of typical continuous PDFs [153]

The key characteristics of each distribution are defined as below:

- **Mean value (μ)**: The mean of a set of values, commonly termed the average or arithmetic mean, represents the central value of the data. For a set of n discrete samples $x_1, x_2, \ldots, x_n$, the mean is calculated as [162]:

$$\mu = \frac{1}{n}\sum_{i=1}^{n} x_i \tag{3.10}$$

  For a continuous function $f(x)$ over the interval $[a,b]$, the mean value is calculated as follows [162]:

$$\mu = \frac{1}{b-a}\int_a^b f(x)\,dx \tag{3.11}$$

  The expected value $E(X)$ of a continuous random variable X is defined by:

$$E(X) = \int_{-\infty}^{\infty} x f(x)\, dx \tag{3.12}$$

- **Standard Deviation (σ)**: It quantifies the dispersion of a dataset relative to its mean. A higher standard deviation indicates more significant variability among data points. The standard deviation is computed as follows [162]:

$$\sigma = \sqrt{\frac{1}{n}\sum_{i=1}^{n}(x_i - \mu)^2} \tag{3.13}$$

- **Variance (Var)**: It measures the spread of data points by calculating the average of the squared deviations from their mean value. The variance is the square of the standard deviation, as [162]:

$$\mathrm{Var} = \sigma^2 = \frac{1}{n}\sum_{i=1}^{n}(x_i - \mu)^2 \tag{3.14}$$

  The variance of the random variable X with a finite mean μ is defined by the following equation [162]:

$$\mathrm{Var}(X) = E\left[(X-\mu)^2\right] = E\left[X^2\right] - (E[X])^2 \tag{3.15}$$

  The standard deviation of X is defined as follows:

$$\sigma(X) = \sqrt{\mathrm{Var}(X)} \tag{3.16}$$

In power system uncertainty modeling, the most frequently used continuous PDFs are discussed below:

3.3.3.1 Gaussian (Normal) distribution

The Gaussian distribution, also known as the normal distribution, is one of the most fundamental probability distributions in statistics, widely used in various fields. The Gaussian distribution is characterized by its bell-shaped curve and is defined by the following PDF [161]:

$$f(x) = \frac{1}{\sigma\sqrt{2\pi}} e^{-\frac{(x-\mu)^2}{2\sigma^2}}, \quad -\infty < x < \infty \tag{3.17}$$

where x represents any possible value that the measurement can assume. μ is the mean, determining the center of the distribution. σ is the standard deviation of the

distribution, and σ^2 is the variance, which controls the spread of the distribution. The expected value and variance of a normal distribution are given by:

$$E(X) = \mu \tag{3.18}$$

$$\text{Var}(X) = \sigma^2 \tag{3.19}$$

Random variables with different means and variances can be modeled by the Gaussian (Normal) PDF with appropriately selected parameters for the center and spread of the distribution. Figure 3.4 gives an example of several Gaussian distributions with selected values of μ and σ^2.

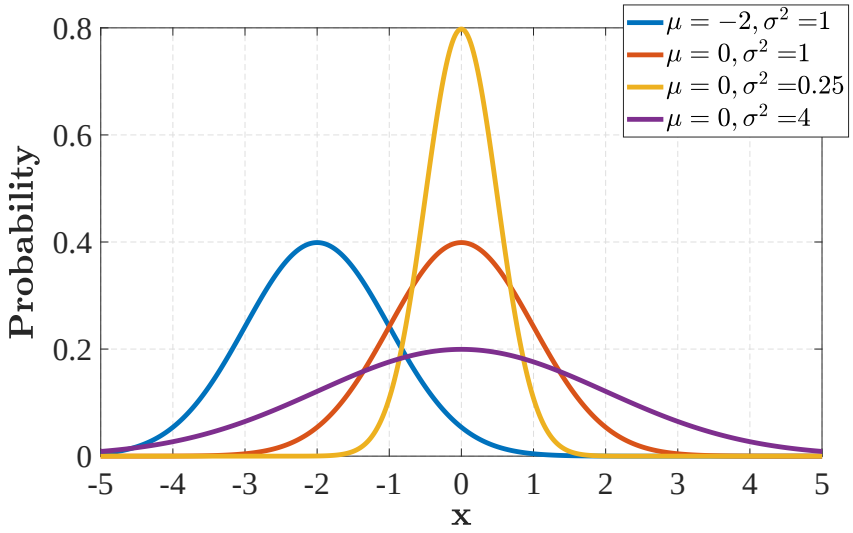

Figure 3.4: Gaussian PDFs with chosen values of μ and σ^2

3.3.3.2 Weibull distribution

The Weibull distribution is commonly employed to describe various types of observed component failures and natural phenomena. It is widely used in reliability and survival analysis, failure modeling, and wind speed characterization. The distribution's parameters offer substantial flexibility, enabling the representation of systems with increasing, decreasing, or constant failure rates over time. The PDF of the Weibull distribution for a random variable is expressed as follows [163]:

$$f(x) = \left(\frac{k}{c}\right)\left(\frac{x}{c}\right)^{k-1} e^{-(\frac{x}{c})^k}, \quad x > 0 \tag{3.20}$$

where $k > 0$ is the shape parameter, which determines the behavior of the distribution. $c > 0$ is the scale parameter, which controls the spread of the distribution. The mean value and variance of the Weibull function are [162, 163]:

$$\mu = E(X) = c\Gamma(1+k^{-1}) \tag{3.21}$$

$$\sigma^2 = \mathrm{Var}(X) = c^2\Gamma(1+2k^{-1}) - \mu^2 \tag{3.22}$$

Where the Gamma function Γ is defined as:

$$\Gamma(x) = \int_0^\infty t^{x-1}e^{-t}\,dt \tag{3.23}$$

Figure 3.5 illustrates the flexibility of the Weibull PDF through curves generated for various selected values of shape parameter k and scale parameter c.

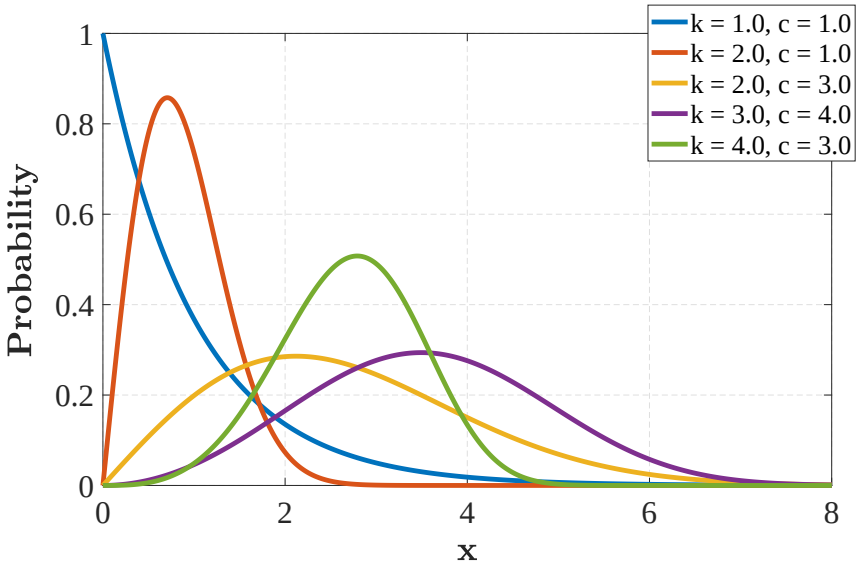

Figure 3.5: Weibull PDF with chosen values of k and c

- **Rayleigh distribution:** A special case of the Weibull distribution with a shape parameter $k = 2$, where the mean and variance are given by [163]:

$$\mu = c\frac{\sqrt{\pi}}{2}, \quad \sigma^2 = \frac{(4-\pi)}{4}c^2 \tag{3.24}$$

The key advantages of the Weibull distribution are cited as follows [163]:

1. It is defined by two parameters (shape k and scale c), making it more general and flexible than the single-parameter Rayleigh distribution, while being less complex than five-parameter models such as the bivariate normal distribution.

2. Numerous studies have demonstrated that the Weibull distribution provides an accurate fit to wind speed data collected across diverse geographic regions.

3. When the Weibull parameters at a specific height are known, reliable methodologies exist for estimating the corresponding parameters at other heights.

The characteristics of wind speed are influenced by several environmental factors, including geographical location, topography, and local climatic conditions. These characteristics can be effectively estimated through statistical analysis of observed wind speed frequency distributions in the target region.

3.3.3.3 Beta distribution

The beta distribution is a continuous probability distribution defined on the interval $[0,1]$. It is commonly used in Bayesian statistics, reliability analysis, and modeling uncertainties in power systems and renewable energy. The beta distribution for a random variable is expressed as [161]:

$$f(x;\alpha,\beta) = \frac{\Gamma(\alpha+\beta)}{\Gamma(\alpha)\Gamma(\beta)} x^{\alpha-1}(1-x)^{\beta-1}, \quad 0 < x < 1 \tag{3.25}$$

where $\alpha, \beta > 0$ are the shape parameters and Γ is the gamma function. The mean value and variance of the beta distribution are:

$$\mu = E[X] = \frac{\alpha}{\alpha+\beta} \tag{3.26}$$

$$\sigma^2 = \mathrm{Var}(X) = \frac{\alpha\beta}{(\alpha+\beta)^2(\alpha+\beta+1)} \tag{3.27}$$

The parameters α and β determine the shape of the beta PDF, allowing it to take various forms. As shown in Figure 3.6, when $\alpha = \beta$, the distribution is symmetric about $x = 0.5$. However, different choices of α and β result in asymmetric distributions.

The Beta distribution offers several advantages when modeling random variables bounded within a finite interval, such as solar irradiance or PV power output:

1. It is defined on the interval $[0,1]$, making it well-suited for representing normalized quantities such as solar power outputs, probabilities, and proportions.

2. With two shape parameters (α and β), the Beta distribution provides a high degree of flexibility, allowing it to represent a wide variety of distribution shapes (e.g., uniform, U-shaped, skewed, or bell-shaped).

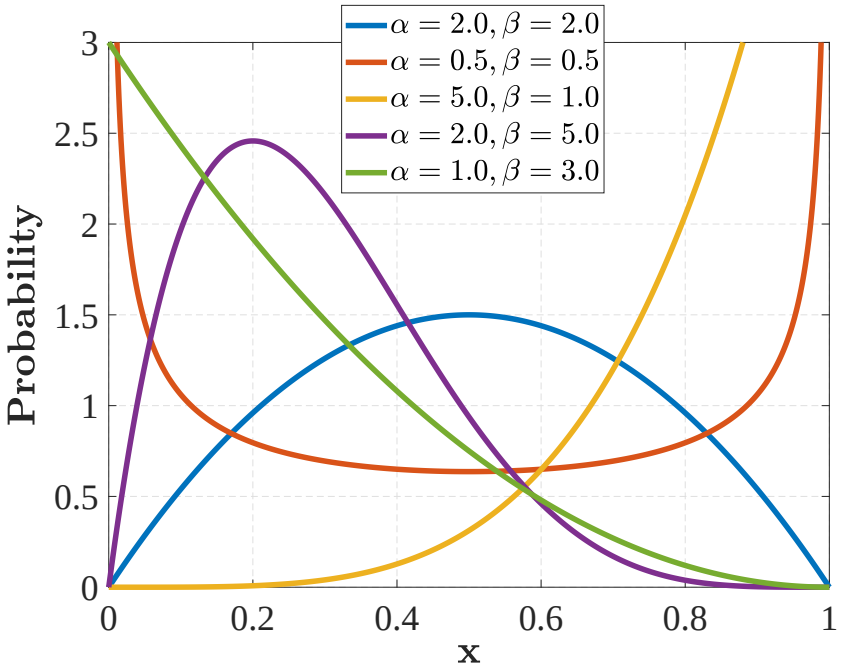

Figure 3.6: Beta PDFs with chosen values of α and β

3. Several previous studies have confirmed that the Beta distribution accurately models the variability of solar irradiance and PV power generation across different climate zones.

4. Unlike the Gaussian distribution, the Beta distribution inherently avoids assigning probability to physically impossible outcomes, such as negative values, ensuring realistic modeling of bounded physical phenomena.

3.4 Modern power systems uncertainties modeling

This section details the modeling approach for various uncertainties. First, different time-varying voltage-dependent load models are defined. Subsequently, the uncertainties associated with wind generator power and solar photovoltaic generator power, which depend on meteorological factors such as wind speed, solar irradiance, and ambient temperature, are thoroughly analyzed. Thus, an integrated generation-load model is developed.

3.4.1 Load modeling

The time-varying voltage-dependent load model, also known as the time-varying load model, represents a load that fluctuates based on both time and voltage. Accordingly,

the voltage-dependent load model presented in [164], which accounts for time-varying load at a given period t, is expressed as follows:

$$\begin{cases} P_k(t) = P_{ok}(t) \times V_k^{\alpha}(t) \\ Q_k(t) = Q_{ok}(t) \times V_k^{\beta}(t) \end{cases} \tag{3.28}$$

Where P_k represents the active power and Q_k denotes the reactive power injected at bus k and time t. P_{ok} is the nominal active load, while Q_{ok} is the nominal reactive load at the rated voltage at bus k. $V_k(t)$ is the per-unit voltage magnitude at bus k, and the parameters α and β are, respectively, the voltage exponents corresponding to the active and reactive load voltage, as presented in Table 3.1 [165].

Table 3.1: Voltage-dependent load types and their corresponding exponents [165]

Load types	α	β
Constant	0	0
Residential	0.92	4.04
Commercial	1.51	3.40
Industrial	0.18	6.00

3.4.2 Renewable energy resources (RESs) modeling

3.4.2.1 Wind speed modeling

The stochastic wind speed variation over each period t (*1 hour* in this study) is modeled using the Weibull PDF [166, 167]. The Weibull PDF for wind speed w^t (in m/s) at the t^{th} hour can be expressed as the following equation:

$$f_w^t(w) = \left(\frac{k^t}{c^t}\right)\left(\frac{w^t}{c^t}\right)^{(k^t-1)} \times \exp\left[-\left(\frac{w^t}{c^t}\right)^{k^t}\right] \text{ for } w^t > 0,\ c^t > 0 \text{ and } k^t > 0 \tag{3.29}$$

The shape factor k^t and scale factor c^t at the t^{th} hour are determined using the following expressions:

$$k^t = \left(\frac{\sigma_w^t}{\mu_w^t}\right)^{-1.086} \tag{3.30}$$

$$c^t = \frac{\mu_w^t}{\Gamma(1+1/k^t)} \tag{3.31}$$

here, μ_v^t and σ_v^t represent the mean and standard deviation of wind speed, which is computed using the historical data for each t^{th} hour

3.4.2.2 Solar irradiance modeling

The stochastic variability of solar irradiance can be described using the beta PDF, as in [166, 168]. Over each timeframe 't' (considered as *1 hour* in this study), the beta PDF for solar irradiance i^t in (kW/m^2) is expressed as follows:

$$f_i^t(i) = \begin{cases} \frac{\Gamma(\alpha^t+\beta^t)}{\Gamma(\alpha^t)\Gamma(\beta^t)}(i^t)^{\alpha^t-1}(1-i^t)^{\beta^t-1}, & 0 \le i^t \le 1;\ \alpha^t, \beta^t \ge 0 \\ 0, & \text{otherwise} \end{cases} \tag{3.32}$$

where β^t and α^t represent the shape parameters of the beta PDF, and Γ denotes the gamma function.

The shape parameters of the beta PDF can be determined using the mean (μ_i^t) and standard deviation (σ_i^t) of solar irradiance for the corresponding period.

$$\beta^t = (1-\mu_i^t)\left(\frac{\mu_i^t(1+\mu_i^t)}{(\sigma_i^t)^2} - 1\right) \tag{3.33}$$

$$\alpha^t = \mu_i^t \times \frac{\beta^t}{1-\mu_i^t} \tag{3.34}$$

3.4.2.3 Power generation model

To accurately estimate the power produced by WT and solar PV arrays, the continuous PDF for a specified time frame is divided into intervals, or spans, where the wind speed and solar irradiance fall within defined ranges [103]. Consequently, the power outputs from both the WT and solar PV systems are calculated based on all potential probabilities within each hour.

a) Power generation by WT

The average power output of the WT for a specific hour 't', denoted as (P_{WT}^t), is computed as follows [169, 170]:

$$P_{WT}^t = \sum_{k=1}^{N_w} PG_{WTk} \times P_w(w_k^t) \tag{3.35}$$

Where k represents the phase variable and N_w denotes the total number of discrete wind speed phases, w_k^t refers to the wind speed in the k^{th} phase at the t^{th} hour.

The probability of wind speed for each phase k during any given hour is estimated using:

$$P_w(w_k^t) = \int_{w_{k,min}^t}^{w_{k,max}^t} f_w^t(w)dw \quad \text{for} \quad k = 1 \dots N_w \tag{3.36}$$

The power output of the WT is influenced by the wind speed at its location and the turbine's specific characteristics, with the relationship following the non-linear performance curve defined by the manufacturer. The generated power of the WT at the average wind speed w_{ak} for the k^{th} phase can be calculated using [166]:

$$PG_{WTk} = \begin{cases} 0 & w_{ak} < w_{cin} \quad \text{or} \quad w_{ak} > w_{cout} \\ \left(\alpha \times w_{ak}^3 + \beta \times P_{rated}\right) & w_{cin} \leq w_{ak} \leq w_N \\ P_{rated} & w_n \leq w_{ak} \leq w_{cout} \end{cases} \tag{3.37}$$

where P_{rated} refers to the WT's maximum power output, and w_{cout} represents the wind speed at which the turbine ceases operation (cut-out speed). The constants α and β are calculated based on the cut-in wind speed w_{cin} and the nominal wind speed w_n, as expressed in the following equations:

$$\alpha = \frac{P_{rated}}{\left(w_n^3 - w_{cin}^3\right)} \tag{3.38}$$

$$\beta = \frac{w_{cin}^3}{\left(w_{cin}^3 - w_n^3\right)} \tag{3.39}$$

According to Equation (3.37), wind power generation exhibits a discrete pattern across different wind speed regions. The non-linear power curve illustrates the theoretical correlation between wind speed and the wind turbine's output, which is primarily controlled by three wind speed levels: the cut-in speed w_{cin}, the rated speed w_{rated}, and the cut-out speed w_{cout} [171, 172]. These levels define four distinct operational regions of the turbine, with their respective probabilities as plotted in Figure 3.7.

At low wind speeds in the **first region**, below the cut-in speed w_{cin}, the turbine does not generate power due to insufficient wind speeds. In the **second region**, once the wind speed exceeds w_{cin}, the turbine begins generating power, which increases nonlinearly with the wind speed until it reaches the rated wind speed w_{rated}, where the turbine produces its maximum output P_{rated}. Beyond this region, the power output remains constant in the **third region** thanks to power control mechanisms until the wind speed reaches the cut-out speed w_{cout} (see Figure 3.7). Finally, in the **fourth**

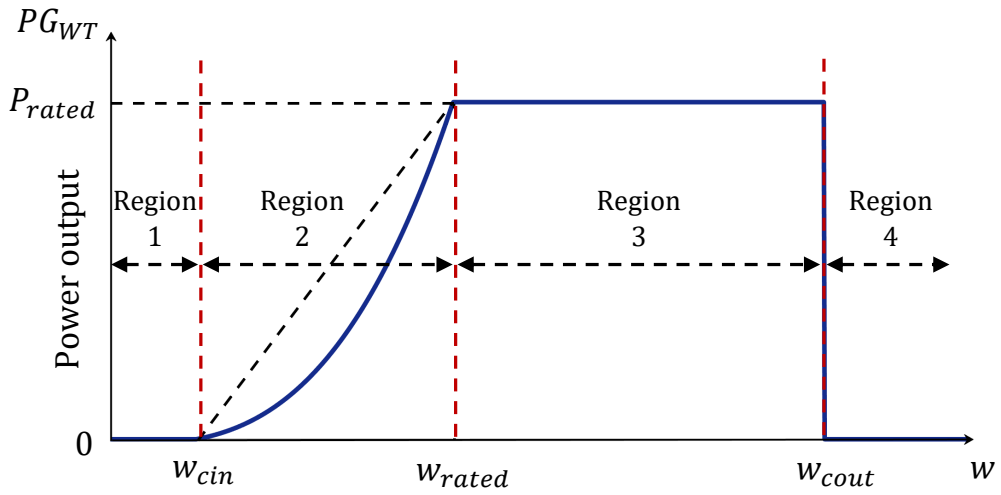

Figure 3.7: Non-linear power curve of a wind turbine

region, when the wind speed exceeds w_{cout}, the turbine stops working to prevent damage.

b) Power generation by solar PV

The average power output of solar PV at a given hour 't', denoted as (P_{PV}^t), can be calculated as follows:

$$P_{PV}^t = \sum_{k=1}^{N_i} PG_{PVk} \times P_i(i_k^t) \tag{3.40}$$

where N_i symbolizes the total number of discrete solar irradiance phases, and i_k^t refers to the k^{th} phase of solar irradiance at the t^{th} hour. The probability of solar irradiance for each phase k at any given hour is estimated as follows:

$$P_i(i_k^t) = \int_{i_{k,min}^t}^{i_{k,max}^t} f_i^t(i)di \tag{3.41}$$

The power output of solar PV arrays depends on both the solar irradiance and the ambient temperature at the installation site. The power generated by the solar PV panels at the average solar irradiance (i_{ak}) for the k^{th} phase can be estimated as demonstrated in Equation (3.42) [76, 169].

$$PG_{PVk}(i_{ak}) = N_{PVmod} \times FF \times V_k \times I_k \tag{3.42}$$

where N_{PVmod} indicates the total count of PV modules, FF refers to the fill factor, and V_k and I_k represent the voltage and current of the cell at the k^{th} phase, respectively. These parameters can be determined using the following equations [76, 169]:

$$V_k = V_{oc} - K_v \times T_{ck} \tag{3.43}$$

$$FF = \frac{V_{MMP} \times I_{MMP}}{V_{oc} \times I_{sc}} \tag{3.44}$$

$$T_{ck} = T_a^t + i_{ak}\left(\frac{N_{OT} - 20}{0.8}\right) \tag{3.45}$$

$$I_k = i_{ak}[I_{sc} + K_i(T_{ck} - 25)] \tag{3.46}$$

In the equations above, $T_{ck}(^\circ C)$ represents the cell temperature at the k^{th} phase, K_v and K_i are the temperature coefficients for voltage $(V/^\circ C)$ and current $(A/^\circ C)$, respectively. V_{MMP} and I_{MMP} denote the voltage (V) and current (A) at the maximum power point, while V_{oc} and I_{sc} represent the open circuit voltage (V) and short circuit current (A), respectively. N_{OT} is the nominal operating temperature of the cell $(^\circ C)$, and T_a^t is the hourly average ambient temperature $(^\circ C)$.

3.5 Conclusion

This chapter provided a concise yet comprehensive overview of the methods employed to address parameter uncertainties in modern power systems, exploring various approaches such as probabilistic and possibilistic methods, hybrid models, information gap decision theory, robust optimization, and interval analysis. Different voltage-dependent load models with time-varying characteristics were defined to reflect realistic consumption patterns. Additionally, the stochastic behavior of renewable energy sources is modeled using appropriate probability density functions, specifically the Beta and Weibull distributions for solar photovoltaic and wind turbine power generations, respectively. This methodological framework offers valuable guidance for planners and operators, enabling robust and informed decision-making in the face of increasing uncertainty and variability inherent in modern power systems.

Chapter 4

Optimization and Metaheuristic Algorithms

4.1 Introduction

Optimization has emerged as a powerful tool for solving complex engineering and mathematical problems. It plays a central role in identifying the most effective solutions by adjusting decision variables within a defined search space and according to a specified quantitative criterion. The goal may be to either maximize or minimize a specific objective function, depending on the nature of the problem.

In electrical engineering, optimization presents multiple challenges, stemming from both the inherent characteristics of the problem and the requirements of the developer. These challenges may involve linear, nonlinear, integer, or stochastic optimization, each introducing different complexities and uncertainty. Simultaneously, user needs, such as achieving global optimality, solution reliability and accuracy, reasonable computational time, etc., must be satisfied. Addressing these challenges has been the focus of numerous research employing various optimization techniques. Deterministic methods typically depend on calculating a search direction based on derivatives concerning system design parameters. These methods are only effective in the limited case when the desired solution is assumed to be close to a known starting point for this search. To overcome this limitation, researchers have increasingly explored the development and application of metaheuristic algorithms for complex design problems in electrical engineering.

A metaheuristic algorithm is a search strategy designed to find the optimal or near-optimal solutions to complex optimization problems that are otherwise difficult or impractical to solve using traditional deterministic methods [173]. In real-world scenarios characterized by incomplete information and limited resources, obtaining an exact solution is often unfeasible, making the use of metaheuristics both imperative and

efficient to find a quasi-optimal solution. Their emergence represents one of the most significant advancements in optimization over recent decades. Numerous metaheuristic algorithms have been proposed and successfully applied across multiple applications to tackle nonlinear, non-convex, and large-dimensional optimization problems. Those techniques rely on probabilistic and random transition mechanisms. Consequently, metaheuristics are particularly advantageous as they have proven to be a compromise tool for identifying the best solutions with less computational effort than deterministic or greedy approaches, which enables effective decision-making and optimal resource allocation in complex systems [174].

In this chapter, we present the optimization definition and principle and explore the widely used nature-inspired metaheuristic optimization algorithms in the electrical engineering field, such as Grey Wolf Optimization (GWO) and Jellyfish Search Optimization (JSO), as well as two recently developed algorithms, namely the Black-Winged Kite Algorithm (BKA) and the Frilled Lizard Optimization (FLO), all of which are proposed and implemented in the present study. By critically analyzing the advantages and limitations of various metaheuristic approaches, researchers and practitioners can make more informed and strategic decisions in selecting and tailoring these methods to address complex optimization challenges in distribution networks. We will also introduce an Improved Frilled Lizard Optimization (IFLO) algorithm, designed to address complex optimization problems with enhanced efficiency and robustness. Specifically, we will enhance the standard FLO algorithm by incorporating three advanced strategies to improve its search capabilities and achieve a more effective balance between the exploration and exploitation phases. The chapter concludes with a comprehensive evaluation of the IFLO performance, using a set of 23 benchmark functions. This assessment includes a comprehensive comparison with several state-of-the-art metaheuristic algorithms, offering insights into the efficacy of the proposed IFLO. The analysis incorporates statistical evaluations, convergence curves, and boxplots generated from multiple independent runs.

4.2 Optimization process

Optimization is often reduced to mathematical solution techniques, to which the encountered failures are subsequently attributed. However, as with most problems to be solved, optimization must follow a systematic approach consisting of different steps, as illustrated in Figure 4.1. This process begins with clearly defining the problem and formulating a mathematical model, followed by selecting an appropriate solution method to explore potential solutions. While these steps may proceed sequentially,

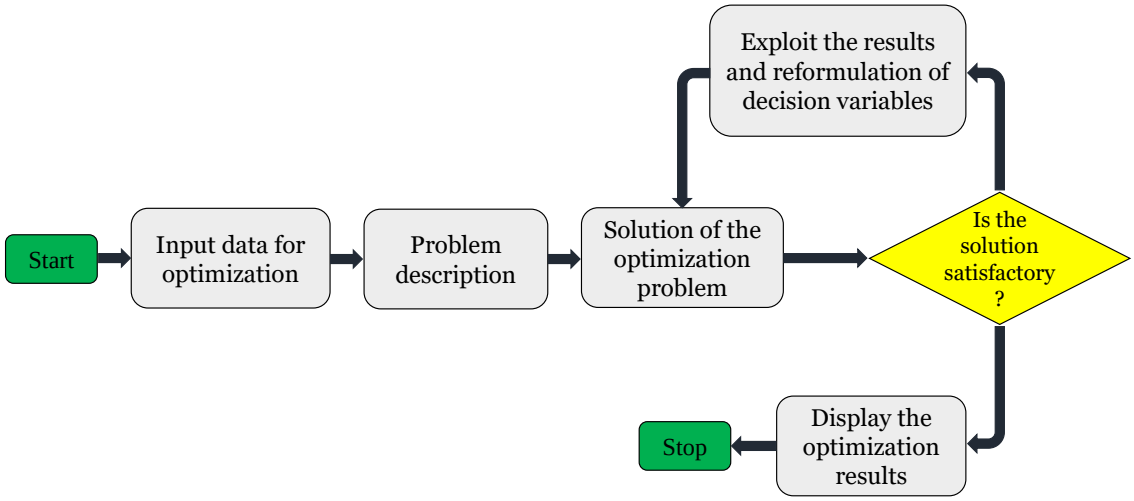

Figure 4.1: Steps for solving an optimization problem

iterative processes and feedback loops are often essential to ensuring optimization objectives are met [175, 176]. The process continues until the convergence criterion is satisfied.

4.3 Formulation of the optimization problem

The formulation of the optimization problem is a fundamental step in the design process, as it directly influences the success of subsequent stages. This stage is not straightforward, since the selection of design variables is seldom unique, and current computational resources can only handle a limited number of variables. The design problem, as defined by the specifications, must be translated into an equivalent mathematical formulation. This transformation is the most delicate phase of the design process, as multiple formulations are often possible, especially in defining the objective functions and constraints that represent the system's performance. Specifically, it involves the definition of [177]:

4.3.1 Objective function

The objective function represents one of the key outputs of the optimization problem, defining the goal it aims to achieve. It can typically assume one of two forms: either a cost function to be minimized, such as production cost, energy consumption, operational expenditure, or development time, or a performance indicator to be maximized, including parameters like profit, system efficiency, or transmission factor. The choice of the desired objective function is essential in formulating the optimization problem,

as it not only specifies the nature of the optimization problem but also significantly influences the modeling strategy employed for its resolution.

In single-objective optimization, the determination of the objective function is generally straightforward. For example, when the task involves identifying the design parameters of a system that meets predefined performance criteria, the objective function may be expressed as the deviation between the achieved and the desired performance metrics. However, in more complex optimizations requiring accommodating multiple objectives, some of which may be conflicting, all objectives must be considered simultaneously. This introduces additional complexity to the optimization process, necessitating an appropriate and balanced objective function formulation. A well-defined objective function is therefore essential for guiding the optimization algorithm towards achieving a well-balanced and satisfactory solution [178].

4.3.2 Control parameters

Control parameters or decision variables are adjustable factors within a system that directly influence its performance. These parameters can encompass various forms, such as geometric dimensions, material properties, or structural configurations. They can be either quantitative or qualitative and may be continuous or discrete. The identification and number of control parameters play a crucial role in defining the structure and complexity of the optimization problem. Raising the number of adjustable variables can expand the search space, thereby increasing the possibility of discovering better solutions. However, this also leads to increased computational efforts and optimization processing times [178, 179].

4.3.3 Constraints

Constraints are commonly imposed by the designer and play a crucial role in ensuring that the optimization process produces feasible and robust solutions. These constraints may encompass requirements related to permissible geometric configurations, the physical validity of the adopted model, production capabilities, safety standards, or operational limitations necessary for proper system functioning [178]. Additionally, device-specific constraints might involve adherence to operational temperature ranges, environmental conditions, or compliance with relevant regulatory standards throughout the device's lifecycle. Such constraints are formulated based on the designer's expertise and specific objectives, thereby guiding the optimization algorithm toward solutions that are both technically sound and contextually appropriate. Ethical considerations,

strategic requirements, and personal design preferences can also be encoded to shape the solution space [180, 181].

By incorporating these constraints, the optimization process delivers optimal outcomes that are both feasible and applicable in real-world scenarios.

4.4 Optimization methods

Optimization methods refer to a wide range of techniques employed to find the best possible solution to a problem within a defined search space and a given set of constraints. These methods are essential in various fields, including engineering, economics, and computer science, and they aim to either maximize or minimize an objective function, depending on the problem. Optimization problems in electrical engineering pose several challenges, including user requirements, problem characteristics, and computational time constraints. While many studies rely on exact solution methods that guarantee optimality, there are some cases where solutions of satisfactory quality are sought without the guarantee of optimality but with the benefit of reduced computational time [11, 182].

Optimization methods can broadly be classified into two main categories: conventional methods and metaheuristic methods.

4.4.1 Conventional methods

Conventional methods involve techniques based on well-established mathematical frameworks for problem-solving, commonly categorized into two groups:

4.4.1.1 Analytical techniques

Analytical techniques model the optimization problem using a set of mathematical equations and aim to derive a direct or exact solution through conventional analytical procedures. These methods are valued for their straightforward implementation and short computation time while ensuring convergence toward optimal solutions [74]. However, their applicability and computational efficiency can be limited when dealing with large-scale or highly complex systems.

4.4.1.2 Deterministic techniques

Deterministic techniques form a class of mathematical approaches that iteratively improve an initial solution to converge toward an optimum. These techniques are conventionally divided into two categories: Linear Programming, which addresses

problems with linear objective functions and constraints, and Nonlinear Programming, which accommodates nonlinearity in either the objective function or the constraints. However, these techniques suffer from limitations including computational complexity as the number of decision variables grows, requiring substantial computation time, and may become trapped in local optima when applied to non-convex and large-scale optimization problems [183, 184]

4.4.2 Metaheuristic methods

The term metaheuristic is derived from two Greek words: "meta," meaning "beyond" or "at a superior level," and "heuristic," referring to the act of "finding" or "discovering." [185]. Metaheuristics are a class of optimization algorithms, also called approximation algorithms, designed to address complex and computationally challenging problems where traditional mathematical methods may be ineffective or impractical. These algorithms offer a solution to optimization problems often faced by engineers and decision-makers. Typically, metaheuristics are stochastic, meaning they incorporate randomness, and iterative, meaning they refine solutions progressively over multiple iterations. As search algorithms, they aim to understand the structure of a problem and approximate its optimal solution effectively [177].

The search process in metaheuristics is guided by two primary phases: exploration and exploitation, with strategies inspired by natural phenomena, such as biological evolution, animal behavior, and physical processes. The exploration phase enables the algorithm to investigate unexplored areas of the solution space in search of potential local optima. In contrast, the exploitation phase utilizes the insights gained during the exploration phase to focus on the most promising regions of the solution space and refine the search toward the nearest local optimum. In this later phase, the goal is to achieve the best possible solution [11].

These methods are considered global optimization techniques, as their primary objective is to identify the global optimum of a given function while avoiding entrapment in local optima. Figure 4.2 illustrates the distinction between local and global optima in an optimization problem.

4.5 Various optimization algorithms

This section presents a detailed overview of the optimization algorithms developed and implemented in Chapter 5, including the Grey Wolf Optimization (GWO) and the Jellyfish Search Optimization (JSO), as well as two recently developed methods: the

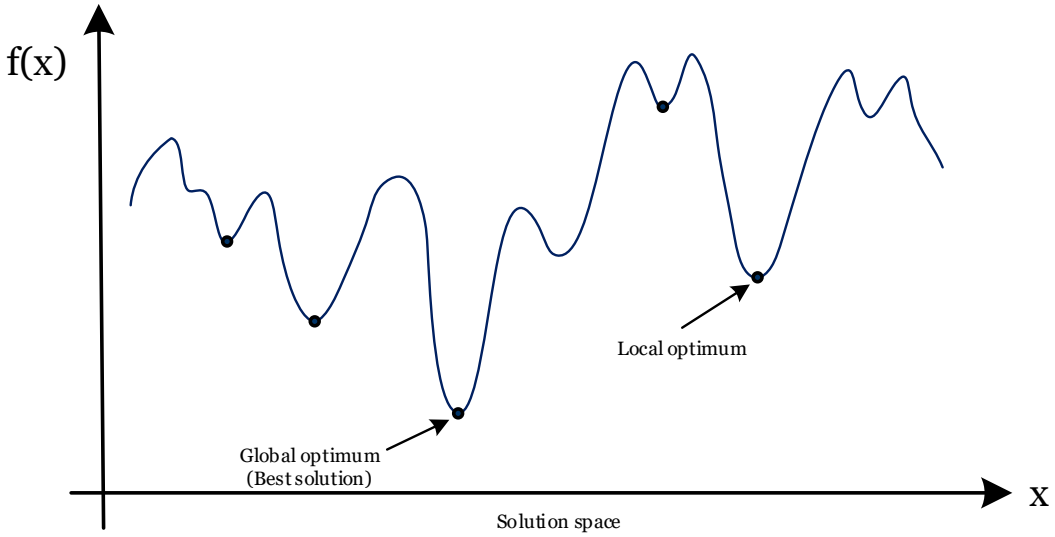

Figure 4.2: Local optima and global optima

Black-Winged Kite Algorithm (BKA) and the Frilled Lizard Optimization (FLO). The latter will be improved and introduced in the next section.

4.5.1 Grey wolf optimization (GWO) algorithm

The Grey Wolf Optimizer (GWO) is a biologically inspired algorithm introduced by Mirjalili and Lewis [186]. The GWO simulates the cooperative hunting behavior and hierarchical leadership structure of grey wolves in the wild. To mathematically model the social hierarchy of wolves, they are categorized into four groups based on their fitness levels. The best solution is designated as the alpha (α) wolf. The subsequent solutions, ranked second and third, are termed beta (β) and delta (δ) wolves. The remaining solutions are termed as omega (ω), representing the subordinate wolves that follow the guidance of the top three to achieve the global optimum solution. Figure 4.3 illustrates the social hierarchy of grey wolves in nature.

The optimization process in GWO is structured around three main behavioral phases observed in wolf hunting: searching for prey, encircling the prey, and attacking the prey. The algorithm begins by initializing a population of candidate solutions (wolves) with randomly generated positions. These wolves then interact and evolve according to the modeled social dynamics, driving the search toward global optimum.

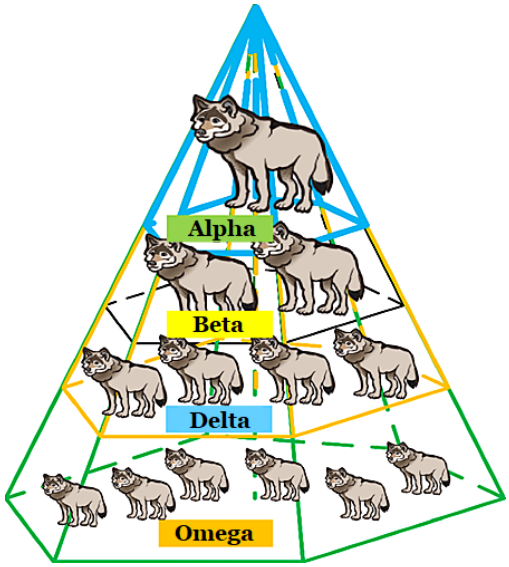

Figure 4.3: Hierarchical levels of the grey wolves [186]

4.5.1.1 Hunting strategy: Exploration phase

As previously described, grey wolves strategically surrounding their prey during the hunting process (see Figure 4.4 (a)) To mathematically model this encircling behavior, the following equations have been developed [186]:

$$\vec{M} = |\vec{C} \cdot \vec{X}_p(t) - \vec{X}_w(t)| \tag{4.1}$$

$$\vec{X}(t+1) = \vec{X}_p(t) - \vec{A} \cdot \vec{M} \tag{4.2}$$

In the above equations, t denotes the current iteration number; $\vec{M}$ represents the distance vector between a grey wolf and its prey; $\vec{X}_p$ refers to the position vector of the prey, while $\vec{X}$ indicates the position vector of a grey wolf. The operator "$\cdot$" denotes element-wise multiplication. The coefficient vectors $\vec{A}$ and $\vec{C}$ are computed as follows:

$$\vec{A} = 2\vec{a} \cdot \vec{r}_1 - \vec{a} \tag{4.3}$$

$$\vec{C} = 2 \cdot \vec{r}_2 \tag{4.4}$$

The parameter $\vec{a}$ decreases linearly from 2 to 0 over the course of iterations, thereby balancing exploration and exploitation. The vectors $\vec{r}_1$ and $\vec{r}_2$ denote random values uniformly distributed within the interval $[0, 1]$.

Operating a simulated social hierarchy and encircling mechanism, the GWO algorithm efficiently navigates the search space to identify optimal solutions for the

optimization problem. The algorithm holds the top three candidate solutions at each iteration, labeled as α, β, and δ, which serve as guiding leaders. The remaining search agents, including the ω wolves, update their positions based on these select solutions. This mechanism is mathematically realized through the iterative application of the following equations, which emulate the hunting dynamics of grey wolves and enable the algorithm to exploit promising regions of the solution space:

$$\vec{M}_\alpha = |\vec{C}_1 \cdot \vec{X}_\alpha - \vec{X}| \tag{4.5}$$
$$\vec{M}_\beta = |\vec{C}_2 \cdot \vec{X}_\beta - \vec{X}| \tag{4.6}$$
$$\vec{M}_\delta = |\vec{C}_3 \cdot \vec{X}_\delta - \vec{X}| \tag{4.7}$$

$$\vec{X}_1 = \vec{X}_\alpha - \vec{A}_1 \cdot \vec{M}_\alpha \tag{4.8}$$
$$\vec{X}_2 = \vec{X}_\beta - \vec{A}_2 \cdot \vec{M}_\beta \tag{4.9}$$
$$\vec{X}_3 = \vec{X}_\delta - \vec{A}_3 \cdot \vec{M}_\delta \tag{4.10}$$

$$\vec{X}(t+1) = \frac{\vec{X}_1 + \vec{X}_2 + \vec{X}_3}{3} \tag{4.11}$$

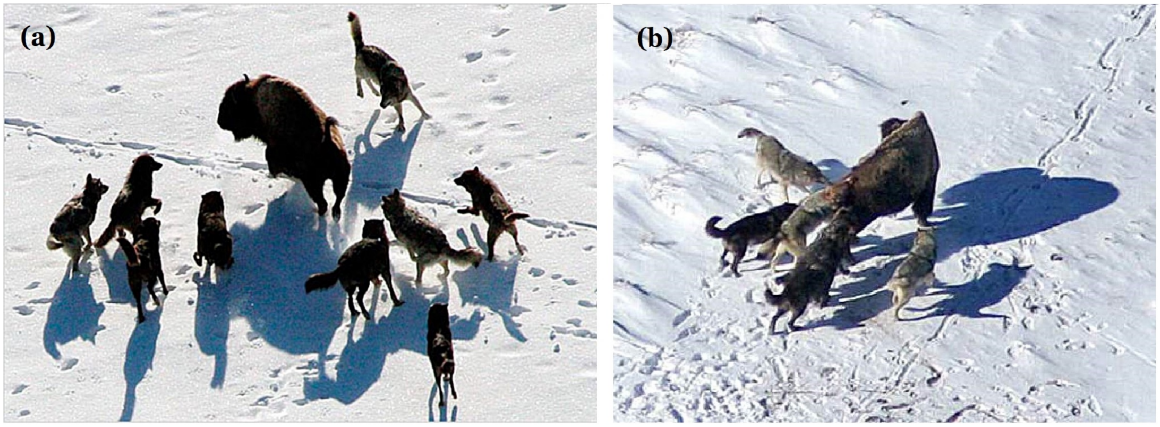

Figure 4.4: (a) Surrounding the prey, (b) Attacking the prey [186]

4.5.1.2 Attacking strategy: exploitation phase

Grey wolves terminate the hunt by attacking the prey once it ceases to move, as illustrated in Figure 4.4(b). To mathematically represent this behavior of approaching the prey, the parameters a and A are decreased linearly with the progression of iterations. This mechanism causes the search agents to diverge when $|\vec{A}| > 1$ and

converge when $|\vec{A}| < 1$. During each iteration, the three leading wolves, α, β, and δ, are identified and stored as the best solutions found thus far. The remaining wolves update their positions using Equations (4.5) to (4.11), based on the locations of these leading wolves. Finally, the α wolf, once the stopping criterion is satisfied, is considered the optimal solution. Figure 4.5 illustrates the pseudo code of the GWO algorithm.

Initialize the grey wolf population X_i *for* $i = 1, 2, ..., N_{pop}$
Initialize a, A, *and* C
Calculate the fitness of each search agent
$X_\alpha \leftarrow$ *the best search agent*
$X_\beta \leftarrow$ *the second best search agent*
$X_\delta \leftarrow$ *the third best search agent*
while $t <$ *Max number of iterations* **do**
    for *each search agent* **do**
        Update the position of the current search agent using equation (4.11)
    end for
    Update a, A, *and* C
    Calculate the fitness of all search agents
    Update X_α, X_β, *and* X_δ
    $t \leftarrow t + 1$
end while
return X_α

Figure 4.5: Pseudo code of the GWO algorithm

4.5.2 Jellyfish search optimizer (JSO) algorithm

The Artificial Jellyfish Search Optimizer (JSO) is a nature-inspired metaheuristic algorithm introduced by Chou and Truong in 2021 [187]. It emulates the collective movement and the adaptive foraging strategy of jellyfish in the ocean. The algorithm models two primary modes of jellyfish locomotion: passive motion, driven by ocean currents, which facilitates global exploration, and active motion within a swarm, which enables local exploitation by allowing individuals to move toward more promising areas based on the positions of other individuals.

Biologically, jellyfish exhibit features that allow them to control their movements. They contract their underside like an umbrella mechanism to push out water and propel themselves forward. They also use their tentacles to catch and release venom that immobilizes their prey. These natural traits are abstracted into the algorithm's structure to balance exploration and exploitation. A key feature of the JSO is integrating a time control mechanism, which governs the switching between passive and active movement, which then converges into a jellyfish bloom, as depicted in Figure 4.6 [188].

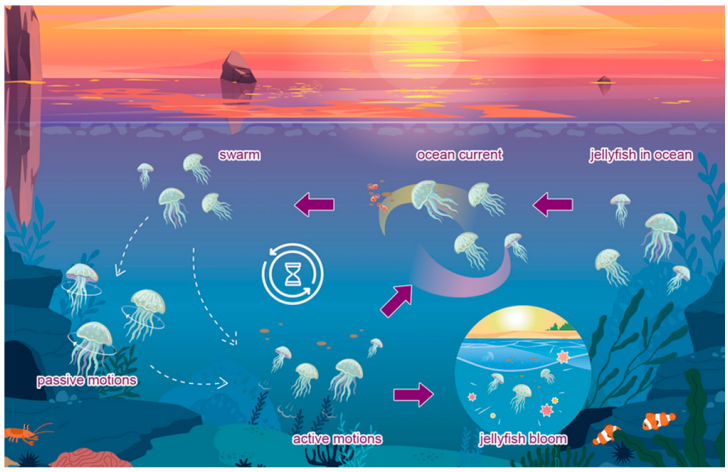

Figure 4.6: Jellyfish movements in ocean [188]

The optimization process begins with a randomly initialized population and iteratively updates the positions of jellyfish until a defined stopping criterion is satisfied. Due to its adaptability, simplicity, and robust performance, JSO has shown competitive performance in addressing a wide range of complex optimization problems.

The following subsections present the mathematical modeling of jellyfish behavior and movements in the ocean.

4.5.2.1 Ocean current

The direction of the ocean current, denoted as $\overrightarrow{\text{trend}}$, is determined by calculating the average of the vectors pointing from each jellyfish's position to the current jellyfish with the best position in the population, using [187]:

$$\overrightarrow{\text{trend}} = P^* - \beta \times \text{rand}(0,1) \times \mu \tag{4.12}$$

where, P^* represents the jellyfish currently occupying the best position within the swarm, β is a distribution coefficient, and μ denotes the mean position of all jellyfish in the population.

The updated position of each jellyfish is then determined by

$$P_i(t+1) = P_i(t) + \text{rand}(0,1) \times (P^* - \beta \times \text{rand}(0,1) \times \mu) \tag{4.13}$$

4.5.2.2 Jellyfish swarm motions

Jellyfish exhibit two distinct types of motions within a swarm: passive motion (Type A) and active motion (Type B). During the initial stages of swarm formation, the majority of jellyfish exhibit Type A motion. However, over time, they increasingly exhibit Type

B motion. The jellyfish's motion of type A, which involves local exploration around the jellyfish's current position and the corresponding updated location of each jellyfish, is mathematically expressed as follows [187]:

$$P_i(t+1) = P_i(t) + \delta \times \text{rand}(0,1) \times (U_{ba} - L_{ba}) \tag{4.14}$$

Here, δ denotes the motion coefficient, while U_{ba} and L_{ba} represent the upper and lower bounds of the search space, respectively.

The jellyfish's motion of type B reflects active movement within the swarm, where each jellyfish adjusts its position based on interactions with other individuals. Specifically, one jellyfish moves toward another based on food availability at their respective locations. Equations (4.15 - 4.17) provide the simulation of type B motion, including the step calculation, direction of motion, and updated location of a jellyfish, as follows [187]:

$$\overrightarrow{\text{Step}} = \text{rand}(0,1) \times \overrightarrow{\text{Direction}} \tag{4.15}$$

$$\overrightarrow{\text{Direction}} = \begin{cases} P_j(t) - P_i(t) & \text{if } h(P_i) \geq h(X_j) \\ P_i(t) - P_j(t) & \text{if } h(P_i) < h(X_j) \end{cases} \tag{4.16}$$

$$P_i(t+1) = P_i(t) + \overrightarrow{\text{Step}} \tag{4.17}$$

where h represents the objective function that evaluates the position P_i.

A time control mechanism is utilized to determine the motion type over time. This mechanism governs both type A and type B motions within the swarm, as well as the movements of jellyfish toward ocean currents. The formulation of the time control mechanism is expressed in the following equation:

$$c(t) = \left| \left(1 - \frac{t}{Max_{iter}}\right) \times (2 \times rand(0,1) - 1) \right| \tag{4.18}$$

where t denotes time, represented as the iteration number, and Max_{iter} refers to the maximum number of iterations, which is a predefined parameter. Figure 4.7 illustrates the pseudo code of the JFO algorithm.

4.5.3 Black-winged kite algorithm (BKA)

The Black-Winged Kite Algorithm (BKA) is a novel nature-inspired optimization method introduced by Jun Wang et al. in 2024 [189]. This algorithm is based on the migratory and predatory behaviors of the black-winged kite, a bird known

Initialize the jellyfish population P_i *for* $i = 1, 2, ..., N_{pop}$
Compute the quantity of food for each jellyfish candidate
$P^* \leftarrow$ *the jellyfish at location currently with most food*
Initialize time: $t = 1$
repeat
  for *each jellyfish* **do**
    Compute the time control (c) *using Equation (4.18)*
    if $c \geq 0.5$ **then** ▷ Jellyfish follows ocean current
      Determine ocean current using Equation (4.12)
      Update the position of jellyfish using Equation (4.13)
    else ▷ Jellyfish moves inside the swarm
      if $rand \geq (1-c)$ **then** ▷ Jellyfish exhibits Type A motion (Passive)
        Update the position of jellyfish using Equation (4.14)
      else ▷ Jellyfish exhibits Type B motion (Active)
        Determine the direction of jellyfish using Equation (4.16)
        Update the position of jellyfish using Equation (4.17)
      end if
    end if
    Check boundaries and compute quantity of food at new location
    Update both the individual position (P_i) *and the best food location* (P^*)
  end for
  $t \leftarrow t + 1$
until $t \geq$ Max number of iterations
Display the best results

Figure 4.7: Pseudo code of the JFO algorithm

for its exceptional migratory patterns and hunting strategies. By emulating these natural behaviors, the BKA effectively explores the solution space and resolves complex optimization problems. The following subsections provide a detailed mathematical modeling of the black-winged kite's biological behavior and search movements within the solution space.

4.5.3.1 Initialization phase

The BKA process begins with the random generation of an initial population. Each candidate solution, representing the position of a black-winged kite (B), is structured in matrix form as follows [189]:

$$B = \begin{bmatrix} B_{1,1} & \cdots & B_{1,k} & \cdots & B_{1,dim} \\ \vdots & \ddots & \vdots & \ddots & \vdots \\ B_{i,1} & \cdots & B_{i,k} & \cdots & B_{i,dim} \\ \vdots & \ddots & \vdots & \ddots & \vdots \\ B_{n,1} & \cdots & B_{n,k} & \cdots & B_{n,dim} \end{bmatrix} \tag{4.19}$$

where n denotes the total number of candidate solutions, *dim* represents the size of the optimization problem, and B_{ij} refers to the j^{th} dimension of the i^{th} black-winged kite. The initial positions of the black-winged kites are generated using a uniform distribution within the predefined search boundaries.

$$P_i = B_{lb} + \text{rand}(B_{Ub} - B_{Lb}), \tag{4.20}$$

where i ranges from 1 to n, B_{Lb} and B_{Ub} represent the lower and upper bounds of the i^{th} black-winged kite in the j^{th} dimension, respectively, and *rand* denotes a uniformly distributed random value in the interval $[0, 1]$.

4.5.3.2 Attacking behavior

As a predator of small grassland mammals and insects, the black-winged kite demonstrates adaptive flight behaviors by adjusting its wing and tail angles according to wind speed. During hunting, it hovers quickly to observe potential prey and then swiftly dives to capture it. This predatory mechanism reflects a combination of exploratory and exploitative search strategies. Figure 4.8(a) shows the hovering phase, where the black-winged kite maintains balance with outstretched wings, while Figure 4.8(b) depicts the moment just before the high-speed rush toward its target. The mathematical model below describes the attack behavior of the black-winged kite [189]:

$$z_{t+1}^{ij} = \begin{cases} z_t^{ij} + k(1 + \sin(r)) \times z_t^{ij}, & \text{if } \rho < r \\ z_t^{ij} + k \times (2r - 1) \times z_t^{ij}, & \text{else} \end{cases} \tag{4.21}$$

with

$$k = 0.05 \times e^{-2 \times \left(\frac{t}{T}\right)^2} \tag{4.22}$$

In the equations above, $z^{ij}t$ and $z^{ij}t+1$ represent the positions of the i^{th} Black-winged kite in the j^{th} dimension at the t^{th} and $(t+1)^{\text{th}}$ iterations, respectively. The variable r represents a uniformly distributed random number in the range $[0, 1]$, while ρ is a constant set to 0.9. T symbolizes the maximum number of iterations, and t indicates the current iteration count.

4.5.3.3 Migration behavior

Bird migration is a complex behavioral process affected by various environmental factors, including climate variability and food availability. To adapt to seasonal changes, many bird species migrate from northern to southern regions during winter

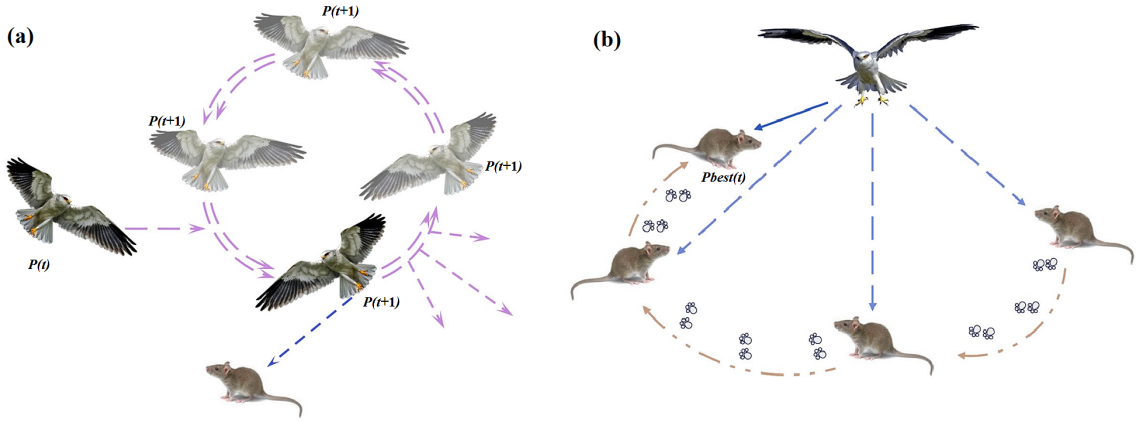

Figure 4.8: (a) Black-winged kites hovering in the air, waiting for attack, and (b) hovering in the air, searching for prey [189]

in search of more favorable living conditions and abundant resources. Usually, this migration is guided by leaders whose navigational abilities are critical to the flock's success. A hypothesis is proposed to model the migration behavior: if the fitness of a given individual in the population is lower than that of a randomly selected one, the leader will give up leadership and integrate into the migrating group, signifying its unsuitability to guide others. Conversely, if the individual's fitness value exceeds that of the random population, it continues to lead the group toward the destination. This mechanism allows the dynamic identification and selection of the best leaders, thereby enhancing the efficiency and success of the migration process. The migration behavior of black-winged kites is modeled mathematically as follows [189]:

$$z_{t+1}^{ij} = \begin{cases} z_t^{ij} + \mathcal{C}(0,1) \times \left(z_t^{ij} - L_i^j\right), & F_i < F_{ri} \\ z_t^{ij} + \mathcal{C}(0,1) \times \left(L_i^j - y \times z_t^{ij}\right), & \text{else} \end{cases} \tag{4.23}$$

with

$$y = 2 \times \sin\left(r + \frac{\pi}{2}\right) \tag{4.24}$$

In the above model, L_i^j denotes the leading scorer of the Black-winged kite in the j^{th} dimension at the t^{th} iteration. z_t^{ij} and z_{t+1}^{ij} represent the position of the i^{th} Black-winged kite in the j^{th} dimension at iteration steps t and $t+1$, respectively. The term F_i refers to the fitness value associated with the current position of the i^{th} kite in the j^{th} dimension, while F_{ri} corresponds to the fitness value of a randomly selected position in the same dimension and iteration. The operator $\mathcal{C}(0,1)$ represents the Cauchy mutation. Figure 4.9 illustrates the pseudo code of the BKA algorithm.

Input: Objective function $f(x)$, population size N_{pop}, max iterations T_{max}
Output: Best solution X_{best}
Initialize population P_i *for* $i = 1, 2, ..., N_{pop}$ *within bounds*
Evaluate fitness F *of each individual*
while $t < T_{max}$ **do**
Phase 1: Attacking behavior
    if $\rho < r$ **then**
        $z_{t+1}^{ij} = z_t^{ij} + k(1 + \sin(r)) \times z_t^{ij}$
    else
        $z_{t+1}^{ij} = z_t^{ij} + k \times (2r - 1) \times z_t^{ij}$
    end if
Phase 2: Migration behavior
    Select a random individual r
    if $F_i < F_r i$ **then** ▷ Leader gives up
        $z_{t+1}^{ij} = z_t^{ij} + \mathcal{C}(0, 1) \times \left(z_t^{ij} - L_i^j\right)$
    else ▷ Continue to lead
        $y = 2 \times \sin(r + \pi/2)$
        $z_{t+1}^{ij} = z_t^{ij} + \mathcal{C}(0, 1) \times \left(L_i^j - y \times z_t^{ij}\right)$
    end if
    Apply boundary constraints and update fitness
    Update X_{best} *if improved*
end while
return X_{best}

Figure 4.9: Pseudo code of the BKA algorithm

4.5.4 Frilled lizard optimization (FLO) algorithm

The Frilled Lizard Optimization (FLO) algorithm, introduced in 2024 by Ibraheem Abu Falahah et al. [190], is a recent bio-inspired metaheuristic that mimics the predatory behavior of the frilled lizard in nature. This lizard waits patiently for prey, staying motionless until prey appears, then launching a rapid attack and feeding on it before retreating to the safety of the treetops. This intelligent behavioral pattern, characterized by a balance between patience and rapid action, enables the FLO to efficiently explore the solution space, refine candidate solutions, and strategically converge toward optimal results. Figure 4.10 shows a live picture of a frilled lizard.

The following subsections provide the mathematical modeling of frilled lizard behavior in nature.

4.5.4.1 Initialization

The FLO algorithm initiates the search process by generating a population of randomly distributed candidate solutions within the defined search space. Each individual in the population, representing a frilled lizard, corresponds to a potential solution and

Figure 4.10: Frilled lizard taken from Pinterest

is structured as a vector, as described in Equation (4.25). The entire set of these candidate solutions is collectively represented by a matrix illustrated in Equation (4.26). Throughout the iterative optimization process, the algorithm continuously evaluates the fitness of each solution and selects the most optimal candidate at each iteration [190].

$$x_{i,k} = Lb + rand \times (UB - LB) \quad k = 1, 2, ..., dim. \tag{4.25}$$

$$X = \begin{bmatrix} X_1 \\ \vdots \\ X_i \\ \vdots \\ X_n \end{bmatrix} = \begin{bmatrix} x_{1,1} & \cdots & x_{1,k} & \cdots & x_{1,dim} \\ \vdots & \ddots & \vdots & \ddots & \vdots \\ x_{i,1} & \cdots & x_{i,k} & \cdots & x_{i,dim} \\ \vdots & \ddots & \vdots & \ddots & \vdots \\ x_{n,1} & \cdots & x_{n,k} & \cdots & x_{n,dim} \end{bmatrix} \tag{4.26}$$

where X represents the population matrix of the FLO algorithm, while X_i corresponds to the i^{th} candidate solution. Each element $x_{i,k}$ within this matrix represents the k^{th} decision variable of the i^{th} solution. dim defines the optimization problem dimension, while n indicates the total number of frilled lizards.

4.5.4.2 Hunting Strategy: Exploration phase

One of the distinctive natural behaviors of the frilled lizard is its sit-and-wait hunting strategy, in which it remains unmoving and attacks prey immediately upon detection. This behavior inspires substantial shifts in the positions of candidate solutions within

the search space, thereby improving the global exploration capability of the algorithm. In the initial stage of the FLO algorithm, the position of each individual in the population is updated by simulating this predatory behavior. Specifically, each frilled lizard identifies other individuals with better fitness values as prey and updates its position accordingly, as formulated in Equation (4.27) [190].

$$P_i = \{X_j : F_j < F_i \text{ and } j \neq i\}, \quad i = 1, 2, \ldots, n \text{ and } j \in \{1, 2, \ldots, n\} \tag{4.27}$$

Here, P represents the set of potential prey for the i^{th} frilled lizard, where each X_j denotes a member of the population with a better fitness value compared to that of the i^{th} frilled lizard. The term F_j corresponds to the objective function value associated with the candidate solution X_j.

The FLO algorithm assumes that each frilled lizard randomly chooses one candidate from its set of potential prey and then attacks it. This predatory action is simulated by updating the lizard's position based on its movement toward the selected prey, as expressed in Equation (4.28). If the newly generated position yields a better fitness value than the current one, it is adopted as the new position of the corresponding individual following Equation (4.29) [170, 190].

$$x_{i,k}^{P1} = x_{i,k} + rand \times (SP_{i,k} - I \cdot x_{i,k}), \quad i = 1, 2, \ldots, n, \text{ and } k = 1, 2, \ldots, dim \tag{4.28}$$

$$X_i = \begin{cases} X_i^{P1}, & F_i^{P1} < F_i \\ X_i, & \text{else} \end{cases} \tag{4.29}$$

where X_i^{P1} denotes the newly generated position of the i^{th} frilled lizard during the initial phase of the FLO algorithm. The component $x_{i,k}^{P1}$ refers to the k^{th} dimension of this new position, while F_i^{P1} represents its corresponding objective function value. The term $SP_{i,k}$ indicates the k^{th} dimension of the selected prey position for the i^{th} lizard, and I is a randomly selected integer from the set $\{1, 2\}$.

4.5.4.3 Moving up the Tree: Exploitation phase

After feeding, the frilled lizard climbs to the top of a nearby tree. This natural behavior is emulated in the FLO algorithm to perform refining solutions, resulting in minor positional adjustments that enhance the algorithm's local search capability. In the second phase of the FLO process, individual positions are updated based on the modeled

retreat behavior of the frilled lizard. A new candidate position for each individual is determined using Equation (4.30). If this new position yields an improved objective function value, it replaces the previous one, as specified in Equation (4.31) [170, 190].

$$x_{i,k}^{P2} = x_{i,k} + (1-2\,rand)\cdot\frac{(UB_k - LB_k)}{t}, \quad i = 1,2,\ldots,n, \quad k = 1,2,\ldots,dim, \quad t = 1,2,\ldots,T_{max} \tag{4.30}$$

$$X_i = \begin{cases} X_i^{P2}, & \text{if } F_i^{P2} < F_i \\ X_i, & \text{else} \end{cases} \tag{4.31}$$

Here, X_i^{P2} represents the newly generated position of the i^{th} frilled lizard during the second phase of the FLO algorithm, while $x_{i,k}^{P2}$ denotes its k^{th} decision variable. The corresponding objective function value is given by F_i^{P2}. t indicates the current iteration number, and T_{max} denotes the maximum number of iterations allowed. Figure 4.11 illustrates the pseudo code of the FLO algorithm.

Input: Objective function $f(x)$, population size N_{pop}, max iterations T_{max}
Output: Best solution X_{best}
Initialize population matrix randomly using Equation (4.25)
Evaluate fitness $F_i = f(X_i)$ for each X_i
for $t = 1$ to T_{max} **do**
    for *each frilled lizard X_i* **do**
Phase 1: Hunting strategy ▷ Exploration
        Identify candidate prey P_i using Equation (4.27)
        Randomly select the prey for the i^{th} frilled lizard
        Calculate the new position of i^{th} frilled lizard using Equation (4.28)
        Update position using attack strategy (Equation (4.29)) $\rightarrow X_i^{P1}$
Phase 2: Moving up the Tree ▷ Exploitation
        Calculate the new position of the ith frilled lizard using Equation (4.30)
        Update position using retreat strategy (Equation (4.31)) $\rightarrow X_i^{P2}$
    end for
    Update X_{best} if a better solution is found
end for
return X_{best}

Figure 4.11: Pseudo code of the FLO algorithm

4.6 Improved Frilled Lizard Optimization (IFLO) algorithm

The ongoing advancements in engineering and scientific domains have created increasingly complex optimization problems, posing significant challenges for existing conventional algorithms. Consequently, there has been a growing research interest in improving algorithms to address these rising complexities. The pursuit of algorithmic improvement has emerged as a pivotal research focus, aiming to enhance both the efficiency and adaptability of optimization techniques [191].

One notable stride in this process of algorithm improvement involves the incorporation of advanced strategies designed to improve robustness, convergence speed, and avoid premature convergence.

In our specific study, improvements were implemented within the FLO algorithm, originally designed to emulate the natural hunting behavior of the frilled lizard. The proposed improvements include the incorporation of three distinct strategies: fitness distance balance (FDB), quasi-opposite-based learning (QOBL), and Cauchy mutation (CM), each contributing distinctively to improving the algorithm's performance. The integration of these strategies serves the purpose of further amplifying its exploration capabilities while addressing limitations linked to premature convergence and constrained exploration and effectively escaping local optima traps. The subsequent subsections provide a detailed mathematical description of each incorporated improvement strategy.

4.6.1 Fitness Distance Balance (FDB)

The FDB strategy serves as an effective selection mechanism in optimization algorithms, particularly enhancing the exploration process by evaluating candidate solutions according to their fitness and proximity to the optimal solution [192, 193]. By prioritizing solutions that exhibit both better objective values and minimal distances to the current optimal solution, FDB enables the algorithm to effectively explore new areas while refining promising regions. The distance of the current candidate solution (DP_i) from the best solution (P_{best}) is calculated as follows:

$$DP_i = \sqrt{\sum_{k=1}^{dim} (x_{i,k} - P_{best,k})^2}, \quad \forall i \in \{1, 2, \ldots, n\},\ P_i \neq P_{\text{best}} \tag{4.32}$$

Subsequently, two vectors are constructed to represent the fitness and distance values of all candidate solutions. The distance vector DP and the fitness vector F are created as follows:

$$DP = [DP_1, DP_2, \ldots DP_n] \tag{4.33}$$

$$F = [F_1, F_2, \ldots F_n] \tag{4.34}$$

In the final stage of the FDB method, a score is computed for each candidate solution to guide the selection process using the following formula:

$$S_{FDBi} = \omega \times (1 - normF_i) + (1 - \omega) \times normDP_i \tag{4.35}$$

where normF_i and normDP_i denote the normalized fitness and distance values of the i^{th} candidate solution, respectively. The parameter $\omega \in [0,1]$ is a weighting coefficient that regulates the relative influence of fitness and distance score. It is dynamically adjusted throughout the optimization process and can be formulated as follows:

$$\omega = 0.5 \times \left(1 + \frac{t}{T}\right) \tag{4.36}$$

4.6.2 Quasi-Opposite-Based Learning (QOBL)

QOBL is an enhanced strategy derived from oppositional-based learning, designed to improve the exploration and exploitation capabilities of the algorithm [194, 195]. QOBL enhances the search process by simultaneously considering both the current candidate solutions and their quasi-opposite counterparts, thereby increasing the probability of convergence toward the global optimum. Let a candidate solution be represented as $X(x_1, x_2, \ldots, x_{\text{dim}})$, where each decision variable $x_k \in [LB_k, UB_k] \quad \forall k \in \{1, 2, \ldots, dim\}$ is defined as $Y(y_1, y_2, \ldots y_{dim})$. Each opposite point y_k is calculated as $y_k = LB_k + UB_k - x_k$, and the midpoint is obtained as:

$$M_k = \frac{LB_k + UB_k}{2} \tag{4.37}$$

To generate a quasi-opposite point y_k^q, which is statistically more probable to be closer to the optimal solution than the opposite point y_k, the following formulation is applied:

$$y_k^q = \begin{cases} M_k + rand \times (y_k - M_k) & \text{if } y_k < M_k \\ y_k + rand \times (M_k - y_k) & \text{otherwise} \end{cases} \tag{4.38}$$

where *rand* is the uniformly distributed random number in the range of [0, 1].

4.6.3 Cauchy Mutation (CM)

CM is integrated into the FLO algorithm to enhance its exploration capabilities more thoroughly across the solution space. This strategy introduces significant variability into the population using a CM operator, thereby allowing the algorithm to escape local optima traps and preventing premature convergence [196, 197]. The Cauchy distribution, a continuous probability distribution characterized by two parameters, μ and σ, governs this mutation. The probability density function of the one-dimensional Cauchy distribution is mathematically expressed as:

$$f(z;\sigma,\mu) = \frac{1}{\pi}\frac{\sigma}{\sigma^2+(z-\mu)^2}, \quad z \in (-\infty,\infty), \tag{4.39}$$

When $\sigma = 1$ and $\mu = 0$, the Cauchy probability density function simplifies to its standard form, which is given by:

$$f(x;1,0) = \frac{1}{\pi(z^2+1)}, \quad z \in (-\infty,\infty), \tag{4.40}$$

The formula for the standard Cauchy distribution is represented by Equation (4.41):

$$\text{cauchy}(0,1) = \tan\left[\pi\left(\xi - 0.5\right)\right], \quad \xi \in [0,1]. \tag{4.41}$$

Equation (4.42) is employed to apply the CM operator on newly generated candidate positions.

$$X_i^{t+1} = X_i^t + \alpha \otimes \text{Cauchy}(0,1) \otimes (X_i^t - X_{best}) \tag{4.42}$$

where α symbolizes the step size and $\otimes$ denotes the entrywise multiplication operator. Figure 4.12 show a psuedo code of the proposed IFLO algorithm.

4.7 Simulation results

The effectiveness and robustness of the suggested Improved Frilled Lizard Optimization (IFLO) algorithm were rigorously assessed through a comparison with several well-known and recently developed optimization methods, including the Grey Wolf Optimizer (GWO) [186], Dingo Optimization Algorithm (DOA) [198], Harris Hawks optimization (HHO) [199], Whale Optimization Algorithm (WOA) [200], Chernobyl Disaster Optimizer (CDO) [201], Black-winged Kite Algorithm (BKA) [189], and the standard Frilled Lizard Optimization (FLO) [190]. All these algorithms and simulations were carried out using MATLAB R2021a on a computing platform equipped with

Input: Objective function $f(x)$, population size N_{pop}, max iterations T_{max}
Output: Best solution X_{best}
Initialize population matrix randomly using Equation (4.25)
Evaluate fitness $F_i = f(X_i)$ *for each* X_i
for $t = 1$ to T_{max} **do**
    for *each frilled lizard* X_i **do**
Phase 1: Hunting strategy ▷ Exploration
        Identify candidate prey P_i *using Equation (4.27)*
        Randomly select the prey for the i^{th} *frilled lizard*
        Calculate the new position of i^{th} *frilled lizard using Equation (4.28)*
        Update position using attack strategy (Equation (4.29)) $\rightarrow X_i^{P1}$
Phase 2: Moving up the Tree ▷ Exploitation
        Calculate the new position of the ith frilled lizard using Equation (4.30)
        Update position using retreat strategy (Equation (4.31)) $\rightarrow X_i^{P2}$
The proposed modifications:
        Apply the FDB selection strategy to update the Frilled Lizard's position and assign the best found solution
        Update the Frilled Lizard's position using QOBL and assign the best found solution
        Update the Frilled Lizard's position based on CM and assign the best found solution
    end for
    Update X_{best} *if a better solution is found*
end for
return X_{best}

Figure 4.12: Pseudo code of the proposed IFLO algorithm

an Intel(R) Core(TM) i5-7200U CPU @ 2.50 GHz, 8.00 GB of RAM, and a 64-bit Windows operating system.

4.7.1 IFLO evaluation on standard benchmark functions

At the beginning, we wanted to test the efficacy of the suggested IFLO algorithm using a set of 23 standard benchmark functions, encompassing unimodal, multimodal, and fixed-dimension multimodal categories, as detailed in Appendix B [202–204]. The parameter settings used for all compared algorithms are provided in Table 4.1. Each algorithm was evaluated over 30 independent trial runs, and the results were systematically recorded.

4.7.1.1 Analysis of the statistical results

In this case, the performance of the suggested IFLO algorithm was compared with several optimization methods, including GWO [186], DOA [198], HHO [199], WOA [200],

Table 4.1: Setting parameters of each algorithm

Algorithm	**Parameter**	**Setting Value**
GWO [186]	Population size	30
	T_{max}	300
	a	[2,0]
DOA [198]	Population size	30
	T_{max}	300
	P	0.5
	Q	0.7
	$\beta 1$	[-2,2]
	$\beta 2$	[-1,1]
HHO [199]	Population size	30
	T_{max}	300
	E_o	[-1,1]
WOA [200]	Population size	30
	T_{max}	300
	$a1 = a2$	[2,0]
	b	1
	l	[-1,1]
CDO [201]	Population size	30
	T_{max}	300
	r	rand[0,1]
BKA [189]	Population size	30
	T_{max}	300
	p	0.9
FLO [190]	Population size	30
	T_{max}	300
	I	rand[1,2]
IFLO	Population size	30
	T_{max}	300
	I	rand[1,2]

CDO [201], BKA [189], and the standard FLO [190]. Table 4.2 displays the statistical outcomes, consisting of the best, average, worst, and standard deviation (SD) values for all algorithms. As observed from the table, the proposed IFLO consistently outperforms other compared methods across all benchmark functions. These findings demonstrate the superior optimization capability and robustness of the proposed IFLO algorithm in achieving optimum results.

Table 4.2: Statistical results of optimization algorithms on the benchmark functions

Function	Measure	GWO [186]	DOA [198]	HHO [199]	WOA [200]	CDO [201]	BKA [189]	FLO [190]	**IFLO**
F1	Best	1.287E-16	4.120E-247	3.766E-75	2.197E-54	1.892E-82	6.818E-63	5.179E-245	**0**
	Average	3.442E-15	2.167E-28	1.767E-60	3.221E-42	8.327E-79	7.522E-44	6.963E-227	**0**
	Worst	1.858E-14	6.500E-27	5.218E-59	4.059E-41	8.524E-78	2.256E-42	2.022E-225	**0**
	SD	3.834E-15	1.187E-27	9.522E-60	9.726E-42	1.912E-78	4.120E-43	0	**0**
F2	Best	5.297E-10	1.376E-124	2.489E-38	3.446E-35	1.189E-43	3.106E-31	1.549E-122	**0**
	Average	1.316E-09	3.737E-23	7.004E-33	9.276E-30	6.960E-41	1.741E-28	7.132E-114	**0**
	Worst	3.509E-09	1.111E-21	7.354E-32	1.942E-28	4.876E-40	1.143E-27	2.118E-112	**0**
	SD	7.725E-10	2.028E-22	1.650E-32	3.561E-29	1.070E-40	3.153E-28	3.865E-113	**0**
F3	Best	5.384E-04	2.714E-289	1.232E-63	2.866E+04	6.503E-71	2.358E-62	3.595E-212	**0**
	Average	8.805E-02	8.763E-36	1.089E-45	6.282E+04	3.142E-54	3.884E-49	1.374E-162	**0**
	Worst	4.287E-01	2.629E-34	2.028E-44	1.089E+05	9.421E-53	7.588E-48	4.121E-161	**0**
	SD	1.086E-01	4.800E-35	4.235E-45	1.963E+04	1.720E-53	1.549E-48	7.372E-162	**0**
F4	Best	2.486E-04	2.368E-151	2.575E-37	8.811E-02	7.006E-40	2.378E-31	4.299E-125	**0**
	Average	6.748E-04	6.268E-25	5.684E-31	5.360E+01	1.267E-37	4.300E-24	7.956E-117	**0**
	Worst	1.494E-03	1.331E-23	1.580E-29	8.827E+01	7.342E-37	1.289E-22	1.236E-115	**0**
	SD	3.103E-04	2.562E-24	2.880E-30	3.300E+01	1.861E-37	2.353E-23	3.019E-116	**0**
F5	Best	2.593E+01	2.882E+01	1.471E-04	2.787E+01	2.789E+01	2.733E+01	0	**0**
	Average	2.747E+01	2.892E+01	3.370E-02	2.841E+01	2.819E+01	2.826E+01	0	**0**
	Worst	2.877E+01	2.899E+01	3.283E-01	2.881E+01	2.874E+01	2.896E+01	0	**0**
	SD	8.984E-01	4.198E-02	6.005E-02	3.590E-01	2.243E-01	4.958E-01	0	**0**
F6	Best	2.234E-01	3.497E+00	7.151E-07	1.753E-01	7.500E+00	1.554E+00	0	**0**
	Average	9.570E-01	5.636E+00	4.801E-04	8.839E-01	7.500E+00	3.049E+00	0	**0**
	Worst	1.996E+00	6.898E+00	3.278E-03	1.690E+00	7.500E+00	6.414E+00	0	**0**
	SD	4.891E-01	8.675E-01	7.050E-04	4.102E-01	0	1.224E+00	0	**0**
F7	Best	1.639E-03	3.961E-05	2.108E-05	2.851E-05	8.888E-06	8.786E-05	5.163E-06	**5.354E-07**
	Average	3.711E-03	8.825E-04	2.981E-04	5.719E-03	1.630E-04	5.436E-04	8.908E-05	**5.209E-05**
	Worst	9.103E-03	2.949E-03	2.256E-03	2.886E-02	7.011E-04	1.413E-03	3.692E-04	**1.438E-04**
	SD	1.653E-03	9.445E-04	4.127E-04	6.123E-03	1.401E-04	3.324E-04	7.645E-05	**3.517E-05**
F8	Best	-8.063E+03	-6.554E+03	-1.257E+04	-1.256E+04	-5.167E+03	-1.050E+04	-1.257E+04	**-1.257E+04**
	Average	-6.010E+03	-4.724E+03	-1.256E+04	-9.889E+03	-3.728E+03	-8.817E+03	-9.597E+03	**-1.079E+04**
	Worst	-3.426E+03	-3.455E+03	-1.235E+04	-6.684E+03	-2.936E+03	-7.081E+03	-8.681E+03	**-9.016E+03**
	SD	1.028E+03	7.277E+02	4.002E+01	1.912E+03	4.744E+02	8.633E+02	1.353E+03	**1.807E+03**
F9	Best	4.093E-12	0	0	0	0	0	0	**0**
	Average	8.162E+00	0	0	0	1.088E+02	0	0	**0**
	Worst	2.349E+01	0	0	0	2.512E+02	0	0	**0**
	SD	6.094E+00	0	0	0	1.149E+02	0	0	**0**
F10	Best	4.975E-09	8.882E-16	8.882E-16	4.441E-15	4.441E-15	8.882E-16	8.882E-16	**8.882E-16**
	Average	1.156E-08	1.007E-15	8.882E-16	7.046E-15	4.441E-15	1.007E-15	8.882E-16	**8.882E-16**
	Worst	3.124E-08	4.441E-15	8.882E-16	1.510E-14	4.441E-15	4.441E-15	8.882E-16	**8.882E-16**
	SD	5.925E-09	6.486E-16	0	2.273E-15	0	6.486E-16	0	**0**
F11	Best	2.554E-15	0	0	0	0	0	0	**0**
	Average	6.080E-03	0	0	5.407E-02	3.404E-03	0	0	**0**
	Worst	3.807E-02	0	0	5.527E-01	2.346E-02	0	0	**0**
	SD	1.099E-02	0	0	1.470E-01	6.600E-03	0	0	**0**

Table 4.2: Statistical results of optimization algorithms on the benchmark functions (Continued)

Function	Measure	GWO [186]	DOA [198]	HHO [199]	WOA [200]	CDO [201]	BKA [189]	FLO [190]	**IFLO**
F12	Best	2.042E-02	2.512E-01	6.700E-08	1.570E-02	1.106E+00	6.368E-02	1.571E-32	**1.571E-32**
	Average	5.770E-02	5.677E-01	2.588E-05	5.879E-02	1.451E+00	1.890E-01	1.571E-32	**1.571E-32**
	Worst	1.400E-01	1.626E+00	1.245E-04	4.630E-01	1.669E+00	6.891E-01	1.571E-32	**1.571E-32**
	SD	3.109E-02	2.770E-01	3.245E-05	8.221E-02	2.723E-01	1.611E-01	5.567E-48	**5.567E-48**
F13	Best	4.533E-01	2.119E+00	1.323E-06	2.817E-01	3.547E-01	1.188E+00	1.350E-32	**1.350E-32**
	Average	8.546E-01	2.861E+00	2.315E-04	7.618E-01	5.825E-01	2.090E+00	1.350E-32	**1.350E-32**
	Worst	1.479E+00	3.156E+00	8.604E-04	1.442E+00	8.250E-01	2.998E+00	1.350E-32	**1.350E-32**
	SD	2.540E-01	2.634E-01	2.270E-04	3.073E-01	1.146E-01	4.718E-01	5.567E-48	**5.567E-48**
F14	Best	9.980E-01	9.980E-01	9.980E-01	9.980E-01	8.937E+00	9.980E-01	9.980E-01	**9.980E-01**
	Average	5.761E+00	2.670E+00	1.592E+00	2.837E+00	1.506E+01	1.295E+00	9.982E-01	**9.980E-01**
	Worst	1.267E+01	5.929E+00	5.929E+00	1.076E+01	1.830E+01	4.950E+00	1.003E-00	**9.980E-01**
	SD	4.386E+00	1.766E+00	1.285E+00	2.618E+00	2.611E+00	8.677E-01	9.639E-04	**0**
F15	Best	3.160E-04	3.075E-04	3.081E-04	3.086E-04	3.164E-04	3.075E-04	3.196E-04	**3.075E-04**
	Average	5.806E-03	2.918E-03	4.139E-04	8.229E-04	3.740E-04	2.492E-03	7.698E-04	**3.111E-04**
	Worst	2.036E-02	2.255E-02	1.630E-03	2.252E-03	7.761E-04	2.036E-02	1.661E-03	**3.266E-04**
	SD	8.930E-03	6.435E-03	2.357E-04	6.231E-04	9.749E-05	6.071E-03	4.607E-04	**4.821E-06**
F16	Best	-1.032E+00	-1.032E+00	-1.032E+00	-1.032E+00	-1.029E+00	-1.032E+00	-1.032E+00	**-1.032E+00**
	Average	-1.032E+00	-1.032E+00	-1.032E+00	-1.032E+00	-1.004E+00	-1.032E+00	-1.029E+00	**-1.032E+00**
	Worst	-1.032E+00	-1.032E+00	-1.032E+00	-1.032E+00	-9.999E-01	-1.032E+00	-1.012E+00	**-1.032E+00**
	SD	6.438E-08	1.803E-10	6.040E-08	8.293E-09	8.734E-03	5.455E-16	5.022E-03	**6.584E-16**
F17	Best	3.979E-01	3.979E-01	3.979E-01	3.979E-01	3.979E-01	3.979E-01	3.979E-01	**3.979E-01**
	Average	3.980E-01	3.979E-01	3.980E-01	3.979E-01	4.058E-01	3.979E-01	4.216E-01	**3.979E-01**
	Worst	3.996E-01	3.979E-01	3.987E-01	3.981E-01	5.820E-01	3.979E-01	6.257E-01	**3.979E-01**
	SD	3.115E-04	3.243E-16	1.690E-04	4.157E-05	3.334E-02	0	5.690E-02	**0**
F18	Best	3.000E+00	3.000E+00	3.000E+00	3.000E+00	3.000E+00	3.000E+00	3.000E+00	**3.000E+00**
	Average	3.000E+00	3.000E+00	3.000E+00	3.000E+00	3.182E+01	3.000E+00	9.163E+00	**3.000E+00**
	Worst	3.001E+00	3.004E+00	3.000E+00	3.000E+00	8.404E+01	3.000E+00	3.131E+01	**3.000E+00**
	SD	1.192E-04	6.823E-04	5.150E-06	2.125E-07	3.510E+01	3.141E-15	9.370E+00	**1.330E-15**
F19	Best	-3.863E+00	-3.863E+00	-3.863E+00	-3.863E+00	-3.862E+00	-3.863E+00	-3.862E+00	**-3.863E+00**
	Average	-3.862E+00	-3.828E+00	-3.858E+00	-3.852E+00	-3.858E+00	-3.863E+00	-3.705E+00	**-3.863E+00**
	Worst	-3.860E+00	-3.090E+00	-3.852E+00	-3.810E+00	-3.848E+00	-3.863E+00	-2.907E+00	**-3.863E+00**
	SD	7.728E-04	1.439E-01	3.401E-03	1.323E-02	3.347E-03	4.025e-13	1.814E-01	**2.710E-15**
F20	Best	-3.322E+00	-3.322E+00	-3.277E+00	-3.321E+00	-3.314E+00	-3.322E+00	-3.128E+00	**-3.322E+00**
	Average	-3.271E+00	-3.185E+00	-3.011E+00	-3.238E+00	-3.219E+00	-3.293E+00	-2.629E+00	**-3.290E+00**
	Worst	-3.084E+00	-2.578E+00	-2.600E+00	-3.031E+00	-3.101E+00	-3.202E+00	-1.953E+00	**-3.203E+00**
	SD	7.157E-02	1.473E-01	1.596E-01	1.006E-01	5.720E-02	5.082E-02	3.297E-01	**5.348E-02**
F21	Best	-1.015E+01	-1.015E+01	-9.825E+00	-1.015E+01	-9.627E+00	-1.015E+01	-1.015E+01	**-1.015E+01**
	Average	-8.212E+00	-7.597E+00	-5.201E+00	-8.578E+00	-5.374E+00	-9.652E+00	-9.139E+00	**-1.015E+01**
	Worst	-2.369E+00	-2.630E+00	-4.996E+00	-2.627E+00	-2.795E+00	-2.630E+00	-5.055E+00	**-1.015E+01**
	SD	2.867E+00	2.977E+00	8.734E-01	2.594E+00	1.510E+00	1.909E+00	1.915E+00	**6.019E-15**
F22	Best	-1.040E+01	-1.040E+01	-5.088E+00	-1.040E+01	-6.926E+00	-1.040E+01	-1.040E+01	**-1.040E+01**
	Average	-1.040E+01	-7.430E+00	-5.077E+00	-7.817E+00	-5.240E+00	-9.958E+00	-9.741E+00	**-1.040E+01**
	Worst	-1.039E+01	-2.766E+00	-5.029E+00	-1.836E+00	-3.209E+00	-3.724E+00	-5.088E+00	**-1.040E+01**
	SD	2.244E-03	3.313E+00	1.405E-02	3.169E+00	9.806E-01	1.694E+00	1.679E+00	**4.665E-16**
F23	Best	-1.054E+01	-1.054E+01	-5.128E+00	-1.053E+01	-7.510E+00	-1.054E+01	-1.054E+01	**-1.054E+01**
	Average	-9.992E+00	-7.595E+00	-5.037E+00	-5.368E+00	-5.503E+00	-9.866E+00	-9.82E+00	**-1.054E+01**
	Worst	-2.422E+00	-2.419E+00	-2.764E+00	-1.676E+00	-2.675E+00	-3.833E+00	-5.128E+00	**-1.054E+01**
	SD	2.058E+00	3.476E+00	4.295E-01	2.850E+00	1.218E+00	2.045E+00	1.782E+00	**1.143E-15**

4.7.1.2 Analysis of convergence curves

The convergence curve of the suggested IFLO algorithm is illustrated in Figure 4.13, alongside other efficient optimization techniques, including GWO [186], DOA [198], HHO [199], WOA [200], CDO [201], BKA [189], and the original FLO [190]. According to the convergence curves, the suggested IFLO achieves faster convergence across unimodal, multimodal, and fixed-dimension multimodal benchmark functions. Notably, IFLO surpasses the performance of the original FLO by reaching the optimal solution more swiftly. This improved performance can be attributed to the proposed enhancements, which effectively strengthen both the exploration and exploitation capabilities of the algorithm, thereby enabling a more efficient convergence toward optimal solutions.

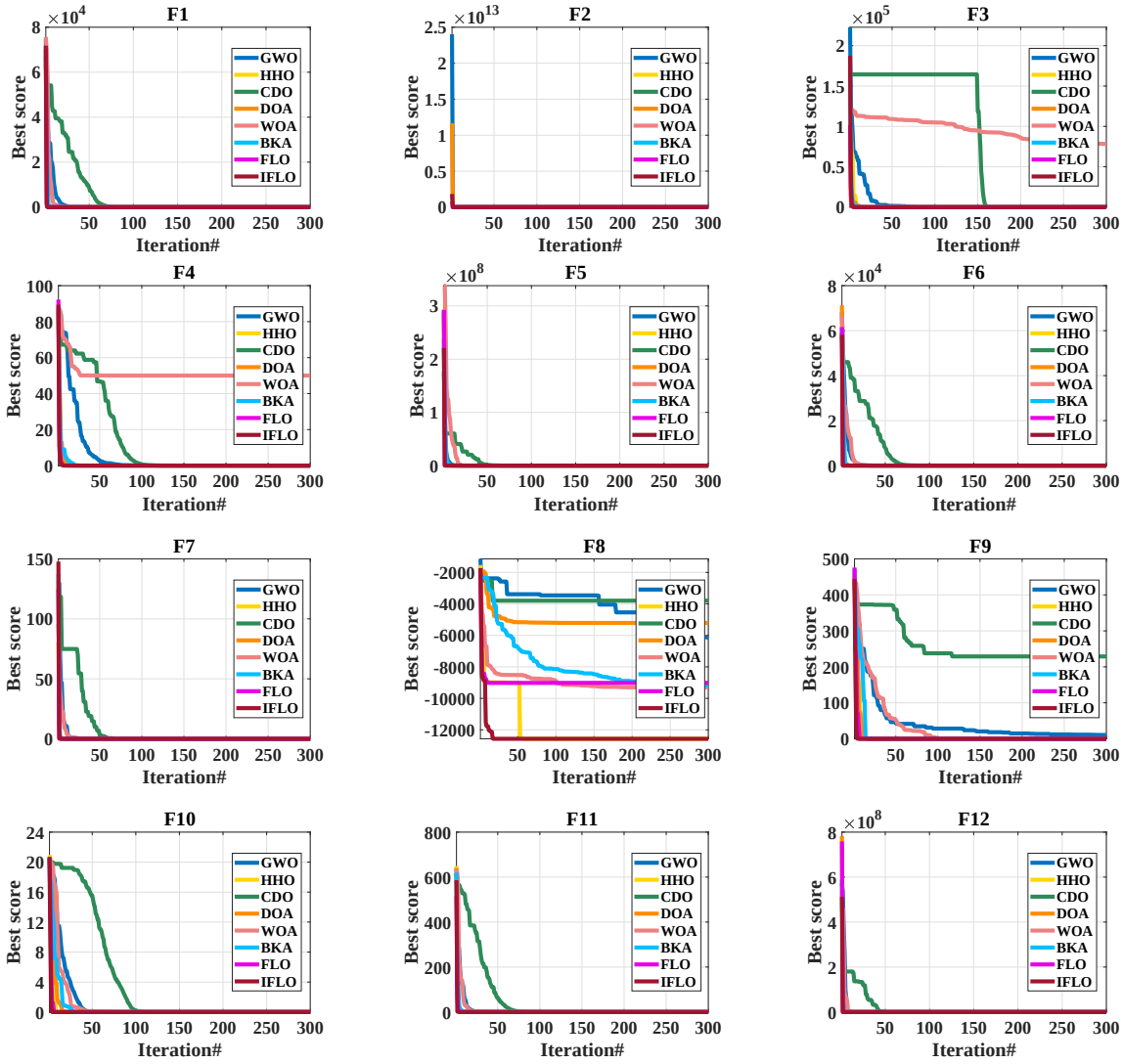

Figure 4.13: Comparative convergence analysis of algorithms on benchmark functions

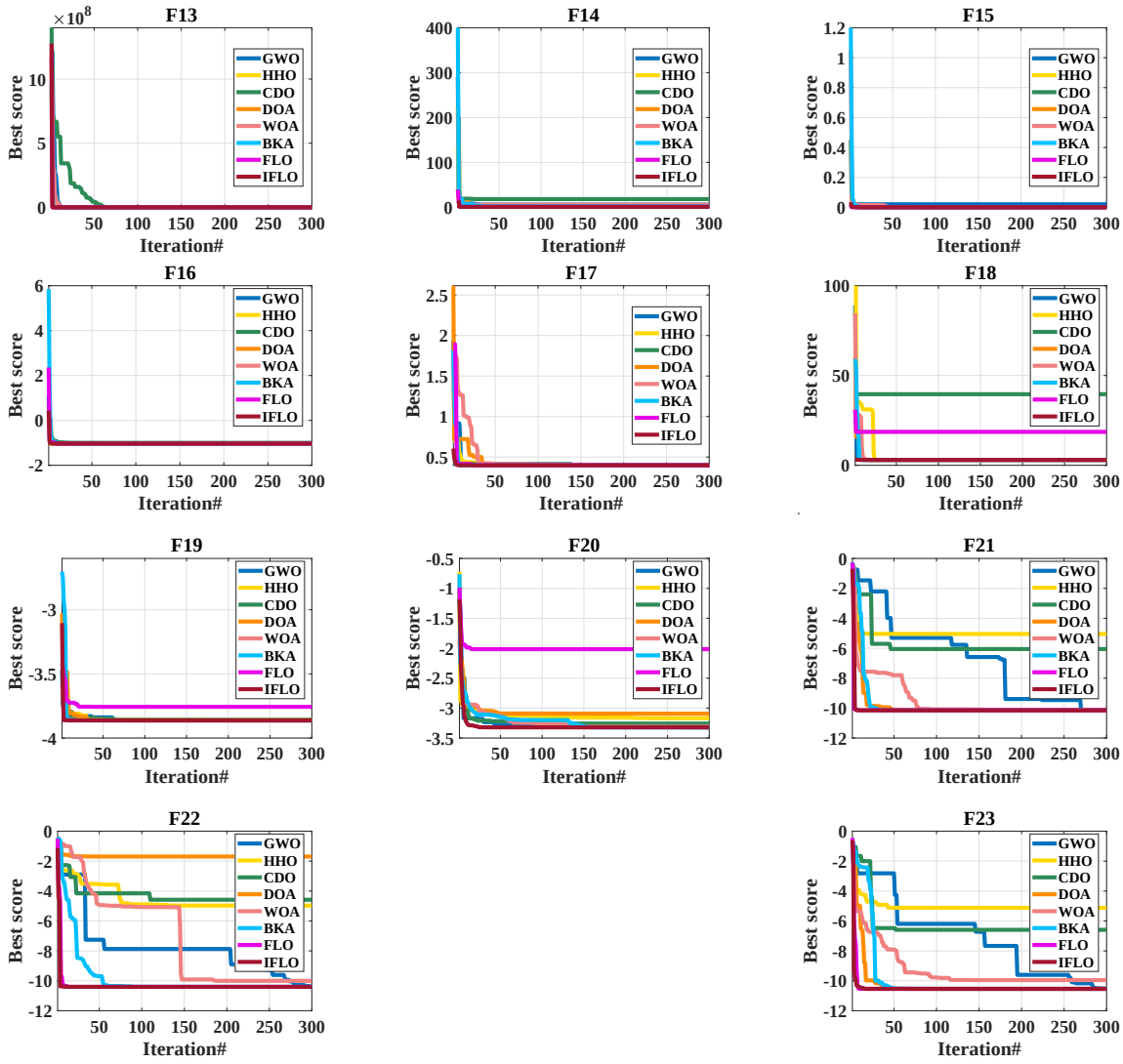

Figure 4.13: Comparative convergence analysis of algorithms on benchmark functions (continued)

4.7.1.3 Analysing data using Boxplots

Boxplots serve as an effective means for visualizing the statistical distribution of data, particularly through quartile representation, and are widely used to emphasize key features such as central tendency, spread, and the presence of outliers. In this study, Figure 4.14 presents a comparative boxplot analysis of the proposed IFLO algorithm against several well-established and efficient optimizers. These boxplots provide a statistical summary of the performance distributions derived from multiple simulation runs across 23 benchmark functions. A narrower boxplot observed for the IFLO algorithm indicates lower variance, signifying that it delivers more stable and consistent results concerning solution quality and convergence speed. This consistency

also implies reduced sensitivity to random initialization and fewer outliers. Contrarily, the wider boxplots of other algorithms on certain benchmark functions reveal higher variability, underscoring less reliable performance and a diminished ability to achieve the optimal optimization goals. Moreover, the occurrence of outliers in the boxplots of the compared algorithms underscores their occasional performance degradation in certain problems. This variability indicates a lack of robustness in handling diverse optimization scenarios. Hence, the IFLO algorithm exhibits a more stable performance with minimal outliers, reinforcing its superiority in terms of consistency across a wide range of benchmark functions and simulation scenarios.

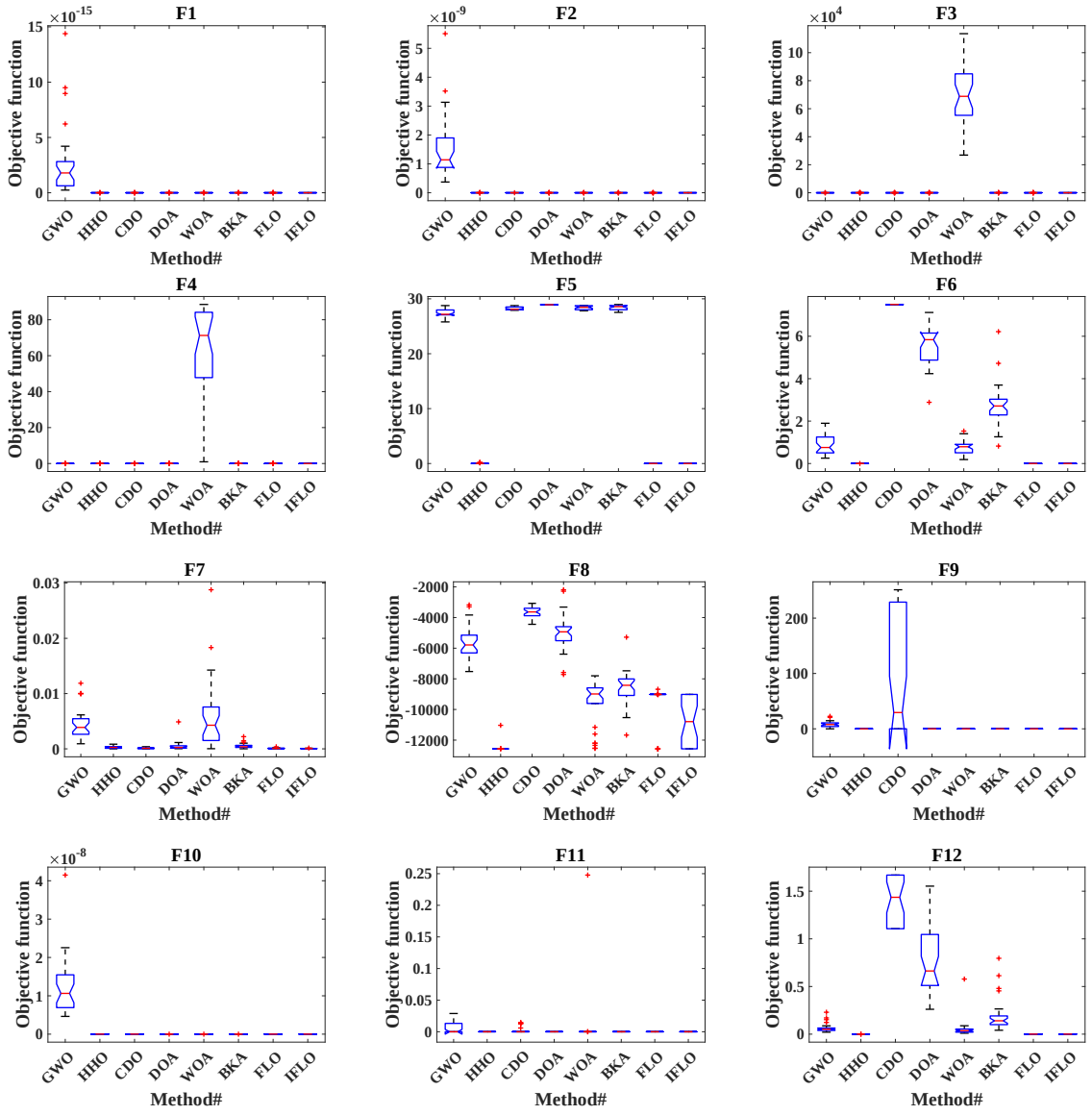

Figure 4.14: Statistical comparison of various optimizers using boxplots on test function

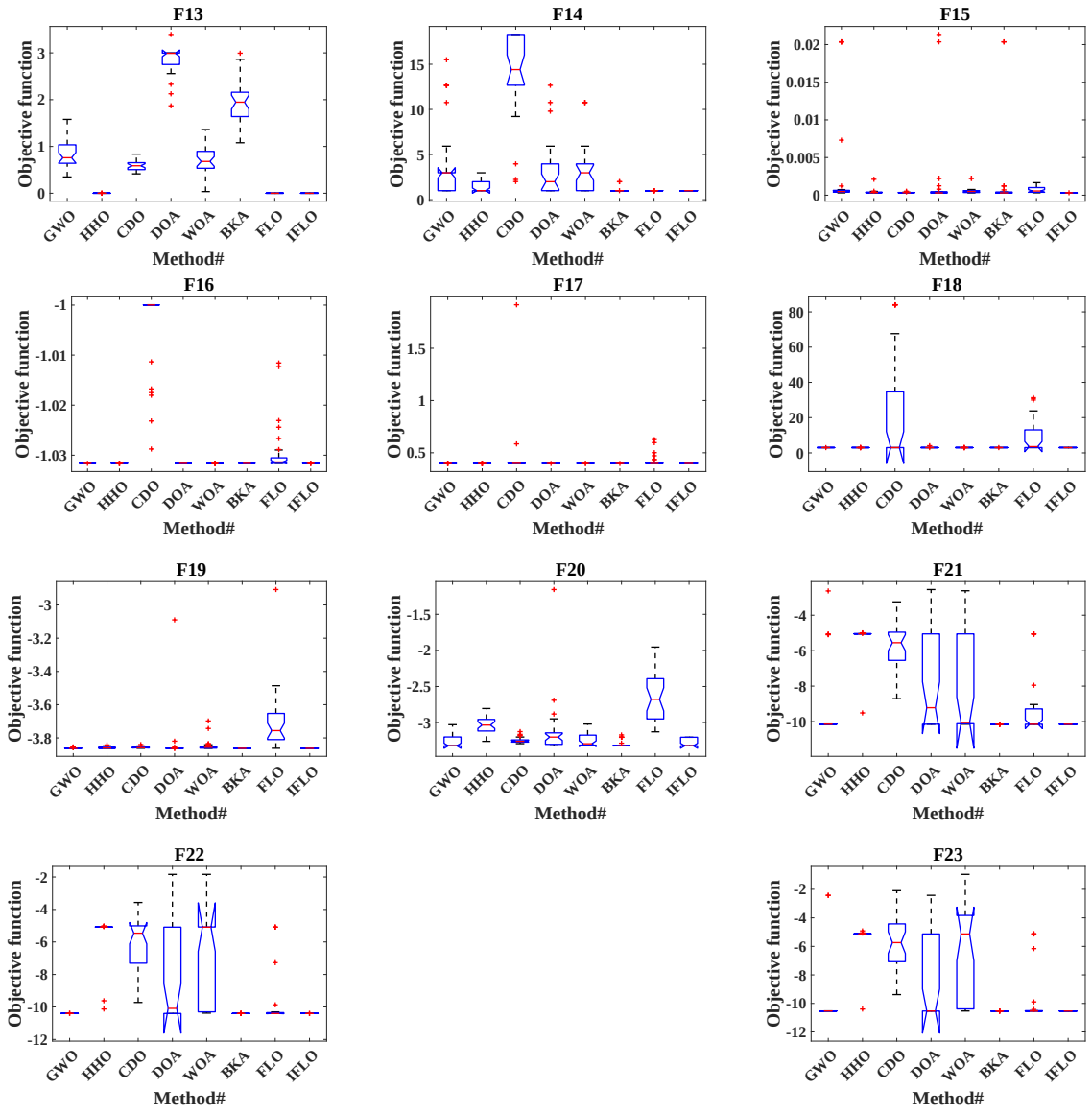

Figure 4.14: Statistical comparison of various optimizers using boxplots on test function (Continued)

4.8 Conclusion

In this chapter, we explored the foundational principles of optimization and distinguished between exact optimization methods and metaheuristic techniques. We provided an in-depth description of various metaheuristic optimization algorithms, providing the mathematical modeling inspired by their natural behaviors. Particular attention was given to the proposed Improved Frilled Lizard Optimization (IFLO) algorithm, which incorporates three advanced strategies, including fitness distance balance (FDB), quasi-opposite-based learning (QOBL), and Cauchy mutation (CM) to

strengthen the algorithm's search capabilities and establish a more effective balance between the exploration and exploitation processes.

The performance of the IFLO algorithm was rigorously evaluated using a set of 23 benchmark test functions and compared against several well-established and recent optimization algorithms, including Grey Wolf Optimizer (GWO), Dingo Optimization Algorithm (DOA), Harris Hawks Optimization (HHO), Whale Optimization Algorithm (WOA), Chernobyl Disaster Optimizer (CDO), Black-winged Kite Algorithm (BKA), and the conventional Frilled Lizard Optimization (FLO). The comparative analysis, drawn from statistical evaluations, convergence curves, and boxplot visualizations, confirmed the superior performance level of the suggested IFLO technique. Specifically, the algorithm consistently achieved higher-quality solutions and demonstrated faster convergence over these existing methods.

Overall, the proposed modifications effectively enhanced exploration capability, mitigated the risks of premature convergence, and improved the algorithm's ability to escape local optima traps, thereby ensuring robust and reliable performance across a diverse set of optimization problems.

Chapter 5

Solving the Optimal Planning Problem of Renewable Energy Sources in Distribution Grids

5.1 Introduction

The integration of renewable energy source-based distributed generation (RES-based DG), as said in Chapter One, plays a crucial role in enhancing network performance. However, when not optimally planned, incorporating these energy sources may lead to increased power losses, significant voltage deviations, and reduced system stability [8]. Therefore, the optimal allocation and sizing of DG units are essential to ensure their beneficial impact on the overall operation and reliability of the distribution system.

Solving the optimal planning problem of RES-based DG in distribution grids presents a complex optimization challenge that must consider various operational constraints and inherent uncertainties, including fluctuations in load demand and the intermittent nature of renewable energy generation. To effectively address these challenges, advanced optimization techniques are needed to determine the most suitable locations, sizes, and operating power factors of DG units in non-convex search spaces while satisfying system constraints and maintaining power quality standards. Traditional methods often fail to locate the global optimum as they can become trapped in local minima.

To overcome the limitations of conventional optimization techniques, this chapter introduces a novel Improved Frilled Lizard Optimizer (IFLO), specifically developed to address the optimal planning problem of renewable energy sources, namely wind turbines (WT) and solar photovoltaic (SPV) systems, within radial distribution grids (RDGs). This chapter is structured to examine the applied algorithm across two distinct cases. In the first case, a single-objective optimization problem is addressed

without considering uncertainty in load or generation, focusing solely on minimizing active power losses within the IEEE 69-bus medium-scale distribution system. The second case involves a more complex and realistic case study applied to the IEEE 85-bus large-scale distribution system. Here, a multi-objective optimization framework is adopted, incorporating uncertainties in both load and generation over a seasonal planning horizon. The objectives in this scenario are to simultaneously minimize average annual active power losses and voltage deviation while maximizing the yearly average voltage stability index, all within the bounds of operational constraints. This approach reflects practical and forward-looking planning goals for modern distribution systems.

The effectiveness of the proposed IFLO algorithm is rigorously compared to other well-established and efficient methods, including GWO, JSO, BKA, and the original FLO, all of which are also proposed and implemented in this chapter.

5.2 RES-based DG planning without uncertainties

In this case study, we focus on an analysis conducted on a system operating under peak load conditions within a controlled environment free from uncertainties. This deterministic setup simplifies the optimization process by neglecting any uncertainties related to load demand or renewable generation outputs, thereby enabling a direct evaluation of the algorithm's performance under ideal operating conditions. This preliminary investigation serves as a foundational step, providing a clearer understanding of system dynamics, unraveling its inherent characteristics, and paving the way for more complex analyses that account for uncertainty. These visualizations contribute to a deeper, holistic understanding of the key dynamic elements that influence power systems, aiding in strategic decision-making and resource planning.

5.2.1 Problem Description

The primary objective of this initial case of DG planning problem is to minimize active power losses in the distribution grid while adhering to all system operational constraints. Referring to Figure 5.1, the branch's active power loss, denoted as P_{iloss} is expressed as follows:

$$P_{iloss} = R_{bi} I_{bi}^2 = R_{bi} \frac{P_{i+1}^2 + Q_{i+1}^2}{|V_{i+1}|^2} \tag{5.1}$$

Similarly, The branch's reactive power loss, denoted as Q_{iloss}, is given by

$$Q_{iloss} = X_{bi} I_{bi}^2 = X_{bi} \frac{P_{i+1}^2 + Q_{i+1}^2}{|V_{i+1}|^2} \tag{5.2}$$

where P_{i+1} and Q_{i+1} denote the active and reactive power demands at bus $i+1$, respectively. V_{i+1} represents the voltage magnitude at the same bus. I_{bi} refers to the current flowing through the branch i, while R_{bi} and X_{bi} denote the corresponding branch resistance and reactance, respectively.

The total active power loss, indicated by TP_{loss}, is expressed as

$$TP_{loss} = \sum_{i=1}^{N_b} P_{iloss} \tag{5.3}$$

The corresponding total reactive power loss, indicated by TQ_{loss}, is given by

$$TQ_{loss} = \sum_{i=1}^{N_b} Q_{iloss} \tag{5.4}$$

where N_b represents the total number of branches.

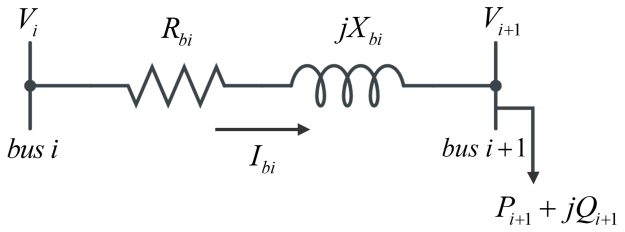

Figure 5.1: Equivalent two-bus model of the grid

5.2.2 System limitations

The proposed optimization methods must adhere to all system constraints, including voltage limits (minimum and maximum), DG unit location and capacity, power balance, permissible DG power factor range, and thermal limits. A detailed description of each constraint is provided below.

5.2.2.1 Equality constraints

The power balance equations are defined as equality constraints expressed as follows:

$$P_{\text{sub}} + \sum P_{\text{DG}} = \sum P_{\text{i,loss}} + \sum P_{\text{d}} \tag{5.5}$$

$$Q_{\text{sub}} + \sum Q_{\text{DG}} = \sum Q_{\text{i,loss}} + \sum Q_{\text{d}} \tag{5.6}$$

where P_{sub} and Q_{sub} symbolize the active and reactive power injected by the substation into the distribution grid, respectively. P_{DG} and Q_{DG} represent the active and reactive power contributions from the DGs. P_{d} and Q_{d} correspond to the active and reactive power demands of loads. The power losses within the system are represented by $P_{\text{i,loss}}$ for active power loss and $Q_{\text{i,loss}}$ for reactive power loss.

5.2.2.2 Inequality constraints

- DG location limits: DGs can be placed on any bus in the system, except the slack bus as follow:

$$2 \leq DG_{\text{loc}} \leq N_b \tag{5.7}$$

- Bus voltage limits: The voltage magnitude at each bus is constrained within the following bounds (in per unit):

$$0.95 \leq V_i \leq 1.05 \tag{5.8}$$

- DG capacity limits: The generation limits of DGs are defined as follows:

$$\sum P_{DG} \leq P_d, \sum Q_{DG} \leq Q_d \tag{5.9}$$

- Thermal limit: The current in each branch must not exceed its maximum allowable capacity, as follows:

$$I_i \leq I_{i,max} \tag{5.10}$$

- DG power factor limits: The PF range for each DG unit can be set as:

$$0.7 \leq PF_{DG} \leq 1 \tag{5.11}$$

5.2.3 Simulation Results and Discussions

The developed IFLO algorithm is initially implemented and tested on the IEEE 69 bus medium-scale system [146] without considering any uncertainty. The system load flow calculations are carried out using the backward/forward-sweep method [87, 138], chosen for its accuracy, simplicity, and computational efficiency. The study seeks to determine the optimal placement and sizing of DG units in the RDG to reduce total active power losses while respecting all operational constraints. The optimization process examines two operating PFs of DG units across two distinct scenarios:

- **Scenario 1:** DGs integration operating at unity power factor (unity-PF)
- **Scenario 2:** DGs integration operating at optimal power factor (optimal-PF) within the permissible range specified in Equation (5.11)

For each scenario, system performance is recorded for configurations with one, two, and three DG units. The effectiveness of the proposed IFLO method is evaluated by comparing its outcomes against other well-established and effective optimization techniques, including GWO, JSO, BKA, and the original FLO, which are also proposed and implemented in this study, along with other existing optimization methods from the literature. A common population size of 100 and a maximum of 100 iterations are applied to each algorithm to ensure a fair comparison.

5.2.3.1 Scenario 1: DGs integration operating at unity-PF

In this scenario, DGs are assumed to generate only active power, typical of solar PV arrays. Table 5.1 presents the optimal DG placement and sizing results identified by the proposed IFLO algorithm, alongside results produced by additional techniques implemented in this study, including GWO, JSO, BKA, and the original FLO. It also includes results from techniques in the literature addressing the same optimization problem, such as Particle Swarm Optimization (PSO) [205] and the Modified Gravitational Search Algorithm (MGSA) [87]. Upon reviewing the table, the IFLO algorithm matches or outperforms other methods in achieving the optimum results. With a single DG integrated into the RDG, IFLO lowers the system's active power losses from 224.961 kW/102.147 kVAr to 83.192 kW/40.523 kVAr. The optimal placement is at bus 61, with a recommended size of 1872.647 kW. This solution raises the lowest voltage of node 65 from 0.9092 p.u. to 0.9789 p.u. The new lowest voltage node becomes node 27, whose voltage is 0.9683 p.u. The average execution time was 5.93 seconds.

For two DG units installed, the IFLO further lowers active power losses to 71.658 kW. The optimal siting involves installing a 1781.467 kW unit at bus 61 and a 531.175 kW unit at bus 17. This configuration raises the minimum system voltage from the base case value of 0.9092 p.u. to 0.9790 p.u. at bus 65, providing a slightly better performance than other methods. Indicatively, the mean execution time for our developed IFLO was 6.46 seconds. When three DG units are integrated, the IFLO algorithm effectively determines their optimal locations and sizes, outperforming other methods by achieving the lowest power losses of 69.419 kW. The most suitable locations are buses 11, 61, and 17, with the minimum system voltage reaching 0.9790 pu at bus 65. Roughly, the average execution time of the proposed IFLO was 6.59 seconds.

Figures 5.2 - 5.4 display the convergence curves of the different optimization methods for configurations with one, two, and three DG units, respectively. In every case, IFLO

Table 5.1: Results of integrating 1, 2, and 3 DGs with unity power factor into the RDG

Scenario	Method	Optimal Location	Optimal Sizes (kW)	TP_{loss} (kW)	TQ_{loss} (kVAr)	V_{min} /**Bus**
No DGs	-	-	-	224.961	102.147	0.9092/**65**
1 DG	MGSA [87]	61	1820.81	83.28	40.64	0.9682/**27**
	PSO [205]	61	1870	83.22	-	-
	GWO	61	1872.589	83.192	40.523	0.9683/**27**
	JSO	61	1872.647	83.192	40.523	0.9683/**27**
	BKA	61	1872.647	83.192	40.523	0.9683/**27**
	FLO	61	1872.647	83.192	40.523	0.9683/**27**
	IFLO	**61**	**1872.647**	**83.192**	**40.523**	**0.9683/27**
2 DGs	MGSA [87]	61 17	1786.90 573.24	71.73	-	-
	PSO [205]	61 17	530 1870	71.68	-	-
	GWO	61 18	1781.353 530.296	71.660	35.935	0.9789/**65**
	JSO	61 17	1781.464 531.174	71.659	35.933	0.9789/**65**
	BKA	61 17	1781.467 531.175	71.659	35.933	0.9789/**65**
	FLO	22 61	487.272 1787.444	72.126	36.133	0.9789/**65**
	IFLO	**61** **17**	**1781.467** **531.175**	**71.658**	**35.933**	**0.9790/65**
3 DGs	MGSA [87]	15 61 63	562.65 1190.11 523.31	71.90	-	-
	PSO [205]	11 17 61	460 440 1700	69.54	-	-
	GWO	20 61 66	358.812 1723.270 503.666	69.732	35.069	0.9788/**65**
	JSO	67 18 61	368.882 477.379 1666.482	70.002	35.199	0.9768/**65**
	BKA	61 66 18	1726.930 459.695 399.268	69.675	35.051	0.9790/**65**
	FLO	20 11 61	378.125 635.620 1637.144	69.718	35.052	0.9768/**65**
	IFLO	**11** **61** **18**	**526.827** **1718.966** **380.052**	**69.410**	**34.953**	**0.9790/65**

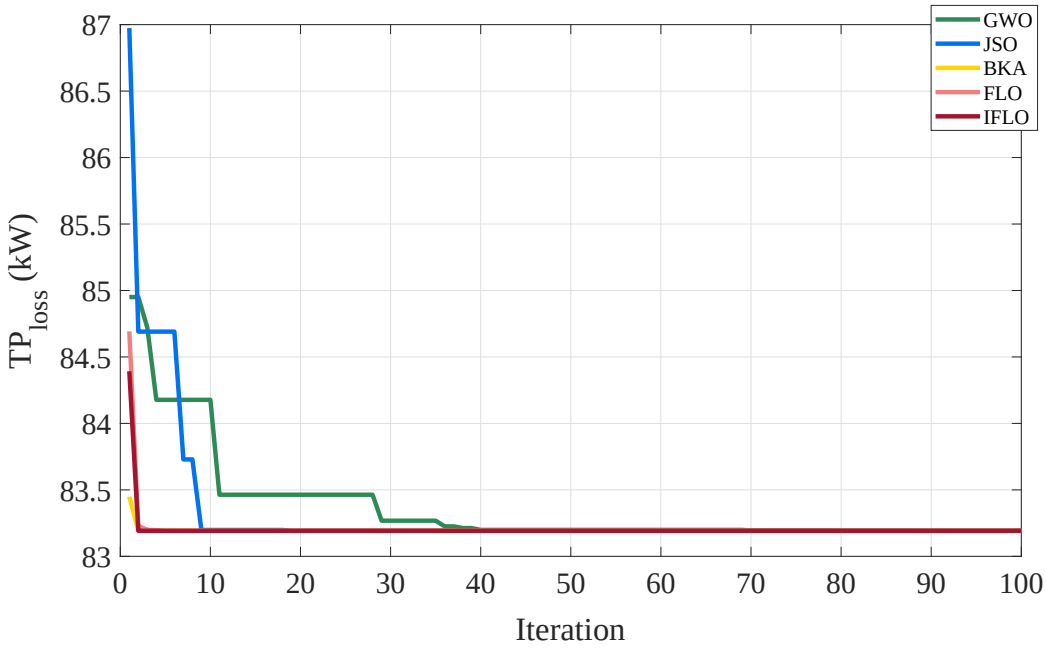

Figure 5.2: Convergence curves for single DG optimisation at Unity-PF

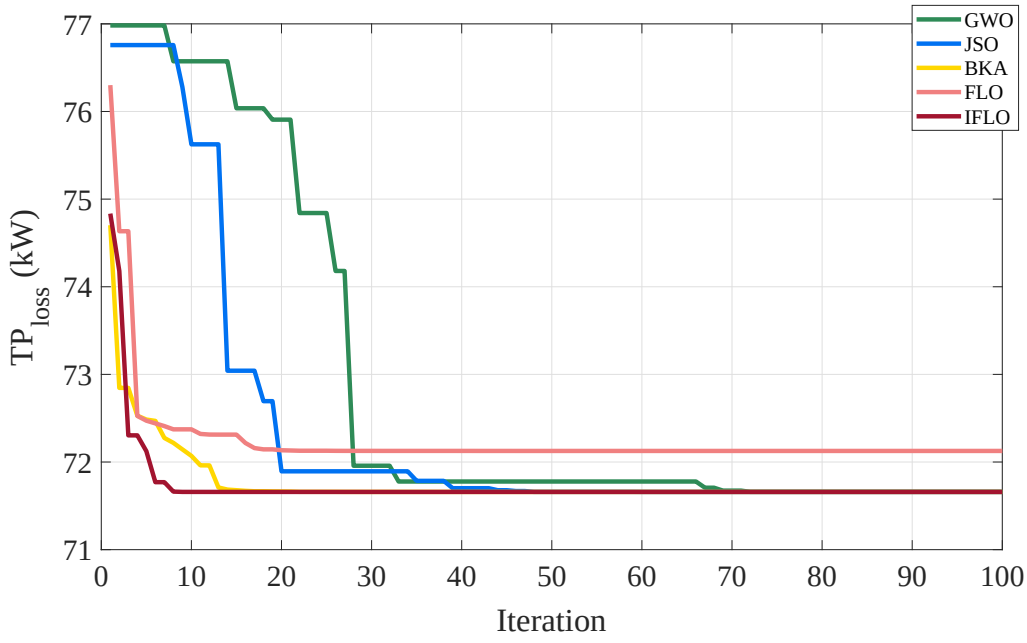

Figure 5.3: Convergence curves for two DG optimisation at Unity-PF

demonstrates a faster convergence rate, achieves the optimum fitness value, and does so in markedly fewer iterations than the competing algorithms.

Figure 5.5 illustrates the voltage profiles recorded with and without DG integration relative to the base case. The plot demonstrates that the voltage level improves

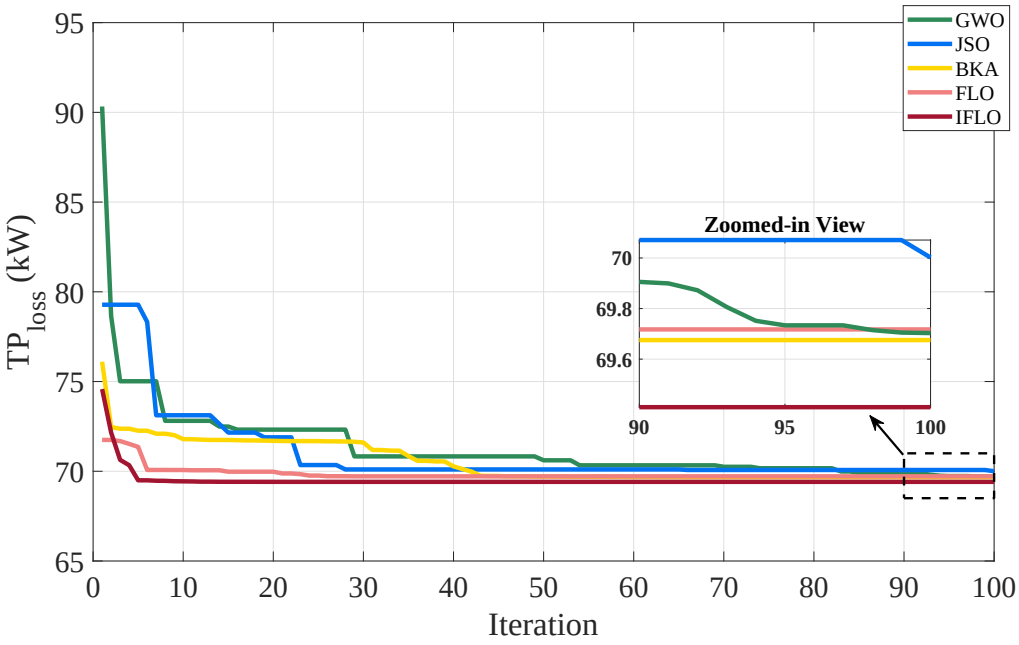

Figure 5.4: Convergence curves for three DG optimisation at Unity-PF

following the integration of DG units, with the most significant enhancements observed when two or three DGs are installed.

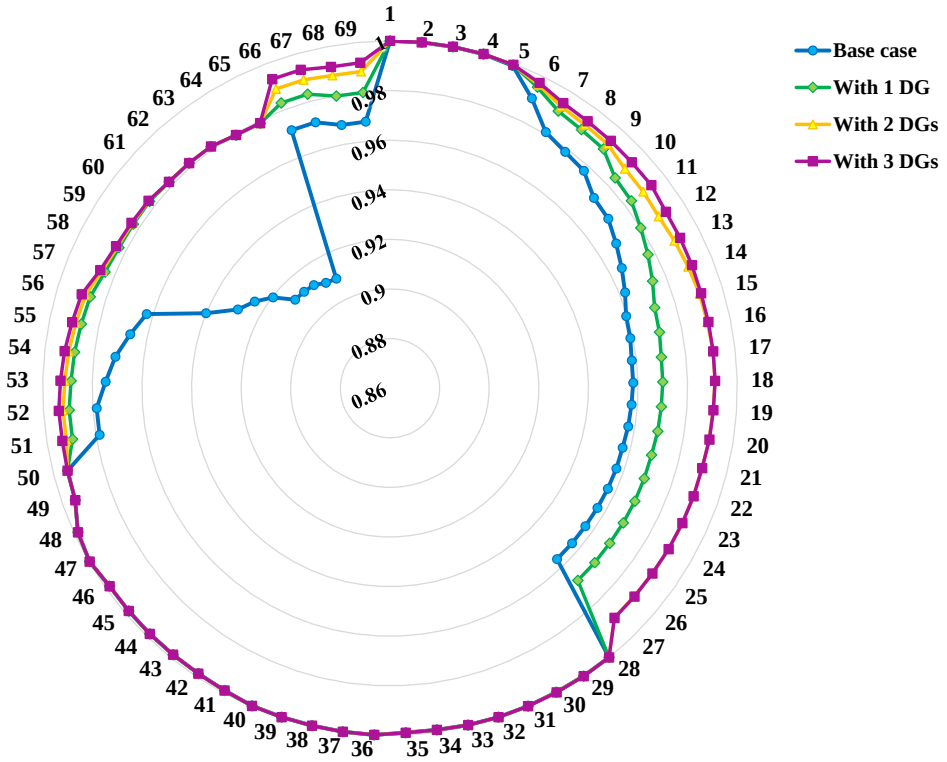

Figure 5.5: Voltage profile of RDG before and after DG integration at unity-PF

5.2.3.2 Scenario 2: DGs integration operating at optimal-PF

Unlike the former scenario, where DG units were assumed to supply solely active power, this scenario considers DGs capable of generating both active and reactive powers, typical of wind turbines. Here, the DG's power factor is treated as an additional decision variable, ranging from 0.7 to 1. In simpler words, the optimization process simultaneously determines the three parameters of optimal placement, sizing, and PF of each DG unit. The corresponding reactive power output is calculated based on the active power and the optimized PF. Accordingly, the optimization problem is formulated as a three-dimensional problem for a single DG operating at an optimal PF, and it expands to six and nine dimensions when considering two and three DG units, respectively.

Table 5.2 summarizes the optimal locations, sizes, and PFs for one, two, and three DGs integrated into the RDG without imposing a fixed unity-PF, alongside the corresponding reductions in system active losses, reactive losses, and improvements in minimum voltages. Likewise, the obtained results are compared with those from other proposed and implemented efficient algorithms, along with findings from previous state-of-the-art studies, to confirm the effectiveness of the proposed approach. Once again, the results in Table 5.2 demonstrate the superior performance of the proposed IFLO algorithm in solving the optimal DG planning problem compared to other methods. This scenario confirms that operating DG units at optimal PFs leads to significantly greater reductions in power losses and improvements in voltage profiles than Scenario 1, where DGs were assumed to operate at unity PF.

Figures 5.6 - 5.8 illustrate the convergence curves of the various optimization methods for scenarios involving one, two, and three DG units operating at optimal PFs, respectively. In each case, the proposed IFLO algorithm exhibits a faster convergence rate and attains the optimal fitness value within significantly fewer iterations than other compared algorithms. For indicative purposes, the average execution time for our developed IFLO was 6.63 seconds. This accelerated convergence and superior optima are attributable to the enhanced strategies embedded in IFLO, which help it avoid premature convergence on local minima while rapidly steering the search toward the global optimum.

Comparing the two scenarios, operating DG units at optimal PFs delivers a marked improvement in system performance over operation at unity PF, underscoring the benefits of flexible PF operation. Moreover, as displayed in Figure 5.9, a significant enhancement in voltage profiles across all buses is observed. The results presented in Table 5.1 and Table 5.2 validate the effectiveness of the proposed IFLO algorithm,

Table 5.2: Results of integrating 1, 2, and 3 DGs with optimal power factor into the RDG

Scenario	Method	Optimal Location	Optimal Sizes (kW)/**PF**	TP_{loss} (kW)	TQ_{loss} (kVAr)	V_{min} **/Bus**
No DGs	-	-	-	224.961	102.147	0.9092/**65**
1 DG	MGSA [87]	61	1820.59/**0.815**	23.15	14.38	0.9724/**27**
	PSO [205]	61	2220/**0.81**	23.20	-	-
	GWO	61	1825.968/**0.815**	23.147	14.375	0.9724/**27**
	JSO	61	1828.412/ **0.815**	23.147	14.369	0.9725/**27**
	BKA	61	1828.412/ **0.815**	23.147	14.369	0.9725/**27**
	FLO	61	1828.412/ **0.815**	23.147	14.369	0.9725/**27**
	IFLO	**61**	**1828.412/0.815**	**23.147**	**14.369**	**0.9725/27**
2 DGs	MGSA [87]	61 18	1647.04/**0.812** 456.31/**0.826**	7.89	8.52	0.9923/**69**
	PSO [205]	61 17	2130/**0.81** 630/**0.82**	7.20	-	-
	GWO	61 14	1670.270/ **0.783** 641.932/**0.870**	8.520	8.387	0.9942/**50**
	JSO	61 17	1736.379/**0.814** 522.596/**0.827**	7.202	8.042	0.9942/**50**
	BKA	18 61	525.530/**0.833** 1732.700/**0.813**	7.204	8.046	0.9942/**50**
	FLO	18 61	630.599/ **0.862** 1597.907/ **0.782**	8.189	8.370	0.9934/**65**
	IFLO	**17** **61**	**522.042/0.828** **1734.674/0.814**	**7.201**	**8.044**	**0.9943/50**
3 DGs	MGSA [87]	61 64 17	970.82/**0.715** 722.92/**0.902** 601.04/**0.789**	8.61	8.47	0.9943/**50**
	PSO [205]	11 18 61	660 **0.83** 460 **0.81** 2060 **0.81**	4.61	-	-
	GWO	21 61 15	282.944/**0.816** 1701.814/**0.784** 202.984/**0.891**	7.459	8.199	0.9935/**69**
	JSO	18 61 50	473.975/**0.827** 1703.679/**0.815** 637.569/**0.845**	5.188	2.784	0.9930/**69**
	BKA	23 61 12	336.425/ **0.821** 1663.489/ **0.808** 404.234/ **0.756**	4.652	6.960	0.9943/**50**
	FLO	22 11 61	425.437/**0.797** 526.497/**0.777** 1479.322/**0.781**	6.212	7.493	0.9911/**65**
	IFLO	**11** **61** **18**	**494.322/0.813** **1674.327/0.814** **378.861/0.833**	**4.267**	**6.758**	**0.9943/50**

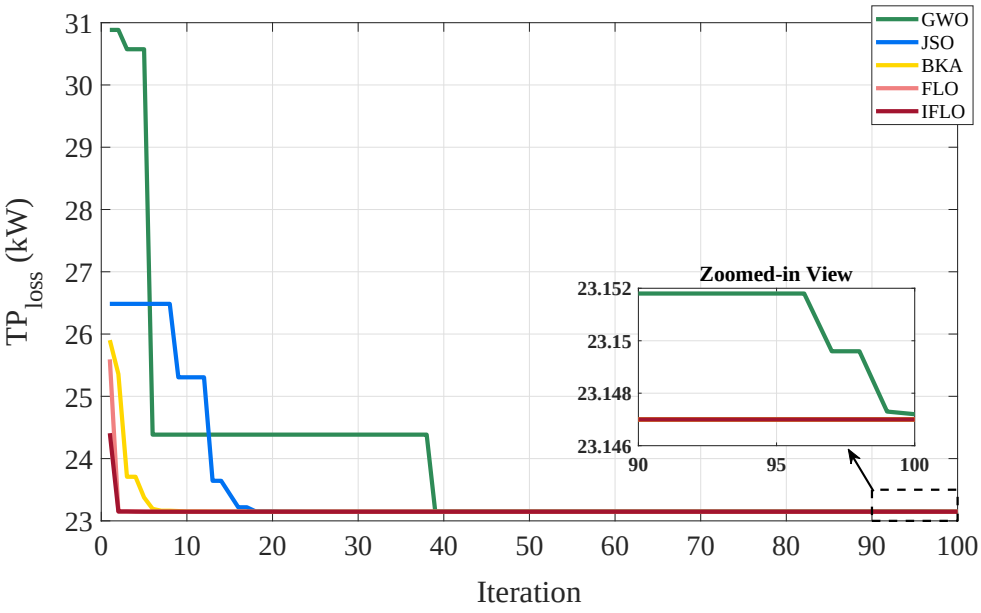

Figure 5.6: Convergence curves for one DG optimization at Optimal-PF

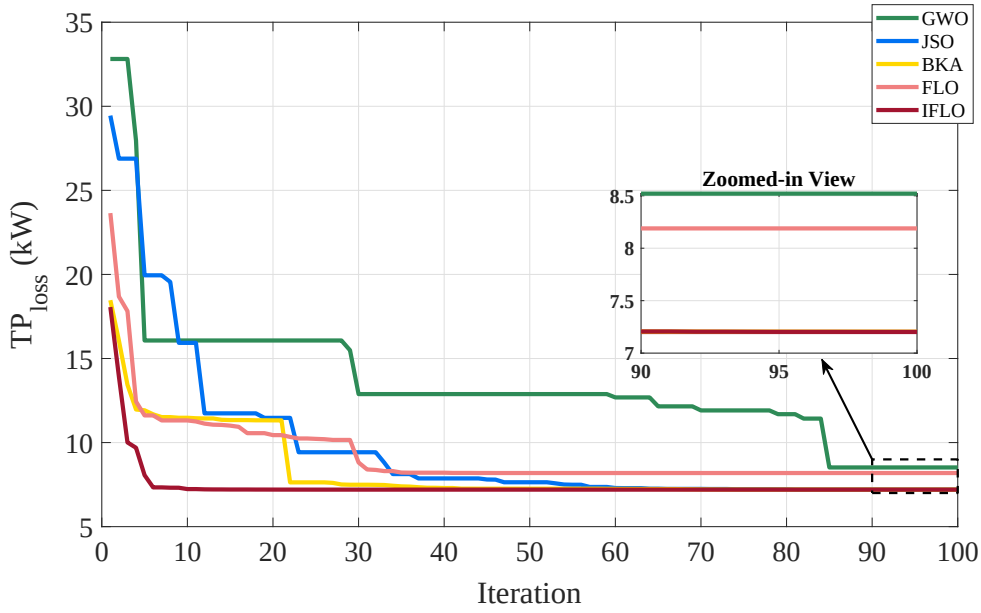

Figure 5.7: Convergence curves for two DG optimization at Optimal-PFs

demonstrating its capability to address problems involving multiple decision variables and expanded search spaces.

By neglecting uncertainties associated with load demand and renewable energy generation, the study highlights the potential of the proposed optimization method to enhance system performance over other conventional methods, under idealized

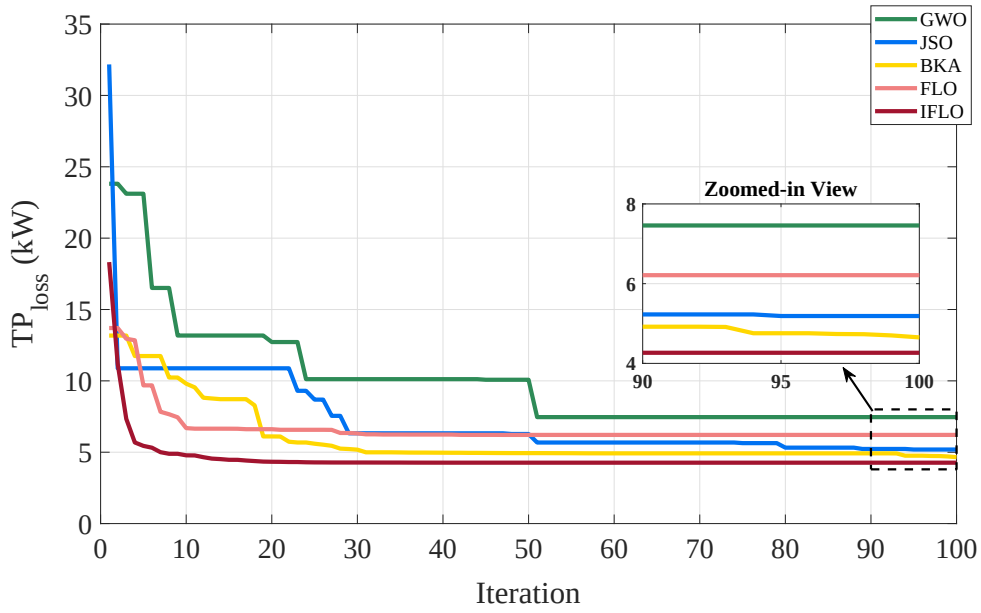

Figure 5.8: Convergence curves for three DG optimization at Optimal-PFs

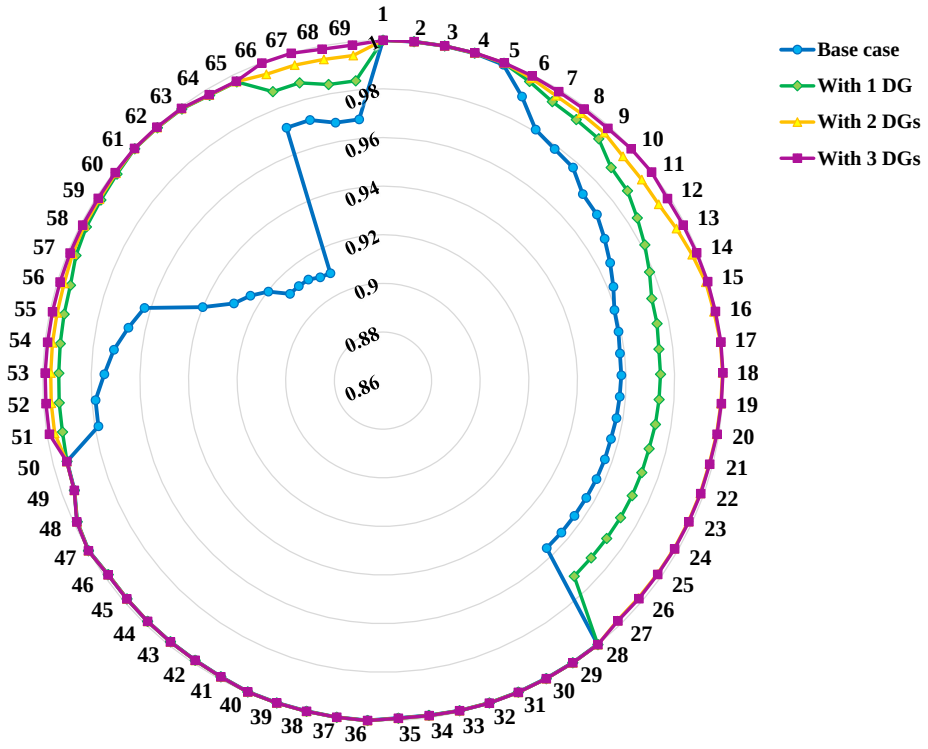

Figure 5.9: Voltage profile of RDG before and after DG integration at optimal-PFs

conditions. However, while these results provide valuable insights, they serve as a benchmark for evaluating the performance of the optimization approach under more complex and realistic scenarios, where uncertainty plays a significant role.

5.3 RES planning considering uncertainties

In this section, we delve into a more complex optimization framework that accounts for uncertainties in both load demand and power generation within a larger distribution grid while addressing multiple objective functions. This realistic scenario captures the inherent variability of distribution grids integrating RESs. The presence of these uncertainties significantly increases the complexity of the optimization problem, requiring the application of sophisticated techniques capable of effectively addressing this dynamic optimization challenge. To this end, we apply our proposed IFLO algorithm to concurrently determine the optimal number and placement of WTs and SPV strings, as well as the optimal PF settings of the WTs, within an 85-bus large-scale distribution system [147].

The multi-objective functions include minimizing average annual power losses and voltage deviation while maximizing the yearly average voltage stability index, all within operational constraints. This study incorporates real-world uncertainties in RES, including variations in wind speed, solar irradiance, ambient temperature, and time-varying load demand, using historical data collected from a study region located in the south of Algeria over a seasonal planning horizon. The proposed IFLO approach is compared against other established and efficient optimization techniques, which are also proposed and implemented in this work.

Finally, a comprehensive analysis of the results will be conducted to gain a deeper understanding of the system's behavior under uncertain conditions, offering insights into both the challenges and potential opportunities that may arise. This analysis facilitates predictive decision-making through a nuanced, data-driven assessment of probabilistic outcomes.

5.3.1 Problem description with uncertainty

This work case addresses the challenge of achieving optimal grid operation by solving the optimal planning problem for RESs, specifically WTs and SPV arrays, alongside determining the optimal PF settings for the WTs within the RDG. Under uncertain conditions, the optimization must be adapted to account for the variability in key parameters. The following subsections present the detailed mathematical formulations of the three objective functions and the associated constraints.

5.3.1.1 Objective functions

The objective functions examined in this case study are as follows:

a) Power loss reduction: RDGs are particularly prone to high real power losses, primarily due to their elevated resistance to reactance (R/X) ratios. Assessing and minimizing these losses is essential for improving the overall operational efficiency of the grid. Following load flow analysis, the annual average power loss can be expressed as follows:

$$APloss = \frac{\sum_{t=1}^{N_t} \sum_{i=1}^{N_b} R_{bi} \left| \frac{V_i^t - V_{i+1}^t}{R_{bi} + jX_{bi}} \right|^2}{N_t} \tag{5.12}$$

where V_i and V_{i+1} denote the voltage magnitudes at the sending bus i and the receiving bus $i+1$ at the t^{th} hour, respectively. R_{bi} and X_{bi} represent the resistance and reactance of the i^{th} branch. N_b is the total number of branches, and N_t is the total number of time periods (hours).

b) Voltage deviation minimization: Voltage deviation quantifies the deviation of bus voltage magnitudes from a specified reference value, V_{ref}, typically set to 1 p.u. Minimizing VD is essential for ensuring compliance with operational standards and maintaining power quality. The annual average total voltage deviation (AVD) can be formulated as follows:

$$AVD = \frac{\sum_{t=1}^{N_t} \sum_{i=1}^{N} \left(V_{\text{ref}} - |V_i^t| \right)^2}{N_t} \tag{5.13}$$

Here, N denotes the total number of buses, and V_i^t represents the voltage magnitude at bus i during the t^{th} hour.

c) Voltage stability index maximization:

As discussed in Chapter Two, the Voltage Stability Index (VSI) reflects the power system's ability to maintain stable voltage levels under varying load conditions. For reliable grid operation, the VSI should remain greater than zero across all buses in the distribution grid. Buses exhibiting lower VSI values are more vulnerable to voltage instability. Therefore, maximizing the VSI is essential to ensure system stability. The mathematical expression for the VSI at the $(i+1)^{\text{th}}$ bus in a radial distribution grid at the t^{th} hour is given as follows [206]:

$$VSI_{i+1}^t = |V_i^t|^4 - 4(P_{di+1}^t R_{bi} + Q_{di+1}^t X_{bi})|V_i^t|^2 - 4(P_{di+1}^t X_{bi} - Q_{di+1}^t R_{bi})^2 \tag{5.14}$$

where P^t_{di+1} and Q^t_{di+1} represent the active and reactive power demands, respectively, at the $(i+1)^{\text{th}}$ bus during the t^{th} hour. The annual average voltage stability index (AVSI) for the entire distribution grid can be expressed as follows:

$$AVSI = \frac{\sum_{t=1}^{N_t} \sum_{i=1}^{N-1} VSI^t_{i+1}}{N_t} \tag{5.15}$$

The optimization problem simultaneously considers the three aforementioned objective functions. A weighted aggregation sum method is employed to formulate the multi-objective function. Accordingly, the fitness function is defined as follows:

$$Fitness = \delta_1 F_1 + \delta_2 F_2 + \delta_3 F_3 \tag{5.16}$$

with,

$$\sum_{i=1}^{3} \delta_i = 1,\ \delta_i \in [0,1] \tag{5.17}$$

The following formulas are used to normalize the objective functions:

$$F_1 = \frac{APloss}{APloss_{base}} \tag{5.18}$$

$$F_2 = \frac{AVD}{AVD_{base}} \tag{5.19}$$

$$F_3 = \frac{AVSI}{AVSI_{base}} \tag{5.20}$$

where F_1, F_2, and F_3 denote the normalized objective functions, and δ_1, δ_2, and δ_3 are the corresponding weighting factors, chosen as 0.5, 0.25, and 0.25, respectively [207].

5.3.1.2 System constraints

In addressing the optimal planning problem of RESs, the proposed approach must satisfies all system constraints, including both equality and inequality constraints, as outlined below.

a) **Equality constraints** Maintaining a balance between power generation and the total power demand, including losses, is essential to prevent reverse power flow, which can potentially harm the system. These power balance constraints are formulated as follows:

$$P_{\text{sub}}^{t} + \sum_{i=1}^{N_f} P_{\text{WT}}^{t} \times n_{\text{WT},i} + \sum_{i=1}^{N_f} P_{\text{PVS}}^{t} \times n_{\text{PVS},i} = \sum_{j=2}^{N} P_{d,j}^{t} + \sum_{j=1}^{Nb} P_{loss,j}^{t} \tag{5.21}$$

$$Q_{\text{sub}}^{t} + \sum_{i=1}^{N_f} Q_{\text{WT}}^{t} \times n_{\text{WT},i} = \sum_{j=2}^{N} Q_{d,j}^{t} + \sum_{j=1}^{Nb} Q_{loss,j}^{t} \tag{5.22}$$

where P_{sub}^{t} and Q_{sub}^{t} denote the total active and reactive power supplied by the substation to the distribution grid at the t^{th} hour, respectively. P_{WT}^{t} and P_{PVS}^{t} represent the power generated by WTs and SPV strings at the t^{th} hour, respectively. N_f indicates the number of farms, while $n_{\text{WT},i}$ and $n_{\text{PV},i}$ denote the number of installed WT and SPV units in the i^{th} farm. $P_{d,j}^{t}$ and $Q_{d,j}^{t}$ correspond to the active and reactive power demands at branch j during time period t. The total active and reactive power losses in branch j at time t are represented by $P_{loss,j}^{t}$ and $Q_{loss,j}^{t}$, respectively.

b) Inequality constraints

- RES-based DG location limit: Each type of DG can be installed at any bus in the system, except at the slack bus (substation), as expressed below:

$$2 \leq DG_{loc,j} \leq N \quad j \in type \tag{5.23}$$

- Bus voltage limit: The voltage level at each bus must be held within specified standard limits in real-time, as given below:

$$V_{min} \leq V_{i}^{t} \leq V_{max} \tag{5.24}$$

  In the inequality above, V_{min} and V_{max} represent the minimum and maximum permissible voltage levels at any bus during each hour.

- RES-based DG penetration limits: The total rated capacity of the integrated RESs must not exceed the overall system load demand, as described below:

$$\sum_{i=1}^{N_f} P_{\text{WT,rated}}^{t} \times n_{\text{WT},i} + \sum_{i=1}^{N_f} P_{\text{PVS,rated}}^{t} \times n_{\text{PVS},i} \leq \sum_{j=2}^{N} P_{d,j}^{t} \tag{5.25}$$

- WT power factor limit: The PF of each wind farm is treated as an adjustable parameter within the optimization process, enabling reactive power support when needed. It falls within the following range:

$$PF_{min} \leq PF_i \leq PF_{max} \quad i = 1, 2, \ldots, N_f \tag{5.26}$$

Accordingly, the reactive power supplied by each wind farm at each hour t is defined as a function of the active power and PF as expressed below:

$$Q^t_{\mathrm{WT}} \times n_{\mathrm{WT},i} = P^t_{\mathrm{WT}} \times n_{\mathrm{WT},i} \times \tan\left(cos^{-1}(PF_i)\right) \quad i = 1, 2, \ldots, N_f \tag{5.27}$$

On the other side, SPV arrays are assumed to operate at a unity-PF, as they are typically designed to generate only active power, without supplying or absorbing reactive power.

- Thermal limit: To ensure line security, the current flowing through branch i at the t^{th} hour, denoted as I^t_{bi}, must remain below its specified maximum limit, as expressed below:

$$I^t_{bi} \leq I^{\max}_{bi} \quad i = 1, 2, \ldots, N_b \tag{5.28}$$

where $I^{\max}_{bi}$ symbolizes the maximum current-carrying capacity of the i^{th} branch.

5.3.2 Data analysis

Analyzing local weather data alongside load patterns is a critical initial step in addressing the optimal planning problem of RESs into distribution grids. The system under study is assumed to follow the standard time-varying load profile of the IEEE-RTS [64, 169]. The annual load is divided into four seasons: summer, autumn, winter, and spring. Each seasonal load is represented by the hourly load of a day (24 hours), resulting in a total of 96 hours (24 × 4) that represent the entire year's load profile (8760 hours). Accordingly, the seasonal hourly load profile is illustrated in Figure 5.10.

Historical data on wind speed, solar irradiance, and ambient temperature were collected from the In Salah region, a province located in central Algeria, in the Sahara, over a decade (from 01 January 2012 to 31 December 2021). These data are accessible through the NASA website [208]. Figure 5.11 shows the precise location of In Salah Province.

For this study, each year is divided into four seasons: summer (May to July), autumn (August to October), winter (November to January), and spring (February to April). Each season is represented by a day of 24 hours, capturing the hourly variability of RESs during that season. Consequently, the entire year is represented

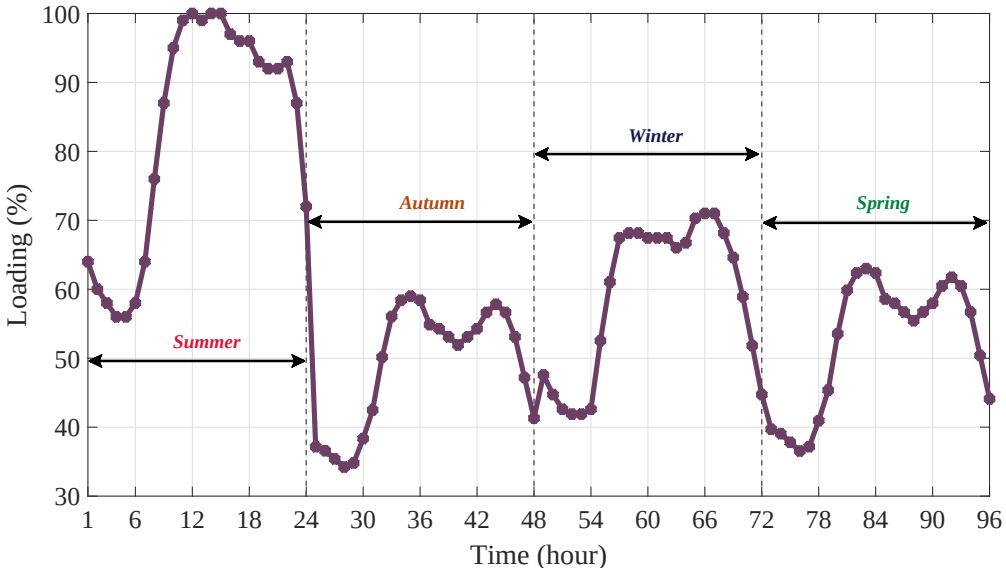

Figure 5.10: Seasonal hourly load profile

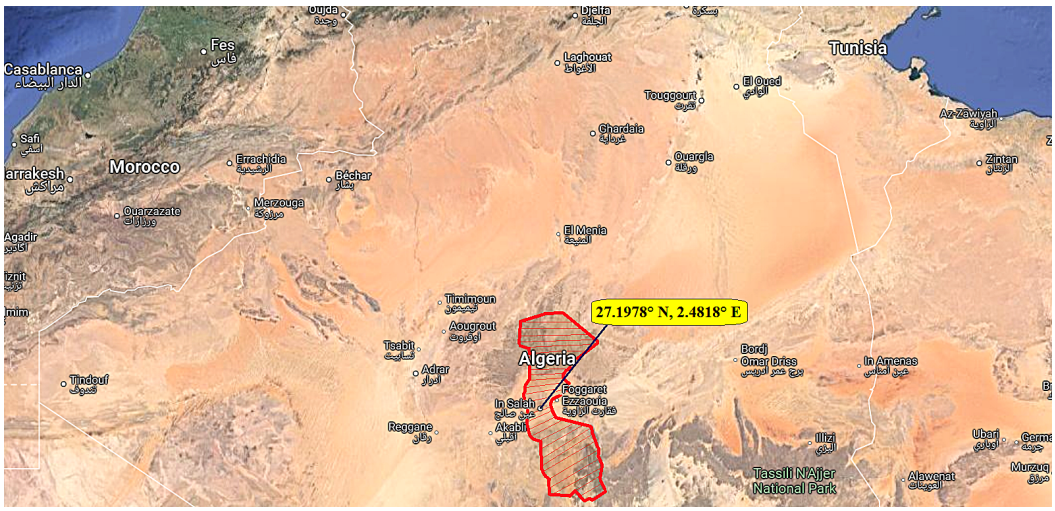

Figure 5.11: Geographical location of the studied area shown on Google Maps

by four seasonal days, totaling 96 hours. Weibull and beta PDFs are then generated for each hour to accurately fit the hourly seasonal wind speed and solar irradiance, respectively. The adjustment steps are set at 1 m/s for wind speed and 0.05 kW/m^2 for solar irradiance. For illustration, the probability distributions of wind speed for the 22$^{\text{nd}}$ hour in summer and solar irradiance for the 14$^{\text{th}}$ hour in spring are shown in Figure 5.12 and Figure 5.13, respectively.

The ambient temperature is represented by averaging the hourly temperature values for each season. Accordingly, the seasonal hourly average temperatures are depicted in Figure 5.14.

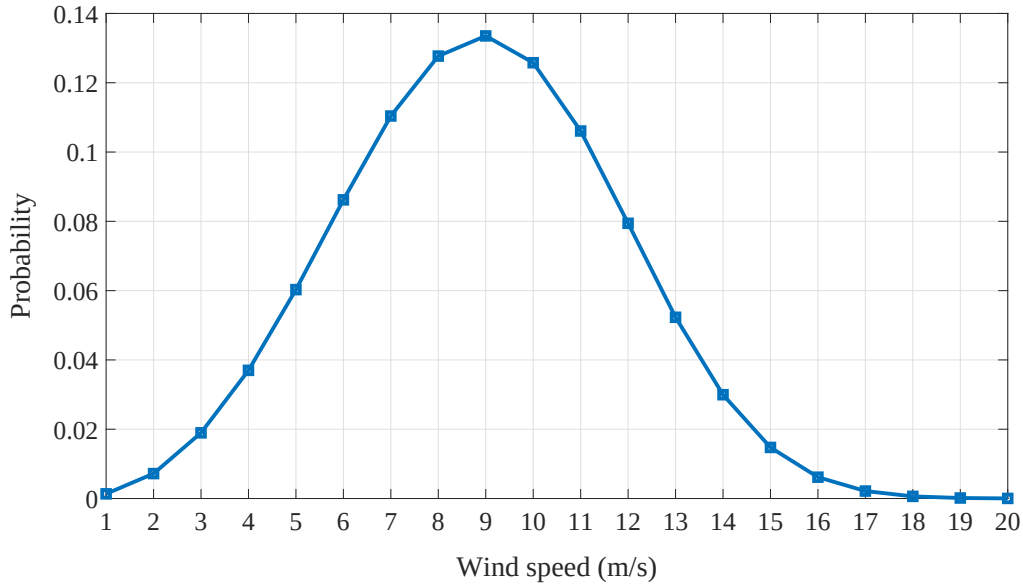

Figure 5.12: Weibull PDF of wind speed for the 22$^{\text{nd}}$ hour of summer (for $k = 3.4217$ and $c = 9.8850$).

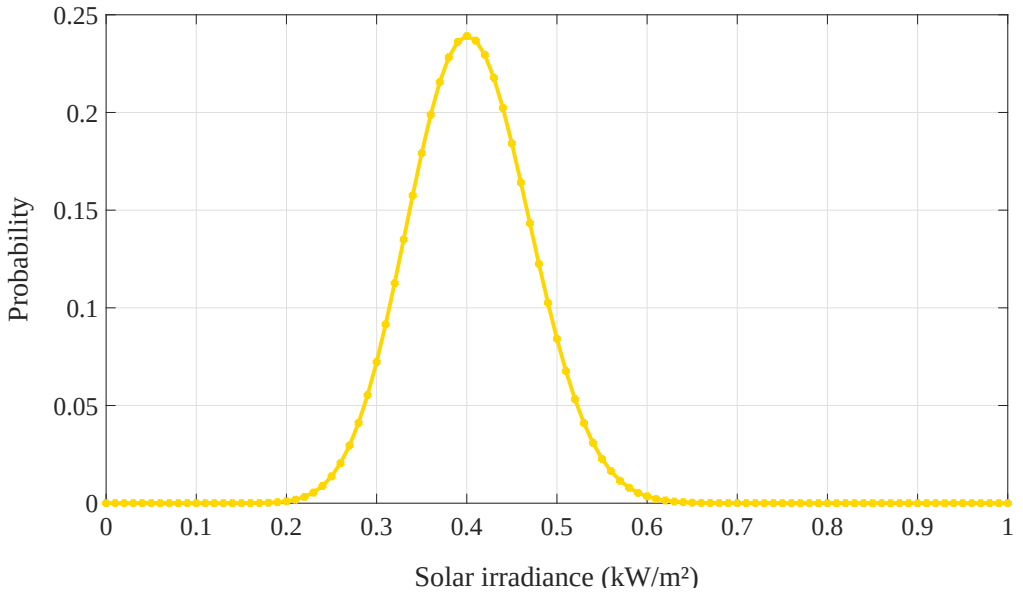

Figure 5.13: Beta PDF of solar irradiance for the 14$^{\text{th}}$ hour of spring (for μ=0.4042 and σ= 0.1012)

5.3.3 Simulation Results and Discussions

The proposed IFLO algorithm is applied to the 85-bus large-scale RDG of 11 kV [147]. The developed load-generation model serves as input data to address the optimal planning problem of RESs into the distribution grid. Load flow analysis is performed

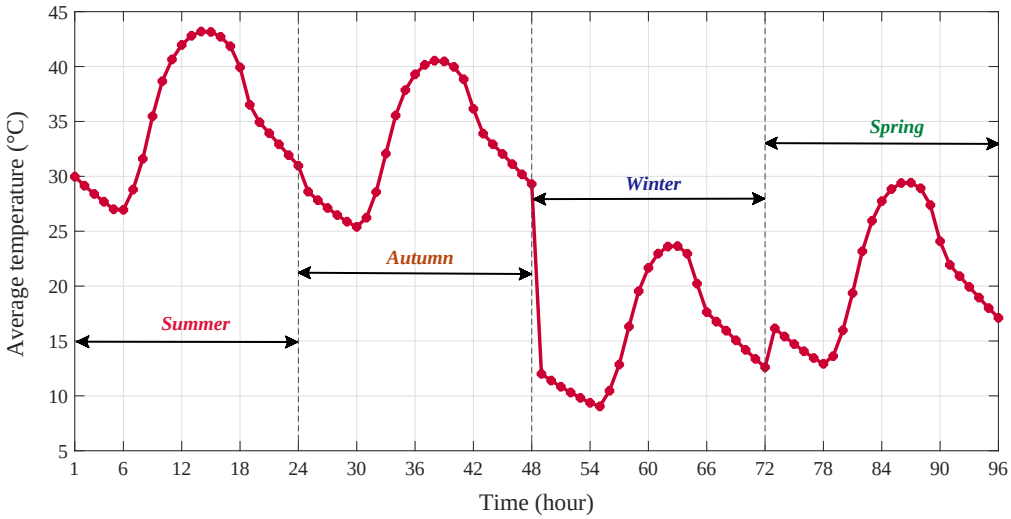

Figure 5.14: Seasonal hourly average temperature

using the backward/forward sweep method [138], which is well-suited for radial grid structures. A schematic representation of the optimization flow process adopted in the proposed framework is shown in Figure 5.15.

This study examines the integration of two wind farms and two solar farms into the RDG. The WTs employed have a rated capacity of 250 kW each, while each SPV string comprises 20 panels, yielding a total output rated at 4.4 kW per string. The technical specifications of both the SPV modules and WTs are summarized in Table 5.3 [103].

To evaluate the performance of the proposed IFLO algorithm, a comparative analysis is conducted against three well-established and effective optimization techniques, namely

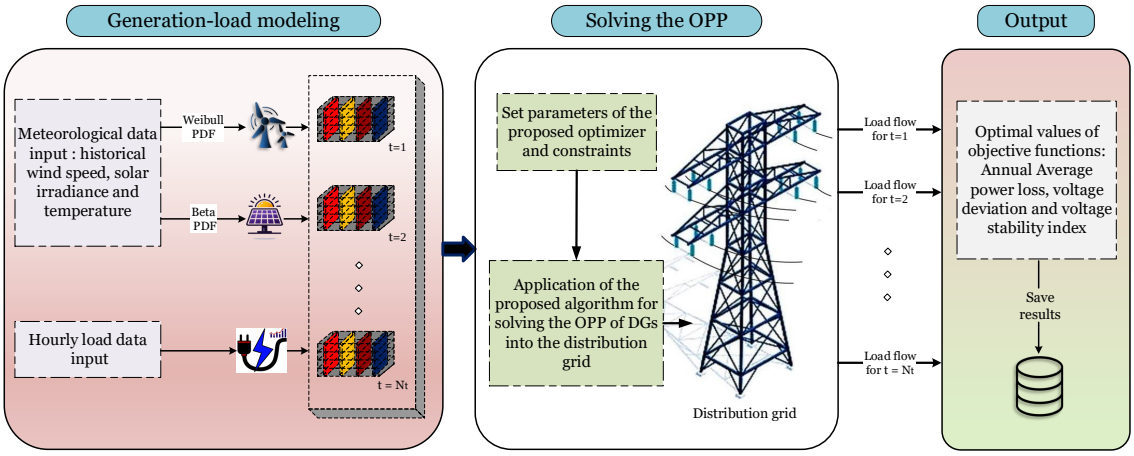

Figure 5.15: Optimization flow process for addressing the optimal planning problem of RESs into the RDG

Table 5.3: Technical Parameters of SPV and WT unit

Parameters	Value
SPV unit	
Current at maximum power point, I_{MPP}	7.76 A
Voltage at maximum power point, V_{MPP}	28.36 V
Short circuit current, I_{sc}	8.38 A
Open circuit voltage, V_{oc}	36.96 V
Nominal cell operating temperature, N_{OT}	49 °C
Current temperature coefficient, K_i	0.00545 A/°C
Voltage temperature coefficient, K_v	0.1278 V/°C
WT unit	
Rated output power, P_{rated}	250 kW
Cut-in speed, w_{in}	3 m/s
Rated speed, w_{N}	12 m/s
Cut-out speed, w_{out}	25 m/s

GWO, BKA, and the original FLO algorithm. All algorithms are applied to the same dataset to ensure consistency and fairness in comparison. The population size and maximum number of iterations are fixed at 30 and 50, respectively, as detailed in Table 5.4, along with the operational system constraints. The modeling of uncertainties associated with WTs, SPV systems, and load demand is discussed in detail in Chapter Three, within the context of the hourly planning horizon.

Table 5.4: Parameters values limitations

Parameters	Value
Number of population	30
Maximum iterations	50
Voltage boundaries [108]	$0.9\,p.u \leq V_i^t \leq 1.05\,p.u$
Size of WT units	$0 \leq WT \leq 10$ turbines
Size of SPV strings	$0 \leq SPV \leq 584$ strings
WT Power factor	$0.7 \leq PF \leq 1$
SPV system power factor	1

Table 5.5 summarizes the energy management results for the 85-bus system using the different optimization techniques, both before and after the integration of RES units. These results underscore the system performance enhancements achieved through the suitable installation of WTs and SPV strings. In the base case, without any RES integration, the annual average power losses, voltage deviation, and voltage stability

Table 5.5: Optimal planning results for RESs integration into the 85-bus RDG

Specification	Without RESs	With RESs installation			
		GWO	BKA	FLO	IFLO
RES Parameters					
Optimal location of SPV farms	–	46 29	42 51	45 48	52 70
Optimal number of SPV strings	–	25 84	114 12	83 103	74 55
Optimal rated power of SPV farms (kW)	–	110 370	502 53	365 453	326 242
Optimal location of WT farms	–	63 34	34 68	35 64	35 68
Optimal number of installed WT units	–	1 7	5 3	4 3	5 3
Optimal rated power of WT farms (kW)	–	250 1750	1250 750	1000 750	1250 750
Optimal PF of WTs (kW)	–	1 0.7000	0.7068 0.7005	0.7264 0.7066	0.7000 0.7000
System Performance Metrics					
Annual average Ploss (kW)	118.2953	46.0170	35.6760	40.0428	**35.1939**
Annual average VD (p.u)	0.30662	0.0790	0.0688	0.0753	**0.0659**
Annual average VSI (p.u)	1.3744	1.1757	1.1359	1.1515	**1.1315**
Annual average min VSI (p.u)	0.7355	0.8566	0.8856	0.8737	**0.8884**
Annual average min voltage (p.u)	0.9252	0.9614	0.9696	0.9663	**0.9704**
Best fitness value	-	0.47277	0.41347	0.44013	**0.40834**

Note: Bolded values represent the best obtained solutions.

index were recorded at 118.2953 kW, 0.30662 p.u., and 0.7355 p.u., respectively. Following the incorporation of RES units, the proposed IFLO algorithm effectively determines optimal control parameters for WTs and SPV strings, resulting in a significant reduction in annual average power losses to 35.1939 kW (a 70.25% decrease), a reduction in voltage deviation to 0.0659 p.u. (an improvement of 78.51%), and an increase in the voltage stability index to 0.8884 p.u. (a 20.79% enhancement).

The optimal placements for WT farms are determined at Buses 35 and 68, with 5 and 3 WT units installed, respectively. For SPV farms, the optimal locations are Buses 52 and 70, comprising 74 and 55 SPV strings, respectively. This corresponds to WT ratings of 1250 kW and 750 kW and SPV ratings of 326 kW and 242 kW, respectively. According to the obtained results in Table 5.5, it is evident that the proposed IFLO

algorithm exhibits superior performance over other methods, namely GWO, BKA, and the original FLO, in achieving optimum results.

Figure 5.16 and Figure 5.17 display the predicted seasonal power generation from each WT and SPV farm. These figures demonstrate the variability in power output throughout the year due to changes in key uncertain factors such as wind speed, solar irradiance, and ambient temperature.

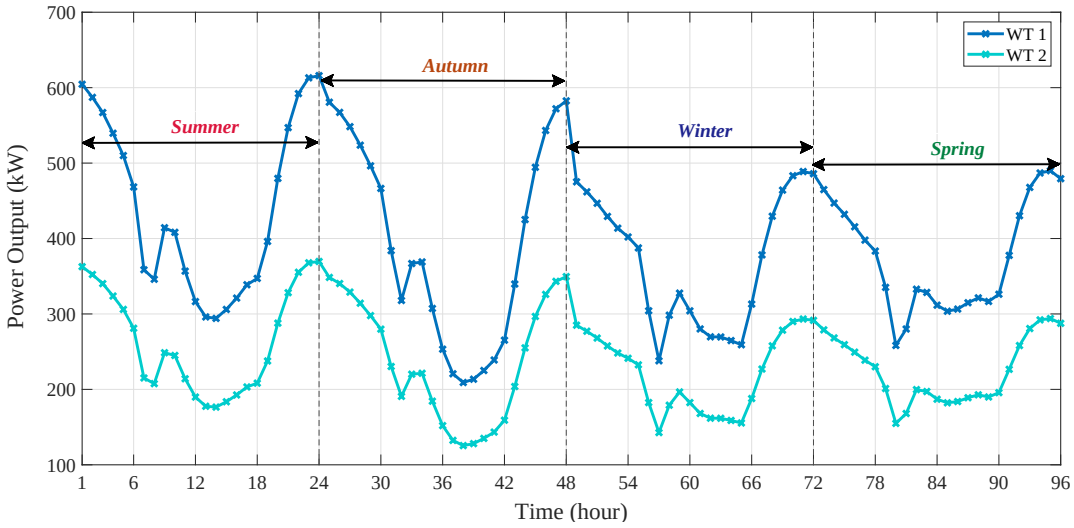

Figure 5.16: Predicted hourly seasonal power generated by wind farms

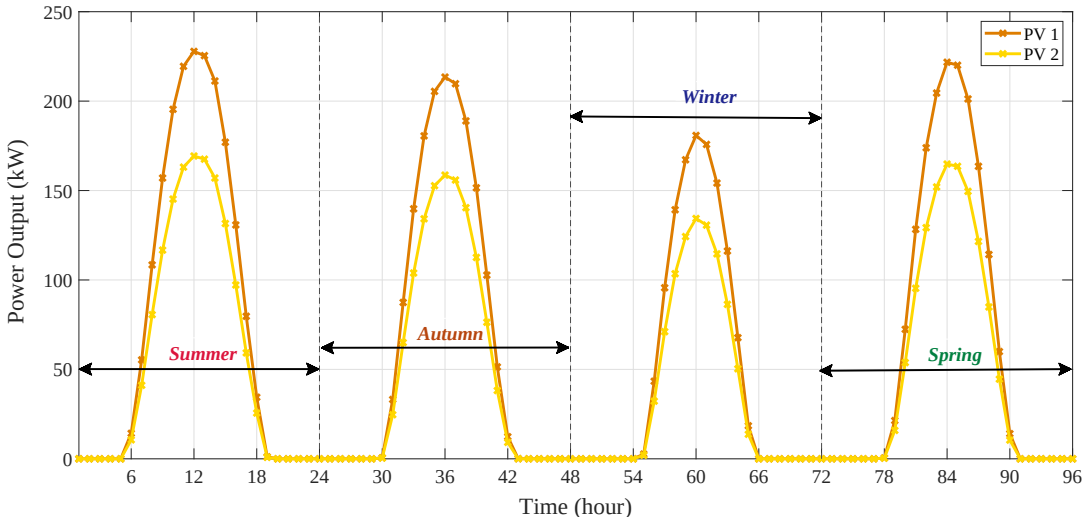

Figure 5.17: Predicted hourly seasonal power generated by SPV farms

Figure 5.18 and Figure 5.19 show the system voltage profiles of both with and without RES integration. It is clear from these figures that there is a significant enhancement in voltage levels following the incorporation of WT units and SPV strings.

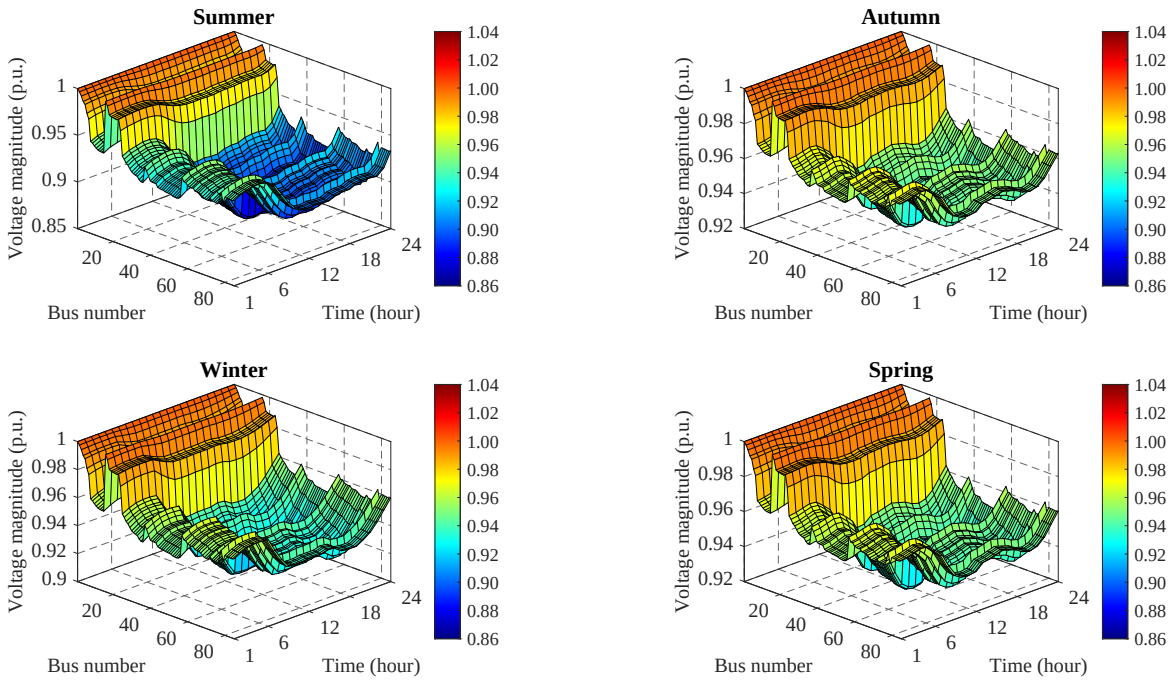

Figure 5.18: Seasonal voltage profiles for the 85-bus RDG without RESs integration

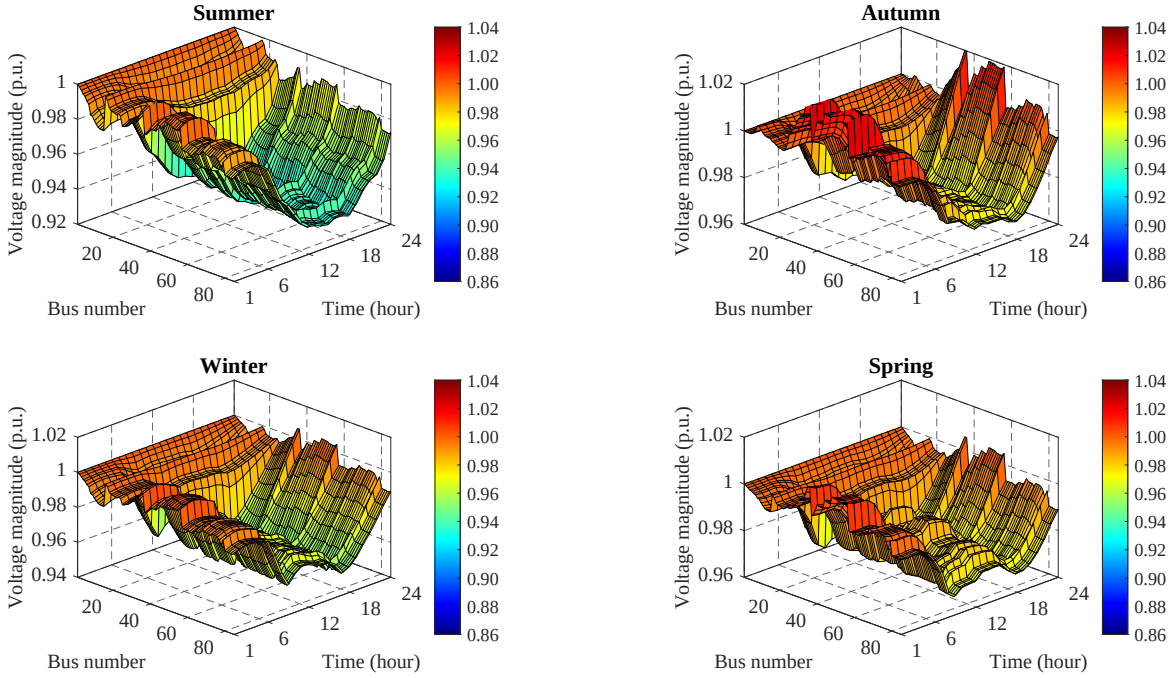

Figure 5.19: Seasonal voltage profiles for the 85-bus RDG in the presence of RESs

Moreover, as shown in Figure 5.20, the incorporation of RES leads to a notable reduction in power losses across seasons of the year, particularly during peak load periods, demonstrating the impact of RES in improving system efficiency and reducing energy costs. Additionally, Figure 5.21 depicts the positive effect of RES integration

on voltage stability, with a consistent improvement observed throughout seasons of the year. These findings further underscore the benefits of RES integration in maintaining stable and reliable voltage levels.

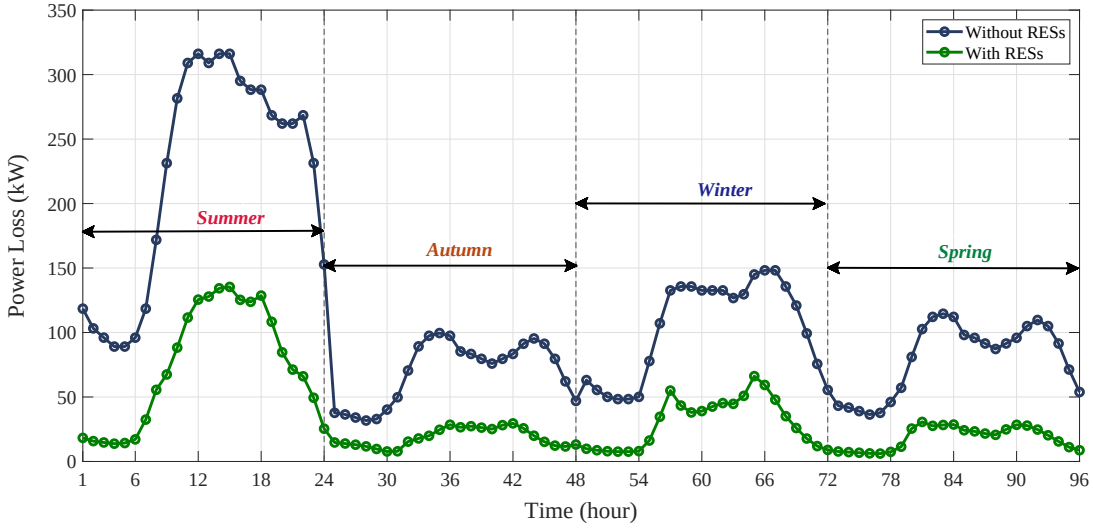

Figure 5.20: Seasonal power losses for the 85-bus RDG without and with the integration of RESs

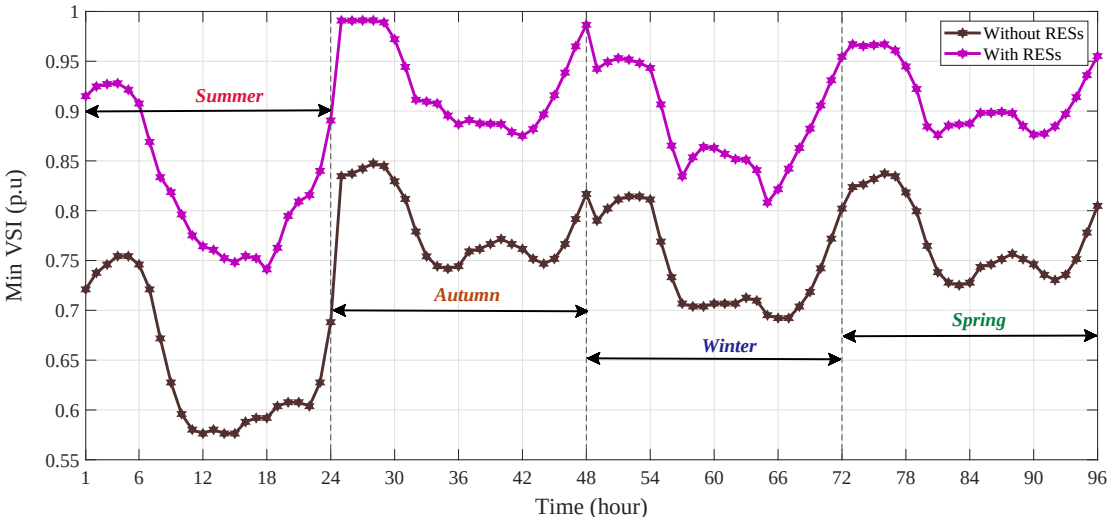

Figure 5.21: Minimum VSI recorded at prior and after the integration of RESs for each season and hour

Table 5.6 provides a performance comparison of fitness values obtained by the IFLO algorithm against other efficient optimization techniques, namely GWO, BKA, and the original FLO. The results demonstrate that the proposed method outperforms the others across key performance metrics: mean, best, and worst values, demonstrating its robustness and effectiveness in addressing the optimal planning problem of RESs.

Table 5.6: Fitness value comparison of algorithms

Algorithm	Best	Average	Worst	SD
GWO	0.47277	0.48293	0.50171	0.008884
BKA	0.41347	0.425872	0.44654	0.012735
FLO	0.44013	0.45965	0.47262	0.010950
IFLO	**0.40834**	**0.40960**	**0.41207**	**0.001232**

Note: Bolded values represent the best obtained solutions.

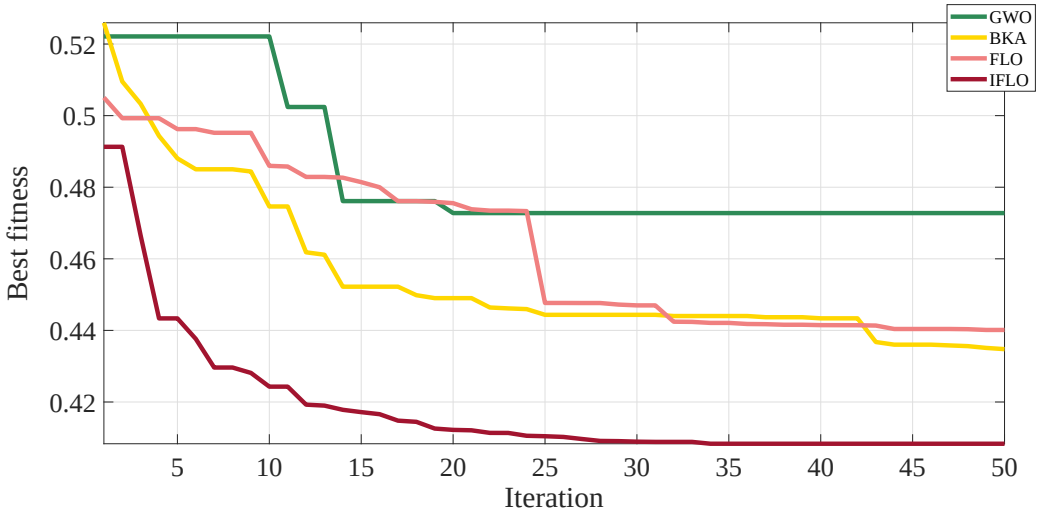

Figure 5.22: Convergence behavior of various algorithms addressing the optimal planning problem of RESs in the 85-bus RDG

Besides, Figure 5.22 presents the convergence behavior for the RES integration problem in the RDG. The proposed IFLO algorithm demonstrates the fastest convergence and achieves the lowest fitness value among the compared methods. As an indication, the mean convergence time achieved with the proposed IFLO was 246.66 seconds per iteration, which is very acceptable. This enhanced performance is attributed to the improvement strategies incorporated within the algorithm.

5.4 Conclusion

This chapter tackled the complex challenge of the optimal planning problem for renewable energy sources (RESs), specifically the integration of wind turbines (WTs) and solar photovoltaic (SPV) farms into distribution grids. A comprehensive analysis and comparison were conducted to evaluate the performance of the proposed Improved Frilled Lizard Optimization (IFLO) algorithm against other recent and efficient optimization techniques, including GWO, JSO, BKA, and the original FLO, all of which were also proposed and implemented in this study. The chapter examined two distinct

case studies. The first addressed a single-objective optimization problem, focusing solely on minimizing active power losses within the common IEEE 69-bus medium-scale distribution system without accounting for uncertainties. In contrast, the second case study considered a further complex and realistic scenario based on the IEEE 85-bus large-scale distribution system. Here, uncertainties in both load and generation were incorporated over a seasonal planning horizon, in which a multi-objective optimization framework is adopted, including minimizing average annual active power losses and voltage deviation while maximizing the yearly average voltage stability index. The results demonstrate that the proposed IFLO algorithm significantly outperforms conventional optimization methods in terms of convergence speed and solution quality. Moreover, the detailed investigation conducted under uncertainty further confirmed the efficacy and robustness of the IFLO technique in selecting appropriate control parameters in the presence of uncertain factors.

In summary, the IFLO algorithm offers a valuable and efficient optimization tool for the sustainable and reliable planning of RES units in distribution grids. By leveraging this approach, significant reductions in power losses, enhancements in voltage profiles, improvements in grid voltage stability, and overall increases in network efficiency and robustness can be achieved. Consequently, the proposed method supports the development of smart planning and operational strategies, facilitating present and future applications in modern power system planning.

Conclusion and Future Work

The continued increase in energy consumption has positioned distribution networks as a central focus from an optimization perspective. Distributed generation (DG) presents a promising pathway to mitigate power losses, reduce voltage drops, enhance system stability, lower carbon emissions, alleviate heavy loading, and boost long-term system reliability. However, the unplanned integration of such DG units can negatively impact the operational performance of distribution grids. In this context, the work presented in this thesis addressed the challenge of the optimal planning of renewable energy sources (RESs)-based DG, specifically wind turbines and solar photovoltaic systems integration within radial distribution grids of various sizes and complexities.

Accordingly, we have identified the optimal locations and sizes for integrating solar photovoltaic and wind energy sources into the IEEE 69-bus medium-scale and 85-bus large-scale distribution grids. This was achieved by developing a novel approach, the Improved Frilled Lizard Optimizer (IFLO) algorithm, specifically designed to address the optimal planning problem for renewable energy integration. This approach incorporates advanced strategies to enhance its search capabilities and prevent premature convergence or entrapment in local minima. In addition, other recent algorithms, including GWO, JSO, BKA, and the original FLO, were also proposed and implemented within this thesis to enable a comprehensive comparative analysis. The impact of RES integration on key system performance metrics, such as active power losses, voltage deviation, and voltage stability index, was thoroughly analyzed through single and multi-objective function formulations. The backward/forward sweep method was employed for the load flow solution due to its accuracy, robustness, and computational efficiency, utilizing a topology-based approach.

The study accounted for uncertainties inherent to renewable energies to ensure their reliable integration into distribution grids. Uncertainty modeling based on probability density functions involved considering seasonal variation in wind speed, solar irradiance availability, and fluctuation in ambient temperature throughout the year, alongside the seasonal fluctuation in load demand. This analysis was supported by a decade of historical meteorological data collected from the In Salah region of Algeria, all within a

time-dependent generation-load model to develop robust and resilient renewable energy integration strategies. Simulation results demonstrate that the newly developed IFLO algorithm significantly outperforms other conventional methods, including GWO, JSO, BKA, and the original FLO, in terms of convergence speed toward the global optimum and solution quality across all scenarios.

This research presented a foundation for understanding the potential benefits and limitations of incorporating renewable energy into electrical grids. The developed methodological framework provides valuable guidance for planners and operators, enabling robust and informed decision-making in the face of the increasing uncertainty and variability inherent in modern power systems. Besides, the proposed IFLO approach offers a powerful and promising optimization tool for enhancing multiple performance metrics, paving the way to effective and sustainable system integration while demonstrating its applicability to real-world scenarios.

Looking ahead, this research opens several promising directions for future investigations. The following recommendations are proposed for future work:

- Examining recent optimization techniques for solving the optimal planning problem of RES while accounting for uncertainty. Additionally, enhancing the search capabilities of these algorithms by integrating newly advanced strategies to more effectively explore the search space.
- A promising area for further research is the integration of electric vehicle (EV) charging stations alongside RES into distribution grids, considering uncertainties related to EVs, electricity pricing fluctuations, and load growth.
- Expanding the current framework by considering additional emerging factors such as cost-effectiveness, grid resilience under extreme conditions, and grid capacity expansion.
- Explore and investigate advanced forecasting techniques, such as machine learning-based models, to manage uncertainty effectively.
- Future research could investigate the optimization of distributed energy resources, such as rooftop solar panels, small-scale wind turbines, and battery storage systems, within distribution grids. This includes studying their impact on distribution system security, voltage regulation, and power quality issues, such as frequency balance, voltage stabilization, and reactive power regulation.
- Optimization in the presence of demand response programs, where consumers adjust their power usage during peak times in response to price signals, could be integrated into optimization frameworks to enhance network performance and reduce operational costs.

References

[1] Muhammad Shahroz Sultan, Syed Ali Abbas Kazmi, Abdullah Altamimi, Zafar A. Khan, and Dong Ryeol Shin. Multi-Objective Optimization-Based Approach for Optimal Allocation of Distributed Generation Considering Techno-Economic and Environmental Indices. *Sustainability (Switzerland)*, 15(5):4306, 2023.

[2] Mohamed A. Tolba, Hegazy Rezk, Mujahed Al-Dhaifallah, and Ayman A. Eisa. Heuristic optimization techniques for connecting renewable distributed generators on distribution grids. *Neural Computing and Applications*, 32(17):14195–14225, 2020.

[3] Essam A. Al-Ammar, Kiran Farzana, Asad Waqar, Muhammad Aamir, Saifullah, Azhar Ul Haq, Muhammad Zahid, and Memoona Batool. ABC algorithm based optimal sizing and placement of DGs in distribution networks considering multiple objectives. *Ain Shams Engineering Journal*, 12(1):697–708, 2021.

[4] Muhammad Imran Akbar, Syed Ali Abbas Kazmi, Omar Alrumayh, Zafar A. Khan, Abdullah Altamimi, and M. Mahad Malik. A Novel Hybrid Optimization-Based Algorithm for the Single and Multi-Objective Achievement with Optimal DG Allocations in Distribution Networks. *IEEE Access*, 10:25669–25687, 2022.

[5] Khoa H. Truong, Perumal Nallagownden, Irraivan Elamvazuthi, and Dieu N. Vo. A Quasi-Oppositional-Chaotic Symbiotic Organisms Search algorithm for optimal allocation of DG in radial distribution networks. *Applied Soft Computing Journal*, 88:106067, 2020.

[6] Mahzan Dalawir, Maher Azzouz, and Ahmed Azab. Optimal allocation of wind-based distributed generators and STATCOMs using a hierarchical stochastic programming approach. *Electric Power Systems Research*, 237:110960, 2024.

[7] Mohammad Nasir, Ali Sadollah, Eneko Osaba, and Javier Del Ser. A Novel Metaheuristic Approach for Loss Reduction and Voltage Profile Improvement in Power Distribution Networks Based on Simultaneous Placement and Sizing of Distributed Generators and Shunt Capacitor Banks. In *Lecture Notes in Computer Science (including subseries Lecture Notes in Artificial Intelligence and Lecture Notes in Bioinformatics)*, volume 12489 LNCS, pages 64–76. Springer, 2020.

[8] Saleh Ba-swaimi, Renuga Verayiah, Vigna K. Ramachandaramurthy, and Ahmad K. ALAhmad. Long-term optimal planning of distributed generations and battery energy storage systems towards high integration of green energy considering uncertainty and demand response program. *Journal of Energy Storage*, 100:113562, 2024.

[9] Ling Ling Li, Xing Da Fan, Kuo Jui Wu, Kanchana Sethanan, and Ming Lang Tseng. Multi-objective distributed generation hierarchical optimal planning in distribution network: Improved beluga whale optimization algorithm. *Expert Systems with Applications*, 237:121406, 2024.

[10] Giscard M. Binini, Josiah L. Munda, and Olawale M. Popoola. Optimal location, sizing and scheduling of distributed energy storage in a radial distribution network. *Journal of Energy Storage*, 94:112499, 2024.

[11] Abdelkader Boukaroura. Contribution à la modélisation et à l'optimisation des réseaux de distribution sous incertitudes. PhD thesis, University of Oum El Bouaghi, 2021.

[12] Boris Berseneff. Réglage de la tension dans les réseaux de distribution du futur. PhD thesis, Grenoble University, 2010.

[13] Marjorie Cosson. Stabilité du réseau électrique de distribution. Analyse du point de vue automatique d'un système complexe. PhD thesis, Paris Saclay University, 2016.

[14] Poul H. Andersen, John A. Mathews, and Morten Rask. Integrating private transport into renewable energy policy: The strategy of creating intelligent recharging grids for electric vehicles. *Energy Policy*, 37(7):2481–2486, 2009.

[15] Yujun HE. Contribution au réglage de la tension sur un réseau HTA avec producteurs. Apport de la flexibilité de la demande. PhD thesis, CentraleSupélec, 2015.

[16] Chabane Djabali. Contribution à l'optimisation de la reconfiguration des réseaux de distribution en présence de la production décentralisée. PhD thesis, Ferhat Abbas University, Setif 1, 2021.

[17] Sarfaraz Nawaz, Ankit Vijayvargiya, and Abhishek Gupta. Optimal Allocation of Capacitor in Radial Distribution System. *International Journal of Electrical and Computer Engineering (IJECE)*, 7(2):748–753, 2017.

[18] David Infield and Leon Freris. *Renewable energy in power systems*. John Wiley & Sons, 2nd edition, 2020.

[19] J. M. Yusta, H. M. Khodr, and A. J. Urdaneta. Optimal pricing of default customers in electrical distribution systems: Effect behavior performance of demand response models. *Electric Power Systems Research*, 77(5-6):548–558, 2007.

[20] Réseau de Transport d'Électricité (RTE). *Courbes de consommation*. Available at : https://www.services-rte.com/fr/visualisez-les-donnees-publiees-par-rte/courbes-de-consommation.html, consulté en 2025.

[21] Magdi S. Mahmoud, Nezar M. Alyazidi, and Mohamed I. Abouheaf. Adaptive intelligent techniques for microgrid control systems: A survey. *International Journal of Electrical Power and Energy Systems*, 90:292–305, 2017.

[22] Zhenya Liu. Innovation in Global Energy Interconnection Technologies. In Zhenya Liu, editor, *Global Energy Interconnection*, pages 239–272. Academic Press, Boston, 2015.

[23] Isaac Ortega-Romero, Xavier Serrano-Guerrero, Antonio Barragán-Escandón, and Chistopher Ochoa-Malhaber. Optimal Integration of Distributed Generation in Long Medium-Voltage Electrical Networks. *Energy Reports*, 10:2865–2879, 2023.

[24] Prem Prakash and Dheeraj K. Khatod. Optimal sizing and siting techniques for distributed generation in distribution systems: A review. *Renewable and Sustainable Energy Reviews*, 57:111–130, 2016.

[25] Mohammed Hamouda Ali. Optimal planning of electrical network with renewable energy sources. PhD thesis, Al-Azhar University, 2021.

[26] A Omri. Analyse de la transition vers les énergies renouvelables en Tunisie: Risques, enjeux et stratégies à adopter. thèse de doctorat, Université De Sfax Ecole doctorale des sciences économiques, gestion et informatique Unité de recherche en économie de développement, France, 2016.

[27] Mohammed Telidjane. Modélisation des panneaux photovoltaïques et adaptation de la cyclostationnarité pour le diagnostic. PhD thesis, University of Lyon, 2017.

[28] Adil Mansouri, Abdelmounime El Magri, Rachid Lajouad, Ilyass El Myasse, El Khlifi Younes, and Fouad Giri. Wind energy based conversion topologies and maximum power point tracking: A comprehensive review and analysis. *e-Prime Advances in Electrical Engineering, Electronics and Energy*, 6:100351, 2023.

[29] Sonelgaz official website. https://www.sonelgaz.dz, 2025.

[30] G. S. Stavrakakis and A. Pouliezos. 2.10 - Electrical Parts, Control Systems and Power Electronics of Wind Turbines. *Comprehensive Renewable Energy, Second Edition: Volume 1-9*, 1-9:279–352, 2022.

[31] Daniel Stratton, Daniel Martino, Kemper Lewis, and John Hall. Selection of sustainable wind turbine tower geometry and material using multi-level decision making. In *Proceedings of the ASME Design Engineering Technical Conference*, volume 2A, page V02AT03A027. American Society of Mechanical Engineers, 2014.

[32] Tony Burton, Nick Jenkins, David Sharpe, and Ervin Bossanyi. *Wind Turbine Installations and Wind Farms*, chapter 9, pages 525–564. John Wiley & Sons, Ltd, 2011.

[33] J. Gordon Leishman. *Aerodynamics of horizontal axis wind turbines*, volume 1, chapter 3, pages 1–69. John Wiley & Sons, Ltd, 2011.

[34] Md Rabiul Islam, Youguang Guo, and Jianguo Zhu. A review of offshore wind turbine nacelle: Technical challenges, and research and developmental trends. *Renewable and Sustainable Energy Reviews*, 33:161–176, 2014.

[35] Vestas Wind Systems A/S. *Products - Turbines*. https://www.vestas.com/en/products/turbines, 2014.

[36] Atul Kumar, Muhammad Zafar Ullah Khan, and Bishwajeet Pandey. Wind Energy: A Review Paper. *Gyancity Journal of Engineering and Technology*, 4(2):29–37, 2018.

[37] Shifeng Wang and Sicong Wang. Impacts of wind energy on environment: A review. *Renewable and Sustainable Energy Reviews*, 49:437–443, 2015.

[38] Sukanta Roga, Shawli Bardhan, Yogesh Kumar, and Sudhir K. Dubey. Recent technology and challenges of wind energy generation: A review. *Sustainable Energy Technologies and Assessments*, 52:102239, 2022.

[39] U.S. Department of Energy. *Office of Energy Efficiency and Renewable Energy*. https://www.energy.gov/eere/office-energy-efficiency-renewable-energy, accessed in 2025.

[40] Peter Enevoldsen and George Xydis. Examining the trends of 35 years growth of key wind turbine components, *Energy for Sustainable Development*, vol. 50, pp. 18–26, 2019.

[41] Mladen Bošnjaković, Marko Katinić, Robert Santa, and Dejan Marić. Wind Turbine Technology Trends. *Applied Sciences (Switzerland)*, 12(17):8653, 2022.

[42] Fabian Wagner. Renewables in Future Power Systems. *Renewables in future power systems: implications of technological learning and uncertainty*, pages 3–20, 2014.

[43] A. Maafi. A survey on photovoltaic activities in Algeria. *Renewable Energy*, 20(1):9–17, 2000.

[44] Kacem Gairaa and Yahia Bakelli. Solar energy potential assessment in the Algerian south area: Case of Ghardaïa region. *Journal of Renewable Energy*, 2013(1):496348, 2013.

[45] Sivasami Kolandasamy and Thangalakshmi Sivalingam. Impact of Panel Materials on Solar Cell Performance. in *Innovations in Perovskite Solar Cell Materials and Devices*, IntechOpen, 2024, ch. 3. 2024.

[46] M. Halbwax, T. Sarnet, Ph Delaporte, M. Sentis, H. Etienne, F. Torregrosa, V. Vervisch, I. Perichaud, and S. Martinuzzi. Micro and nano-structuration of silicon by femtosecond laser: Application to silicon photovoltaic cells fabrication. *Thin Solid Films*, 516(20):6791–6795, 2008.

[47] Nikolaos F. Voudoukis. Photovoltaic Technology and Innovative Solar Cells. *European Journal of Electrical Engineering and Computer Science*, 2(1), 2018.

[48] S. M.Amir Al Zumahi, M. Khairul Basher, Nourin Arobi, M. Momtazur Rahman, Ahmed M. Tawfeek, M. A.Rafiq Akand, M. Mahbubur Rahman, M. Nur-E-Alam, and M. Khalid Hossain. High-efficiency silicon solar cells designed on experimentally achieved nano-engineered low-reflective silicon surface. *Journal of Optics (India)*, pages 1–15, 2024.

[49] Subhash Chander, A Purohit, Anshu Sharma, S P Nehra, M S Dhaka, and Others. A study on photovoltaic parameters of mono-crystalline silicon solar cell with cell temperature. *Energy Reports*, 1:104–109, 2015.

[50] Angel Antonio Bayod-Rújula. Solar photovoltaics (PV). In Francesco Calise, Massimo Dentice D'Accadia, Massimo Santarelli, Andrea Lanzini, and Domenico Ferrero, editors, *Solar Hydrogen Production: Processes, Systems and Technologies*, pages 237–295. Academic Press, 2019.

[51] Enrico Barbier. Geothermal energy technology and current status: An overview. *Renewable and Sustainable Energy Reviews*, 6(1-2):3–65, 2002.

[52] Juan Carlos Ríos Fernández. Integration capacity of geothermal energy in supermarkets through case analysis. *Sustainable Energy Technologies and Assessments*, 34:49–55, 2019.

[53] Alison Bartle. Hydropower potential and development activities. *Energy Policy*, 30(14):1231–1239, 2002.

[54] D. Azofra, E. Martínez, E. Jiménez, J. Blanco, F. Azofra, and J. C. Saenz-Díez. Comparison of the influence of photovoltaic and wind power on the Spanish electricity prices by means of artificial intelligence techinques. *Renewable and Sustainable Energy Reviews*, 42:532–542, 2015.

[55] Changhai Liu, Min Hu, Wenzhi Gao, Jian Chen, Yishan Zeng, Daozhu Wei, Qingjun Yang, and Gang Bao. A high-precise model for the hydraulic power take-off of a raft-type wave energy converter. *Energy*, 215:119107, 2021.

[56] Sisty Basil Massawe and AO Olorunnisola. The Environmental Challenges of Biomass Utilisation for Combined Heat and Power Generation in a Paper Mill in Tanzania. *Journal of Fundamentals of Renewable Energy and Applications*, 06(01):2, 2015.

[57] Nima Norouzi and Maryam Fani. The prioritization and feasibility study over renewable technologies using fuzzy logic: A case study for Takestan plains. *Research Article Journal of Energy Management and Technology (JEMT)*, 5(2):12, 2020.

[58] Elkadhi Hayfa and Ben Hamida Rania. The impact of the biomass energy use on CO2 emissions: A Panel data model for 15 countries. In *IREC 2014 - 5th International Renewable Energy Congress*, pages 1–6. IEEE, 2014.

[59] Chandrasekaran Venkatesan, Raju Kannadasan, Mohammed H. Alsharif, Mun Kyeom Kim, and Jamel Nebhen. A novel multiobjective hybrid technique for siting and sizing of distributed generation and capacitor banks in radial distribution systems. *Sustainability (Switzerland)*, 13(6):3308, 2021.

[60] Sambaiah Sampangi Kola. A review on optimal allocation and sizing techniques for DG in distribution systems. *International Journal of Renewable Energy Research (IJRER)*, 8(3):1236–1256, 2018.

[61] Atma Ram Gupta and Ashwani Kumar. Optimal placement of D-STATCOM using sensitivity approaches in mesh distribution system with time variant load models under load growth. *Ain Shams Engineering Journal*, 9(4):783–799, 2018.

[62] Badreddine Bendriss, Samir Sayah, and Abdellatif Hamouda. Optimization of distributed generations within radial distribution systems to enhance system performance. In *Proceedings - 2023 International Conference on Engineering and Advanced Technology, ICEEAT'23*, volume 1, pages 1–6. IEEE, 2023.

[63] Mahmoud G. Hemeida, Abdalla Ahmed Ibrahim, Al Attar A. Mohamed, Salem Alkhalaf, and Ayman M.Bahaa El-Dine. Optimal allocation of distributed generators DG based Manta Ray Foraging Optimization algorithm (MRFO). *Ain Shams Engineering Journal*, 12(1):609–619, 2021.

[64] Duong Quoc Hung, N. Mithulananthan, and Kwang Y. Lee. Optimal placement of dispatchable and nondispatchable renewable DG units in distribution networks for minimizing energy loss. *International Journal of Electrical Power and Energy Systems*, 55:179–186, 2014.

[65] Sneha Sultana and Provas Kumar Roy. Krill herd algorithm for optimal location of distributed generator in radial distribution system. *Applied Soft Computing Journal*, 40:391–404, 2016.

[66] Wen Shan Tan, Mohammad Yusri Hassan, Md Shah Majid, and Hasimah Abdul Rahman. Optimal distributed renewable generation planning: A review of different approaches. *Renewable and Sustainable Energy Reviews*, 18:626–645, 2013.

[67] V. Ajjarapu and B. Lee. Bibliography on voltage stability. *IEEE Transactions on Power Systems*, 13(1):115–125, 1998.

[68] Amirreza Naderipour, Zulkurnain Abdul-Malek, Mohd Wazir Bin Mustafa, and Josep M. Guerrero. A multi-objective artificial electric field optimization algorithm for allocation of wind turbines in distribution systems. *Applied Soft Computing*, 105:107278, 2021.

[69] Imran Ahmad Quadri, S. Bhowmick, and D. Joshi. A comprehensive technique for optimal allocation of distributed energy resources in radial distribution systems. *Applied Energy*, 211:1245–1260, 2018.

[70] Masoud Ahmadipour, Zaipatimah Ali, and Hussein Mohammed Ridha. Enhancing voltage stability and load shedding optimization through a fusion of gravitational search algorithm and particle swarm optimization with deep learning. *Soft Computing*, pages 1–21, 2025.

[71] Aamir Ali, M. U. Keerio, and J. A. Laghari. Optimal Site and Size of Distributed Generation Allocation in Radial Distribution Network Using Multi-objective Optimization. *Journal of Modern Power Systems and Clean Energy*, 9(2):404–415, 2021.

[72] Badreddine Bendriss, Samir Sayah, and Abdellatif Hamouda. Efficient multi-objective optimization approach for solving optimal DG placement and sizing problem in distribution systems. *Journal of Engineering Research (Kuwait)*, 2024.

[73] Umesh Agarwal and Naveen Jain. Distributed Energy Resources and Supportive Methodologies for their Optimal Planning under Modern Distribution Network: a Review. *Technology and Economics of Smart Grids and Sustainable Energy*, 4(1):1–21, 2019.

[74] Zeineb Abdmouleh, Adel Gastli, Lazhar Ben-Brahim, Mohamed Haouari, and Nasser Ahmed Al-Emadi. Review of optimization techniques applied for the integration of distributed generation from renewable energy sources. *Renewable Energy*, 113:266–280, 2017.

[75] A. G. Tsikalakis and N. D. Hatziargyriou. Environmental benefits of distributed generation with and without emissions trading. *Energy Policy*, 35(6):3395–3409, 2007.

[76] Partha Kayal, Sayonsom Chanda, and Chandan Kumar Chanda. An analytical approach for allocation and sizing of distributed generations in radial distribution network. *International Transactions on Electrical Energy Systems*, 27(7):e2322, 2017.

[77] Akanit Kwangkaew, Siriya Skolthanarat, Chalie Charoenlarpnopparut, and Mineo Kaneko. Optimal Location and Sizing of Renewable Distributed Generators for Improving Robust Voltage Stability Against Uncontrollable Reactive Compensation. *IEEE Access*, 11(6):52260–52274, 2023.

[78] M. A. Abdelkader, M. A. Elshahed, and Z. H. Osman. An analytical formula for multiple DGs allocations to reduce distribution system losses. *Alexandria Engineering Journal*, 58(4):1265–1280, 2019.

[79] Sydulu Maheswarapu and Others. A solution to multi-objective optimal accommodation of distributed generation problem of power distribution networks: An analytical approach. *International Transactions on Electrical Energy Systems*, 29(10), 2019.

[80] Murat Cikan and Nisa Nacar Cikan. Optimum allocation of multiple type and number of DG units based on IEEE 123-bus unbalanced multi-phase power distribution system. *International Journal of Electrical Power and Energy Systems*, 144:108564, 2023.

[81] M. Madhusudhan, N. Kumar, and H. Pradeepa. Optimal location and capacity of DG systems in distribution network using genetic algorithm. *International Journal of Information Technology (Singapore)*, 13(1):155–162, 2021.

[82] Badreddine Bendriss, Samir Sayah, and Abdellatif Hamouda. Jellyfish Search Optimizer for Optimal Planning of DG Units Considering Load Levels. In *2024 International Conference on Advances in Electrical and Communication Technologies, ICAECOT 2024*, pages 1–6. IEEE, 2024.

[83] P Dinakara Prasad Reddy, V C Veera Reddy, and T Gowri Manohar. Whale optimization algorithm for optimal sizing of renewable resources for loss reduction in distribution systems. *Renewables: wind, water, and solar*, 4:1–13, 2017.

[84] Mohammed Hamouda Ali, Salah Kamel, Mohamed H. Hassan, Marcos Tostado-Véliz, and Hossam M. Zawbaa. An improved wild horse optimization algorithm for reliability based optimal DG planning of radial distribution networks. *Energy Reports*, 8:582–604, 2022.

[85] Thai Dinh Pham, Thang Trung Nguyen, and Bach Hoang Dinh. Find optimal capacity and location of distributed generation units in radial distribution networks by using enhanced coyote optimization algorithm. *Neural Computing and Applications*, 33(9):4343–4371, 2021.

[86] Nihat Pamuk and Umut Emre Uzun. Optimal Allocation of Distributed Generations and Capacitor Banks in Distribution Systems Using Arithmetic Optimization Algorithm. *Applied Sciences (Switzerland)*, 14(2):831, 2024.

[87] Ahmad Eid. Allocation of distributed generations in radial distribution systems using adaptive PSO and modified GSA multi-objective optimizations. *Alexandria Engineering Journal*, 59(6):4771–4786, 2020.

[88] Ramesh Daravath and Sravana Kumar Bali. Optimal Distributed Energy Resources Placement to Reduce Power Losses and Voltage Deviation in a Distribution System. *Iranian Journal of Science and Technology - Transactions of Electrical Engineering*, pages 1–20, 2025.

[89] Mohamed A. Elseify, Fatma A. Hashim, Abdelazim G. Hussien, and Salah Kamel. Single and multi-objectives based on an improved golden jackal optimization algorithm for simultaneous integration of multiple capacitors and multi-type DGs in distribution systems. *Applied Energy*, 353:122054, 2024.

[90] Younes Ghazagh Jahed, Seyyed Yousef Mousazadeh Mousavi, and Saeed Golestan. Optimal sizing and siting of distributed generation systems incorporating reactive power tariffs via water flow optimization. *Electric Power Systems Research*, 231:110278, 2024.

[91] Talha Enes Gümüş, Selcuk Emiroglu, and Mehmet Ali Yalcin. Optimal DG allocation and sizing in distribution systems with Thevenin based impedance stability index. *International Journal of Electrical Power and Energy Systems*, 144:108555, 2023.

[92] Waseem Sultana and S. D.Sundarsingh Jebaseelan. Optimal allocation of solar PV and wind energy power for radial distribution system using spider monkey optimization. *Sustainable Computing: Informatics and Systems*, 42:100986, 2024.

[93] Priyanka Maurya, Prabhakar Tiwari, and Arvind Pratap. Electric eel foraging optimization algorithm for distribution network reconfiguration with distributed generation for power system performance enhancement considerations different load models. *Computers and Electrical Engineering*, 119:109531, 2024.

[94] Zebin Wang, Yu Li, Guodao Zhang, Xiaotian Pan, and Ji Li. Multi-objective optimization of solar resource allocation in radial distribution systems using a refined slime mold algorithm. *Heliyon*, 10(11), 2024.

[95] Hana Merah, Mohammed Jameel, Abdelmalek Gacem, Djilani Ben Attous, Mohamed Ebeed, and Mariam A. Sameh. Solving single- and multi-objective optimal power flow problems using the spider wasp optimization algorithm. *Electrical Engineering*, pages 1–45, 2025.

[96] Nil Kamal Yadav and Soumyabrata Das. Multi-Objective Optimization for Distributed Generator and Shunt Capacitor Placement Considering Voltage-Dependent Nonlinear Load Models. *Swarm and Evolutionary Computation*, 92:101782, 2025.

[97] Isaiah Adebayo, Yanxia Sun, Emmanuel Ikeh, Sunday Salimon, David Aborisade, and Oluwaseyi Adebiyi. Optimal sizing and allocation of multiple distribution generations for radial distribution networks enhancement using advanced metaheuristic-based osprey optimization algorithm. *Engineering Research Express*, 6(4):45361, 2024.

[98] Olakunle Elijah Olabode, Daniel Oluwaseun Akinyele, Titus Oluwasuji Ajewole, Samuel Okeolu Omogoye, and Akeem Abimbola Raji. Impact of integrating type-1 distributed generation on distribution network using modified genetic algorithm and voltage stability index: a technical and cost–benefit analysis approach. *Journal of Engineering and Applied Science*, 71(1):222, 2024.

[99] Dessalegn Bitew Aeggegn, George Nyauma Nyakoe, and Cyrus Wekesa. An Energy Management System for Multi-Microgrid system considering uncertainties using multi-objective multi-verse optimization. *Energy Reports*, 13:286–302, 2025.

[100] Jhony Andrés Guzmán-Henao, Rubén Iván Bolaños, Brandon Cortés-Caicedo, Luis Fernando Grisales-Noreña, Oscar Danilo Montoya, and Jesús C. Hernández. A multi-objective master–slave methodology for optimally integrating and operating photovoltaic generators in urban and rural electrical networks. *Results in Engineering*, 24:103059, 2024.

[101] Ahmed Fathy, Dalia Yousri, and Ehab F. El-Saadany. A novel memory-based artificial gorilla troops optimizer for installing biomass distributed generators in unbalanced radial networks. *Sustainable Energy Technologies and Assessments*, 68:103885, 2024.

[102] Ahmed Ayman Kandel, Hamdy Kanaan, Tarek Mahmoud, and Bahaa Saad. Efficient reduction of power losses by allocating various DG types using the ZOA algorithm. *Results in Engineering*, 23:102560, 2024.

[103] Partha Kayal and C. K. Chanda. Optimal mix of solar and wind distributed generations considering performance improvement of electrical distribution network. *Renewable Energy*, 75:173–186, 2015.

[104] H. Abdel-Mawgoud, Salah Kamel, Mansur Khasanov, and Tahir Khurshaid. A strategy for PV and BESS allocation considering uncertainty based on a modified Henry gas solubility optimizer. *Electric Power Systems Research*, 191:106886, 2021.

[105] Antônio Sobrinho Campolina Martins, Leandro Ramos de Araujo, and Débora Rosana Ribeiro Penido. Sensibility Analysis with Genetic Algorithm to Allocate

Distributed Generation and Capacitor Banks in Unbalanced Distribution Systems. *Electric Power Systems Research*, 209:107962, 2022.

[106] Mansur Khasanov, Salah Kamel, Essam Halim Houssein, Claudia Rahmann, and Fatma A. Hashim. Optimal allocation strategy of photovoltaic- and wind turbine-based distributed generation units in radial distribution networks considering uncertainty. *Neural Computing and Applications*, 35(3):2883–2908, 2023.

[107] Mansur Khasanov, Salah Kamel, Claudia Rahmann, Hany M. Hasanien, and Ahmed Al-Durra. Optimal distributed generation and battery energy storage units integration in distribution systems considering power generation uncertainty. *IET Generation, Transmission and Distribution*, 15(24):3400–3422, 2021.

[108] Ashraf Ramadan, Mohamed Ebeed, Salah Kamel, Emad M. Ahmed, and Marcos Tostado-Véliz. Optimal allocation of renewable DGs using artificial hummingbird algorithm under uncertainty conditions. *Ain Shams Engineering Journal*, 14(2):101872, 2023.

[109] Kushal Manohar Jagtap, Anup Shukla, and Surya Abhishek Baboria. Optimal planning for distribution networks considering system uncertainties using pseudo-inspired gravitational search algorithm. *Electrical Engineering*, pages 1–20, 2024.

[110] Umme Mumtahina, Sanath Alahakoon, and Peter Wolfs. Optimal Allocation and Sizing of Battery Energy Storage System in Distribution Network Using Mountain Gazelle Optimization Algorithm. *Energies*, 18(2):379, 2025.

[111] Ali Avar and Ehsan Ghanbari. Optimal integration and planning of PV and wind renewable energy sources into distribution networks using the hybrid model of analytical techniques and metaheuristic algorithms: A deep learning-based approach. *Computers and Electrical Engineering*, 117:109280, 2024.

[112] Saleh Ba-swaimi, Renuga Verayiah, Vigna K Ramachandaramurthy, Ahmad K ALAhmad, and Sanjeevikumar Padmanaban. Optimal Planning of Renewable Distributed Generators and Battery Energy Storage Systems in Reconfigurable Distribution Systems with Demand Response Program to Enhance Renewable Energy Penetration. *Results in Engineering*, page 104304, 2025.

[113] Shamte Kawambwa and Daudi Mnyanghwalo. Revenue loss reduction in the electrical distribution networks using distributed generators: A case of Tanzania electrical distribution network. *Journal of ICT Systems*, 2(2):67–80, 2024.

[114] Fude Duan, Ali Basem, Dheyaa J. Jasim, Mahdiyeh Eslami, and Mustafa Okati. A multi-objective improved horse herd optimizer based on convex lens imaging for stochastic optimization of wind energy resources in distribution networks considering reliability and uncertainty. *Scientific reports*, 14(1):29532, 2024.

[115] Ahmed T. Hachemi, Rashad M. Kamel, Mohamed Hashem, Mohamed Ebeed, and Abdelhakim Saim. Reliability and line loading enhancement of distribution systems using optimal integration of renewable energy and compressed air energy storages simultaneously under uncertainty. *Journal of Energy Storage*, 101:113921, 2024.

[116] Mohamed Farhat, Salah Kamel, and Almoataz Y. Abdelaziz. Modified Tasmanian devil optimization for solving single and multi-objective optimal power flow in conventional and advanced power systems. *Cluster Computing*, 28(2):105, 2025.

[117] Mohamed A. Elseify, Salah Kamel, and Loai Nasrat. An improved moth flame optimization for optimal DG and battery energy storage allocation in distribution systems. *Cluster Computing*, 27(10):14767–14810, 2024.

[118] Karthik Nagarajan, Arul Rajagopalan, Mohit Bajaj, R. Sitharthan, Shir Ahmad Dost Mohammadi, and Vojtech Blazek. Optimizing dynamic economic dispatch through an enhanced Cheetah-inspired algorithm for integrated renewable energy and demand-side management. *Scientific Reports*, 14(1):3091, 2024.

[119] Mansur Khasanov, Salah Kamel, Mohamed H. Hassan, and Jose Luis Domínguez-García. Maximizing renewable energy integration with battery storage in distribution systems using a modified Bald Eagle Search Optimization Algorithm. *Neural Computing and Applications*, 36(15):8577–8605, 2024.

[120] Deyaa Ahmed, Mohamed Ebeed, Salah Kamel, Loai Nasrat, Abdelfatah Ali, Mostafa F. Shaaban, and Abdelazim G. Hussien. An enhanced jellyfish search optimizer for stochastic energy management of multi-microgrids with wind turbines, biomass and PV generation systems considering uncertainty. *Scientific Reports*, 14(1):15558, 2024.

[121] Aykut Fatih Güven, Salah Kamel, and Mohamed H. Hassan. Optimization of grid-connected photovoltaic/wind/battery/supercapacitor systems using a hybrid artificial gorilla troops optimizer with a quadratic interpolation algorithm. *Neural Computing and Applications*, pages 1–39, 2024.

[122] Ziad M. Ali, Shady H.E. Abdel Aleem, Ahmed I. Omar, and Bahaa Saad Mahmoud. Economical-Environmental-Technical Operation of Power Networks with High Penetration of Renewable Energy Systems Using Multi-Objective Coronavirus Herd Immunity Algorithm. *Mathematics*, 10(7):1201, 2022.

[123] Md Shadman Abid, Hasan Jamil Apon, Khandaker Adil Morshed, and Ashik Ahmed. Optimal Planning of Multiple Renewable Energy-Integrated Distribution System With Uncertainties Using Artificial Hummingbird Algorithm. *IEEE Access*, 10:40716–40730, 2022.

[124] Mingxuan Lu, Yun Teng, Zhe Chen, and Yu Song. A bi-level optimization strategy of electricity-hydrogen-carbon integrated energy system considering photovoltaic and wind power uncertainty and demand response. *Scientific Reports*, 15(1):18, 2025.

[125] Mahmoud M. Sayed, Mohamed Y. Mahdy, Shady H.E. Abdel Aleem, Hosam K.M. Youssef, and Tarek A. Boghdady. Simultaneous Distribution Network Reconfiguration and Optimal Allocation of Renewable-Based Distributed Generators and Shunt Capacitors under Uncertain Conditions. *Energies*, 15(6):2299, 2022.

[126] Pappu Kumar Saurav, Swapna Mansani, and Partha Kayal. Multi-faceted sustainability improvement in low voltage power distribution network employing DG and capacitor bank. *Computers and Electrical Engineering*, 120:109789, 2024.

[127] Khaled Fettah, Ahmed Salhi, Talal Guia, Abdelaziz Salah Saidi, Abir Betka, Madjid Teguar, Hisham Alharbi, Sherif S.M. Ghoneim, Takele Ferede Agajie, and Ramy N.R. Ghaly. Optimal integration of photovoltaic sources and capacitor banks considering irradiance, temperature, and load changes in electric distribution system. *Scientific reports*, 15(1):2670, 2025.

[128] Fude Duan, Ali Basem, Sadek Habib Ali, Teeb Basim Abbas, Mahdiyeh Eslami, and Mahdi Jafari Shahbazzadeh. An information gap decision theory and improved gradient-based optimizer for robust optimization of renewable energy systems in distribution network. *Scientific Reports*, 15(1):346, 2025.

[129] Olukayode A. Afolabi, Warsame H. Ali, Penrose Cofie, John Fuller, Pamela Obiomon, and Emmanuel S. Kolawole. Analysis of the Load Flow Problem in Power System Planning Studies. *Energy and Power Engineering*, 07(10):509–523, 2015.

[130] William F Tinney and Clifford E Hart. Power Flow Solution by Newton's Method. *IEEE Transactions on Power Apparatus and Systems*, PAS-86(11):1449–1460, 1967.

[131] Tebbakh Noureddine and Labed Djamel. Load flow analysis using newton raphson method in presence of distributed generation. *International Journal of Power Electronics and Drive Systems*, 12(1):489–498, 2021.

[132] Hsiao Dong Chiang. A decoupled load flow method for distribution power networks: algorithms, analysis and convergence study. *International Journal of Electrical Power and Energy Systems*, 13(3):130–138, 1991.

[133] B. Stott and O. Alsac. Fast decoupled load flow. *IEEE Transactions on Power Apparatus and Systems*, PAS-93(3):859–869, 1974.

[134] Smarajit Ghosh and D Das. Method for Load Flow solution of Radial Distribution Systems. *International Conference on MEMS and Optoelectronics Technologies ICMOT-2010*, 146(6):641–648, 2010.

[135] Ahmed R. Abul'Wafa. A network-topology-based load flow for radial distribution networks with composite and exponential load. *Electric Power Systems Research*, 91:37–43, 2012.

[136] K. Vinoth Kumar and M. P. Selvan. A simplified approach for load flow analysis of radial distribution network with embedded generation. In *IEEE Region 10 Annual International Conference, Proceedings/TENCON*, pages 1–6. IEEE, 2008.

[137] Saad Ouali and Abdeljabbar Cherkaoui. An Improved Backward/Forward Sweep Power Flow Method Based on a New Network Information Organization for Radial Distribution Systems. *Journal of Electrical and Computer Engineering*, 2020(1):5643410, 2020.

[138] Adel Ali Abou El-Ela, Ragab A El-Sehiemy, Abdel-Mohsen Kinawy, and Mohamed Taha Mouwafi. Optimal capacitor placement in distribution systems for power loss reduction and voltage profile improvement. *IET Generation, Transmission & Distribution*, 10(5):1209–1221, 2016.

[139] J Duncan Glover, Thomas J Overbye, and Mulukutla S Sarma. *Power system analysis & design*. Cengage Learning, 2017.

[140] Ji Pyng Chiou, Chung Fu Chang, and Ching Tzong Su. Variable scaling hybrid differential evolution for solving network reconfiguration of distribution systems. *IEEE Transactions on Power Systems*, 20(2):668–674, 2005.

[141] J a Michline Rupa and S Ganesh. Power Flow Analysis for Radial Distribution System Using Backward / Forward Sweep Method. *International Journal of Electrical, Computer, Energetic, Electronic and Communication Engineering*, 8(10):1537–1541, 2014.

[142] An Dt Le, M. A. Kashem, M. Negnevitsky, and G. Ledwich. Minimising voltage deviation in distribution feeders by optimising size and location of distributed generation. *Australian Journal of Electrical and Electronics Engineering*, 3(2):147–156, 2007.

[143] Arif Bourzami and Tarek Bouktir. *Contribution à l ' étude de la stabilité des grands réseaux électriques dans un marché de l ' électricité dérégulé en présence des sources d ' énergie renouvelable par la logique floue*. PhD thesis, 2019.

[144] Mohammed Adel Djari and Lahouaria Benasla. Voltage stability assessment using different methods. *Elektrotehniski Vestnik/Electrotechnical Review*, 90(4):206–213, 2023.

[145] M Chakravorty and Debapriya Das. Voltage stability analysis of radial distribution networks. *International Journal of Electrical Power & Energy Systems*, 23(2):129–135, 2001.

[146] Mesut E. Baran and Felix F. Wu. Optimal capacitor placement on radial distribution systems. *IEEE Transactions on Power Delivery*, 4(1):725–734, 1989.

[147] D. B. Prakash and C. Lakshminarayana. Optimal siting of capacitors in radial distribution network using Whale Optimization Algorithm. *Alexandria Engineering Journal*, 56(4):499–509, 2017.

[148] Dulce Fernão Pires, Carlos Henggeler Antunes, and António Gomes Martins. NSGA-II with local search for a multi-objective reactive power compensation problem. *International Journal of Electrical Power and Energy Systems*, 43(1):313–324, 2012.

[149] Vikas Singh, Tukaram Moger, and Debashisha Jena. Uncertainty handling techniques in power systems: A critical review. *Electric Power Systems Research*, 203:107633, 2022.

[150] Mohamed Ebeed and Shady H.E.Abdel Aleem. Overview of uncertainties in modern power systems: uncertainty models and methods. In *Uncertainties in Modern Power Systems*, pages 1–34. Elsevier, 2020.

[151] Paul Wanjoli, Nabil H. Abbasy, and Mohamed M.Zakaria Moustafa. A state-of-the-art review on the modeling and probabilistic approaches to analysis of power systems integrated with distributed energy resources. *Ain Shams Engineering Journal*, 16(1):103198, 2025.

[152] Morteza Aien, Ali Hajebrahimi, and Mahmud Fotuhi-Firuzabad. A comprehensive review on uncertainty modeling techniques in power system studies. *Renewable and Sustainable Energy Reviews*, 57:1077–1089, 2016.

[153] Zhaoyuan Wang, Siqi Bu, Jiaxin Wen, and Can Huang. A comprehensive review on uncertainty modeling methods in modern power systems. *International Journal of Electrical Power and Energy Systems*, 166:110534, 2025.

[154] A. Rezaee Jordehi. How to deal with uncertainties in electric power systems? A review. *Renewable and Sustainable Energy Reviews*, 96:145–155, 2018.

[155] Morteza Aien, Masoud Rashidinejad, and Mahmud Fotuhi-Firuzabad. On possibilistic and probabilistic uncertainty assessment of power flow problem: A review and a new approach. *Renewable and Sustainable energy reviews*, 37:883–895, 2014.

[156] Qianyu Dong, Qiuye Sun, Yujia Huang, Zhibo Li, and Chong Cheng. Hybrid possibilistic-probabilistic energy flow assessment for multi-energy carrier systems. *IEEE access*, 7:176115–176126, 2019.

[157] Yakov Ben-Haim. *Info-gap decision theory: decisions under severe uncertainty*. (2nd ed.), Y. Ben-Haim, Ed. Oxford: Academic Press, pp. 9–36, 2006.

[158] Andrew E B Lim, J George Shanthikumar, and Z J Max Shen. Model uncertainty, robust optimization, and learning. In *Models, methods, and applications for innovative decision making*, pages 66–94. INFORMS, 2006.

[159] Wei Gao, Chongmin Song, and Francis Tin-Loi. Probabilistic interval analysis for structures with uncertainty. *Structural Safety*, 32(3):191–199, 2010.

[160] Peter Olofsson and Mikael Andersson. *Probability, statistics, and stochastic processes*. ch. 8, pp. 444–526, John Wiley & Sons, Ltd, 2012.

[161] J Mohammed. *Analysis of optimal sizing and location of shunt capacitors in active distribution networks*. PhD thesis, University of Belgrade (Serbia), 2018.

[162] Douglas C Montgomery and George C Runger. *Applied statistics and probability for engineers*. John wiley & sons, 2010.

[163] Mohamed Abuella. *Study of Particle Swarm for Optimal Power Flow in Ieee*. Southern Illinois University at Carbondale, 2012.

[164] W. W. Price, C. W. Taylor, G. J. Rogers, K. Srinivasan, C. Concordia, M. K. Pal, Bess, P. Kundur, B. L. Agrawal, J. F. Luini, E. Vaahedi, and B. K. Johnson. Standard Load Models for Power Flow and Dynamic Performance Simulation. *IEEE Transactions on Power Systems*, 10(3):1302–1313, 1995.

[165] Deependra Singh, Devender Singh, and K. S. Verma. Multiobjective optimization for DG planning with load models. *IEEE Transactions on Power Systems*, 24(1):427–436, 2009.

[166] Muhammad Zeeshan Malik, Mahesh Kumar, Amir Mahmood Soomro, Mazhar Hussain Baloch, Mehr Gul, Muhammad Farhan, and Ghulam Sarwar Kaloi. Strategic planning of renewable distributed generation in radial distribution system using advanced MOPSO method. *Energy Reports*, 6:2872–2886, 2020.

[167] Raheela Jamal, Junzhe Zhang, Baohui Men, Noor Habib Khan, Mohamed Ebeed, and Salah Kamel. Solution to the deterministic and stochastic Optimal Reactive Power Dispatch by integration of solar, wind-hydro powers using Modified Artificial Hummingbird Algorithm. *Energy Reports*, 9:4157–4173, 2023.

[168] Ali Selim, Salah Kamel, Essam H. Houssein, Francisco Jurado, and Fatma A. Hashim. A modified Runge–Kutta optimization for optimal photovoltaic and battery storage allocation under uncertainty and load variation. *Soft Computing*, pages 1–21, 2024.

[169] Y. M. Atwa, E. F. El-Saadany, M. M.A. Salama, and R. Seethapathy. Optimal renewable resources mix for distribution system energy loss minimization. *IEEE Transactions on Power Systems*, 25(1):360–370, 2010.

[170] Badreddine Bendriss, Samir Sayah, and Abdellatif Hamouda. A novel improved Frilled Lizard algorithm for solving the optimal planning problem of renewable energy sources within distribution grids under uncertainties. *Energy Conversion and Management*, 326:119465, 2025.

[171] Woldu Tahaguas. Modeling and simulation of power system dynamics for studying the impacts of increasing wind power in a weak grid system. In *Res Electricae Magdeburgenses. Magdeburger Forum zur Elektrotechnik*, volume 94, 2023.

[172] Emelie Sjökvist. Improvement of Wind Power Forecasting and Prediction of Production Losses Caused by Ice Formation on Wind Turbine Blades : A Machine Learning Approach, Umeå University, Department of Physics, 59 pages, 2023.

[173] Kristin P. Bennett and Emilio Parrado-Hernández. The interplay of optimization and machine learning research. *Journal of Machine Learning Research*, 7:1265–1281, 2006.

[174] Srinivasan Balan, Simulated Annealing, and Swarm Intelligence Algorithm. Metaheuristics in Optimization: Algorithmic Perspective. *OR-MS-Tomorrow (2020)*, pages 1–12, 2021.

[175] R. A. Jabr and B. C. Pal. Intermittent wind generation in optimal power flow dispatching. *IET Generation, Transmission and Distribution*, 3(1):66–74, 2009.

[176] Frédéric Héliodore, Amir Nakib, Boussaad Ismail, Salma Ouchraa, and Laurent Schmitt. *Metaheuristics for Intelligent Electrical Networks*, volume 10. John Wiley & Sons, 2017.

[177] Omessaad Hajji. Contribution au développement de méthodes d'optimisation stochastique. Application à la conception des dispositifs électrotechniques. *Thèse de doctorat spécialité Génie électrique, Ecole centrale de Lille, Université des Sciences et Technonlogie, Lille*, pages 1–171, 2003.

[178] Enseignement Sup, Recherche Scientifique, Batna Pr, Par Ketfi, and Nadhir Magister. *Doctorat en sciences Contribution à la gestion des réseaux de distribution en présence de génération d ' énergie dispersée*. PhD thesis, Université de Batna 2, 2014.

[179] Samir Syah. *Application de l'intelligence artificielle pour le fonctionnement optimal des systèmes électrique*. PhD thesis, Ferhat Abbas University, Setif 1, 2018.

[180] Mohd Nadhir Ab Wahab, Samia Nefti-Meziani, and Adham Atyabi. A comprehensive review of swarm optimization algorithms. *PloS one*, 10(5):e0122827, 2015.

[181] Farhad Soleimanian Gharehchopogh and Hojjat Gholizadeh. A comprehensive survey: Whale Optimization Algorithm and its applications. *Swarm and Evolutionary Computation*, 48:1–24, 2019.

[182] Linda Slimani. *Contribution à l'Application de l'Optimisation par des Méthodes Métaheuristiques à l'Écoulement de Puissance Optimal dans un Environnement de l'Électricité Dérégulé*. PhD thesis, Université de Batna 2, 2009.

[183] Rana H.A. Zubo, Geev Mokryani, Haile Selassie Rajamani, Jamshid Aghaei, Taher Niknam, and Prashant Pillai. Operation and planning of distribution networks with integration of renewable distributed generators considering uncertainties: A review. *Renewable and Sustainable Energy Reviews*, 72:1177–1198, 2017.

[184] Singiresu S Rao. *Engineering optimization: theory and practice*. John Wiley & Sons, 2019.

[185] Kenneth Sörensen, Marc Sevaux, and Fred Glover. A history of metaheuristics. *Handbook of Heuristics*, 2-2:791–808, 2018.

[186] Seyedali Mirjalili, Seyed Mohammad Mirjalili, and Andrew Lewis. Grey wolf optimizer. *Advances in engineering software*, 69:46–61, 2014.

[187] Jui Sheng Chou and Dinh Nhat Truong. A novel metaheuristic optimizer inspired by behavior of jellyfish in ocean. *Applied Mathematics and Computation*, 389:125535, 2021.

[188] Mohamed Selmy, Miral Salah Noah, and Islam M Abdelqawee. Optimized and Sustainable PV Water Pumping System with Three-Port Converter , a Case Study : The Al-Kharijah Oasis. pages 227–253, 2024.

[189] Jun Wang, Wen Chuan Wang, Xiao Xue Hu, Lin Qiu, and Hong Fei Zang. Black-winged kite algorithm: a nature-inspired meta-heuristic for solving benchmark functions and engineering problems. *Artificial Intelligence Review*, 57(4):98, 2024.

[190] Ibraheem Abu Falahah, Osama Al-Baik, Saleh Alomari, Gulnara Bektemyssova, Saikat Gochhait, Irina Leonova, Om Parkash Malik, Frank Werner, and Mohammad Dehghani. Frilled Lizard Optimization: A Novel Bio-Inspired Optimizer for Solving Engineering Applications. *Computers, Materials and Continua*, 79(3):3631–3678, 2024.

[191] Mridul Chawla and Manoj Duhan. Levy Flights in Metaheuristics Optimization Algorithms–A Review. *Applied Artificial Intelligence*, 32(9-10):802–821, 2018.

[192] Hamdi Tolga Kahraman, Sefa Aras, and Eyüp Gedikli. Fitness-distance balance (FDB): A new selection method for meta-heuristic search algorithms. *Knowledge-Based Systems*, 190:105169, 2020.

[193] Hamdi Tolga Kahraman, Huseyin Bakir, Serhat Duman, Mehmet Katı, Sefa Aras, and Ugur Guvenc. Dynamic FDB selection method and its application: modeling and optimizing of directional overcurrent relays coordination. *Applied Intelligence*, 52(5):4873–4908, 2022.

[194] Tapas Si, Péricles B.C. Miranda, and Debolina Bhattacharya. Novel enhanced Salp Swarm Algorithms using opposition-based learning schemes for global optimization problems. *Expert Systems with Applications*, 207:117961, 2022.

[195] Koustav Dasgupta, Provas Kumar Roy, and Vivekananda Mukherjee. A Novel Quasi-Oppositional Learning-Based Chaos-Assisted Sine Cosine Algorithm for Hybrid Energy Integrated Dynamic Economic Emission. *IETE Journal of Research*, 70(3):2453–2480, 2023.

[196] Lei Wu, Jiawei Wu, and Tengbin Wang. The improved grasshopper optimization algorithm with Cauchy mutation strategy and random weight operator for solving optimization problems. *Evolutionary Intelligence*, 17(3):1751–1781, 2024.

[197] Xing Wang, Qian Liu, and Li Zhang. An Adaptive Sand Cat Swarm Algorithm Based on Cauchy Mutation and Optimal Neighborhood Disturbance Strategy. *Biomimetics*, 8(2):191, 2023.

[198] Amit Kumar Bairwa, Sandeep Joshi, and Dilbag Singh. Dingo Optimizer: A Nature-Inspired Metaheuristic Approach for Engineering Problems. *Mathematical Problems in Engineering*, 2021(1):2571863, 2021.

[199] Mohammad Shehab, Ibrahim Mashal, Zaid Momani, Mohd Khaled Yousef Shambour, Anas AL-Badareen, Saja Al-Dabet, Norma Bataina, Anas Ratib Alsoud, and Laith Abualigah. Harris Hawks Optimization Algorithm: Variants and Applications. *Archives of Computational Methods in Engineering*, 29(7):5579–5603, 2022.

[200] Seyedali Mirjalili and Andrew Lewis. The Whale Optimization Algorithm. *Advances in Engineering Software*, 95:51–67, 2016.

[201] Hisham A. Shehadeh. Chernobyl disaster optimizer (CDO): a novel meta-heuristic method for global optimization. *Neural Computing and Applications*, 35(15):10733–10749, 2023.

[202] Shijie Zhao, Tianran Zhang, Shilin Ma, and Miao Chen. Dandelion Optimizer: A nature-inspired metaheuristic algorithm for engineering applications. *Engineering Applications of Artificial Intelligence*, 114:105075, 2022.

[203] Momin Jamil and Xin She Yang. A literature survey of benchmark functions for global optimisation problems. *International Journal of Mathematical Modelling and Numerical Optimisation*, 4(2):150–194, 2013.

[204] Marcin Molga and Czesław Smutnicki. Test functions for optimization needs. *Test functions for optimization needs*, 101(c):1–43, 2005.

[205] Satish Kansal, Vishal Kumar, and Barjeev Tyagi. Hybrid approach for optimal placement of multiple DGs of multiple types in distribution networks. *International Journal of Electrical Power and Energy Systems*, 75:226–235, 2016.

[206] Ali Selim, Salah Kamel, and Francisco Jurado. Voltage stability analysis based on optimal placement of multiple DG types using hybrid optimization technique. *International Transactions on Electrical Energy Systems*, 30(10):e12551, 2020.

[207] E. S. Ali, S. M. Abd Elazim, and A. Y. Abdelaziz. Optimal allocation and sizing of renewable distributed generation using ant lion optimization algorithm. *Electrical Engineering*, 100(1):99–109, 2018.

[208] NASA. POWER Data Access Viewer. Available at : https://power.larc.nasa.gov/

Appendix A

Load and line data

Table A.1: Bus data for 69-bus test system

Bus No.	P_L (kW)	Q_L (kVar)
1	0	0
2	0	0
3	0	0
4	0	0
5	0	0
6	2.60	2.20
7	40.40	30
8	75	54
9	30	22
10	28	19
11	145	104
12	145	104
13	8	5.50
14	8	5.50
15	0	0
16	45.50	30
17	60	35
18	60	35
19	0	0
20	1	0.60
21	114	81
22	5.30	3.50
23	0	0
24	28	20
25	0	0
26	14	10
27	14	10

Table A.1: Bus data for 69-bus test system (Continued)

Bus No.	P_L (kW)	Q_L (kVar)
28	26	18.60
29	26	18.60
30	0	0
31	0	0
32	0	0
33	14	10
34	19.50	14
35	6	4
36	26	18.55
37	26	18.55
38	0	0
39	24	17
40	24	17
41	1.20	1
42	0	0
43	6	4.30
44	0	0
45	39.22	26.30
46	39.22	26.30
47	0	0
48	79	56.40
49	384.70	274.50
50	384.70	274.50
51	40.50	28.30
52	3.60	2.70
53	4.35	3.50
54	26.40	19
55	24	17.20
56	0	0
57	0	0
58	0	0
59	100	72
60	0	0
61	1244	888
62	32	23
63	0	0
64	227	162
65	59	42
66	18	13
67	18	13
68	28	20
69	28	20

Table A.2: Line data for 69-bus test system

Line Number	**From bus**	**To bus**	**Resistance (Ω)**	**Reactance (Ω)**
1	1	2	0.0005	0.0012
2	2	3	0.0005	0.0012
3	3	4	0.0015	0.0036
4	4	5	0.0251	0.0294
5	5	6	0.3660	0.1864
6	6	7	0.3811	0.1941
7	7	8	0.0922	0.0470
8	8	9	0.0493	0.0251
9	9	10	0.8190	0.2707
10	10	11	0.1872	0.0619
11	11	12	0.7114	0.2351
12	12	13	1.0300	0.3400
13	13	14	1.0440	0.3450
14	14	15	1.0580	0.3496
15	15	16	0.1966	0.0650
16	16	17	0.3744	0.1238
17	17	18	0.0047	0.0016
18	18	19	0.3276	0.1083
19	19	20	0.2106	0.0696
20	20	21	0.3416	0.1129
21	21	22	0.0140	0.0046
22	22	23	0.1591	0.0526
23	23	24	0.3463	0.1145
24	24	25	0.7488	0.2475
25	25	26	0.3089	0.1021
26	26	27	0.1732	0.0572
27	3	28	0.0044	0.0108
28	28	29	0.0640	0.1565
29	29	30	0.3978	0.1315
30	30	31	0.0702	0.0232
31	31	32	0.3510	0.1160
32	32	33	0.8390	0.2816
33	33	34	1.7080	0.5646
34	34	35	1.4740	0.4873
35	3	36	0.0044	0.0108
36	36	37	0.0640	0.1565
37	37	38	0.1053	0.1230
38	38	39	0.0304	0.0355
39	39	40	0.0018	0.0021
40	40	41	0.7283	0.8509
41	41	42	0.3100	0.3623
42	42	43	0.0410	0.0478

Table A.2: Line data for 69-bus test system (Continued)

Line Number	From bus	To bus	Resistance (Ω)	Reactance (Ω)
43	43	44	0.0092	0.0116
44	44	45	0.1089	0.1373
45	45	46	0.0009	0.0012
46	4	47	0.0034	0.0084
47	47	48	0.0851	0.2083
48	48	49	0.2898	0.7091
49	49	50	0.0822	0.2011
50	8	51	0.0928	0.0473
51	51	52	0.3319	0.1114
52	9	53	0.1740	0.0886
53	53	54	0.2030	0.1034
54	54	55	0.2842	0.1447
55	55	56	0.2813	0.1433
56	56	57	1.5900	0.5337
57	57	58	0.7837	0.2630
58	58	59	0.3042	0.1006
59	59	60	0.3861	0.1172
60	60	61	0.5075	0.2585
61	61	62	0.0974	0.0496
62	62	63	0.1450	0.0738
63	63	64	0.7105	0.3619
64	64	65	1.0410	0.5302
65	11	66	0.2012	0.0611
66	66	67	0.0047	0.0014
67	12	68	0.7394	0.2444
68	68	69	0.0047	0.0016

Table A.3: Bus Data for 85-Bus Test System

Bus No.	P_L (kW)	Q_L (kVar)
1	0	0
2	0	0
3	0	0
4	56	57.13
5	0	0
6	35.28	35.99
7	0	0
8	35.28	35.99
9	0	0
10	0	0
11	56	57.13
12	0	0
13	0	0
14	35.28	35.99
15	35.28	35.99
16	35.28	35.99
17	112	114.26
18	56	57.13
19	56	57.13
20	35.28	35.99
21	35.28	35.99
22	35.28	35.99
23	56	57.13
24	35.28	35.99
25	35.28	35.99
26	56	57.13
27	0	0
28	56	57.13
29	0	0
30	35.28	35.99
31	35.28	35.99
32	0	0
33	14	14.28
34	0	0
35	0	0
36	35.28	35.99
37	56	57.13
38	56	57.13
39	56	57.13
40	35.28	35.99
41	0	0
42	35.28	35.99

Table A.3: Bus Data for 85-Bus Test System (Continued)

Bus No.	P_L (kW)	Q_L (kVar)
43	35.28	35.99
44	35.28	35.99
45	35.28	35.99
46	35.28	35.99
47	14	14.28
48	0	0
49	0	0
50	36.28	37.01
51	56	57.13
52	0	0
53	35.28	35.99
54	56	57.13
55	56	57.13
56	14	14.28
57	56	57.13
58	0	0
59	56	57.13
60	56	57.13
61	56	57.13
62	56	57.13
63	14	14.28
64	0	0
65	0	0
66	56	57.13
67	0	0
68	0	0
69	56	57.13
70	0	0
71	35.28	35.99
72	56	57.13
73	0	0
74	56	57.13
75	35.28	35.99
76	56	57.13
77	14	14.28
78	56	57.13
79	35.28	35.99
80	56	57.13
81	0	0
82	56	57.13
83	35.28	35.99
84	14	14.28
85	35.28	35.99

Table A.4: Line data for 85-bus test system

Line Number	**From bus**	**To bus**	**Resistance (Ω)**	**Reactance (Ω)**
1	1	2	0.108	0.075
2	2	3	0.163	0.112
3	3	4	0.217	0.149
4	4	5	0.108	0.074
5	5	6	0.435	0.298
6	6	7	0.272	0.186
7	7	8	1.197	0.82
8	8	9	0.108	0.074
9	9	10	0.598	0.410
10	10	11	0.544	0.373
11	11	12	0.544	0.373
12	12	13	0.598	0.410
13	13	14	0.272	0.186
14	14	15	0.326	0.223
15	2	16	0.728	0.302
16	3	17	0.455	0.189
17	5	18	0.82	0.340
18	18	19	0.637	0.264
19	19	20	0.455	0.189
20	20	21	0.819	0.340
21	21	22	1.548	0.642
22	19	23	0.182	0.075
23	7	24	0.910	0.378
24	8	25	0.455	0.189
25	25	26	0.364	0.151
26	26	27	0.546	0.226
27	27	28	0.273	0.113
28	28	29	0.546	0.226
29	29	30	0.546	0.226
30	30	31	0.273	0.113
31	31	32	0.182	0.075
32	32	33	0.182	0.075
33	33	34	0.819	0.340
34	34	35	0.637	0.264
35	35	36	0.182	0.075
36	26	37	0.364	0.151
37	27	38	1.002	0.416
38	29	39	0.546	0.226
39	32	40	0.455	0.189
40	40	41	1.002	0.416
41	41	42	0.273	0.113
42	41	43	0.455	0.189

Table A.4: Line data for 85-bus test system (Continued)

Line Number	From bus	To bus	Resistance (Ω)	Reactance (Ω)
43	34	44	1.002	0.416
44	44	45	0.911	0.378
45	45	46	0.911	0.378
46	46	47	0.546	0.226
47	35	48	0.637	0.264
48	48	49	0.182	0.075
49	49	50	0.364	0.151
50	50	51	0.455	0.189
51	48	52	1.366	0.567
52	52	53	0.455	0.189
53	53	54	0.546	0.226
54	52	55	0.546	0.226
55	49	56	0.546	0.226
56	9	57	0.273	0.113
57	57	58	0.819	0.340
58	58	59	0.182	0.075
59	58	60	0.546	0.226
60	60	61	0.728	0.302
61	61	62	1.002	0.415
62	60	63	0.182	0.075
63	63	64	0.728	0.302
64	64	65	0.182	0.075
65	65	66	0.182	0.075
66	64	67	0.455	0.189
67	67	68	0.910	0.378
68	68	69	1.092	0.453
69	69	70	0.455	0.189
70	70	71	0.546	0.226
71	67	72	0.182	0.075
72	68	73	1.184	0.491
73	73	74	0.273	0.113
74	73	75	1.002	0.416
75	70	76	0.546	0.226
76	65	77	0.091	0.037
77	10	78	0.637	0.264
78	67	79	0.546	0.226
79	12	80	0.728	0.302
80	80	81	0.364	0.151
81	81	82	0.091	0.037
82	81	83	1.092	0.453
83	83	84	1.002	0.416
84	13	85	0.819	0.340

Table A.5: Bus Data for the actual Portuguese 94-Bus System

Bus No.	P_L (kW)	Q_L (kVar)
1	0	0
2	22.5	10.9
3	240.3	116.4
4	24.3	11.8
5	0	0
6	0	0
7	28.8	14
8	0	0
9	0	0
10	0	0
11	0	0
12	0	0
13	0	0
14	57.6	27.9
15	0	0
16	0	0
17	18.9	9.2
18	0	0
19	0	0
20	55.8	27
21	40.5	19.6
22	0	0
23	54	26.2
24	0	0
25	0	0
26	46.8	22.7
27	0	0
28	0	0
29	13.5	6.5
30	3.6	1.7
31	18	8.7
32	21.6	10.5
33	9	4.4
34	64.8	31.4
35	65.7	31.8
36	59.4	28.8
37	13.5	6.5
38	161.1	78
39	26.1	12.6
40	134.1	65
41	85.5	41.4
42	41.4	20.1

Table A.5: Bus Data for the actual Portuguese 94-Bus System (Continued)

Bus No.	P_L (kW)	Q_L (kVar)
43	41.4	20.1
44	41.4	20.1
45	21.6	10.5
46	25.2	12.2
47	45.9	22.2
48	36.9	17.9
49	63.9	31
50	68.4	33.1
51	27.9	13.5
52	81	39.2
53	69.3	33.6
54	62.1	30.1
55	35.1	17
56	205.2	99.4
57	31.5	15.3
58	521.1	252.4
59	212.4	102.9
60	39.6	19.2
61	45	21.8
62	17.1	8.3
63	21.6	10.5
64	35.1	17
65	70.2	34
66	34.2	16.6
67	22.5	10.9
68	45.9	22.2
69	33.3	16.1
70	36.9	17.9
71	45	21.8
72	75.6	36.6
73	67.5	32.7
74	27.9	13.5
75	38.7	18.7
76	53.1	25.7
77	65.7	31.8
78	63	30.5
79	67.5	32.7
80	45	21.8
81	9	4.4
82	16.2	7.8
83	67.5	32.7
84	296.1	143.4

Table A.5: Bus Data for the actual Portuguese 94-Bus System (Continued)

Bus No.	P_L (kW)	Q_L (kVar)
85	72	34.9
86	76.5	37.1
87	90.9	44
88	72	34.9
89	63	30.5
90	21.6	10.5
91	36.9	17.9
92	20.7	10
93	17.1	8.3
94	90	43.6

Table A.6: Line data for the actual Portuguese 94-bus system

Line Number	**From bus**	**To bus**	**Resistance (Ω)**	**Reactance (Ω)**
1	1	2	0.1120	0.1873
2	2	3	0.0763	0.1274
3	3	4	0.1891	0.3161
4	4	5	0.2243	0.3749
5	5	6	0.2571	0.4297
6	6	7	0.1340	0.2239
7	7	8	0.2986	0.4991
8	8	9	0.1953	0.3265
9	9	10	0.5097	0.8519
10	10	11	1.5303	1.5101
11	11	12	0.1889	0.1864
12	12	13	0.1816	0.1793
13	13	14	0.0661	0.0653
14	14	15	0.4115	0.4061
15	15	16	0.2584	0.2550
16	16	17	0.2033	0.2006
17	17	18	0.7243	0.7148
18	18	19	0.2162	0.2134
19	19	20	0.3500	0.3454
20	20	21	1.4775	0.3891
21	21	22	0.4500	0.1185
22	22	23	0.7710	0.2030
23	23	24	0.8850	0.2331
24	24	25	0.9915	0.2611
25	25	26	0.3840	0.1011
26	26	27	0.7245	0.1908
27	27	28	1.1850	0.3121
28	28	29	1.2353	0.6899
29	29	30	0.3557	0.1987
30	30	31	0.9494	0.3406
31	31	32	0.6899	0.3853
32	32	33	1.5707	0.8773
33	5	34	1.2655	0.4540
34	5	35	0.1688	0.0943
35	35	36	0.2741	0.1531
36	36	37	0.2552	0.1426
37	6	38	0.4165	0.2326
38	6	39	1.4835	0.3907
39	39	40	1.8000	0.4740
40	40	41	0.5177	0.2892
41	41	42	0.7148	0.3992
42	8	43	1.0575	0.2785

Table A.6: Line data for the actual Portuguese 94-bus system (Continued)

Line Number	**From bus**	**To bus**	**Resistance (Ω)**	**Reactance (Ω)**
43	43	44	0.5198	0.2903
44	44	45	0.3341	0.1866
45	9	46	0.3490	0.1949
46	10	47	0.5771	0.3223
47	47	48	0.3598	0.2009
48	48	49	0.7688	0.4294
49	49	50	0.2599	0.1451
50	50	51	0.8654	0.4833
51	10	52	0.5248	0.5179
52	52	53	0.1737	0.1714
53	53	54	0.6148	0.6068
54	54	55	0.1980	0.1954
55	55	56	0.1980	0.1954
56	56	57	0.2850	0.2813
57	57	58	0.1429	0.1410
58	58	59	0.3409	0.1904
59	59	60	0.3679	0.2055
60	60	61	0.3591	0.2006
61	61	62	0.3503	0.1957
62	62	63	0.4219	0.2356
63	63	64	1.5380	0.5517
64	64	65	0.9788	0.3511
65	65	66	1.4911	0.5349
66	11	67	0.9690	0.2552
67	67	68	0.6705	0.1766
68	12	69	0.4354	0.2432
69	13	70	0.4631	0.2586
70	70	71	0.2707	0.1512
71	15	72	0.6683	0.3732
72	72	73	0.8525	0.4762
73	16	74	0.3314	0.1851
74	18	75	0.4050	0.2262
75	19	76	0.4367	0.2439
76	19	77	0.3416	0.1908
77	77	78	0.2113	0.1180
78	78	79	1.1249	0.4035
79	79	80	1.1738	0.6556
80	80	81	0.6190	0.3457
81	81	82	0.5684	0.3174
82	20	83	0.8393	0.3011
83	83	84	0.2133	0.1191
84	84	85	0.3645	0.2036

Table A.6: Line data for the actual Portuguese 94-bus system (Continued)

Line Number	**From bus**	**To bus**	**Resistance (Ω)**	**Reactance (Ω)**
85	85	86	0.3206	0.1791
86	22	87	0.7675	0.4286
87	24	88	1.5914	0.5709
88	25	89	0.7020	0.3921
89	25	90	20.743	0.7441
90	90	91	0.6780	0.2432
91	91	92	0.5738	0.3205
92	27	93	0.5913	0.3303
93	28	94	1.1865	0.3124

Appendix B

Benchmark test functions

Table B.1: Unimodal functions.

Function	Dim	Range	Global F_{min}
$f_1(z) = \sum_{j=1}^{n} z_j^2$	30	$[-100, 100]$	0
$f_2(z) = \sum_{j=1}^{n} \lvert z_j \rvert + \prod_{j=1}^{n} \lvert z_j \rvert$	30	$[-10, 10]$	0
$f_3(z) = \sum_{j=1}^{n} \left(\sum_{i=1}^{j} z_i \right)^2$	30	$[-100, 100]$	0
$f_4(z) = \max_j \quad \lvert z_j \rvert, \quad 1 \leq j \leq n$	30	$[-100, 100]$	0
$f_5(z) = \sum_{j=1}^{n-1} \left[100(z_{j+1} - z_j^2)^2 + (z_j - 1)^2 \right]$	30	$[-30, 30]$	0
$f_6(z) = \sum_{j=1}^{n} ([z_j + 0.5])^2$	30	$[-100, 100]$	0
$f_7(z) = \sum_{j=1}^{n} j z_j^4 + \text{rand}(0, 1)$	30	$[-1.28, 1.28]$	0

Table B.2: Multimodal functions.

Function	Dim	Range	Global F_{min}
$f_8(z) = \sum_{j=1}^{n} -z_j \sin\left(\sqrt{\lvert z_j \rvert}\right)$	30	$[-500, 500]$	-12569.5
$f_9(z) = \sum_{j=1}^{n} \left[z_j^2 - 10\cos(2\pi z_j) + 10 \right]$	30	$[-5.12, 5.12]$	0
$f_{10}(z) = -20\exp\left(-0.2\sqrt{\frac{1}{n}\sum_{j=1}^{n} z_j^2}\right) - \exp\left(\frac{1}{n}\sum_{j=1}^{n}\cos(2\pi z_j)\right) + 20 + e$	30	$[-32, 32]$	0
$f_{11}(z) = \frac{1}{4000}\sum_{j=1}^{n} z_j^2 - \prod_{j=1}^{n}\cos\left(\frac{z_j}{\sqrt{j}}\right) + 1$	30	$[-600, 600]$	0
$f_{12}(z) = \frac{\pi}{n}\left\{10\sin^2(\pi x_1) + \sum_{j=1}^{n-1}\left[(x_j - 1)^2\left(1 + 10\sin^2(\pi x_{j+1})\right)\right] + (x_n - 1)^2\right\} + \sum_{j=1}^{n} u(z_j, 10, 100, 4)$	30	$[-50, 50]$	0
$f_{13}(z) = 0.1\left\{\sin^2(3\pi z_1) + \sum_{j=1}^{n-1}(z_j - 1)^2\left[1 + \sin^2(3\pi z_j + 1)\right] + (z_n - 1)^2\left[1 + \sin^2(2\pi z_n)\right]\right\} + \sum_{j=1}^{n} u(z_j, 5, 100, 4)$ $u(z_j, a, b, c) = \begin{cases} b(z_j - a)^c, & z_j > a \\ 0, & -a \leq z_j \leq a \\ b(-z_j - a)^c, & z_j < -a \end{cases}$	30	$[-50, 50]$	0

Table B.3: Fixed-dimension multimodal benchmark functions.

Function	Dim	Range	Global F_{min}
$f_{14}(z) = \left[\frac{1}{500} + \sum_{i=1}^{25} \frac{1}{i+\sum_{j=1}^{2}(z_j - a_{ij})^6}\right]^{-1}$	2	$[-65.536, 65.536]$	0.998
$f_{15}(z) = \sum_{j=1}^{11} \left[b_j - \frac{z_j(b_j^2+b_j z_2)}{b_j^2+b_j z_3+z_4}\right]^2$	4	$[-5, 5]$	0.00030
$f_{16}(z) = 4z_1^2 - 2.1z_1^4 + \frac{1}{3}z_1^6 + z_1 z_2 - 4z_2^2 + 4z_2^4$	2	$[-5, 5]$	-1.0316
$f_{17}(z) = \left(z_2 - \frac{5.1}{4\pi^2}z_1^2 + \frac{5}{\pi}z_1 - 6\right)^2 + 10\left(1 - \frac{1}{8\pi}\right)\cos z_1 + 10$	2	$[-5, 5]$	0.3979
$f_{18}(z) = \left[1 + (z_1 + z_2 + 1)^2 \left(19 + 14z_1 + 3z_1^2 - 14z_2 + 6z_1 z_2 + 3z_2^2\right)\right] \times \left[30 + (2z_1 - 3z_2)^2 (18 - 32z_1 + 12z_1^2 - 48z_2 - 36z_1 z_2 + 27z_2^2)\right]$	2	$[-2, 2]$	3
$f_{19}(z) = -\sum_{j=1}^{4} c_j \exp\left[-\sum_{i=1}^{3} a_{ji}(z_i - p_{ji})^2\right]$	3	$[1, 3]$	-3.86
$f_{20}(z) = -\sum_{j=1}^{4} c_j \exp\left[-\sum_{i=1}^{6} a_{ji}(z_i - p_{ji})^2\right]$	6	$[0, 1]$	-3.32
$f_{21}(z) = -\sum_{j=1}^{5} \left[(z - a_j)(z - a_j)^T + c_j\right]^{-1}$	4	$[0, 10]$	-10.1532
$f_{22}(z) = -\sum_{j=1}^{7} \left[(z - a_j)(z - a_j)^T + c_j\right]^{-1}$	4	$[0, 10]$	-10.4028
$f_{23}(z) = -\sum_{j=1}^{10} \left[(z - a_j)(z - a_j)^T + c_j\right]^{-1}$	4	$[0, 10]$	-10.5363